Endocytic recycling regulates extracellular matrix assembly by cancer associated fibroblasts to promote ovarian cancer cell invasion

A thesis submitted to the University of Manchester for the degree of Doctor of Philosophy in the Faculty of Biology, Medicine and Health

2023

Matthew J. Hartshorn

School of Biological Sciences

Division of Cell Matrix Biology and Regenerative Medicine

Contents

Word count: 63,075

List of figures

List of Tables

Abbreviations

AA	Antibiotic-antimycotic
AEBP1	Adipocyte enhancer binding protein 1
APJ	Apelin/apelin receptor
Arp2/3	Actin-related protein 2/3
BAR	Bin-amphiphysin-Rvs
BSA	Bovine serum albumin
CA-MSC	Cancer-associated MSC
CAF	Cancer associated fibroblasts
CHEVI	Class C homologs in endosome–vesicle interaction
CLIC	Clathrin-independent carrier
COPII	Coat protein complex II
CORVET	Class C core vacuole/endosome tethering
CRISPR	Clustered regularly interspaced short palindromic repeats
CSF-1	Colony-stimulating factor
Ct	Cycle threshold
ddH_2O	Double-distilled water
DMEM	Dulbecco's Modified Eagle Medium
DTC	Disseminated tumour cell
DTT	Dithiothreitol
ECM	Extracellular matrix
EdU	Ethynyl-2′-deoxyuridine
EE	Early endosome
EGF	Epidermal growth factor
EGFR	Epidermal growth factor receptor
EHD2	EH-domain containing 2
EMT	Epithelial-to-mesenchymal transition
ER	Endoplasmic reticulum

ERC	Endocytic recycling compartment
FABP4	Fatty acid binding protein 4
FACS	Fluorescence-activated cell sorting
FAK	Focal adhesion kinase
FAP	Fibroblast activation protein
FBS	Fetal bovine serum
FERARI	Factors for endosome recycling and Rab interactions
FGF	Fibroblast growth factor
FSP-1	Fibroblast-specific protein-1
GAP	GTPase activating protein
GDP	Guanosine-diphosphate
GEEC	GPI-anchored protein-enriched early endosomal compartment
GEF	Guanine nucleotide exchange factor
GFP	Green fluorescent protein
GLO	Gulconolactone oxidase
GTP	Guanosine-triphosphate
GTPase	Guanosine triphosphatases
HDF	Human dermal fibroblasts
HGF	Hepatocyte growth factor
HGSOC	High-grade serous ovarian cancer
HOPS	Homotypic fusion and vacuole protein sorting
IL-6	Interleukin-6
IL-8	Interleukin-8
ILV	Intraluminal vesicle
JIP	JNK-interacting protein
LE	Late endosome
LOX	Lysyl oxidase
M6PR	Mannose-6-phosphate receptor
Methocel	RPMI medium with methylcellulose

MMP	Matrix metalloproteinase
mNG	mNeonGreen
MOC	Manchester ovarian cancer
MSC	Mesenchymal stem cell
MVB	Multivesicular body
NFs	Normal fibroblasts
NK	Natural killer
NNMT	Nicotinamide N-methyltransferase
OC	Ovarian cancer
PARPI	Poly (ADP-ribose) polymerase inhibitor
PBS	Phosphate buffered saline
PDGFA	Platelet-derived growth factor A
PEI	Polyethylenimine
PFA	Paraformaldehyde
PRELP	Prolargin
PTMs	Post-translational modifications
RaB11-FIP5	Rab11 family-interacting protein 5
RGD	Arg-Gly-Asp
RT-qPCR	Quantitative reverse transcription PCR
scRNA-seq	Single-cell RNA sequencing
SDS-PAGE	Sodium dodecyl-sulfate polyacrylamide gel electrophoresis
SHG	Second-harmonic generation
SIK2	Salt-inducible kinase 2
SMA	α-smooth muscle actin
STIC	Serous tubal intraepithelial carcinoma
TAMs	Tumour-associated macrophages
TBS-T	Tris-buffered saline-Tween 20
TGFβ	Transforming growth factor beta
TGN	Trans-Golgi network
TIP47	Tail-interacting protein of 47 kD

TME	Tumour microenvironment
Treg	T regulatory
VEGF	Vascular endothelial growth factor
WASH	Wiskott-Aldrich syndrome protein and scar homolog
WASP	Wiskott-Aldrich syndrome protein

Abstract

High-grade serous ovarian cancer (HGSOC) is the most common and lethal form of ovarian cancer. Early-stage diagnosis is rare due to the subtle nature of symptoms, and at later stages metastasis is common. The omentum is a preferential site for metastatic tumour formation, as it provides a HGSOC supportive tumour microenvironment (TME), an aspect of which is the extracellular matrix (ECM), assembled primarily by cancer associated fibroblasts (CAFs). Whilst it is known that fibrillar collagen-rich ECM in the omentum is associated with HGSOC progression, the molecular mechanisms involved in ECM assembly within the TME are poorly understood. Although endocytic recycling has been implicated in basement membrane ECM assembly, and in the remodelling of the ECM protein fibronectin, its role in ECM assembly within the HGSOC TME remains unclear. We found that Kuramochi HGSOC cells were minimally invasive in collagen hydrogels, but their co-culture with CAFs isolated from HGSOC metastases within spheroids significantly enhanced invasion. CAF-conditioned medium was insufficient to promote HGSOC invasion, however substantial collagen remodelling was detected in the vicinity of co-culture spheroids, suggesting that CAFs directly influenced the ECM to support invasion. An siRNA screening approach was used to deplete key endocytic recycling regulator Rab GTPases, and Arf6, in CAFs to identify those required to promote HGSOC invasion. Depletion of Arf6, or Rab4a and Rab4b in combination, resulted in a reduced capacity of two primary CAF lines to facilitate HGSOC invasion in 3D.

We next analysed the influence of Arf6, Rab14, Rab4a and Rab4b, on ECM assembly. Fibronectin is thought to be important in generating fibrillar collagen matrix, however its assembly was unaffected by recycling regulator depletion. Instead, depletion of Arf6, or Rab14, inhibited collagen I deposition by CAFs, with collagen monomer secretion remaining unaffected. Recently, the uptake of secreted collagen and it's recycling via an unknown route, has been implicated in fibrillar collagen assembly. Measuring the uptake of exogenous collagen I monomers by CAFs, demonstrated that Arf6 depletion significantly elevated collagen I uptake. However, there was a significant delay in the reappearance of internalised collagen as fibrils at the cell surface, suggesting that Arf6 regulates the deposition of endocytosed and recycled collagen. Furthermore, live-cell imaging revealed that Arf6 localised to sites of exogenous collagen fibrillogenesis in CAFs overexpressing Arf6-mNeonGreen. Together, our data demonstrate key roles for endocytic recycling in the support of HGSOC progression by CAFs, and specifically implicate Arf6 in collagen assembly within the TME.

Declaration

No portion of the work referred to in the thesis has been submitted in support of an application for another degree or qualification of this or any other university or other institute of learning.

Copyright statement

i. The author of this thesis (including any appendices and/or schedules to this thesis) owns certain copyright or related rights in it (the "Copyright") and s/he has given The University of Manchester certain rights to use such Copyright, including for administrative purposes.

ii. Copies of this thesis, either in full or in extracts and whether in hard or electronic copy, may be made only in accordance with the Copyright, Designs and Patents Act 1988 (as amended) and regulations issued under it or, where appropriate, in accordance with licensing agreements which the University has from time to time. This page must form part of any such copies made.

iii. The ownership of certain Copyright, patents, designs, trademarks and other intellectual property (the "Intellectual Property") and any reproductions of copyright works in the thesis, for example graphs and tables ("Reproductions"), which may be described in this thesis, may not be owned by the author and may be owned by third parties. Such Intellectual Property and Reproductions cannot and must not be made available for use without the prior written permission of the owner(s) of the relevant Intellectual Property and/or Reproductions.

iv. Further information on the conditions under which disclosure, publication and commercialisation of this thesis, the Copyright and any Intellectual Property and/or Reproductions described in it may take place is available in the University IP Policy (see http://documents.manchester.ac.uk/DocuInfo.aspx?DocID=24420), in any relevant Thesis restriction declarations deposited in the University Library, The University Library's regulations (see http://www.library.manchester.ac.uk/about/regulations/) and in The University's policy on Presentation of Theses.

Acknowledgments

I would like to firstly thank my supervisor Patrick Caswell for the opportunity to join his lab and for his guidance and supervision during my PhD project. I would also like to thank Richard Edmondson for his supervision, Caitlin Waddell for her provision of primary cells from patient samples, and Joan Chang for her guidance and collaboration during the final year of my PhD. I would also like to thank Wellcome for the funding of my studentship.

I am grateful to the Caswell lab members, both past and present, for their support and friendship during my PhD. In particular I would like to thank Jakub Gemperle, Eleanor Hinde, Joe Hetmanski and Soledad Astrada Feijer, as well as Ieva Norvaisaite for her work during her masters project.

I would like to thank members of the bioimaging, mass spectrometry, flow cytometry core facilities, in particular Peter March for his assistance with microscopy and image processing. I am also grateful to Craig Lawless for his spectrometry data analyses.

Finally, I would like to thank my friends and family for their support and encouragement during my PhD.

Chapter 1: Introduction

1.1 An overview of cancer

Cancers are a group of diseases which together are responsible for around 10 million deaths worldwide per year [1]. In men, the most prevalent cancer types are prostate, lung, and colon cancers, and those in women are cancers of the breast, lung, and colon [2]. Although cancer encompasses over 100 genetically diverse diseases, a number of hallmarks have been defined that can be applied across all cancer types. These describe the functional capabilities gained by cells as they transition towards a malignant state during tumourigenesis, and include, but are not limited to, genomic instability, proliferation, inflammation, induction of angiogenesis, and metastasis [3].

1.2 Ovarian cancer classification and HGSOC development

1.2.1 Ovarian cancer overview

Ovarian cancer (OC) is the seventh most prevalent cancer type in women, accounting for around 4% of all cancer cases [4] [5]. It is the third most common gynaecological cancer, with over 230,000 new patients diagnosed worldwide each year, and is responsible for approximately 150,000 deaths annually [4] [6]. On average, the worldwide 5-year survival rate for OC is between 30-40% [4] [7]. However, the 5-year survival rate for patients can vary greatly depending not only on the OC stage at the time of diagnosis, but also on the histological type of OC detected [4]. Type I tumours are typically low-grade, detected at an early stage (I), and possess mutations in *BRAF* and *KRAS*, whilst lacking mutations in *TP53*. Type II tumours are high-grade, detected at more advanced stages (II, III and IV), and almost always possess mutations in *TP53* [8] [9]. At stage I, the disease is confined to the ovaries and the 5-year survival rate is high at approximately 90%, with the symptoms at this stage including pain in the abdomen, neck and back, as well as abdominal swelling [10] [11]. However, the non-specific and subtle nature of these symptoms results in the majority of OC patients (70%) being diagnosed once the symptoms become more apparent at stages II, III and IV, by which point metastasis has occurred and the 5-year survival rate drops significantly to approximately 20-30% [11] [12].

1.2.2 High-grade serous ovarian cancer (HGSOC) overview

OC can be further classified into four histological subtypes: serous, clear-cell, mucinous and endometrioid [13]. The most common of these subtypes is high-grade serous OC (HGSOC; Type II), accounting for approximately 70% of all OC cases and between 70-80% of all OC deaths [13] [14]. HGSOC tumours are associated with a high level of genetic instability, which arises due to mutations in *TP53* [15]. Furthermore, these tumours are characterised by their highly proliferative, aggressive, and invasive nature, with widespread metastatic dissemination being very common at the time of diagnosis [13] [16]. The origins of HGSOC remain unclear. For many years it was thought that HGSOC originated primarily from the epithelial surface of the ovary, where the inflammation caused by rupture and repair of this surface during ovulation resulted in cell damage and the acquisition of mutations which led to tumour development in the ovary [17]. However, the absence of detectable HGSOC precursor lesions that possess *TP53* mutations within this epithelial surface suggests that the disease may originate elsewhere from the ovary [17] [18]. Over the past 20 years, the epithelial lining of the fallopian tube has emerged as the most likely origin for the majority of HGSOC tumours. Serous tubal intraepithelial carcinoma (STIC) lesions, which are positive for *TP53* mutations, are thought to arise in this epithelial lining and act as the primary HGSOC precursor lesion. The cells within these lesions are believed to be able to transition to the ovary and to develop into primary HGSOC tumours through uncontrolled growth and proliferation following ovarian implantation [18] [19] [20] [21].

1.3 HGSOC treatment

1.3.1 Debulking surgery and chemotherapy

The current standard treatment for HGSOC patients is a combination of cytoreductive debulking surgery and chemotherapy, and has remained largely unchanged for over 30 years [22]. Patients with advanced stage HGSOC will undergo surgical procedures that often include the removal of the fallopian tube, the ovaries, the uterus, and the omentum, as well as other areas where the disease is visible [23]. Patients will also be treated with chemotherapeutic compounds which act as DNA damaging agents through cross-linking, such as cisplatin and carboplatin [24]. Whilst HGSOC tumours are often chemo-responsive, their inherent genetic instability leads to the development of resistance against these compounds and subsequent disease recurrence in approximately 70% of patients within 4-16 months [25] [26].

1.3.2 PARP inhibitors (PARPIs)

Over the last 5 years, poly (ADP-ribose) polymerase inhibitors (PARPIs) have become a promising new addition to the treatment strategy for HGSOC [27]. These compounds offer a more targeted therapy, and take advantage of the synthetic lethality that exists between inhibiting the PARP enzyme in cells that possess germline or somatic loss of function mutations in *BRCA1* or *BRCA2* [28]. However, despite PARPIs drastically improving clinical outcomes for the 22% of patients with HGSOC tumours positive for these mutations, these compounds are ineffective against tumours with functional BRCA1/2 [29] [30]. Furthermore, resistance can arise against PARPIs through a variety of mechanisms, including via the reversion of mutations in *BRCA1/2* that enable functionality to be regained [31]. Whilst recent progress has therefore been made in advancing HGSOC treatment strategies, there still remains a considerable need for the development of new methods if mortality rates associated with the disease are to improve.

1.4 Cancer invasion and metastasis

1.4.1 Overview

One hallmark of cancer in particular, which is a key contributor towards the high mortality rates associated with this group of diseases, is the ability of a malignant cells within a primary tumour to spread to other organs via metastasis [32]. Cancer metastasis involves cells within primary tumours undergoing a series of genetic changes through mutation [33]. During the metastatic cascade for many cancer types, cells will firstly acquire the ability to detach from neighbouring cells through undergoing an epithelial-to-mesenchymal transition (EMT) [34]. This transition then also allows cells to migrate and invade into the surrounding stromal tissue [35].

1.4.2 Mechanisms of cancer cell invasion

Cancer cells that have acquired the ability to invade have been shown to do so either as individual cells, or as a collective, and invading cells can adopt, and switch between, either a mesenchymal or an amoeboid mode of migration [36]. Mesenchymal migration requires the upregulation of integrins and proteases, which allow for extracellular matrix (ECM) proteins to be bound and degraded, respectively. This mode of migration is therefore considered to be most suitable when invasion through a dense, stiffer ECM, is required. In contrast, amoeboid migration allows fast cell movement through small gaps in soft ECM, and is associated with a downregulation of integrins and proteases [36]. Although a full EMT was initially presumed to be required for cancer metastasis, it is now clear that collective migration can occur after cells undergo only a partial EMT, where migratory characteristics are acquired whilst loose cell-cell contacts are retained [37].

1.4.3 Intra- and extravasation

Invasive cancer cells will often migrate towards nearby blood or lymph vessels, where they will then enter into the circulation through intravasation, and one of the advantages of collective cell migration is that survival is more likely during this period for cell clusters [38]. Disseminated tumour cells (DTCs) must then survive in the circulation, undergo extravasation to leave the vascular or lymphatic system, and enter into the stroma of secondary organs [39]. At these stages of the metastatic cascade, large numbers of cancer cells are unable to survive as many of the pro-tumourigenic factors present within the primary organ are no longer available. There is often a latency phase between extravasation and the development of a secondary tumour, due to the necessity of DTCs having to undergo additional genetic alterations in order for the metastatic cascade to be completed [40]. As metastasis is responsible for approximately 90% of cancer-related deaths, it is crucial to better understand the molecular mechanisms which drive this process [41].

1.5 HGSOC metastasis to the omentum

1.5.1 HGSOC metastasises without intra- and extravasation

HGSOC can metastasise using the vasculature through intra- and extravasation, however it differs from the majority of other cancers in that secondary tumours mostly form at distant sites without requiring the blood or lymphatic vessels [42] [43]. Metastasis primarily occurs through the detachment of cells from the primary ovarian tumour, via mechanisms such as hypoxia driven EMT, and entry into the peritoneal cavity [16] [44]. Cells, either as single cells or spheroid aggregates, then use the passive flow of fluid within this cavity to reach sites at which secondary tumours can develop [13] [45]. Disseminated HGSOC cells tend to therefore face fewer challenges when undergoing metastatic spreading compared to most other cancers, a feature that likely contributes to the high mortality rate associated with the disease [46].

1.5.2 HGSOC tropism for the omentum

Although, theoretically, colonisation of any organ accessible from the blood or lymph vessels by DTCs is possible, it is now clear that, for most cancer types, the organs within which secondary tumours form is not random [47]. Each cancer type possesses an organ tropism, where specific organs are favoured for secondary tumour formation over others. This is due to certain organs providing microenvironments that suit the needs of different cancer types in order for their adaptation and development into secondary tumours [48]. Whilst HGSOC has the potential to colonise any of the organs accessible from the peritoneal cavity, disseminated HGSOC cells display a specific affinity for one tissue in particular, the omentum [49]. This apron-like fat pad covers the abdominal cavity and bowel, and primarily acts as a fat storage unit, whilst also having roles in processes such as immune regulation and the exchange of fluid in the peritoneal cavity [42] [43] [50] [51]. The omentum is rich in white adipocytes, as well as other stromal cell types including fibroblasts, mesenchymal stem cells (MSCs) and immune cells, with each of these cell types playing important roles in establishing a tumour microenvironment (TME), or metastatic niche, that facilitates colonisation of the omentum by DTCs [46](Figure 1.1).

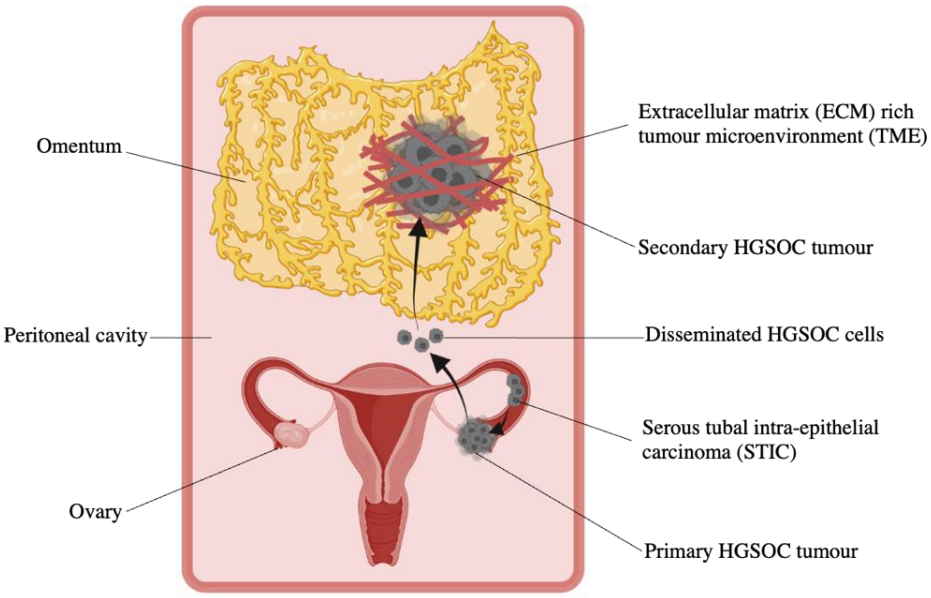

Figure 1.1 - HGSOC cells metastasise from the ovary to the omentum

HGSOC is thought to develop from STIC lesions, which themselves develop from the secretory epithelial cells that line the fallopian tube. STIC cells can transition to the ovary to form a primary HGSOC tumour after implantation. Following an EMT, metastasis primarily occurs via the peritoneal cavity, where disseminated HGSOC cells use the fluid flow within this cavity to reach other sites for secondary tumour formation. HGSOC cells display a tropism for the omentum, as it provides a microenvironment that supports many processes required for cancer cell growth, proliferation, and invasion. One aspect of the microenvironment that supports these processes, is the formation of a dense, fibrillar ECM. Adapted from a figure presented by H Naora and DJ Montell [52].

1.6 Tumour microenvironment (TME) overview

In general, the TME encompasses the non-malignant cells, blood vessels, lymphatic vessels, and non-cellular components such as metabolites and ECM proteins located in the area surrounding a tumour, and in recent years the role of the TME in cancer progression at both primary and secondary sites has become increasingly recognised [53]. Whilst substantial heterogeneity exists between, and within, different cancer types, there are many features shared between their TMEs [54]. A diverse array of non-malignant cell types are recruited into the TME by the tumour, which then drives their adaptation to generate cancer-associated cell types, such that they are able to operate in a way that contributes towards providing conditions for supporting tumour development [55].

1.6.1 Immune cells

There are a number of different immune cell types that have been found to exist within TMEs, including T and B lymphocytes, macrophages, neutrophils, dendritic cells, and natural killer (NK) cells [55] [56]. The role of the immune system in tumour progression is complex, and its impact on a tumour is dictated by which immune cell types are present [57]. For example, cytotoxic CD8+ T lymphocytes are capable of exerting tumour-suppressive effects within the TME. However, high levels of CD4+ T regulatory (Treg) cells are often present in TMEs, which act in an immunosuppressive manner through the modulation of cytotoxic T lymphocyte activity [58]. Similarly, B lymphocytes and macrophages within TMEs can also function in ways that both support and suppress tumour development. B lymphocytes are thought to primarily contribute towards productive immune responses towards a tumour, however it has also become clear in animal models, and in humans, that these cells are capable of secreting specific cytokines which ultimately lead to immune suppression [59]. Macrophages are also prevalent within TMEs, where they become activated to become tumour-associated macrophages (TAMs). TAMs can exist in two distinct activated states, where the M1 state is associated with tumour suppression, and the M2 state contributes towards promoting tumour development [60]. For example, M1 TAMs in the colorectal cancer TME enhance the cancer-cell mediated secretion of factors, such as galectin-3, which drive immune cell recruitment into the tumour vicinity and enable a productive immune response [61]. However, in the case of most TMEs, the interaction of macrophages with tumour cells results in the generation of TAMs that display an immune suppressive M2 phenotype [62]. As well as the ability of M2 TAMs to dampen the immune response in the TME, they have also been shown to enhance angiogenesis, for example through the production of vascular endothelial growth factor (VEGF) [63]. Furthermore, M2 TAMs are thought to collaborate with other non-malignant cell types in TMEs. For example, they have been shown to convert normal fibroblasts (NFs) into cancer-associated fibroblasts (CAFs), which are known to promote tumour progression through a variety of mechanisms, and there is also a cross-talk between these two cell types where CAFs stimulate M2 TAM activity [64].

1.6.2 Angiogenesis

The formation of new blood vessels within TMEs via angiogenesis is vital for tumour progression. Pro- and anti-angiogenic factors regulate this process, and these factors will counteract each other until an angiogenic-switch occurs, where pro-angiogenic factors dominate to drive blood vessel formation [65]. A tumours requirement for blood vessels is primarily the result of nutrient and oxygen availability decreasing as the tumour increases in size [66]. However given the requirement of the majority of cancers for entry into the circulation in order for metastasis to occur, angiogenesis within TMEs also facilitates the spreading of DTCs to secondary sites [67]. The cells within a tumour are capable of stimulating angiogenesis within their TME, however in addition to M2 TAMs, many of the other non-malignant cell types surrounding the tumour can also aid blood vessel formation, including the various other immune cells present, as well as platelets, adipocytes, and CAFs [68]. For example, CAFs have been shown to secrete VEGF to stimulate angiogenesis in the TMEs of various different cancer types, including cancer of the liver and of the stomach [69] [70] [71].

1.6.3 CAFs

Fibroblasts are a common non-malignant cell type within the TME of many different cancers. In healthy organs, NFs predominantly function in the building of connective tissue where they act as the primary synthesisers of ECM, and the precise regulation of ECM synthesis and assembly is essential for organs to function correctly [72]. NFs are known to be heterogeneous, and a number of different phenotypes can be displayed depending on the fibroblast function required at a particular time. For example, in healthy adult organs, fibroblasts are relatively inactive. However, tissue development and repair requires the conversion of these quiescent fibroblasts to a more active, contractile, myofibroblast state, characterised by biomarkers such as α-smooth muscle actin (SMA) and fibroblast activation protein (FAP), enabling them to more efficiently assemble and remodel ECM [72] [73] [74] [75]. The ability of inactive NFs to be reprogrammed to an active, myofibroblast state, is utilised by malignant cells to generate CAFs that assist with tumour development [76].

CAFs are considered as a heterogeneous group of mesenchymal cells, and are capable of carrying out diverse functions within TMEs, including those which support, and suppress, tumourigenesis [77]. In addition to the pro-tumourigenic roles of CAFs in both facilitating angiogenesis through growth factor secretion, and stimulating M2 macrophage function, they are well-established contributors towards the assembly and remodelling of ECM within the TME to support tumour development [78]. The ECM is believed to modulate the vast majority of processes involved in tumour progression, and a dense, stiff, highly cross-linked ECM has been detected within the TMEs of many cancer types. This type of ECM has been extensively shown to allow cancer cells to invade and metastasise, and to proliferate uncontrollably whilst also avoiding cell death and evading the immune system [79]. It is also now clear that, through focal adhesion kinase (FAK) signalling, the ECM can reprogram cancer cell metabolism to stimulate protein biosynthesis which ultimately enables cell survival and proliferation [80]. Finally, the ECM can indirectly enable tumourigenesis, through blocking the accessibility of chemotherapeutic compounds and cytotoxic T lymphocytes to the tumour, whilst also enhancing TAM infiltration [81] [82] [83]. The heterogeneous nature of CAFs within TMEs is exemplified by the fact that as well possessing roles in promoting tumour development, they are now known to also function in a tumour suppressive manner [84]. Whilst evidence in favour of CAFs acting as tumour suppressors is limited relative to that highlighting their tumour promoting functions, it is clear in certain circumstances that the presence of CAFs in TMEs can hinder tumour progression. As an example, the depletion of CAFs in mouse models of pancreatic cancer has been shown to enhance cancer cell invasion and to decrease overall survival through limiting immune cell infiltration [85].

1.7 CAF biomarkers

The biomarkers conventionally used to identify and characterise CAFs are SMA, FAP, fibroblast-specific protein-1 (FSP-1; S100A4) and vimentin [86]. SMA is an actin isoform that is known to contribute towards the ECM assembly and remodelling capacity of myofibroblasts through increasing cell contractility [86]. Whilst expression of SMA is relatively low in NFs, OC-cell derived signalling molecules, such as TGFβ1 and TGFβ3, are known to drive the NF-CAF conversion through elevating SMA expression levels [87] [88] [89]. FAP is a serine protease on the fibroblast cell surface that is thought to have roles both in ECM remodelling through its ability to cleave collagen, and in regulating ovarian CAF proliferation, with increased FAP expression also associated with poor prognosis in HGSOC [90] [91] [92]. FSP-1 is a cytosolic calcium binding protein which can also be secreted by fibroblasts [93] [94]. Studies in mice have demonstrated that CAFs in which FSP-1 has been depleted have a reduced ability to facilitate metastatic colonisation of breast cancer cells [95]. However, although there are a wide variety of suggested roles for FSP-1 in cancer progression, exactly how expression of this protein in CAFs contributes towards their tumour promoting capacity is poorly understood [86] [94]. Since the identification of FSP-1 as a CAF biomarker over 25 years ago, this protein is no longer considered to be fibroblast specific. It is now known that other cell types, including cancer cells, can express FSP-1 and that elevated expression levels are associated with a more aggressive and invasive cancer cell phenotype, and with poor prognosis in cancer patients [93]. This renders FSP-1 as a relatively poor biomarker for CAF identification. Vimentin is an intermediate-filament protein with a role in forming the cytoskeletal network of mesenchymal cells. Whilst vimentin is expressed by CAFs, it is now known that many other cell types also express this protein, such as normal fibroblast populations, adipocytes, and cancer cells. Vimentin is therefore also a relatively poor CAF biomarker [87]. In addition to the conventional biomarkers used for CAF identification, other proteins which are specifically expressed in CAFs have now been identified. For example, collagen XI, which is a known nucleator of collagen I fibrillogenesis, has been identified as a specific biomarker for activated CAFs [96] [97]. High collagen XI expression is associated with poor disease outcomes across a variety of epithelial cancers, and an increase in collagen XI within the omentum of HGSOC patients correlates with disease progression [97] [98].

1.8 Targeting CAFs in the TME to treat cancer

1.8.1 Overview

Since the identification of key mutations in malignant cells that drive cancer progression, such as those which activate the epidermal growth factor receptor (EGFR), or inactivate p53, chemotherapy aiming to inhibit tumour growth has primarily focussed on targeting cancer cells directly. However, during treatment, the development of resistance against chemotherapeutic agents is common, and this is largely attributed to the genetic instability of malignant cells allowing them to develop resistance conferring-mutations [99].

Given that the interactions between cancer cells and their TME are now considered to be crucial contributors towards driving the development of many different cancer types, this opens up the possibility of targeting the TME to hinder tumour development indirectly. The non-malignant cells within TMEs are far more genetically stable, minimising the risk of resistance developing should these cells be targeted [54]. Although there are many differences between TMEs across cancer types, there are also many common features, including the presence of CAFs and their assembled ECM. These common features therefore have the potential to be targeted chemotherapeutically, and due to the multi-faceted role of CAFs in the TME, there is significant potential for them to be targeted in the treatment of cancer. A number of studies have demonstrated how targeting CAFs and the ECM can indirectly hinder tumour progression, with several compounds having entered clinical trials [100].

1.8.2 FAP targeting

Much of the work aiming to target CAFs for cancer treatment has primarily focussed on utilising their cell-surface expression of the CAF biomarker, FAP, as a means of directing cytotoxic compounds or immune cells towards them [101]. Strategies for targeting FAP include the use of antibodies that bind to and inhibit FAP, cytotoxic prodrugs activated by FAP-mediated cleavage, and liposomes that are targeted to FAP and contain chemotherapeutic compounds [102] [103] [104]. Furthermore, approaches aiming to generate an immune response towards CAFs expressing FAP have also been tested [105]. However, despite many of these strategies generating positive results in animal models, none have been sufficiently effective to fully progress through clinical trials [100]. Most other strategies for targeting CAFs revolve around attempts to directly impair their tumour promoting functions in the TME. For example, the CXCL12/CXCR4 signalling axis has been shown to be of particular importance in allowing CAFs to recruit immune and vascular endothelial cells into the TME [106] [107]. In mouse models of breast cancer, the use of an inhibitor compound targeting this axis in CAFs was sufficient to reduce angiogenesis and immunosuppression in the TME [108].

1.8.3 ECM targeting

Attempts have also been made to target the predominantly CAF-assembled ECM within TMEs. The essential role of the ECM in facilitating cancer progression, both directly through supporting tumour growth and invasion, and indirectly by obstructing chemotherapeutic compound and immune cell access to the tumour, renders it an appealing target in cancer therapy [109]. The ECM in the TME may be targeted either via inhibiting the pro-tumourigenic function of ECM components which have already been synthesised and deposited, or alternatively, the processes involved in ECM component synthesis and deposition may be obstructed. For example, the ECM protein tenascin C is highly expressed by malignant cells, and an increase in its levels correlates with the progression of many cancer types, including those of the brain and lung [110]. It has been shown that the use of a tenascin C specific antibody was able to improve the outcome of glioblastoma patients in phase I and II clinical trials, potentially due to the role of this ECM protein in supporting glioblastoma cell migration [111] [112] [113]. With regards to targeting ECM protein deposition within TMEs, efforts have been made aiming to inhibit the synthesis of collagen I, an ECM protein that is of clear importance in cancer

progression, with roles in facilitating malignant cell growth, proliferation, and invasion [114]. In order for collagen to be secreted, triple helical procollagen must first be assembled within the endoplasmic reticulum (ER). A number of ER-resident enzymes function to modify collagen I such that the triple helix can form, such as the collagen prolyl-4-hyroxylases [109]. Inhibition of these enzymes has been demonstrated to significantly reduce metastasis in breast cancer models through impairing collagen I deposition [115] [116]. However, whilst the ECM has an important role in tumour development, it also carries out crucial functions in healthy tissue. As such, although a great deal of evidence exists in support of ECM targeting for cancer treatment, a common issue encountered during attempts to target this aspect of the TME is the non-desirable impact of doing so on healthy tissues [109]. In order for ECM targeting to be an effective strategy in the treatment of cancer, it is essential to identify cancer-specific ECM targets. These targets may include ECM proteins which are significantly more prevalent in TMEs relative to healthy tissue, or cellular components which are of particular importance in ECM synthesis and deposition specifically within TMEs.

Targeting the CAF and ECM components of the TME therefore has great potential as a means to treat various cancer types. However, if this type of approach is to be used effectively in this way, it is crucial to elucidate how TMEs are generated in greater detail, including that found within the HGSOC tumour burdened omentum. Through furthering our understanding of the TME in the omentum, in terms of both its composition and the mechanisms involved in its generation, new targets may be identified for HGSOC treatment through chemotherapeutic intervention.

1.9 The HGSOC metastatic TME

1.9.1 Overview

As the omentum is the preferential site for metastatic HGSOC tumour formation, it is essential to further our understanding of the cellular, and non-cellular, components found within the omental TME. The presence of malignant cells in the omentum is thought to produce various cancer-associated cell types which are capable of assisting with HGSOC colonisation and tumour progression. There is also evidence to suggest that the generation of these various cancer-associated cell types may begin prior to the arrival of disseminated HGSOC cells in the omentum. Through mechanisms including exosome secretion, disseminated HGSOC cells in the peritoneal cavity are able to communicate with normal cell types in the omentum [117]. This is thought to create a pre-metastatic niche which favours omental colonisation, and may in part explain the tropism displayed by HGSOC cells for the omentum during metastasis [118] [119].

1.9.2 White adipocytes

The most abundant cell type in the omentum are the white adipocytes, and in healthy omentum, white adipocytes primarily function as energy storage units. However, they are also responsible for the secretion of over 400 paracrine and endocrine factors, including various adipokines and immune-regulatory cytokines [120]. Evidence has emerged highlighting the importance of the crosstalk that occurs between HGSOC cells and adipocytes in generating a microenvironment that allows for secondary tumour formation [46] [121]. Through converting white adipocytes into cancer-associated adipocytes via this cross-talk, metabolic reprogramming occurs. HGSOC cells in the omentum are able to stimulate the release of adipocyte-derived lipids, which act as an energy source for sustained malignant cell growth and proliferation [122] [123]. White adipocytes in the omentum can also secrete a number of adipokines and other factors that contribute towards secondary tumour formation [46] [124] [125] [126]. For example, they have been shown to secrete interleukin-8 (IL-8) which stimulates OC cell invasion [122]. In addition, white adipocytes can induce metabolic changes in OC cells that enable free fatty acids to be utilised more efficiently [127]. For example, factors secreted by white adipocytes can elevate lipid uptake by OC cells via the apelin/apelin receptor (APJ) signalling pathway [128]. Furthermore, a number of these factors function to upregulate enzymes required for fatty acid metabolism by OC cells, including fatty acid binding protein 4 (FABP4) and salt-inducible kinase 2 (SIK2) [122] [129].

1.9.3 Immune cells

As discussed previously, the role of TAMs and other immune cells in tumour development is well established. Within the healthy omentum, aggregated clusters of immune cells exist, termed “milky spots”, and although rich in various immune cell types which enable defence against pathogens, they have been shown to tolerate cancer cells which subsequently enables omentum colonisation [130] [131]. Interestingly, disseminated HGSOC cells are believed to preferentially colonise the omentum at sites near these clusters, which indicates a direct role for the immune system in HGSOC metastasis [132].

There are multiple different immune cell types found within the HGSOC omental TME, and a degree of heterogeneity in the immune cell composition in the omentum between HGSOC patients has been demonstrated [133]. HGSOC cell-macrophage bidirectional cross-talk is thought to occur in the omentum, through the secretion of many different cytokines, which acts to reprogram resident macrophages into TAMs. TAMs in the HGSOC TME predominantly display the M2 phenotype, and are known to secrete many different factors and enzymes that function to generate an immunosuppressive microenvironment, which in turn facilitates tumour development [46]. For example, TAMs in the omentum are thought to produce exosomes which recruit immunosuppressive Treg cells, and to secrete the chemokine CCL23, which promotes HGSOC cell invasion [134]. Furthermore, TAMs secrete the immunosuppressive and tumourigenic factors VEGF and transforming growth factor beta 1 (TGFβ1) [135] [136].

The impact of T lymphocytes infiltrating the TME on survival and outcome for HGSOC patients varies depending on the subpopulation of these cells present. As in the case of most cancer types, CD8+ T lymphocyte infiltration correlates with better improved outcomes in HGSOC, and a role for these cells has been highlighted in malignant cell clearance [137]. Although some studies have also demonstrated that CD4+ T lymphocytes in the omental TME assist with clearing HGSOC tumours, recent evidence suggests that the presence of this T lymphocyte subpopulation correlates with poor survival [138]. This may be explained by the heterogeneous nature of CD4+ T lymphocytes. Specific subpopulations are able to mobilise other immune cells to generate a productive immune response against the tumour, whereas others, particularly the Treg subpopulation, operate in an immunosuppressive manner [133]. Furthermore, Treg cells within the omental TME have been shown to secrete VEGFA, which stimulates angiogenesis, and platelet-derived growth factor A (PDGFA), which supports CAF growth [139].

The other immune cell types often found within the HGSOC omental TME, are B lymphocytes, natural killer (NK) cells, and dendritic cells [133]. The presence of B lymphocytes in the HGSOC TME is common, and their infiltration, particularly that of B lymphocytes which are CD20+, correlates with improved patient survival [140] [141]. These cells produce a variety of cytokines, which together support a productive immune response for tumour clearance in the omentum. For example, they have been shown to secrete CXCL8, which acts to recruit other immune cell types, including dendritic cells, enabling their maturation such that they can activate CD8+ T lymphocytes [140].

Dendritic cells in the omentum are able to both support and hinder tumour development. Whilst myeloid dendritic cells are capable of aiding tumour clearance, plasmacytoid dendritic cells are immunosuppressive and their presence correlates with poor prognosis [133] [142]. Plasmacytoid dendritic cells are recruited to the HGSOC TME due to the presence of malignant cell-derived factors, such as CXCL12, then following recruitment they can induce angiogenesis, HGSOC metastasis, and impair CD8+ T Lymphocyte function [143]. Finally, NK cells are also present in the TME of HGSOC, and this immune cell type primarily functions to suppress tumour development [133]. For example, HGSOC patient-derived NK cells have been shown to display cytotoxic activity towards HGSOC cells in mice, which resulted in the prevention of metastasis, and were also able to activate other immune cells to hinder HGSOC tumour growth *in vitro*, and in mice [144].

1.9.4 MSCs

Resident MSCs in the omentum can be reprogrammed by HGSOC cells to produce cancer-associated MSCs (CA-MSCs), which have tumour-promoting capabilities. It is known that that the presence of MSCs in co-culture with OC cells enhances OC cell proliferation, invasion, and drug resistance, and this is believed to occur through the secretion of a host of cytokines, such as IL-6, CXCL12 and TGFβ [145] [146] [147] [148] [149]. MSCs are also a source from which CAFs can be derived within the omentum, and HGSOC cell-derived exosomes are responsible for MSC reprogramming [149].

1.9.5 CAFs

In addition to the various immune cells found within the HGSOC TME, CAFs are another stromal cell type present with essential roles in promoting HGSOC colonisation of the omentum and secondary tumour development. As well as from MSCs, CAFs in the omentum are derived from NFs, where HGSOC cells are responsible for their generation through reprogramming, for example via TGFβ secretion [150]. Tumour-CAF bidirectional cross-talk is then responsible for maintaining CAFs in a myofibroblast-like state, and also for stimulating CAFs to perform a number of roles in promoting tumour development in the omentum [151] [152]. CAFs function as the primary ECM remodelling cell type in the TME of most cancer types, and whilst many cell types within the omentum are likely responsible for ECM protein synthesis, including HGSOC cells, TAMs, and white adipocytes, it is the CAFs which predominantly synthesise and assemble these proteins to generate a dense ECM [150] [46] [153] [154] [155] [120] [156] [157] [158]. Work by Delaine-Smith et al. revealed the importance of the cross-talk that occurs between CAFs and OC cells in fibroblast activation [159]. They firstly highlighted TGFβ3 as the most highly expressed TGFβ isoform in OC cells. Secondly, they demonstrated how treatment of omental fibroblasts with this growth factor increases their expression of CAF biomarkers, such as FAP and SMA, and also enhances their ECM protein synthesis and deposition capabilities. This ECM is thought to play crucial roles in the omentum in driving tumour progression, through supporting HGSOC cell growth, proliferation, survival, and invasion [150]. Furthermore, CAFs in the omentum secrete many different growth factors, such as fibroblast growth factor (FGF), hepatocyte growth factor (HGF), and CXCL12, which also stimulate these processes to drive tumour development [151](Figure 1.2).

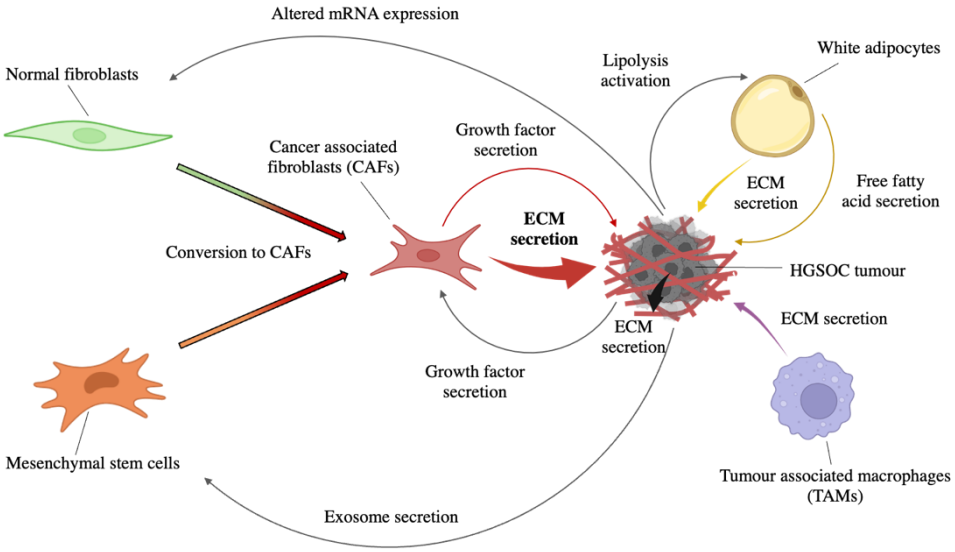

Figure 1.2 – CAFs origins and cell-cell communication within the HGSOC omental TME

There is a great deal of complexity in the different cell types within the HGSOC TME, and in the cell-cell communication that occurs between them. CAFs in the omentum are likely derived from MSCs and NFs, and it is known that HGSOC-secreted factors, such as TGFβ, and exosomes, contribute towards converting these cell types to a CAF-like state. There is then a continual, bidirectional, cross-talk between the HGSOC tumour and the CAFs. The CAF phenotype is maintained by tumour-derived factors, such that the CAFs can carry out a number of processes that support HGSOC cell growth, proliferation, and invasion, including ECM assembly and growth factor secretion. White adipocytes are also activated by HGSOC cells in the omentum, resulting in the secretion of free fatty acids which provide energy for malignant cell growth and proliferation. Furthermore, through this activation, the white adipocytes may also contribute towards the secretion of ECM related proteins. Finally, the immune system plays a crucial role in HGSOC metastasis, and a number of immune cell types, including TAMs, function as immunosuppressants to support tumour development. In addition, TAMs, and the malignant cells themselves, have also been shown to be capable of ECM protein synthesis.

In addition to the tumour-promoting roles of CAFs in the omentum mediated by ECM assembly and growth factor secretion, CAFs are also able to stimulate tumour development via alternative mechanisms. As discussed previously, CAFs are able to communicate bi-directionally with a number of immune cell types within the omentum, which results in the stimulation of their immunosuppressive functions and subsequent tumour development. The cross-talk between CAFs and immune cells in the omentum is complex, and the secretion of a variety of factors by CAFs contributes towards immunosuppression in the TME. For example, factors including CXCL12 and macrophage colony-stimulating factor (CSF-1) are known to be secreted by CAFs which recruit immunosuppressive TAMs to the HGSOC TME [160]. Furthermore, CAFs in the omentum are able to enhance the survival and proliferation of immunosuppressive Treg cells through the production of factors such as CD73 and interleukin-6 (IL-6) [161].

CAFs also exert their pro-tumourigenic effects through mechanisms involving metabolic changes within the HGSOC TME. A role for CAFs has been demonstrated in directly reprogramming HGSOC cells to use glycogen, enabling cell growth and survival as the adipocytes become less abundant with tumour expansion. Glycogen phosphorylase is activated in HGSOC cells through the action of CAF-secreted factors, such as IL-6 and CXCL10 [162] [163]. Furthermore, metabolic reprogramming occurs within CAFs themselves, and these metabolic changes have been shown to contribute towards tumour development in the omentum. For example, nicotinamide N-methyltransferase (NNMT) is a metabolic enzyme that becomes upregulate in CAFs, and is now considered to be crucial in the support of malignant cell growth and metastasis in the HGSOC TME. NNMT plays a role in altering CAF function through its involvement in ECM secretion and assembly, and in pro-tumourigenic cytokine production [164].

1.10 The extracellular matrix (ECM)

1.10.1 Overview

The ECM is a non-cellular, multi-protein assembly, with the mammalian ECM consisting of approximately 300 proteins that make up a core-matrisome, including fibrillar proteins, such as collagen and fibronectin, and proteoglycans, such as versican and aggrecan [165] [166] [167]. The ECM also contains other matrisome-associated components, such as secreted growth factors, and enzymes that are required for the assembly and remodelling of ECM, including lysyl oxidases (LOXs) and matrix metalloproteinases (MMPs) [165] [168] [169]. The two major ECM structures found within the body are the interstitial ECM, and the basement membrane. Both of these ECM structures are able to regulate processes such as cell growth, proliferation, differentiation and angiogenesis, whilst also regulating cell signalling through controlling growth factor abundance [170] [171] [172] [173] [174]. The regulation of these processes is mediated via the interaction of cells with ECM components using a variety of ECM receptors at the cell surface, including integrins and syndecans [175]. Whilst a number of functions are shared between the major ECM structures, they also possess unique properties that enable specific roles to be carried out [176]. The interstitial ECM in connective tissues acts as a scaffold for cells to provide the tissue with structural integrity [177]. However, this type of ECM can exist in different forms, allowing tissues to carry out specific functions. For example, the hierarchical assembly of collagen in tendon offers high-tensile strength through the formation of thick bundles, whereas in the skin, the assembly of collagen to create less compact bundles enables stretching to be withstood [178]. Basement membranes exist as dense, thin sheets, which act as a scaffold for adjacent cell types, such as epithelial and endothelial cells, to anchor them to the underlying connective tissue [178] [179]. Furthermore, basement membranes also play a role in cell signalling, tissue separation and in the protection of tissues from mechanical stress [179] [180]. Although the importance of the ECM in mammalian tissues has been appreciated for many years, the precise mechanisms required for the assembly of individual ECM components into higher-order structures to form a dynamic and complex 3D network are still not yet fully understood.

1.10.2 The ECM in the HGSOC metastatic TME

The composition and architecture of the ECM within the omentum is known to change with HGSOC disease progression. Pearce et al. used a multi-omics approach to compare the ECM composition between HGSOC patient-derived omentum samples with varying disease extents [98] [181]. It was shown that as the disease became more extensive, the complexity of the stromal ECM increased, and proteins such as collagen I, collagen XI, fibronectin, and COMP became more abundant. Furthermore, using second harmonic generation (SHG) microscopy, they were able to demonstrate that changes in collagen organisation occur with disease progression. In samples where the disease extent was relatively minimal, collagen fibres were thin and arranged around the white adipocytes, whereas in samples where the disease was more severe, larger bundles of collagen were observed [98]. These changes that occur in both ECM composition and organisation with HGSOC progression are thought to be important for HGSOC metastasis to the omentum and secondary tumour development [98] [182]. Given the contribution of metastasis to the high mortality rate associated with HGSOC, it is essential to understand the mechanisms involved in assembling the stromal ECM within the HGSOC metastatic TME.

1.10.3 Collagen I synthesis and assembly

The collagens occupy over 30% of the ECM in the human body and are therefore the most predominant family of ECM proteins [183]. This family comprises 28 members in total and can be divided into subtypes, including but not limited to the fibril-forming collagens, the fibril-associated collagens, the network forming collagens, and the transmembrane collagens [183] [184]. The most abundant collagen in connective tissue is the fibril-forming collagen I, and it is this collagen type for which the mechanisms of collagen synthesis, secretion and assembly are best understood [185] [184]. Collagen I is first synthesised as pro-collagen, which is triple helical in structure, primarily consisting of two different polypeptide chains, proα1 encoded by *COL1A1* and proα2 encoded by *COL1A2*, in a 2:1 ratio [186]. However, it has been recently shown that collagen I homotrimers can also be produced, in particular by malignant cells found in pancreatic cancer, and the production of this homotrimeric collagen I was shown to be important for tumour progression [187]. Collagen chains are translated and translocated into the lumen of the ER, where post-translational modifications (PTM) occur which are essential for triple helical pro-collagen to form [184]. For example, procollagen chains are stabilised through the addition of hydroxyl groups by lysyl and prolyl hydroxylases, via enzymatic

reactions that require ascorbic acid [188] [189]. Enzymes within the ER then assist with the formation of an approximately 300 nm pro-collagen triple helical structure, which is then exported from the ER to the Trans-Golgi network (TGN) in a coat protein complex II (COPII) dependent process that can, but does not exclusively, utilise large carriers generated via the action of TANGO1 for this trafficking [190] [191] [192].

Pro-collagen is trafficked through the Golgi network, whilst being subjected to further PTMs, followed by trafficking to the plasma membrane where carrier-plasma membrane fusion occurs, allowing for secretion into the extracellular space and for fibrillogenesis to take place [193] [194]. In certain cell types, such as the fibroblasts found in tendon, fibripositors have been identified, which are specialised membrane invaginations, or protrusions, created via the fusion of collagen-containing carriers with the plasma membrane [195] [194]. In order for procollagen to be processed to form rod-like tropocollagen molecules capable of assembly in the extracellular space, cleavage of the N- and C-termini by specific procollagen proteinases is required [196]. There are two models for how this processing occurs, where the N- and C- termini are cleaved either during procollagen trafficking, or after secretion into the extracellular space [197] [198] [199]. Once secreted and processed, tropocollagen is assembled into higher-order structures through the formation of microfibers, fibrils, fibres, and more complex 3D networks [199]. *In vitro*, collagen is able to self-assemble into fibrils to some extent. However, in order for the more complex networks found *in vivo* to be generated, cells are required to tightly regulate fibril composition, diameter, and length, such that elaborate matrices can be built [200].

Whilst considerable progress has been made over the last century in developing our understanding of collagen assembly *in vivo*, and that of the entire ECM in general, the detailed mechanisms that allow cells to assemble complex 3D matrices are still relatively poorly understood [200]. One mechanism that is known to be of particular importance in ECM assembly, is the binding of cells to secreted ECM components at their cell surface via integrins [201] [202]. Integrins are heterodimeric cell surface receptors that function to link the cytoskeleton within the cell to the ECM. ECM binding to integrins stimulates integrin clustering and initiates downstream intracellular signalling cascades that allow the cell to sense and respond to mechanical stimuli in their microenvironment [203]. Integrins α1β1, α2β1, α10β1 and α11β1, are known to bind monomeric or fibrillar collagens directly, however it is not yet known whether these integrins are essential for collagen fibrillogenesis.

1.10.4 Regulatory collagen family members

There are a number of collagen family members that function in a regulatory capacity within the ECM, which not only control the initiation of collagen fibrillogenesis, but also have roles in regulating ECM organisation [204]. Collagens V and XI are fibril-forming collagens and known initiators/nucleators of collagen fibril formation, where mice in which these collagen types have been depleted display defects in the organisation of collagen fibrils, highlighting the importance of proper initiation of fibrillogenesis in guiding the overall architecture of ECM within a tissue [205] [206] [207]. Collagen V is ubiquitously expressed and, despite being a minor fibril-forming collagen present in small amounts in tissue relative to collagen I, is thought to play an important role in the initiation of collagen I fibrillogenesis [208]. Heterozygous *COL5A1* knockout mice are viable, but have significantly fewer collagen fibrils, and mice that completely lack *COL5A1* are embryonic lethal and are incapable of generating collagen fibrils [205].

The role of collagen XI in the initiation of collagen fibrillogenesis is believed to be of particular importance in cartilage, where it is associated with, and regulates the formation of, collagen II-containing fibrils. Mice completely lacking *COL11A1* have severe cartilage defects with collagen fibrils virtually absent [206] [207]. However, during development, collagen XI expression has been shown to be more ubiquitous, and is also found within tissues that primarily contain collagen I, such as tendons. Mice that lack *COL11A1* in the tendon display defects in fibrillar collagen organisation, where collagen fibrils with a smaller diameter were observed, and this regulation of collagen fibrillogenesis by collagen XI was found to occur during development [209]. Furthermore, collagens XI and V have been shown to coordinate in the regulation of collagen fibril formation in the tendon during development [96].

These nucleators of collagen fibrillogenesis are thought to allow cell types that assemble ECM within tissues, such as fibroblasts, to assemble collagen fibres of specific diameters, allowing for the needs of a given tissue to be met. For example, as mentioned previously, tendon ECM must be able to provide high mechanical strength, and the relatively small amounts of collagen V present likely ensure that fibrils with a large diameter are assembled [204]. In contrast, in the cornea, collagen V levels are higher, ensuring smaller diameter fibrils are assembled which allow for transparency [210].

1.10.5 Fibronectin fibrillogenesis

Fibronectin is a glycoprotein, secreted as a compact, soluble dimer, that becomes bound by integrins including α5β1 and αvβ3 [211] [212]. These integrins bind to specific domains within fibronectin, including its Arg-Gly-Asp (RGD) motif, which induces integrin clustering and focal contact formation [213] [214]. Clustering strengthens the binding of integrins to fibronectin, and actin cytoskeleton-mediated cell contraction facilitates a conformational unfolding of fibronectin dimers such that cryptic fibronectin binding sites are revealed, allowing its polymerisation into fibrils, highlighting the importance of cell contractility in ECM assembly *in vivo* [215] [213] [214] [216] [217] [218].

As well as possessing domains that allow for binding to integrins, fibronectin has a number of modules that enable interactions with other ECM proteins, including collagen, and these interactions are known to be essential for the assembly of complex matrices [219]. For example, fibronectin is known to have multiple collagen I binding domains, and the binding of collagen I to pre-existing fibronectin fibrils is thought to be required for its assembly [220] [216] [221] [222] [223] [224]. However, whilst multiple groups have highlighted a role for fibronectin in collagen I fibrillogenesis, in that collagen I fibrils cannot assemble *in vivo* in its absence, there is also evidence suggesting that fibronectin fibrillogenesis itself can be regulated by collagen I binding [225] [226] [227]. This highlights a more reciprocal relationship between how the assembly of these matrices is regulated. In addition to binding collagen, fibronectin also interacts with and has a role in the assembly of other ECM components, such as the glycoproteins fibrinogen, fibrillin and thrombospondin-1, as well as the proteoglycans versican, perlecan and decorin [228] [229]. These interactions are thought to be important for incorporating other ECM components into the ECM such that it can mature to form a complex matrix [230].

1.11 Endocytic recycling

1.11.1 Overview

A somewhat underappreciated intracellular process with a role in the assembly of ECM is endocytic recycling. This branch of the endosomal membrane trafficking pathway allows cells to return endocytosed cargo, such as integral membrane proteins, and lipids, back to the plasma membrane. Together with the secretory pathway, endocytic recycling offers a means to control how a cell communicates with its environment through regulating integral membrane protein and lipid abundance and organisation at the cell surface [231] [232].

1.11.2 Endocytosis mechanisms

Integral membrane proteins and other cargoes, including receptor bound ligands, can be internalised via a number of mechanisms that can be classified based on their dependence on the clathrin coat protein [233] [234]. Clathrin-mediated endocytosis involves the recruitment of clathrin from the cytosol to the plasma membrane, along with over 50 other proteins that coordinate to drive membrane invagination followed by membrane scission to release a clathrin-coated vesicle into the cytosol. Firstly, a clathrin coat is formed, which together with clathrin consists of adaptor proteins such as the AP2 heterotetramer, as well as a number of other scaffolding proteins [235]. An actin module then assembles at the site of endocytosis which contributes towards membrane bending. This module is made of up of actin filaments, the assembly of which is regulated by the actin-related protein 2/3 (Arp2/3) complex, as well as regulatory components including members of the Wiskott-Aldrich syndrome protein (WASP) family, dynamin, and myosin motor proteins [236] [237] [238]. Constriction of the neck at the invagination is then driven by dynamin, which interacts with, and is thought to be regulated by, Bin-amphiphysin-Rvs (BAR) domain containing proteins. However, the exact role of BAR domain proteins in dynamin regulation is not fully understood, with studies suggesting both stimulatory and inhibitory effects on dynamin function [239] [240]. Uncoating of the vesicle then releases clathrin, and the other proteins involved in clathrin-mediated endocytosis, back into the cytosolic pool for reuse, and allows the vesicle to participate in membrane trafficking towards, and fusion with, the early endosome (EE) compartment [233].

The importance of clathrin-mediated endocytosis in allowing a cell to internalise macromolecules in a specific manner is well established, however there is an increasing number of proteins that are internalised by endocytosis mechanisms that do not require clathrin [233]. For example, cells can use caveolae-mediated endocytosis for macromolecule internalisation, where caveolae are flask-shaped, lipid-rich membrane invaginations with a variety of functions including fatty acid uptake and cell signalling [241] [242]. The formation of caveolae requires the integral membrane protein caveolin-1, the cavin coat proteins, the BAR domain containing Pacsin2, and the EH-domain containing 2 (EHD2) ATPase [243]. In order for these membrane invaginations to detach from the plasma membrane, dynamin is thought to be required. However it is not yet clear whether dynamin acts alone in this role, whether other proteins such as intersectin are also required, or whether detachment can occur independent of dynamin [244] [245] [246]. Following, detachment, caveolae can then be trafficked towards the EE.

Endocytosis can also occur via mechanisms that require neither clathrin nor dynamin, such as the clathrin-independent carrier (CLIC) GPI-anchored protein-enriched early endosomal compartment (GEEC) pathway [247]. This pathway is regulated by several proteins including Arp2/3, as well as the Cdc42 and Arf1 small guanosine triphosphatases (GTPases). Endocytosis via this mechanism occurs without the formation of a coat, where tubulovesicular carriers extend directly from the cell surface and are thought to then fuse with, or to mature into, GEECs [247] [248] [249] [250]. An alternative clathrin and dynamin independent mechanism of endocytosis is macropinocytosis [247]. This process enables large amounts of fluid and macromolecules in the extracellular space to be internalised, where ruffling of the actin cortex generates plasma membrane extensions that allow macropinosomes to form [251]. This endocytic mechanism can occur constitutively, as in the case of a number of immune cell types such as macrophages and dendritic cells, or alternatively it can occur in a signal dependant manner [247]. The formation of macropinosomes by membrane ruffling is regulated by Rac1 and Ras GTPases, as well as by phosphoinositide signalling [252]. Although this mechanism of endocytosis was initially believed to be non-specific, there is evidence to suggest that, in some cases, membrane proteins may be sorted at the site of macropinosome formation. This then allows for the specific internalisation of membrane proteins, and presumably also any cargoes to which they are bound, via this mechanism [253] [254].

1.11.3 Cargo sorting for degradation

Following endocytosis by these mechanisms, internalised cargoes are trafficked to the EE, characterised by the presence of the small GTPase Rab5 on its surface, where cargoes are sorted either for degradation, or for recycling back to the plasma membrane [255]. Internalised cargoes that are to be degraded are sorted into intraluminal vesicles (ILVs) during EE-late endosome (LE) maturation, with this maturation being characterised by a switch from Rab5 to Rab7 on the compartments cytoplasmic surface, and resulting in the formation of a multivesicular body (MVB) [255] [256] [257]. Lysosome-MVB fusion then takes place, where lysosomal hydrolases act to degrade the internalised cargoes present in the lumen of the ILVs [258](Figure 1.3). Importantly, in certain cell types including cancer cells, MVBs can avoid degradation and fuse with the plasma membrane, releasing their contents into the extracellular space as exosomes which act in cell-cell communication [259].

1.11.4 Cargo sorting for recycling

Instead of being sorted for degradation, internalised cargoes at the EE can be sorted for recycling where they are first retrieved from the degradative fate and then trafficked back to the plasma membrane [260]. Cargo retrieval occurs via the generation of tubular retrieval subdomains, that extend from the EE membrane into the cytosol [260] [261]. The membrane remodelling required for the formation of these tubular extensions is driven by Arp2/3 complex mediated-actin polymerisation, with this complex itself being regulated by the Wiskott-Aldrich syndrome protein and scar homolog (WASH) complex [262]. These tubules are then stabilised by BAR domain containing proteins, which sense, and also possibly generate, membrane curvature [263]. Cargo sorting into these tubules primarily occurs in a sequence-dependant manner, where proteins to be recycled possess specific motifs that are recognised by components of the retromer or retriever protein complexes [264] [265]. The recycling of cargoes sorted into tubules back to the plasma membrane can occur via a fast, direct route, or a slow, indirect route [266](Figure 1.3). Cargoes to be recycled via the slow pathway are first trafficked to the endocytic recycling compartment (ERC), which is a distinct population of vesicular and tubular endosomal membranes often located within the cells perinuclear region, that are thought to be derived from EE membrane tabulation events that take place during maturation [267] [268].

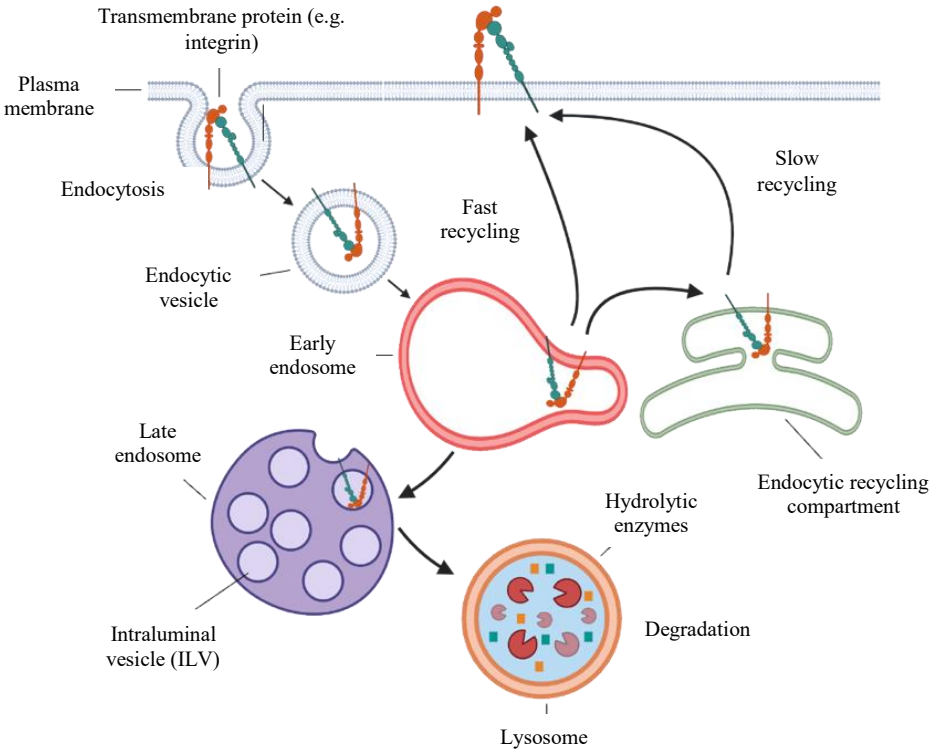

Figure 1.3 – Endocytic recycling pathways return endocytosed cargo back to the plasma membrane

Following endocytosis, internalised cargo is trafficked to the EE for sorting. Cargo can be sorted for degradation, where it is retained within the EE as it matures to form a LE. During maturation, cargo to be degraded is sorted into ILVs, followed by LE-lysosome fusion which allows for cargo degradation via the action of lysosomal hydrolases. Alternatively, endocytosed cargo can be sorted into tubular subdomains of the EE for recycling back to the plasma membrane. Recycling can occur via a fast, direct route, or via a slow, indirect route where cargo is first trafficked to the ERC.

1.11.5 Endocytic recycling regulators – Rab and Arf GTPases

Key regulators of all membrane trafficking events within the cell, including endocytic recycling, are a set of G proteins belonging to the Rab and Arf families of small GTPases, of which there are approximately 60 and 30 members respectively in mammals [269] [270] [271]. These GTPases operate as molecular switches, where they are converted to an active state by the binding of guanosine-triphosphate (GTP), followed by a conversion, via their intrinsic GTPase activity, to an inactive, guanosine-diphosphate (GDP) bound state [272]. Essential regulators of the conversion to the active GTP bound state, are the guanine nucleotide exchange factors (GEFs), which act to facilitate the otherwise slow release of bound GDP and subsequent binding of GTP. The conversion then back to the inactive GDP bound state is regulated by GTPase activating proteins (GAPs) which stimulate the intrinsic, but otherwise very slow, GTPase activity of the G protein [273]. In their GDP bound state, inactive small GTPases are bound by guanine dissociation inhibitors (GDIs), which act to sequester the G protein in the cytosol as a soluble complex through binding their membrane-interacting lipid moieties [274]. GTP binding to the nucleotide binding sites of Rab and Arf proteins triggers large scale, allosteric changes in their conformation, mediated by an interswitch region located between the switch I and switch II regions. These changes allow Rab and Arf proteins, that were previously inactive and sequestered in the cytosol, to firstly interact with membranes following the release of their associated GDI via the action of GDI-displacement factors (GDFs), and secondly to interact with their binding partner proteins, termed effectors [274] [275] [276](Figure 1.4). Within the Rab family of small GTPases, there are a number of subfamilies, where members of each subfamily share distinct sequence motifs [277]. Whilst the members of each subfamily often contribute towards regulating the same aspect of vesicle trafficking, differences can exist between them in terms of their tissue expression, intracellular localisation, and vesicle trafficking dynamics [278, 279]. For example, Rab11a, Rab11b, and Rab25 (11c) are members of the Rab11a subfamily, and function to recycle transmembrane receptor and adhesion complex proteins back to the plasma membrane following internalisation via the ERC. However whereas Rab11a and Rab11b are ubiquitously expressed across tissues, Rab25 is expressed primarily in epithelial cells where it regulates the recycling of cargoes specifically from the apical recycling endosome back to the cell surface [280] [278].

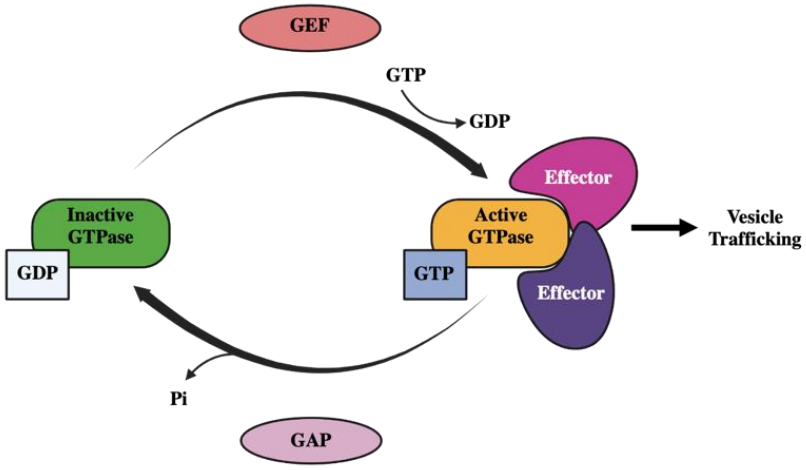

Figure 1.4 – The small GTPase cycle

Rab and Arf small GTPases cycle between an active GTP-bound state, and an inactive GDP-bound state. GEFs facilitate the release of GDP, allowing for GTP binding and conversion to the active state. Once GTP-bound, the active GTPase is capable of membrane association and binding to effector proteins, such that its various roles in regulating membrane trafficking can be carried out. GAPs then stimulate the otherwise slow hydrolysis of GTP to form GDP, rendering the small GTPase in an inactive state.

Specific members of the Rab and Arf families of GTPases have been implicated in the regulation of the fast recycling pathway, such as Rab4 and Rab35, and the slow recycling pathway, such as Rab8, Rab11 and Arf6 [281] [282] [283]. A level of coordination is to be expected between GTPases operating within the same recycling pathway, particularly in the case of the slow recycling pathway that first requires cargo trafficking from the EE to the ERC, followed by transport from the ERC to the plasma membrane. For example, Rab8 and Rab11, which are known to coordinate in the recycling of the transferrin receptor and also during primary ciliogenesis, are thought to regulate EE-ERC trafficking, and ERC-plasma membrane trafficking, respectively [284] [285]. Furthermore, regulators of different recycling pathways can also act in a coordinated manner to control the recycling of specific cargoes. For example, Rab4 and Rab11 have been shown to work in conjunction to mediate the recycling of the angiotensin II type I receptor [286]. The GTPases involved in endocytic recycling can also have roles in other membrane trafficking routes. For example, whilst Rab11 predominantly localises to the ERC, it has also been shown to localise to the TGN, where it acts to regulate transport of cargoes from the TGN to the ERC and the plasma membrane [287] [288].

1.11.6 Rab and Arf effector proteins

Effectors are a diverse set of proteins that allow Rab and Arf GTPases to regulate a variety of processes required for membrane trafficking to occur, including those involved in vesicle budding from donor compartments, vesicle trafficking towards target compartments, membrane tethering, and finally fusion of those trafficked vesicles with target compartment membranes [289]. A large number of effector proteins have been identified for Rab and Arf GTPases, using techniques including genetic screens, affinity chromatography, and proximity labelling techniques, such as BioID [290] [291]. Whilst it was assumed that each effector would bind a specific Rab or Arf protein, there is now evidence to suggest that a single effector can interact with a number of small GTPases, both individually and also simultaneously through multivalent interactions. For example, the MICAL family of Rab effectors have multiple binding sites for different Rab GTPases located within a single interaction domain [292] [293].

In cargo sorting and the formation of vesicles at donor compartments, examples of effectors that have been identified as being of importance include the AP-1 clathrin adaptor, and tail-interacting protein of 47 kD (TIP47) [294] [295]. AP-1 is a Rab4b effector, and their interaction is involved in cargo sorting, such as that of the transferrin receptor, at the early endosome. TIP47 is a Rab9 effector protein, with a role in vesicle budding for the recycling of cargoes including the mannose-6-phosphate receptor (M6PR) from the EE and LE to the TGN [295] [296].

A number of effectors have been implicated in the regulation of vesicle motility during their trafficking from donor to target compartments, including motor proteins which interact directly with Rab and Arf GTPases, as well as effectors which act as adaptors enabling indirect GTPase-motor protein interactions [297]. For example, Rab11 family-interacting protein 5 (Rab11-FIP5) is a Rab11 effector important in the regulation of the slow recycling pathway via its interaction with the kinesin II motor protein [298]. In addition, JNK-interacting protein (JIP) 3 and 4 are Arf6 effectors, which recruit both dynein and kinesin motor proteins to endosomal membranes for the recycling of MT1-MMP [299].

The final steps on the vesicle trafficking pathway involve tethering of the vesicle to the target compartment upon arrival, followed by membrane fusion. Factors required for membrane tethering are also GTPase effector proteins, and classically, have been grouped into those that consist of coiled coils, and those which are complexes made up of several proteins [300]. For example, the exocyst complex is a multiprotein assembly consisting of 8 subunits that functions in vesicle tethering to the plasma membrane, and an effector for GTPases including Rab8, Rab11 and Arf6 [301] [302] [303]. A number of additional GTPase effector membrane tethering complexes have also been identified, including factors for endosome recycling and Rab interactions (FERARI), homotypic fusion and vacuole protein sorting (HOPS), class C core vacuole/endosome tethering (CORVET), and class C homologs in endosome–vesicle interaction (CHEVI) [304] [305]. Furthermore, it has become apparent that Rab GTPases can function more directly as membrane tethers [306]. For example, Rab11a can interact with one of its effectors, class V myosin, to regulate membrane tethering, and Rab11-FIP2 has been highlighted as an additional Rab11a effector that enables myosin motors to interact with vesicles for tethering [307] [308]. Finally, following tethering, membrane fusion is driven by the SNARE protein family of GTPase effector proteins [309] [310].

1.11.7 Endocytic recycling of ECM receptors

As discussed previously, the interactions that occur between cells and the ECM, mediated by receptors at the cell surface, are essential in the regulation of many cellular processes, including growth, survival, proliferation, and migration [175] [311]. Together with lysosomal degradation, endocytic recycling plays a crucial role in regulating ECM receptor function through controlling their availability at the plasma membrane, as well as signalling. Membrane trafficking pathways therefore determine how cells respond to changes in ECM composition and organisation such that they can act accordingly [312]. Rab and Arf GTPases are known to regulate the recycling of a variety of ECM receptors, such as integrins [280] [313]. For example, a role for Rab25 in controlling α5β1 integrin recycling to stimulate cell migration has been demonstrated [280]. Furthermore, Arf6 has been shown to also recycle β1 integrin such that cell migration can occur, and Rab35 has been highlighted as a suppressor of Arf6-mediated β1 recycling to limit migration through enhancing cell adhesion [314].

1.12 Endocytic recycling in ECM assembly

1.12.1 Recycling regulator GTPases in ECM assembly

A number of small GTPases that regulate endocytic recycling have been implicated in various processes linked with ECM assembly and remodelling. Rab10, which is thought to regulate cargo transport through the EE, and from the Golgi apparatus to the plasma membrane, has been shown to be involved in protein secretion to form the basement membrane [315] [316] [317] [318] [319]. Rab4a has been shown to play a role in fibronectin fibrillogenesis by endothelial cells during branching of the vasculature [320]. Another small GTPase that also has an involvement in the process of vascular morphogenesis is Rab11b, which has been shown to regulate fibronectin fibrillogenesis by endothelial cells through its recycling of α5β1 integrin, which is presumably active and bound to cleaved fibronectin. This recycling is thought to coordinate the trafficking of active α5β1 integrin with that of newly synthesised fibronectin, possibly enabling fibronectin secretion to occur at sites where α5β1 integrin is present, and in a state capable of fibronectin binding for the initiation of fibril assembly [321]. However, it is not clear whether the recycling of fibronectin itself is required for fibril assembly, or whether the recycling of the active integrin, coordinated with the trafficking of newly synthesised fibronectin, is sufficient for this process.

1.12.2 Small GTPases in regulating MMP recycling

As well as α5β1 integrin, other cargoes that are recycled in a small GTPase-regulated manner have also been shown to function in ECM assembly and remodelling. MT1-MMP (MMP14) is a membrane anchored MMP, with an established role in ECM remodelling through protein degradation, and is known to be required for the migration and invasion of a variety of cell types through 3D matrices [322]. This MMP is known to be recycled in a Rab and Arf GTPase dependant manner, with Rab8a, Rab14, Rab22a, and Arf6, all playing a role in controlling this recycling [323] [299]. Furthermore, MT1-MMP has been implicated in ECM assembly during the tissue expansion required for tendon development in mice. Cleavage of macromolecules, in particular fibronectin, at fibripositor sites by MT1-MMP was shown to be important for releasing collagen I fibrils from these sites such that they can be assembled into fibres. Fibronectin in this context is thought to act as a bridge between the cell and the collagen fibril on its surface, further emphasising the importance of fibronectin in collagen I assembly [324].

1.12.3 Collagen I recycling in fibrillogenesis

Whilst a number of recycled cargoes, such as integrins and MMPs, have been implicated in fibronectin and collagen I fibrillogenesis, the question of whether or not the recycling of ECM proteins themselves is important for these assembly processes remains unanswered. A recent study highlighting the importance of ECM protein recycling in ECM assembly, demonstrated the involvement of collagen I recycling in its fibrillogenesis by mouse tendon fibroblasts. This recycling process was found to be regulated by a subunit of the CHEVI membrane tethering complex, VPS33B, and is thought to allow fibroblasts to gain spatial control over where the initiation of fibripositor formation occurs at the cell surface [305]. Collagen I fibrillogenesis was shown to require firstly the secretion of soluble collagen I monomers into the extracellular space, followed by the subsequent internalisation and recycling of these monomers to specific sites within the membrane for fibripositor formation [325]. It may be that the collagen presented at the cell surface after internalisation and recycling is sufficient for collagen I assembly via this mechanism. However, the assembly of collagen I fibrils in this fashion likely also involves incorporating additional collagen I monomers that have already been secreted into fibrils.

1.13 Project aims and objectives

Minimal progress has been made in improving HGSOC treatment over the last 30 years. In order to develop more effective treatment strategies, it is essential that new targets are identified for therapeutic intervention. HGSOC metastasis to the omentum correlates with poor prognosis and overall survival, and is considered to be largely responsible for the high mortality rate associated with this disease. The specific conditions within the omental TME act to support colonisation of the omentum by HGSOC cells and subsequent secondary tumour formation. One aspect of this TME that contributes towards supporting multiple aspects of tumour development, including malignant cell growth, proliferation and invasion, is the formation of a dense, fibrillar ECM. Given that the non-malignant cells within the TME are far more genetically stable than HGSOC cells, targeting these cells to indirectly hinder tumour development has considerable potential in the treatment of HGSOC.

In the case of most forms of cancer, CAFs in the TME are considered as the primary cell type responsible for ECM protein synthesis and assembly such that complex 3D networks can be generated. However, the molecular mechanisms involved in the assembly of this type of ECM by CAFs in the omentum remain poorly understood. It is clear that endocytic recycling pathways and the small GTPases involved in their regulation play a crucial role in controlling the processes that guide the generation of complex 3D matrices *in vivo*. In ECM assembly and remodelling, the importance of cargoes, such as integrins, MMPs and ECM proteins in particular, undergoing recycling back to the plasma membrane after internalisation has been demonstrated in a number of contexts both *in vitro* and *in vivo*. However, it is not yet known whether Rab and Arf GTPase regulated-endocytic recycling pathways are required for ECM assembly by the CAFs present in the HGSOC omental metastatic niche. Further investigation into this area, with a particular focus on the identification of small GTPases and associated cargoes that are critical for ECM assembly in this context, could reveal novel targets for therapeutic intervention, where inhibiting their activity may prevent, or at least minimise, HGSOC metastasis to the omentum.

The overall aim of this research project was to identify novel regulators of endocytic recycling required for the assembly of ECM proteins by CAFs in the HGSOC metastatic niche, and to understand their role in controlling the molecular mechanisms involved in ECM assembly.

The primary objectives of this project were as follows:

- Characterise CAFs isolated from HGSOC patient omentum samples in terms of their expression of CAF biomarkers, their ability to assemble ECM proteins of interest, and their capacity for stimulating HGSOC cell invasion in 3D.
- Identify regulators of endocytic recycling required for primary CAFs to assemble ECM proteins and to support HGSOC cell invasion using an siRNA screening approach.
- Investigate the molecular mechanisms involved in the control of ECM assembly by endocytic recycling regulators in CAFs.
- Identify additional ECM proteins that may be of importance in the HGSOC metastatic TME.

Chapter 2: Materials and Methods

2.1 Omentum sample collection and cell culture

Primary fibroblasts were derived from omentum samples obtained from HGSOC patients undergoing cytoreductive debulking surgery at either Saint Mary's hospital, Manchester, or the Christie hospital, Manchester. The removed omentum samples were then processed, either with collagenase and dispase treatment, or using a gentleMACS™ (Miltenyi Biotec, 130-093-235) tissue dissociator according to the manufacturers protocol, to release primary cells as single-cell suspensions for culture. Fibroblasts were isolated from three different types of omentum samples. CAFs and uninvolved fibroblasts were isolated from HGSOC tumour burdened omentum. CAFs were derived from the area of these samples occupied by the tumour and its immediate microenvironment, whereas uninvolved fibroblasts were derived from areas of omentum that were located away from the tumour and that lacked any signs of macroscopic disease. Normal fibroblasts were derived from patients that did not have HGSOC, and instead often had another form of cancer such as early-stage endometrial cancer. All fibroblasts were grown under normoxic conditions, at 37°C with 5% CO_2, in Dulbecco's Modified Eagle Medium (DMEM) – high glucose (Sigma-Aldrich, D6171) containing L-glutamine, with 10% fetal bovine serum (FBS) 1% antibiotic-antimycotic (AA) solution (Sigma-Aldrich, A5955) added (hereafter referred to as complete DMEM). Culture under normoxic conditions likely prohibited cancer cell growth, where growth under hypoxic conditions is favoured. However, to ensure fibroblast monocultures were obtained, cancer cells and other stromal cells, such as mesothelial cells, were removed by subjecting co-cultures to differential trypsinisation [326]. Fibroblast were maintained in culture for no longer than 8 passages, as after this time they are known to become senescent and to lose their CAF-like properties. The primary human dermal fibroblasts (ATCC, PCS-201-012) and the HEK293T cell line were also cultured at 37°C with 5% CO_2 in complete DMEM. The Kuramochi HGSOC cell line was cultured at 37°C with 5% CO_2 in RPMI-1640 medium (Sigma-Aldrich, R8758) containing L-glutamine, with 10% FBS and 1% AA solution added (hereafter referred to as complete RPMI medium).

2.2 Statistical analysis and graph presentation

All statistical analyses were carried out using Graphpad Prism 8 software. All data were tested for normality using the Shapiro-Wilk test. If normally distributed, data were analysed using an unpaired t test (if two groups were to be compared), or a one-way ANOVA with Tukey's multiple comparisons test (if more than two groups were to be compared). All statistically significant results are indicated in the figures. For exogenous fibronectin assembly assays, a two-way ANOVA with Šidák multiple comparisons test was used. Pearson's correlation analysis was used to measure the strength of the relationship between the capacity of CAFs to promote Kuramochi invasion and their contractility. All graph figures were generated using Graphpad Prism 8 software.

2.3 CAF biomarker and ECM protein immunofluorescence staining, microscopy, and analysis

For immunofluorescence, cells were seeded on to ethanol sterilised coverslips, which had been pre-coated with 0.1% gelatin (Sigma-Aldrich, G1393) diluted in PBS by incubation at 37°C with 5% CO_2 for 30 minutes. For staining CAF biomarkers, cells were seeded at a density of 40,000 cells per mL and grown in culture for 4 days. The medium was replaced every 2-3 days, and TGFβ3 was present at a concentration of 10 $ng.mL^{-1}$ in experiments where stated in the figure legend. For the staining of ECM proteins, cells were seeded at a density of 15,000 cells per mL and grown in culture for 10 days, with the medium replaced every 2-3 days. For these experiments, in some cases the medium contained TGFβ3 (10 $ng.mL^{-1}$) and/or ascorbic acid at a concentration of 20 $\mu g\ mL^{-1}$ where stated in the figure legend.

Antibody staining for immunofluorescence microscopy was carried out at room temperature, where cells in culture were firstly washed in phosphate buffered saline (PBS; Sigma-Aldrich, D8537), then fixed in 4% paraformaldehyde (PFA) for 20 minutes. For staining of intracellular proteins, cells were permeabilised at room temperature using 0.2% triton™ X-100 (Sigma, X100) for 5 minutes, whereas for staining extracellular proteins, cells were not permeabilised. Prior to the addition of primary antibodies, cells were treated with 1% bovine serum albumin (BSA) for 1 hour at room temperature to block non-specific antibody binding sites. Primary antibodies (Table 2.1) were added for 1 hour, followed by washing in PBS to remove any unbound antibody. Secondary antibodies (Table 2.2) were added, along with Hoechst 33342 (Invitrogen, H3570) if

nuclear staining was also required, for 1 hour whilst covered. Cells were then washed in PBS to remove any unbound secondary antibody, and in double-distilled water (ddH_2O) to remove the salts from the PBS. If coverslips were used for staining, these were dried briefly, mounted on to glass slides using ProLong™ Gold antifade mountant (Invitrogen, P36980), and left to dry for at least 24 hours. If cells were stained without coverslips, 2.5% Dabco® 33-LV antifade solution diluted in PBS was added.

Antigen	Supplier	Catalogue number	Species and type	Dilution
Alpha smooth muscle actin (αSMA)	Sigma-Aldrich	A2547	Mouse monoclonal	1:100
Fibroblast activation protein (FAP)	Abcam	Ab53066	Rabbit polyclonal	1:100
Collagen XI (Intracellular)	Atlas	HPA058335	Rabbit polyclonal	1:100
Collagen I	Gentaur	OARA02579	Rabbit polyclonal	1:500
Fibronectin	Abcam	Ab6328	Mouse monoclonal	1:100
Collagen XI (Extracellular) (Discontinued)	Atlas	HPA052246	Rabbit polyclonal	1:100
Versican	Developmental Studies Hybridoma Bank	12C5	Mouse monoclonal	1:100

Table 2.1 – Primary antibodies used for immunofluorescence

Antigen	Fluorophore	Supplier	Catalogue number	Species and type	Dilution
Rabbit IgG (H+L)	Alexa Fluor™ 488	ThermoFisher	A11008	Goat polyclonal	1:250
Mouse IgG (H+L)	Alexa Fluor™ 488	ThermoFisher	A32723	Goat polyclonal	1:250
Rabbit IgG (H+L)	Alexa Fluor™ 594	ThermoFisher	A32740	Goat polyclonal	1:250
Mouse IgG (H+L)	Alexa Fluor™ 594	ThermoFisher	A32742	Goat polyclonal	1:250
Rabbit IgG (H+L)	Alexa Fluor™ 647	ThermoFisher	A32733	Goat polyclonal	1:250
Mouse IgG (H+L)	Alexa Fluor™ 647	ThermoFisher	A32728	Goat polyclonal	1:250

Table 2.2 – Secondary antibodies used for immunofluorescence

Cells stained for immunofluorescence microscopy were imaged using either a Zeiss 3i spinning disk confocal microscope, or a Leica SP8 inverted confocal microscope. For spinning disk confocal microscopy, images were acquired using a 3i spinning disk confocal (CSU-X1, Yokagowa) and a Zeiss Z1 Axio-Observer microscope with a 63x/1.40 Plan-Apochromat oil objective. Images were captured with an Evolve ECMCCD camera and Slidebook 6.0 software (3i). All other immunofluorescent staining images were acquired using a Leica SP8 inverted confocal microscope with a 63x/1.40 HC PL APO oil objective and captured using Las X software (Leica). ImageJ was used for all image processing and analysis.

To analyse CAF biomarker expression by immunofluorescence, ImageJ was used to count the number of cells expressing each biomarker over an intensity threshold. For SMA and collagen XI, heterogeneity was clearly visible in their expression levels. Higher threshold values were therefore used for their analysis to ensure only those cells with high levels of expression were counted. For FAP, expression was homogeneous, and a lower threshold value was used.

To analyse ECM protein assembly, two separate methods of analysis were used. Firstly, the fibre area was calculated by thresholding images to remove background staining and measuring the total area, the mean intensity, the minimum intensity, and the maximum intensity for each image. The fibre area was then calculated using the formula (mean intensity/total area)*maximum area. This number was then normalised to the number of cells in each image. To account for differences in staining between biological repeats, these values were normalised within each repeat by dividing the fibre area per cell for each image by the average fibre area per cell for the MOC195CAF untreated condition, or the NS siRNA transfected condition. Secondly, the large fibre index for each image was determined using the ridge detection algorithm within ImageJ, which is an extension of the ridge detection algorithm presented by Steger [327]. We define the fibre index as the area of fibres detected over a given width and length by the algorithm. For these images, a minimum line width of 10 pixels, and a minimum line length of 70 pixels, was used to detect larger fibres only, along with a number of other set parameters that remained constant between all experiments analysed with this algorithm (high contrast = 100, low contrast = 30, sigma = 3.39, lower threshold = 0.17, upper threshold = 1.02). The area of fibres detected was then calculated using the formula (mean intensity/total area)*maximum area, and normalised to cell number for each image to obtain the fibre index per cell. These values were normalised within each repeat as described previously.

2.4 Invasion assays – Spheroid hanging drops and top-down invasion

To study the capacity of primary fibroblasts to stimulate the invasion of Kuramochi cells, the assay predominantly used was the spheroid invasion assay. Spheroids consisted of Kuramochi cells expressing green fluorescent protein (GFP), either as a mono-culture, or as a co-culture with primary fibroblasts stained with the red membrane dye PKH26 (Sigma-Aldrich, PKH26GL) according to the manufacturers protocol. Where stated in the figure legend, fibroblasts were pre-treated with TGFβ3 (10 $ng.mL^{-1}$) for 4 days before mixing with Kuramochi cells. Each spheroid was formed by pipetting 6000 cells, suspended in a 20 µL mixture of RPMI medium with methylcellulose (methocel), on to the lid of a cell culture dish, which was then flipped and placed on a dish containing a small amount of PBS to prevent evaporation of the medium. Hanging drops were incubated overnight at 37°C with 5% CO_2. Spheroids were transferred into a cold, 200 µL collagen I hydrogel mixture, consisting of rat tail collagen I (3 $mg.mL^{-1}$; Corning, 10224442), NaOH (6.8 mM) to naturalise the acetic acid present in the collagen I solution,

2X PBS and FBS- and AA-free RMPI medium. The collagen I mixture containing the suspended spheroids was then transferred to the central well within a 35mm glass bottom imaging dish (Mattek, P35G-1.5-10-C) and left to polymerise for 10 minutes at room temperature, followed by 30 minutes at 37°C. Complete RPMI medium containing ascorbic acid (20 μg mL^{-1}) was added, and spheroids were incubated for 4 days at 37°C with 5% CO_2. Where stated in the figure legend, epidermal growth factor (EGF; 30 $ng.mL^{-1}$) and hepatocyte growth factor (HGF; 100 $ng.mL^{-1}$) were also added to the medium, as they had been used by other members of the lab to stimulate the otherwise relatively non-invasive Kuramochi cells to invade. In some cases, fibroblast conditioned media was added to the Kuramochi spheroids where stated in the figure legend. This was generated by culturing fibroblasts in complete RPMI medium with or without TGFβ3 (10 $ng.mL^{-1}$) added for a minimum of 4 days. Where stated in the figure legend, spheroids were generated as described previously consisting of CAFs as a monoculture, and were grown in culture for 4 days in complete DMEM containing ascorbic acid (20 μg mL^{-1}) before imaging.

Spheroids were imaged at days 0 and 4 using a Leica SP8 confocal microscope, as described previously, with a HC PL APO 10x/0.40 CS2 air objective. For each spheroid, approximately 10 Z-sections were captured to cover the spheroids entire volume, and maximum intensity projections were generated using ImageJ. Spheroid invasion data was analysed in ImageJ, where invading cell area was calculated as a percentage of the total area. To obtain invading cell area and total area, channels were split and the brightness for the channel of interest was adjusted for each image to ensure all invading cells were clearly visible. Images were then thresholded, and the area corresponding to the spheroids central portion was defined. This area was then filled to solve the issue of some images containing a relatively hollow spheroid centre after thresholding due to the top of the spheroid being out of range for the objective. If left unfilled, the hollow spheroid centre would reduce the total area measure and therefore increase the percentage of invading cells. After filling, the total area was measured, along with the area outside the spheroid centre. Invading cell percentages were then normalised within each repeat by dividing each value by the average invading cell area for the Kuramochi mono-culture condition.

The top-down invasion assay approach was also tested in parallel to spheroid invasion method. This involved allowing a collagen I hydrogel mixture, containing the same components as described previously, to polymerise within the wells of a clear bottom 96-well μ-plate (ibidi, 89626) for 10 minutes at room temperature, and 30 minutes at 37°C with 5% CO_2. Cells (50,000 per well), either as a Kuramochi monoculture or a Kuramochi-fibroblast co-culture, were then added on to the hydrogel, followed by the addition of complete RPMI medium containing ascorbic acid (20 μg mL^{-1}). Where stated in the figure legend, EGF and HGF were also added to the medium as described previously. Invasion at day 5 and day 12 was visualised by fluorescence microscopy using a Leica SP8 confocal microscope with a HC PL APO 10x/0.40 CS2 air objective. Las X software (Leica) was used to generate 3D reconstructions of the hydrogels, however this data was not analysed further due to the lack of invasion observed in all conditions.

2.5 Collagen gel contraction assays

Collagen gel contraction assays were carried out using a similar collagen I hydrogel mixture as described previously, although a lower collagen concentration of 2 $mg.mL^{-1}$ was used as this yielded the most reproducible results. Fibroblasts (30,000 per gel), which had been cultured in complete DMEM with or without TGFβ3 (10 $ng.mL^{-1}$) added for 4 days prior, were then mixed with the hydrogel, and transferred to a 35 mm dish where the gel was left to polymerise as described previously. Complete DMEM was added, and gels were incubated for up to 4 days at 37°C with 5% CO_2. Images of the gels at days 0, 1, and 2 were taken in all gel contraction experiments, however, where stated in the figure legend, images were also taken at days 3 and 4. Gel contraction was calculated by measuring gel area at each time point as a percentage of the gel area at day 0. Pearson's correlation analysis was carried out to determine the correlation between fibroblast contractility and their ability to facilitate Kuramochi invasion in the spheroid invasion assays.

2.6 Quantitative reverse transcription PCR (RT-qPCR)

Endocytic recycling regulator expression in primary fibroblasts was measured using RT-qPCR. Cells were grown in culture in complete DMEM for a minimum of 4 days, until a minimum area of 9.6 cm^2 was covered (1 well of a 6-well plate well). For RNA extraction, cells were trypsinised and centrifuged at 4000 rpm for 5 minutes, and an RNeasy kit (Qiagen, 74004) was used according to the manufacturers' protocol. To generate cDNA by reverse transcription, 1 µg of RNA was combined with a dNTP mix (1 mM; Invitroegn, 18427-103) and oligo(dT)23 primer (1 µM; Invitrogen, 58862), in a final volume of 10 µL. Following gentle mixing and a brief centrifugation, the reaction was incubated for 10 minutes at 70°C to allow for primer annealing, with the reaction then being placed on ice to cool. Reverse transcriptase (200 U; Promega, M170A), reverse transcriptase buffer (Promega, M531A), and RNase inhibitor (20 U; NEB, M0314S), were added to the reaction and the volume brought to 20 µL. Following a 10-minute incubation at room temperature to allow for primer elongation, the reaction was incubated at 37°C for 50 minutes. The reverse transcriptase was then denatured by heating to 90°C for 10 minutes, and the cDNA product was diluted by adding 100 µL. Each qPCR reaction was carried out by mixing cDNA (0.4 ng. μL^{-1}) with PowerUp™ SYBR™ Green Master Mix (Applied Biosystems, A25776) and forward and reverse qPCR primers (0.5 µM) for each target sequence. All forward and reverse primers used were predesigned and purchased from Sigma-Aldrich (Table 2.3). The qPCR reactions were carried out using an AriaMX RT-qPCR machine (Agilent Technologies, G8830A), where the cDNA was denatured by heating to 95°C for 2 minutes, following by 40 amplification cycles of 95°C for 15 seconds, primer and SYBR green probe binding at 55°C for 15 seconds, and primer extension for 1 minute at 72°C. Within each biological repeat, qPCR reactions were carried out in triplicate and the average cycle threshold (Ct) value was calculated. The ΔCt value was then calculated by subtracting the average Ct for the housekeeping gene, GAPDH, from the average Ct value for each recycling regulator target gene. The relative expression of each gene was then calculated, where relative expression = $2^{-\Delta Ct}$.

Target	Forward primer sequence (5'-3')	Reverse primer sequence (5'-3')
Rab25	AAAACAATGGACTGCTCTTC	GATTTCTTTCAGGACAGTCTC
Rab11a	ACATCAGCATATTATCGTGG	GACGTAGATCACTCTTATTGC
Rab11b	GAACAACTTGTCCTTCATCG	AGATCTCTGTGAGGATGTTC
Rab4a	ACTAGCACTAAGGATTCTGG	ACAATGTGTTTTCTAGCAGG
Rab4b	ACGACTTCCTCTTCAAATTC	TCTGTAGCGTCACAGTCTTC
Rab8a	GAGAGTGTAATATGGCGAAG	CCTATGGTGGAGATAAAAGTG
Rab8b	ATGAATGACAGCAATTCAGC	GAGTTCATCAAAGTAGCGAG
Rab10	ATCACAACCTCCTACTACAG	GCTCATCTATGTTTCTAAGCC
Rab13	AGAACTGGATGAAAAGCATC	CCACATTCATACTGGATTTAGC
Rab14	ATTTATGGCTGATTGTCCTC	CATAGACCATAAGAGCTCCC
Rab22a	AAAGAATTGGGTGAAAGAGC	AATTGCATGAATAGAGTCGG
Rab22b	TTTATGACCAAAACTGTGCC	AATGAATGAAACCGTTCCTG
Rab35	GTGGAAGAGATGTTCAAC	TTTCTTTCGTTTACTGTTCT
Arf6	CTTAATGAGCATTCTCCACC	TCAAAAGAAGAGAAAGTGGC
Rab5a	GGTTAAAGAACTTCAGAGGC	TTCCTGGAAATCTACTGCTC
Rab5b	ACGTATGGTGGAGTATGAAG	CAACTTCTTAGCTATTGCCAG
Rab5c	CATGGCAATAGCTAAGAAGC	CGATTGGTTAGAGTGGATTC
Rab21	AAGGATGATAGAAACAGCAC	CATCAATAATCTGTACACCTCG
GAPDH	CAATGACCCCTTCATTGACC	GACAAGCTTCCCGTTCTCAG

Table 2.3 – RT-qPCR primer sequences

2.7 Gene silencing for the endocytic recycling regulator screen

To determine which regulators of endocytic recycling were required for primary CAFs to facilitate the invasion of Kuramochi cells out of spheroids and to assemble ECM proteins of interest, an siRNA screen was used. The levels of each regulator protein were depleted using siRNA-mediated RNAi, and cells were used in spheroid invasion assays and ECM assembly assays. To ensure any positive results were not due to non-specific effects of an siRNA, and also not specific to primary fibroblasts derived from only one patient, all positive results observed following the use of one siRNA in CAFs derived from one patient were validated with a second siRNA in CAFs derived from a different patient.

In order to deplete the levels of each endocytic recycling regulator, the RNAi and the clustered regularly interspaced short palindromic repeats (CRISPR)-cas9 approaches were tested. CRISPR-cas9 technology was used in the form of the lentiCRISPRv2 vector system, which aimed to generate a number of CAF lines in which each recycling regulator had been knocked out through gene editing. To test the feasibility of this approach, 3 pairs of DNA oligos encoding a gRNA sequence targeting Rab11a were cloned separately into the lentiCRISPRv2 plasmid (Addgene, plasmid #52961) according to the protocol developed by the Zhang lab [328](Table 2.4). After plasmid preparation, the success of the cloning procedure was assessed by sequencing each plasmid prior to use.

Target	Forward oligo sequence (5'-3')	Reverse oligo sequence (5'-3')
Rab11a (Exon 2)	CACCGCATTTCGAGTAAATCGAGAC	AAACGTCTCGATTTACTCGAAATGC
Rab11a (Exon 3)	CACCGCATATGAAAATGTAGAGCGA	AAACTCGCTCTACATTTTCATATGC
Rab11a (Exon 3)	CACCGGAGTGATCTACGTCATCTCA	AAACTGAGATGACGTAGATCACTCC

Table 2.4 – gRNA encoding DNA sequences cloned into the lentiCRISPRv2 vector

The 3 lentiCRISPRv2 plasmids into which each pair of oligos had been cloned were then used to transfect HEK293T cells. This transfection was carried out by firstly diluting polyethylenimine (PEI; 108 µg.mL^{-1}) in Opti-MEM (ThermoFisher, 31985047) to a final volume of 250 µL. This was then combined with a 250 µL mixture of Opti-MEM consisting of all three different lentiCRISPRv2-Rab11a plasmids (5 µg total), and the pMDLg (Addgene, plasmid #12251), pVSV-G (Addgene, plasmid #138479) and pRSV-Rev (Addgene, plasmid #12253) plasmids (2.5 µg of each). Following a 20-minute incubation at room temperature, the PEI/plasmid mixture was added dropwise to cells in 5 mL Opti-MEM, cells were incubated at 37°C with 5% CO_2 for 6-8 hours, and the medium containing the transfection mixture was replaced with complete DMEM. Viral particle containing medium was then collected 72 hours post-transfection, centrifuged at 1000 rpm for 5 minutes, and filtered through a 0.45 µm pore size filter to remove cell debris. Polybrene (6µg.mL^{-1}) was used to enhance transduction efficiency, and was added both to the primary fibroblasts 2 hours prior to viral media addition, as well as to the viral media after filtration. The filtered viral media was then added to the fibroblasts for 24 hours, followed by replacement of this media with complete DMEM. After 2-3 days,

successfully transduced cells were selected for using puromycin (0.75 µg.mL^{-1}) (Gibco, P8833) treatment for 7-8 days. Importantly, it was decided that we would not subject primary fibroblasts to clonal expansion, and that we would proceed with a mixed population of cells. This was due to the slow growth rate of the primary fibroblasts likely preventing a single cell from generating a cell population of sufficient size for use in downstream experiments. The success of the Rab11a knockout was assessed using sodium dodecyl-sulfate polyacrylamide gel electrophoresis (SDS-PAGE) and western blotting, with samples collected at 1 day and 14 days after the puromycin had been removed from the culture medium.

The second approach used to deplete endocytic recycling regulator protein levels was RNAi mediated by siRNA. All siRNAs used were predesigned, Silencer™ Select siRNAs (ThermoFisher), and the knockdown efficiency of 2-3 siRNA oligos per target GTPase was tested (Table 2.5). To transfect primary fibroblasts, Lipofectamine™ 2000 Transfection Reagent (ThermoFisher, 11668019) was used primarily, however, where stated in the figure legend the Fuse-It-siRNA (Ibidi, 60510) transfection method was also tested according to the manufacturer's protocol. Each siRNA (80 nM total), either individually or in combination, was mixed with Opti-MEM, combined with Lipofectamine™ 2000 in Opti-MEM and incubated for 20 minutes at room temperature for 20 minutes. The siRNA-Lipofectamine™ 2000 mixture was diluted 1:1 by dropwise addition to primary fibroblasts in Opti-MEM, which were then incubated at 37°C with 5% CO_2 for 6-8 hours, after which time the transfection mixture was replaced with complete DMEM. The success of each knockdown was assessed either by western blotting for Rab11a (siRNA 1) and Rab11b (siRNA 1), with cell lysates collected day 5 and day 10 post-transfection, or by RT-qPCR due to the lack of antibody availability for the other endocytic recycling regulators targeted in the screen, with RNA isolated at day 2 and day 8 post-transfection.

Target	Catalogue number	Sense sequence	Anti-sense sequence
Non-silencing control	4390843	Undisclosed	Undisclosed
Rab11a 1	4390824 ID number S16702	CAACAAUGUGGUUCCUAUUtt	AAUAGGAACCACAUUGUUGct
Rab11a 2	4390824 ID number S16703	GAGAUUUACCGCAUUGUUUtt	AAACAAUGCGGUAAAUCUCtg
Rab11b 1	4390824 ID number S17648	GCAUUCAAGAACAUCCUCAtt	UGAGGAUGUUCUUGAAUGCtt
Rab11b 2	4390824 ID number S17647	CUAACGUAGAGGAAGCAUUtt	AAUGCUUCCUCUACGUUAGtg
Rab4a 1	4390824 ID number S11675	GGUCCGUGACGAGAAGUUAtt	UAACUUCUCGUCACGGACCtg
Rab4a 2	4390824 ID number S11676	GAACGAUUCAGGUCCGUGAtt	UCACGGACCUGAAUCGUUCtt
Rab4b 1	4390824 ID number S28800	GGAAGACUGUGAAGCUACAtt	UGUAGCUUCACAGUCUUCCca
Rab4b 2	4390824 ID number S28802	GCACUAUCCUCAACAAGAUtt	AUCUUGUUGAGGAUAGUGCgg
Rab5a 1	4390824 ID number S11678	GGAAGAGGAGUAGACCUUAtt	UAAGGUCUACUCCUCUUCCtc
Rab5a 2	4390824 ID number S11679	CAAGCCUAGUGCUUCGUUUtt	AAACGAAGCACUAGGCUUGat
Rab5b 1	4392420 ID number S11683	GGUAUUACGUUUUGUCAAAtt	UUUGACAAAACGUAAUACCag
Rab5b 2	4392420 ID number S11682	GGAGCGAUAUCACAGCUUAtt	UAAGCUGUGAUAUCGCUCCtg
Rab5b 3	4392420 ID Number S11681	CGACAUUACUAAUCAGGAAtt	UUCCUGAUUAGUAAUGUCGta
Rab5c 1	4390824 ID Number S11708	GGACAGGAGCGGUAUCACAtt	UGUGAUACCGCUCCUGUCCag
Rab 5c 2	4390824 ID Number S11710	GCAAUGAACGUGAACGAAAtt	UUUCGUUCACGUUCAUUGCag
Rab8a 1	4390824 ID number S8679	GCAAGAGAAUUAAACUGCAtt	UGCAGUUUAAUUCUCUUGCca
Rab8a 2	4390824 ID number S8680	GAGUCAAAAUCACACCGGAtt	UCCGGUGUGAUUUUGACACcc
Rab8b 1	4392420 ID number S28633	GAAAGAUUCCGAACAAUCAtt	UGAUUGUUCGGAAUCUUUCct
Rab8b 2	4392420	CGAUAGAACUAGAUGGAAAtt	UUUCCAUCUAGUUCUAUCGtt

	ID number S28634		
Rab8b 3	4392420 ID number S28635	GAAUGAUCCUGGGUAACAAtt	UUGUUACCCAGGAUCAUUCtt
Rab10 1	4392420 ID number S21390	GGACGACAAAAGAGUUGUAtt	UACAACUCUUUUGUCGUCCat
Rab10 2	4392420 ID number S21391	GGAUGAUGCCUUCAAUACUtt	AGUAUUGAAGGCAUCAUCCga
Rab10 3	4392420 ID number S21392	CCAAUAGACUUCAAGAUCAtt	UGAUCUUGAAGUCUAUUCCta
Rab13 1	4392420 ID number S11690	GAGCGGUUCAAGACAAUAAtt	UUAUUGUCUUGAACCGCUCtt
Rab13 2	4392420 ID number S11691	GGAAUCCGAUUUUUCGAAAtt	UUUCGAAAAAUCGGAUUCCat
Rab13 3	4392420 ID number S11692	GAUCCGCACUGUGGAUAUAtt	UAUAUCCACAGUGCGGAUCtt
Rab14 1	4390824 ID number S28311	GAAAAUCUAUCAGAACAUUtt	AAUGUUCUGAUAGAUUUUCtt
Rab14 2	4390824 ID number S28312	GGUCUAUGAAUAUCACUAGAtt	UCUAGUGAUAUCAUAGACCat
Rab21 1	4390824 ID number S22823	GGGUCCAAUUUACUACAGAtt	UCUGUAGUAAAUUGGACCCaa
Rab21 2	4390824 ID number S22824	GGGUCAAAGAAUUACGGAAtt	UUCCGUAAUUCUUUGACCCag
Rab22a 1	4392420 ID number S32992	UGAGCUACAUAAAUUCCUAtt	UAGGAAUUUAUGUAGCUCAtt
Rab22a 2	4392420 ID number S32993	CAGCUAUAAUCGUUUAUGAtt	UCAUAAACGAUUAUAGCUGca
Rab22a 3	4392420 ID number S32994	CGCCGACUCUAUUCAUGCAtt	UGCAUGAAUAGAGUCGGCGta
Rab22b (31) 1	4392420 ID number S21731	GGAAUACGCUGAAUCCAUAtt	UAUGGAUUCAGCGUAUUCCtt
Rab22b (31) 2	4392420 ID number S21732	CAAUGGAACAAUCAAAGUUtt	AACUUUGAUUGUUCCAUUGtt
Rab22b (31) 3	4392420 ID number S21733	GAACUUCACAAGUUCCUCAtt	UGAGGAACUUGUGAAGUUCat
Arf6 1	4390824 ID number S1565	GUCUCAUCUUCGUAGUGGAtt	UCCACUACGAAGAUGAGACct
Arf6 2	4390824 ID number S1566	AGACGGUGACUUACAAAAAtt	UUUUUGUAAGUCACCGUCUcc

Table 2.5 – Small GTPase targeting siRNA oligo sequences used during the siRNA screen

2.8 SDS-PAGE and western blotting

Cell lysates for SDS-PAGE and western blotting were obtained from cells covering a minimum area of 9.6 cm^2 (1 well of a 6-well plate well). Cells were firstly washed with cold PBS on ice, followed by the addition of cell lysis buffer consisting of NaCl (200 mM), Tris (75 mM), NaF (15 mM), Na3Vo4 (1.5 mM), EDTA (7.5 mM), EGTA (7.5 mM), TritonX-100 (1.5%), IGEPAL CA-630 (0.75%), leupeptin (50 $\mu g.mL^{-1}$), aprotinin (50 $\mu g.mL^{-1}$) and AEBSF (1 mM). Cell lysates were scraped from the cell culture dish, and centrifuged at 14,000 RCF for 10 minutes at 4°C to pellet cell debris. The supernatants were then mixed with sample buffer, consisting of Tris (pH 6.8; 0.35 M), glycerol (38%), bromophenol blue (0.012%), SDS (10.3%) and dithiothreitol (DTT; 350 mM), and heated to 95°C for 10 minutes. Samples were loaded into the wells of NuPAGE™ 4 to 12%, Bis-Tris gels (ThermoFisher, NP0322BOX), together with 4 µL of precision plus protein standard molecular weight marker (Bio-Rad, 1610394**),** and run at 100 V for 3 hours in NuPAGE™ MOPS SDS running buffer (Invitrogen, NP0001). For collagen I secretion assays (methods section 2.12.), samples were loaded into the wells of 6% Tris-glycine gels (ThermoFisher, XP00065BOX) with wedge wells to allow for up 80 µL of sample to be loaded. Protein transfer to 0.2 µm nitrocellulose membranes (Amersham, GE10600001) was carried out using a Trans-Blot Turbo Transfer System (Bio-Rad, 1704150EDU) according to the manufacturer's protocol. Membranes were washed in Tris-buffered saline-Tween 20 (TBS-T) buffer and blocked in casein blocking buffer (Sigma-Aldrich, B6429) to prevent non-specific antibody binding. Membranes were incubated with primary antibodies in casein blocking buffer for 1 hour on a rocker at room temperature, then washed three times in TBS-T and incubated with fluorophore conjugated-secondary antibodies diluted in casein blocking buffer for 1 hour on a rocker at room temperature. Antibody-bound proteins were then visualised using an Odyssey® CLx system (LI-COR) and images were processed using ImageJ.

Antigen	Supplier	Catalogue number	Species and type	Dilution
Rab11a	Cell Signalling	2413	Rabbit polyclonal	1:1000
Rab11b	Cell Signalling	2414	Rabbit polyclonal	1:1000
Collagen I	Kerafast	ENH018-FP	Rabbit polyclonal	1:1000
Fibronectin	Sigma-Aldrich	F3648	Rabbit polyclonal	1:1000
Tubulin	Abcam	Ab7291	Mouse monoclonal	1:3000

Table 2.6 – Primary antibodies used for western blotting

2.9 5-ethynyl-2′-deoxyuridine (EdU) cell proliferation assays

The proliferative capacity of primary fibroblasts following siRNA treatment was assessed using the Click-iT™ EdU Alexa Fluor™ 488 imaging kit (ThermoFisher, C10337) according to the manufacturer's protocol. Cells were seeded at a density of 20,000 cells per mL and grown in culture for 5 days in the presence TGFβ3 (10 $ng.mL^{-1}$). Nuclei were then stained with Hoechst 33342 as described previously. A minimum of 150 cells per condition were imaged using an Olympus inverted fluorescence microscope with a 20x/0.40 LWD C A20 objective, and cell proliferation was measured as the percentage of cells positive for the EdU stain.

2.10 Exogenous fibronectin assembly assay

Primary fibroblasts were seeded into wells of a clear bottom 96-well μ-plate, pre-coated with 0.1% gelatin, at a density of 5000 cells per well and cultured for a minimum of 4 days in complete DMEM with TGFβ3 (10 $ng.mL^{-1}$). Fluorophore conjugated exogenous fibronectin (HiLyte Fluor™ 488; Cytoskeleton Inc, FNR02) was added to each well (5 $\mu g.mL^{-1}$) for 5, 15, 30 or 60 minutes, then cells were washed in PBS and fixed in PFA (4%) for 20 minutes at room temperature. Nuclei were stained with Hoechst 33342 and 2.5% Dabco® 33-LV diluted in PBS was added. Images of assembled fibronectin fibres were acquired using a Leica SP8 inverted confocal microscope, where a single z-section was captured with as much fibronectin in focus as possible. ImageJ was used for all image processing, and analysis was carried out using the ridge detection algorithm as described previously, however a minimum line length of 5 pixels was used to ensure smaller fibres were also detected.

2.11 Second-harmonic generation (SHG) microscopy

To visualise the organisation of collagen in the vicinity of spheroids within collagen I hydrogels, SHG microscopy was used. Following imaging of spheroids for invasion analysis, spheroids within hydrogels were washed once in PBS and then fixed in PFA (4%) for 20 minutes at room temperature. Hydrogels were washed three times in PBS to remove PFA, 2.5% Dabco® 33-LV diluted in PBS was added, and stored at 4°C until imaging. Prior to imaging, Dabco® 33-LV was replaced with PBS. The SHG microscopy images were captured using a Leica SP8 upright multi-photon microscope with a 25x/0.95 L HC Fluotar water immersion dipping objective and a MaiTai MP laser (Spectra-Physics) at 880 nm. Z-sections were acquired covering approximately 55 µm and maximum intensity projections were generated using ImageJ software. Images were analysed by quantifying collagen fibre size in the spheroid vicinity using the ridge detection algorithm as described previously, however a minimum line length of 150 pixels was used to detect only large, non-bundled fibres. To ensure only fibres in the spheroid vicinity were measured, ridge detection was restricted to an area around each spheroid of approximately 40,000 pixels in size.

2.12 Collagen I monomer secretion assays

Primary CAFs were seeded at a density of 50,000 cells per mL and grown in culture for 24 hours before transfection with siRNA. Cells were then grown in culture for 72 hours in the presence of TGFβ3 (10 ng.mL^{-1}) and ascorbic acid (20 µg mL^{-1}), after which time the conditioned medium was collected and prepared for SDS-PAGE and western blotting as described previously. Samples were loaded into 6% Tris-glycine gels to allow for a large volume to be loaded. Due to the absence of an available loading control for conditioned media, Ponceau staining (ThermoFisher, 17435103) was used to ensure comparable levels of total protein were loaded in each lane.

2.13 Cy3-Collagen I uptake and deposition assays

Primary CAFs were seeded at a density of 40,000 cells per mL, then grown in culture for 3-4 days in the presence of TGFβ3 (10 ng.mL^{-1}). Cells were transfected with siRNA, the media was replaced with complete DMEM, then the following day exogenous rat tail collagen I (Corning; 10 µg.mL^{-1}), labelled with the Cy3 fluorophore (Joan Chang, Kadler lab, University of Manchester; Cy3-Col I), was added directly to the media for 1 hour. Cells were then trypsinised and prepared for flow cytometry and re-seeding by resuspension in PBS. Approximately 30% of cells were used to determine the percentage of cells with internalised Cy3-Col I by flow cytometry, which was carried out using a BD LSRFortessa™ system, with non-Cy3-Col I treated cells used as negative controls for gating. The remaining trypsinised cells were then re-seeded on to coverslips pre-coated with 0.1% gelatin and grown for 24 hours in complete DMEM, followed by replacement of the medium with complete DMEM containing ascorbic acid (20 µg mL^{-1}). Cells were fixed in PFA as described previously, 24 hours post-ascorbic acid addition, and Cy3-Col I deposition was imaged by confocal microscopy. Deposition analysis was performed using ImageJ software, where the total Cy3-Col I fibre area was measured and normalised to nuclei number. The fibre area for each image was then divided by the average fibre area for the non-silencing condition to normalise values within each biological repeat.

2.14 Expressing mNeonGreen (mNG) and Arf6-mNeonGreen (Arf6-mNG) in CAFs with lentiviral transduction

MNG and Arf6-MNG (6 µg) cloned into the pLX304 vector (Addgene, plasmid #25890; Konstantina Nikolatou, Bryant lab, University of Glasgow) were transfected into HEK293T cells at 60% confluency in a T75 flask, along with psPAX2 (Addgene, plasmid #12260) (4.5 µg) and pCMV-VSV-G (Addgene, #8454; 3 µg). The transfection was carried out using PEI, and the media containing viral particles was used to transduce primary CAFs, as described previously. Transduced CAFs were selected for with blasticidin (ThermoFisher, A1113903; 4 µg.mL^{-1}) treatment for 7-8 days. The cells used for imaging experiments were not sorted using fluorescence-activated cell sorting (FACS), as the proliferation of CAFs sorted using this technique was greatly reduced. As the population of cells used for imaging therefore expressed each construct at varying levels, cells with very low expression or very high expression were ignored.

2.15 Live-cell imaging of Cy3-Col I

Cy3-Col I uptake by CAFs, and Arf6 –mNG localisation to sites of Cy3-Col I assembly, was visualised using live-cell imaging. CAFs expressing mNG or Arf6-mNG were seeded into the wells of 8 chamber µ-slides (Ibidi, 80807), at a density of 33,000 cells per mL, and treated with TGFβ3 (10 $ng.mL^{-1}$). Cells were labelled with CellMask™ deep red actin tracking stain (ThermoFisher, A57245) according to the manufacturer's protocol, and the staining solution was replaced with Opti-Klear™ buffer (ab275938) ready for imaging. Cy3-Col I was added (10 $\mu g.mL^{-1}$), and cells were imaged immediately using spinning disk confocal microscopy with a 63x/1.40 oil objective as described previously, within a chamber pre-warmed to 37°C. Cells were imaged at 2-minute intervals for 2.5-3 hours. Z-stacks were captured at each time point, covering 7.5 µm in total with 0.5 µm per section. Images were captured with Slidebook 6.0 software as described previously, Imaris 9.9.1 software was used to generate 3D reconstructions and ImageJ software was used to generate maximum intensity projections.

2.16 HGSOC patient omentum sample mass spectrometry

For the comparison of ECM protein composition between diseased, uninvolved, and normal omentum samples, 15 different omentum samples, including three pairs of matched diseased and uninvolved samples from the same patient, were processed to enrich ECM proteins, and analysed by mass spectrometry. Snap frozen samples, with a diameter of approximately 0.5 cm^3, were homogenised with a pestle and mortar in 1 mL of TB buffer containing Tris (10 mM), NaCl (150 mM), EDTA (25 mM), Triton X-100 (1%), Leupeptin (25 μg. $mL^{-1)}$, Aprotinin (25 μg. mL^{-1}) and AEBSF (0.5 mM). Homogenised samples were incubated on a rotator at 4°C overnight, then centrifuged at 14,000 RCF for 10 minutes at 4°C. Pellets were then resuspended in PBS+ with Benzonase ® nuclease (250 units.mL^{-1}, Sigma-Aldrich, E1014) added and incubated for 30 minutes at 4°C. Samples were centrifuged for 10 minutes at 14,000 RCF and at 4°C, and western blot sample buffer was added to pellets. To ensure that ECM proteins had been enriched and that cytoplasmic proteins had been depleted in the final pellet during sample processing, a number of samples across the three categories, together with their corresponding supernatants collected at each centrifugation step, were subjected to SDS-PAGE and western blot analysis. This analysis was carried out using fibronectin as an ECM protein marker and tubulin as a cytoplasmic protein marker (Table 2.6).

Samples were prepared for mass spectrometry using the gel-top method. This was then followed by in-gel digestion and protein quantification by the mass spectrometry facility at the University of Manchester using the Orbitrap Exploris™ 480 mass spectrometer. Data analysis was carried out in house by Craig Lawless. MaxQuant 1.6.3.4 software was used to generate protein and peptide intensity values. The human proteome, downloaded from Uniprot (February, 2020), with variable modifications of methionine and proline oxidation, protein acetylation and cysteine carbamidomethylation, was then used to search spectra against. MSqRob software was used to make statistical comparisons between samples belonging to each of the three categories. Quantified proteins were classified into matrix and non-matrix using the matrisome database, and each class was independently submitted to MSqRob. To determine significant changes in protein abundance between samples, a q-value threshold of 0.05 was used, whereas a q-value threshold of 0.15 was used to identify near-significant changes.

Chapter 3: Characterisation of primary fibroblasts isolated from HGSOC patient omentum samples

3.1 Overview

CAFs present in the TME of many different cancer types are known to be very heterogeneous in the phenotypes they display. A number of subpopulations are believed to exist, where each subpopulation expresses different biomarkers and is capable of carrying out different functions, allowing tumour growth to be assisted through a variety of mechanisms [329]. Whilst myofibroblast-like CAFs that generate aberrant ECM are abundant in TMEs, other populations can also be present [330]. CAFs that have immunosuppressive properties can exist, for example a subpopulation of ovarian CAFs have been shown to recruit and activate immunosuppressive $CD25^{+}FOXP3^{+}$ T cells [331]. Furthermore, CAFs which rather than promote tumour development act as inhibitors of this process, can also be present within the TME. For example, in breast cancer, the ability of a CAF subpopulation to suppress tumour growth through secreting Slit2 and activating Robo1 signalling in the tumour has been demonstrated [332].

In order to understand how CAFs within the HGSOC omental TME generate an ECM that contributes towards tumour development, primary fibroblasts were isolated from HGSOC patient omentum samples and characterised. Given the heterogeneity that is known to exist between CAF subpopulations, it was crucial to firstly evaluate the extent of the heterogeneity present in isolated CAF populations through assessing the expression of a panel of known CAF biomarkers by immunofluorescence microscopy. Secondly, using immunofluorescence, isolated fibroblasts were characterised based on their ability to assemble an ECM that consisted of proteins which are known to become more abundant in the omentum TME with HGSOOC disease progression. Finally, spheroid invasion assays were used to measure the capacity of isolated fibroblasts to assemble and remodel ECM in a way that facilitates the invasion of the Kuramochi HGSOC cell line in 3D culture. In addition, the contribution of fibroblast activation state towards CAF function was investigated by comparing CAF biomarker expression, ECM assembly/remodelling, and Kuramochi invasion promoting-ability between omentum derived-CAFs, omentum derived-NFs, and primary human dermal fibroblasts (HDFs). This was then further evaluated by carrying out these comparisons in the presence or absence of TGFβ3, a known HGSOC-cell derived fibroblast activator [159].

3.2 CAF biomarker expression by primary fibroblasts isolated from HGSOC patient tumour burdened omentum samples

3.2.1 Overview

Immunofluorescence microscopy with a panel of known CAF biomarkers was used firstly to confirm that the fibroblasts isolated from HGSOC patient omentum samples were CAF-like in nature, and secondly to evaluate the degree of heterogeneity present in isolated CAF populations. The CAF biomarker panel used consisted of SMA, FAP and collagen XI. Collagen XI was included, as in comparison to normal tissues where levels are thought to be relatively low, high collagen XI expression in CAFs derived from pancreatic and ovarian tumours has been detected [333] [334]. Furthermore, collagen XI has also been included in stromal gene signatures associated with poor clinical outcomes in OC and breast cancer [182] [[335]. Whilst FSP-1 and vimentin have been used extensively as CAF biomarkers in the past, they were omitted from this panel on the basis of their lack of specificity for CAFs. The expression of SMA, FAP and collagen XI was assessed in all isolated CAF populations used throughout this project, and similar biomarker expression levels and localisations were observed across all CAF populations used. The abundance of SMA and FAP positive fibroblasts within the omentum has been shown to increase with HGSOC disease progression, and high FAP expression by omental CAFs is thought to facilitate cancer cell proliferation, invasion, and resistance to chemotherapy [98] [333].

3.2.2 SMA, FAP and collagen XI expression in CAFs

The expression of SMA within each isolated CAF population was heterogeneous, where whilst SMA was expressed in all cells, the level of expression was variable. Many cells expressed high levels of SMA, with bright, large SMA fibres clearly visible, whereas other cells displayed far lower levels of expression (Figure 3.1a). These large fibres likely correspond to more contractile, filament bundles/stress fibres of SMA, and suggest that fibroblasts positive for these fibres were more contractile and myofibroblast-like in nature, therefore rendering them more capable of ECM assembly and remodelling [336] [337] [338]. These data indicated that a level of heterogeneity existed within isolated CAF populations with regards to their expression levels of SMA.

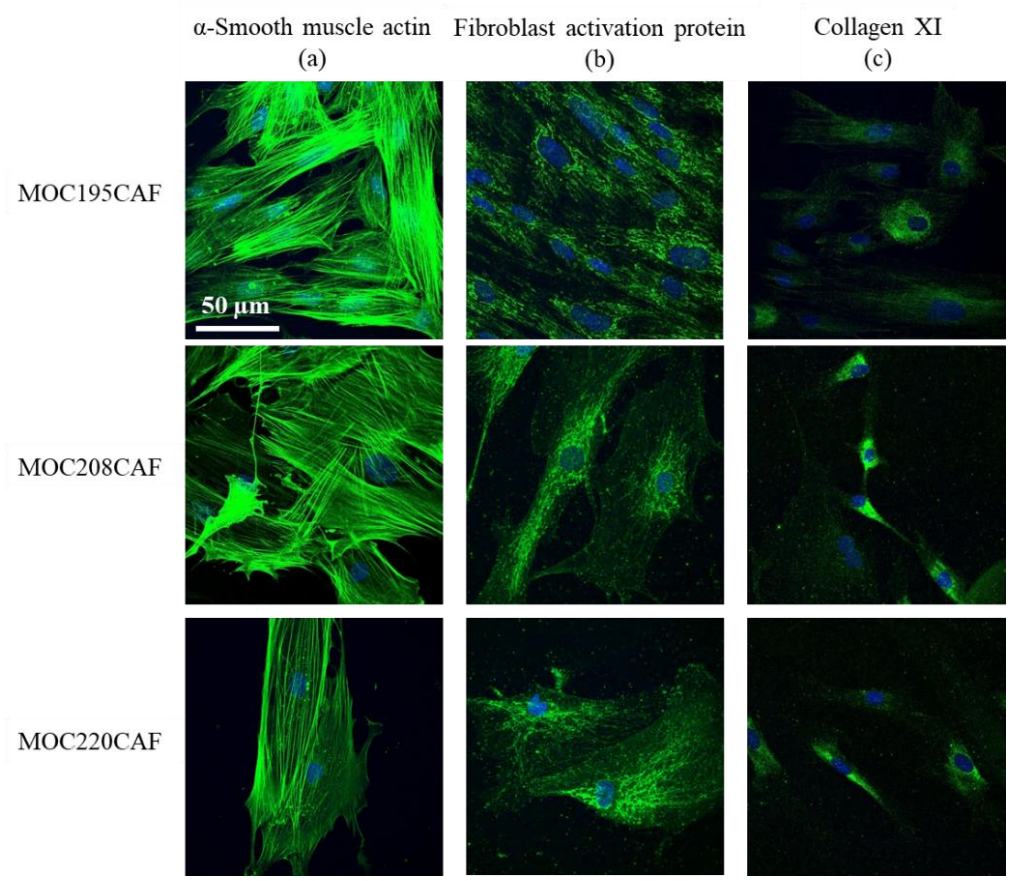

Figure 3.1 – Omentum derived CAFs express SMA, FAP and collagen XI

Primary CAFs were immunostained to detect expression of SMA, FAP and collagen XI after 4 days in culture (N = 3). Representative images of three example CAF lines isolated from HGSOC tumour burdened omentum samples, MOC195, MOC208 and MOC220, are shown (a) Representative images of SMA expression (b) Representative images of FAP expression. (c) Representative images of collagen XI expression. Nuclei were stained with Hoechst 33342. Scale bar = 50 µm. Maximum intensity projections of z-stacks are shown.

Surprisingly, despite others observing heterogeneity in FAP expression by CAFs, CAFs isolated from HGSOC patient omentum samples homogeneously expressed FAP, where a similar expression level and localisation was observed within, and across, all samples [87]. Although FAP functions as a membrane-bound serine protease, its localisation was predominantly reticular in appearance with some diffuse plasma membrane localisation also observed, suggesting it localised primarily within the ER (Figure 3.1b). The expression of collagen XI within all isolated CAF populations was heterogeneous. Although all cells expressed this biomarker to some extent, with a mostly retiuclar localisation observed, there was variation in its expression levels, where a proportion of cells displayed far higher levels of expression than others (Figure 3.1c). Taken together, these results indicate that the populations of fibroblasts isolated from HGSOC patient omentum samples had CAF-like properties in that all biomarkers were expressed, however a degree of heterogeneity was present, with SMA and collagen XI expressed at varying levels within each population.

3.3 Comparison of SMA, FAP and collagen XI expression between primary CAFs, NFs and HDFs

3.3.1 Overview

To determine whether CAF biomarker expression varied depending on fibroblast activation state, immunofluorescence microscopy was used to compare SMA, FAP and collagen XI expression between omentum derived CAFs (MOC195) and NFs (MOC198), as well HDFs isolated from the skin, which were included as a non-omental control. Whereas CAFs were derived from HGSOC patient omentum samples, NFs were isolated from omentum samples removed from patients that did not have HGSOC. Instead, these patients often had some other form of cancer, such as early-stage endometrial cancer. In addition, these comparisons were also carried out in the presence or absence of TGFβ3. The purpose of doing so was firstly to evaluate the impact of treatment with this growth factor on the activation state of fibroblast populations, and secondly to establish whether isolated CAFs could be pushed towards a state similar to that of a myofibroblast capable of ECM assembly/remodelling, and facilitating HGSOC cell invasion.

3.3.2 SMA expression in CAFs, NFs and HDFs

Although differences in SMA expression between omentum derived CAFs and NFs were expected, SMA was surprisingly similar between these fibroblast populations, with comparable percentages of cells possessing large SMA stress fibres (Figure 3.2a, 3.2c). HDFs expressed SMA at far lower levels, where only a small percentage of cells were positive for SMA stress fibres (Figure 3.2a, 3.2c). These results suggested that omentum-derived CAFs and NFs were more myofibroblast-like in nature than HDFs.

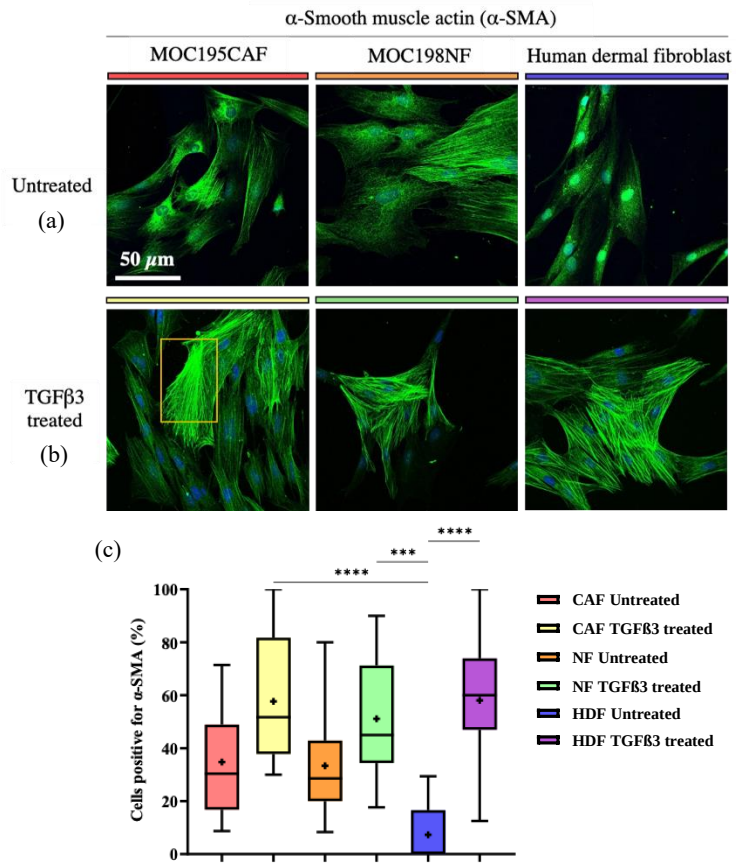

Figure 3.2 – TGFβ3 treatment increases SMA expression in CAFs, NFs and HDFs

*Primary CAF, NFs and HDFs were immunostained to detect SMA expression after 4 days in culture, in the presence or absence of TGFβ3 (N = 3). (a) Representative images of SMA expression in untreated CAFs, NFs and HDFs. (b) Representative images of SMA expression in TGFβ3 (10 ng.mL^{-1}) treated CAFs, NFs and HDFs. (c) Percentages of cells positive for large SMA stress fibres (yellow box in (b)) in CAFs, NFs and HDFs in the presence or absence of TGFβ3 are shown. Quantification of data from three biological replicates, statistical analysis by Kruskal-Wallis test (***p<0.001, ****p<0.0001). All statistically significant results are shown. Nuclei were stained with Hoechst 33342. Scale bar = 50 μm. Maximum intensity projections of z-stacks are shown.*

3.3.3 The effect of TGFβ3 treatment on SMA expression

In order to understand the effect of TGFβ3 treatment on CAF, NF and HDF SMA expression, fibroblasts were cultured in the presence or absence of this growth factor. Treatment with TGFβ3 elevated SMA expression in all three fibroblast types, and was sufficient to increase SMA expression in HDFs to levels comparable with those observed in TGFβ3 treated CAFs and NFs (Figure 3.2a, 3.2b, 3.2c). These results confirmed the already established role of TGFβ3 as a potent activator of fibroblasts, and highlighted how this growth factor may be used to convert a more heterogeneous fibroblast population to one that is more homogenous. For future experiments aiming to understand the mechanisms involved in ECM assembly and remodelling by the myofibroblast subpopulation of CAFs in the omentum, heterogenous CAF populations could be pre-treated with TGFβ3 as a means to push them towards a more homogeneous, activated myofibroblast-like state.

3.3.4 FAP expression in CAFs, NFs and HDFs with TGFβ3 treatment

It was observed previously that FAP expression by all HGSOC patient derived CAF lines was relatively homogeneous, where all cells were positive for this biomarker (Figure 3.1a). Whilst this was to be expected, comparisons between FAP levels in CAFs, NFs and HDFs surprisingly revealed that NFs and HDFs expressed FAP to the same extent as CAFs (Figure 3.3a, 3.3c). As approximately 100% of cells show FAP expression prior to TGFβ3 treatment, the addition of this growth factor was unable to raise expression levels any further (Figure 3.3b, 3.3c).

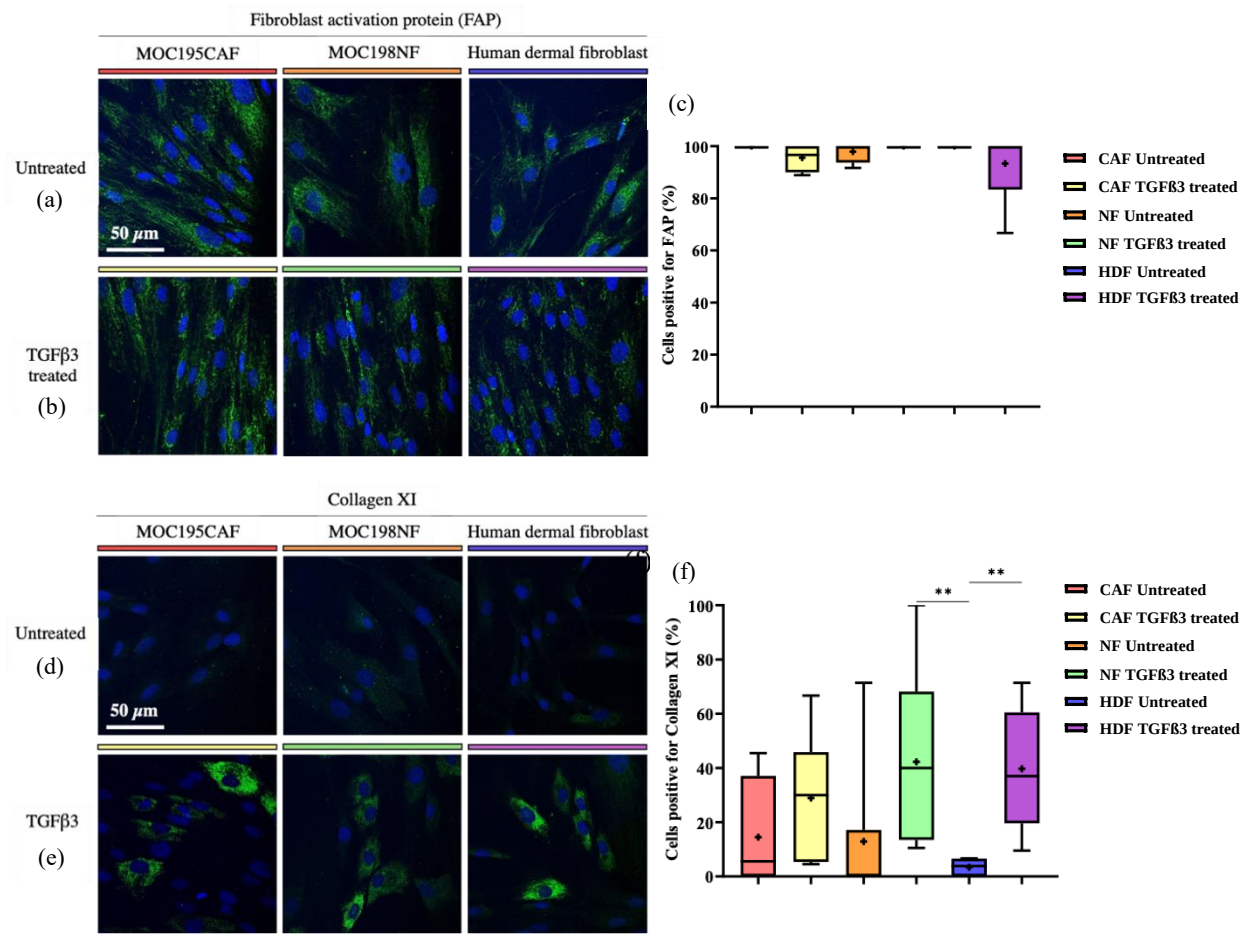

Figure 3.3 – TGFβ3 treatment increases collagen XI expression in CAFs, NFs and HDFs, whereas FAP expression is unaffected

*Primary CAF, NFs and HDFs were immunostained to detect FAP and collagen XI expression after 4 days in culture, in the presence or absence of TGFβ3 (N = 3). (a) Representative images of FAP expression in untreated CAFs, NFs and HDFs. (b) Representative images of FAP expression in TGFβ3 (10 ng.mL^{-1}) treated CAFs, NFs and HDFs. (c) Quantification of merged data from three biological replicates, and statistical analysis by Kruskal-Wallis test, of FAP expression by CAFs, NFs and HDFs in the presence or absence of TGFβ3. The percentages of cells positive for FAP are shown. (d) Representative images of collagen XI expression in untreated CAFs, NFs and HDFs. (e) Representative images of collagen XI expression in TGFβ3 (10 ng.mL^{-1}) treated CAFs, NFs and HDFs. (f) Quantification of merged data from three biological replicates, and statistical analysis by Kruskal-Wallis test (**p<0.01), of collagen XI expression by CAFs, NFs and HDFs in the presence or absence of TGFβ3. The percentages of cells positive for collagen XI are shown. All statistically significant results are shown. Nuclei were stained with Hoechst 33342. Scale bar = 50 μm. Maximum intensity projections of z-stacks are shown.*

3.3.5 Collagen XI expression in CAFs, NFs and HDFs with TGFβ3 treatment

The previous characterisation of isolated omental CAF populations revealed similar collagen XI expression patterns between all populations tested, with heterogeneity then existing within each population (Figure 3.1c). However, despite a number of cells within each isolated population displaying moderate levels of collagen XI expression during this initial characterisation, when expression of this biomarker was compared between CAFs, NFs and HDFs in the presence or absence of TGFβ3, CAF collagen XI expression was far lower than that observed previously. Whilst CAFs were maintained in culture under the same conditions for no longer than 8 passages, it was clear that some CAF-like properties, such as high collagen XI expression, were to some extent lost prior to this, posing a problem for further experiments aiming to study the behaviour of myofibroblast-like CAF populations. As well as in the CAFs, relatively low collagen XI levels were also detected in the NFs and HDFs, with the lowest expression detected in HDFs (Figure 3.3d, 3.3f). Clearly visible increases in collagen XI levels were then observed following treatment of each fibroblast type with TGFβ3, although only the increase in expression by HDFs following treatment was statistically significant (3.3e, 3.3f).

These data suggested that the presence of large SMA stress fibres, FAP positivity and expression of collagen XI are each important biomarkers for CAFs isolated from omentum metastases. Furthermore, these data indicated that collagen XI expression can be lost over time in culture. Changes in the properties of cultured primary CAFs was to be expected as passage number increased. As with SMA, the capacity of TGFβ3 treatment to elevate collagen XI levels in CAFs provided an important method for ensuring that primary CAFs used in downstream experiments were maintained in a myofibroblast-like CAF state.

3.4 Investigating the dependence of CAFs on ascorbic acid for collagen I fibrillogenesis

3.4.1 Overview

Collagen I is known to be deposited and assembled into thick bundles within the HGSOC TME, and levels of collagen I in the omentum increase with disease progression [98]. Furthermore, it is known that collagen I ECM is involved in enhancing the invasiveness of OC cells through β1 integrin mediated adhesion, and also for that of other cancer cell types [339] [340]. It was therefore crucial to understand how CAFs within the omentum assemble collagen I, beginning with evaluating their dependence on ascorbic acid for this process.

Ascorbic acid is thought to be an essential cofactor for the hydroxylation of procollagen proline and lysine residues within the ER, which subsequently stabilises procollagen chains, and allows triple helical procollagen to form ready for secretion via the Golgi apparatus [189]. Human cells are unable to synthesise ascorbic acid, as they lack a functional form of the gulconolactone oxidase (GLO) enzyme which acts to catalyse the final step in its biosynthetic pathway [341]. It has therefore been established for decades that collagen I secretion and assembly by human fibroblasts requires the addition of ascorbic acid [342] [343] [188]. We hypothesised that ascorbic acid would be an essential cofactor required by CAFs in the omentum for collagen deposition.

3.4.2 The effect of ascorbic acid on collagen I assembly by CAFs

To investigate the dependence of primary CAFs on ascorbic acid for collagen I synthesis and deposition, CAFs treated with TGFβ3 were grown in culture for 10 days in the presence or absence of ascorbic acid, and assembled collagen I was visualised using immunofluorescence microscopy in non-permeabilised cells. These data were quantified by measuring the total fibre area after thresholding, which was then normalised to cell number (Figure 3.5). Overall, across three biological repeats, ascorbic acid stimulated collagen I fibre assembly, where a significant increase in collagen I fibre area was observed and measured (Figure 3.4g). However, interestingly, ascorbic acid was not absolutely required for this assembly process, and across all three biological repeats, small amounts of collagen I could be assembled in the absence of ascorbic acid. In the second and third biological repeats, ascorbic acid enhanced the deposition of collagen I fibres by primary CAFs, with statistically significant, and non-statistically significant but clearly visible, increases measured, respectively (Figure 3.4b, 3.4c, 3.4e, 3.4f). However, in the first biological repeat, ascorbic acid did not stimulate collagen I deposition, and primary CAFs had the capacity to deposit collagen I fibres in the absence of ascorbic acid to the same extent as those cultured in its presence (Figure 3.4a, 3.4d). As ascorbic did enhance collagen I assembly in most cases, ascorbic acid was included in the culture medium for all downstream experiments aiming to further understand the mechanisms of ECM assembly utilised by CAFs.

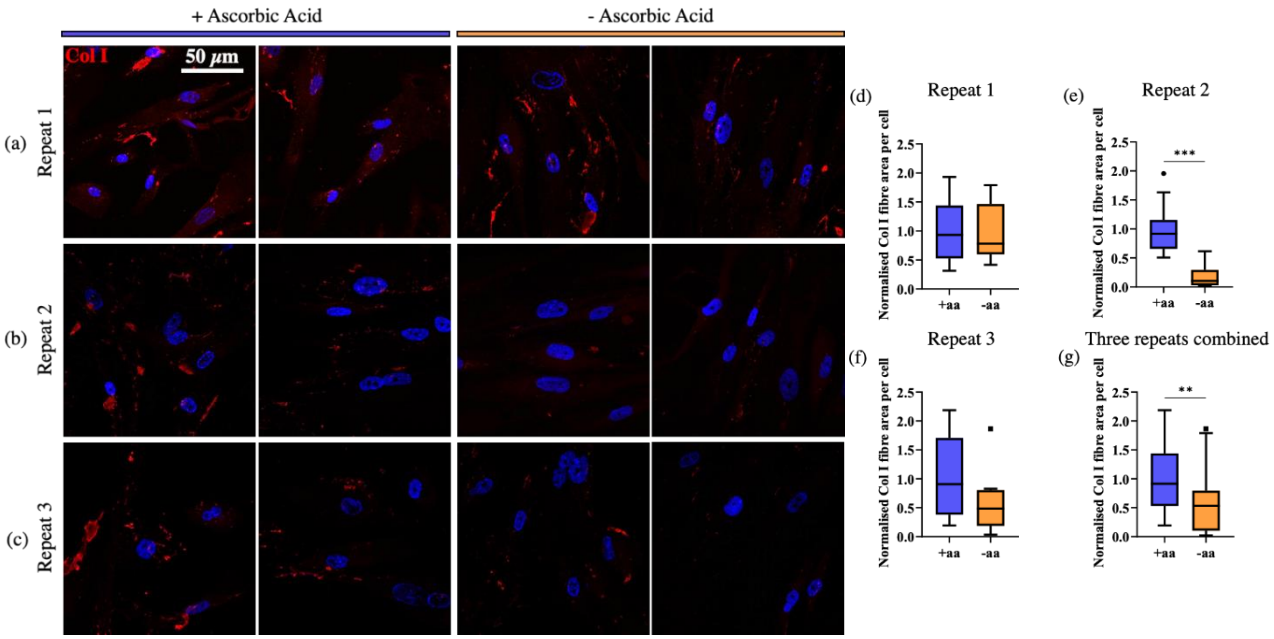

Figure 3.4 – Ascorbic acid enhances, but is not essential for, collagen I deposition by CAFs

*Primary CAFs (MOC194) were immunostained without permeabilisation to detect collagen I deposition after 10 days in culture, in the presence of TGFβ3 (10 ng.mL^{-1}), in the presence or absence of ascorbic acid (20 μg.mL^{-1}; N = 3). Representative images are shown from biological repeats 1(a), 2 (b), and 3 (c), of collagen I deposition by CAFs in the presence or absence of ascorbic acid. (d) Quantification, and statistical analysis by unpaired t-test, of collagen I fibre area deposited by CAFs in biological repeat 1. (e) Quantification, and statistical analysis by Mann-Whitney test (***p<0.001), of collagen I fibre area deposited by CAFs in biological repeat 2. (f) Quantification, and statistical analysis by Mann-Whitney test, of collagen I fibre area deposited by CAFs in biological repeat 3. (g) Quantification, and statistical analysis by Mann-Whitney test (**p<0.01), of data merged from three biological replicates. All statistically significant results are shown. Nuclei were stained with Hoechst 33342. Scale bar = 50 μm. Maximum intensity projections of z-stacks are shown.*

3.5 Collagen I, fibronectin, collagen XI and versican deposition by CAFs, NFs and HDFs

3.5.1 Overview

Once it had been established that CAF-mediated collagen I fibrillogenesis was stimulated by ascorbic acid, the effect of fibroblast activation state on the deposition of collagen I, fibronectin, collagen XI and versican, all of which become more abundant in the omentum with HGSOC progression, in 2D culture was investigated. CAFs, NFs, and HDFs, were grown in culture for 10 days in the presence or absence of TGFβ3 and immunofluorescence microscopy was used to visualise the deposition of collagen I, fibronectin, collagen XI, and versican, as fibres in the extracellular space. The importance of ascorbic acid in the assembly of fibronectin, collagen XI and versican was not investigated. However, given that ascorbic acid stimulated collagen I assembly by CAFs, and that an interdependence is thought to exist between the assemblies of different ECM proteins, ascorbic acid was included in the growth medium [225].

3.5.2 Quantification of ECM protein deposition

In order to quantify these data, two different methods of analysis were used. Firstly, total fibre area was measured and normalised to cell number, giving the overall area of fibres present per cell in each image. Secondly, a large fibre index value was calculated for each image using the ridge detection algorithm within ImageJ software. We define fibre index as the area of fibres detected over a given width and length by the ridge detection algorithm. This enabled only fibres over a specified width (10 pixels) and length (70 pixels) to be detected and measured (Figure 3.5). Large fibre index values were then normalised to cell number for each image.

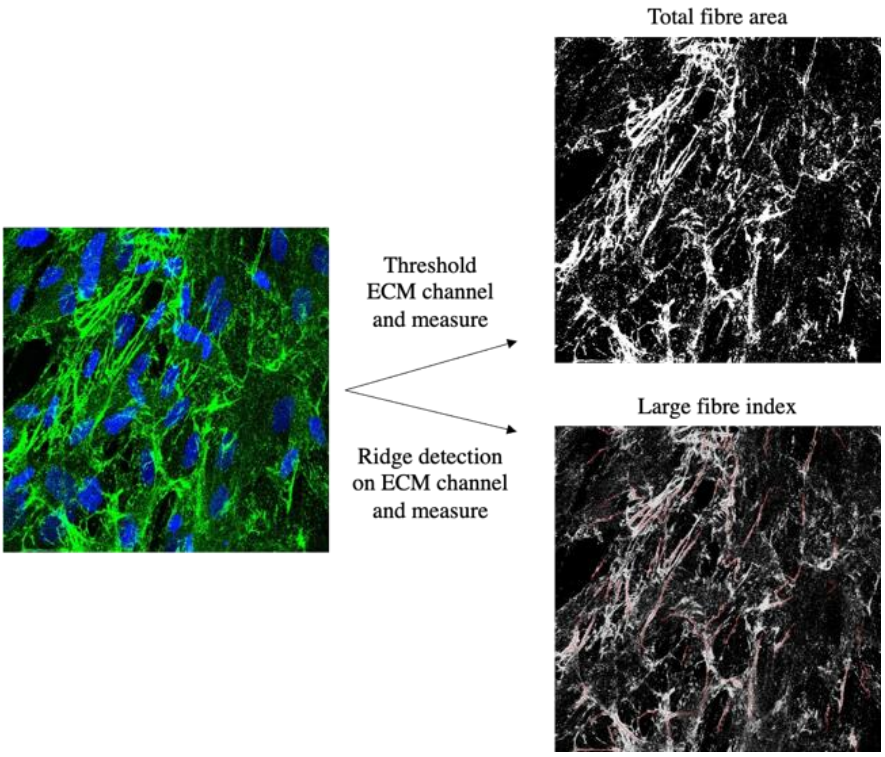

Figure 3.5 – ECM deposition analysis by total fibre area and large fibre index

Collagen I, fibronectin, collagen XI and versican deposition by CAFs, NFs and HDFs was visualised by fluorescence microscopy following immunostaining of non-permeabilised cells. Images were analysed by measuring total fibre area, where the ECM protein channel was thresholded and the total area was measured, and large fibre index, where the ridge detection algorithm was used to identify and measure only those fibres with a minimum width of 10 pixels and a minimum length of 70 pixels. Detected fibres are shown in red. All measured values were normalised to cell number for each image.

3.5.3 Collagen I deposition by CAFs, NFs and HDFs with TGFβ3 treatment

The measurement of total collagen I fibre area revealed that, when untreated, CAFs and NFs were more competent in collagen I assembly than HDFs, with a significantly greater total fibre area detected in CAFs and NFs compared to HDFs (Figure 3.6a, 3.6c). This was to be expected based on the SMA staining observed previously, as HDFs were the least activated of the three fibroblast types and therefore less likely to assemble ECM (Figure 3.2a). TGFβ3 treatment of CAFs or NFs did not significantly alter collagen I deposition, despite this treatment elevating expression of SMA in both of these fibroblast types (Figure 3.2). Whilst treatment with TGFβ3 was previously sufficient to elevate SMA expression levels in HDFs to those observed in TGFβ3 treated CAFs and NFs, this treatment did not stimulate collagen I deposition to the same level as that observed in untreated, or TGFβ3 treated, CAFs and NFs (Figure 3.6b, 3.6c).

Image analysis by measurement of collagen I large fibre index revealed that whilst the amount of large fibres assembled by CAFs was unaffected by TGFβ3 treatment, this treatment resulted in a significant reduction in large fibre assembly by HDFs (Figure 3.6b, 3.6d). The large fibre index was also reduced in NFs with TGFβ3 treatment, however this reduction was not statistically significant (Figure 3.6b, 3.6d).

These data suggest that fibroblast activation state impacts upon collagen I deposition to some extent, as CAFs and NFs were more capable of collagen I deposition than HDFs. However, interestingly, TGFβ3 treatment did not significantly increase collagen I deposition by CAFs, NFs, or HDFs. As TGFβ3 treated HDFs remained unable to deposit collagen I to the same extent as TGFβ3 treated, or untreated, CAFs and NFs, this suggests that these omentum-derived fibroblasts may possess properties, in addition to SMA expression, that allow for excessive collagen I deposition. Furthermore, as treatment of CAFs and NFs with TGFβ3 did not enhance their collagen I deposition capacity, these fibroblast types may have already reached their maximum capacity for collagen I assembly prior to treatment, such that any stimulation was unable to increase deposition further.

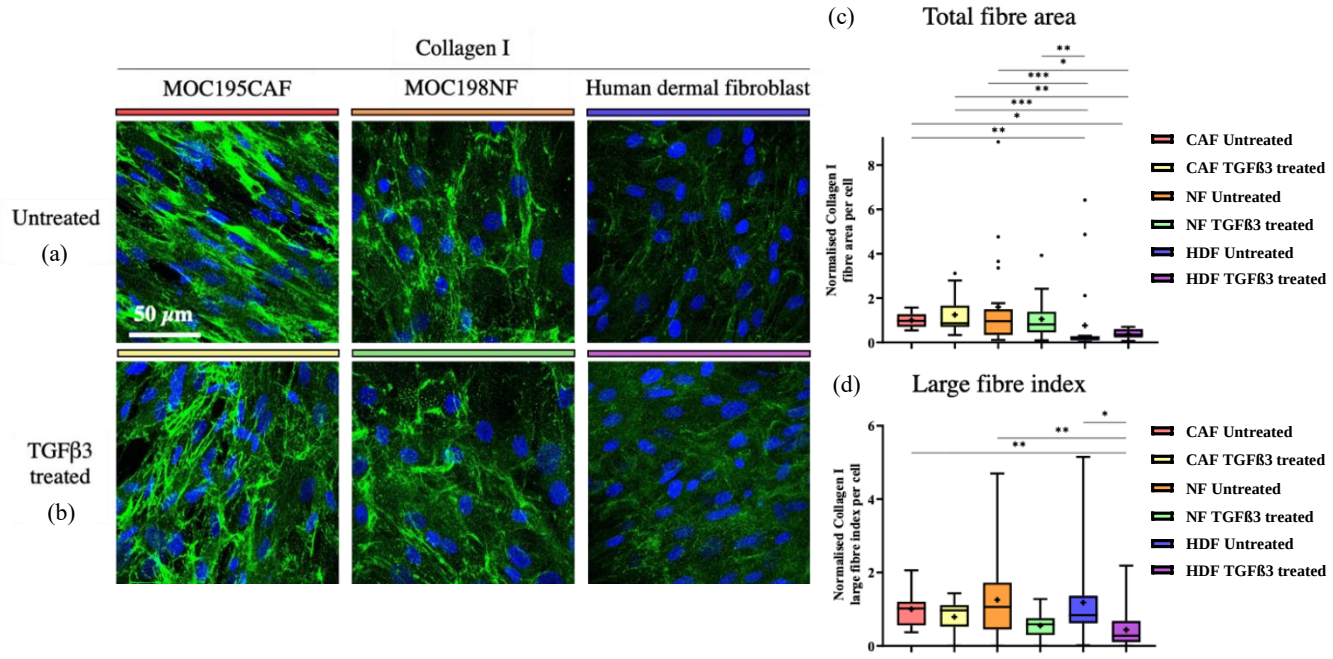

Figure 3.6 – CAFs and NFs assemble collagen I more efficiently than HDFs

*Primary CAFs, NFs and HDFs were immunostained without permeabilisation to detect collagen I deposition after 10 days in culture, in the presence of ascorbic acid (20 µg.mL^{-1}), and in the presence or absence of TGFβ3 (10 ng.mL^{-1}; n=3). (a) Representative images of collagen I deposition by untreated treated CAFs, NFs and HDFs. (b) Representative images of collagen I deposition by TGFβ3 treated CAFs, NFs and HDFs. (c) Quantification of merged data from three biological replicates, and statistical analysis by Kruskal-Wallis test (*p<0.05, **p<0.01, ***p<0.001), of total collagen I fibre area deposited by untreated and TGFβ3 treated CAFs, NFs and HDFs. (d) Quantification of merged data from three biological replicates, and statistical analysis by Kruskal-Wallis test (*p<0.05, **p<0.01), of collagen I large fibre index deposited by untreated and TGFβ3 treated CAFs, NFs and HDFs. All statistically significant results are shown. Nuclei were stained with Hoechst 33342. Scale bar = 50 µm. Maximum intensity projections of z-stacks are shown.*

3.5.4 Fibronectin deposition by CAFs, NFs and HDFs with TGFβ3 treatment

Evaluating the assembly of fibronectin by CAFs, NFs, and HDFs, in response to TGFβ3 treatment revealed interesting results. It was expected that CAFs would have the highest capacity for assembling fibronectin fibres, in particular following TGFβ3 treatment. However, measuring total fibronectin fibre area highlighted that the NFs were the most capable of carrying out fibronectin fibrillogenesis, followed by the HDFs, with the CAFs assembling the least amount of fibres (Figure 3.7a, 3.7c). TGFβ3 treatment did not significantly elevate the total area of fibronectin deposited by the three fibroblast types (Figure 3.7b, 3.7c). Similarly, measuring the large fibronectin fibre index also resulted the same pattern of deposition, where the NFs, when untreated or TGFβ3 treated, deposited the highest amount of large fibres, with the CAFs depositing the least. TGFβ3 treatment also did not alter the amount of large fibres deposited by any of the three fibroblast types (Figure 3.7a, 3.7b, 3.7d).

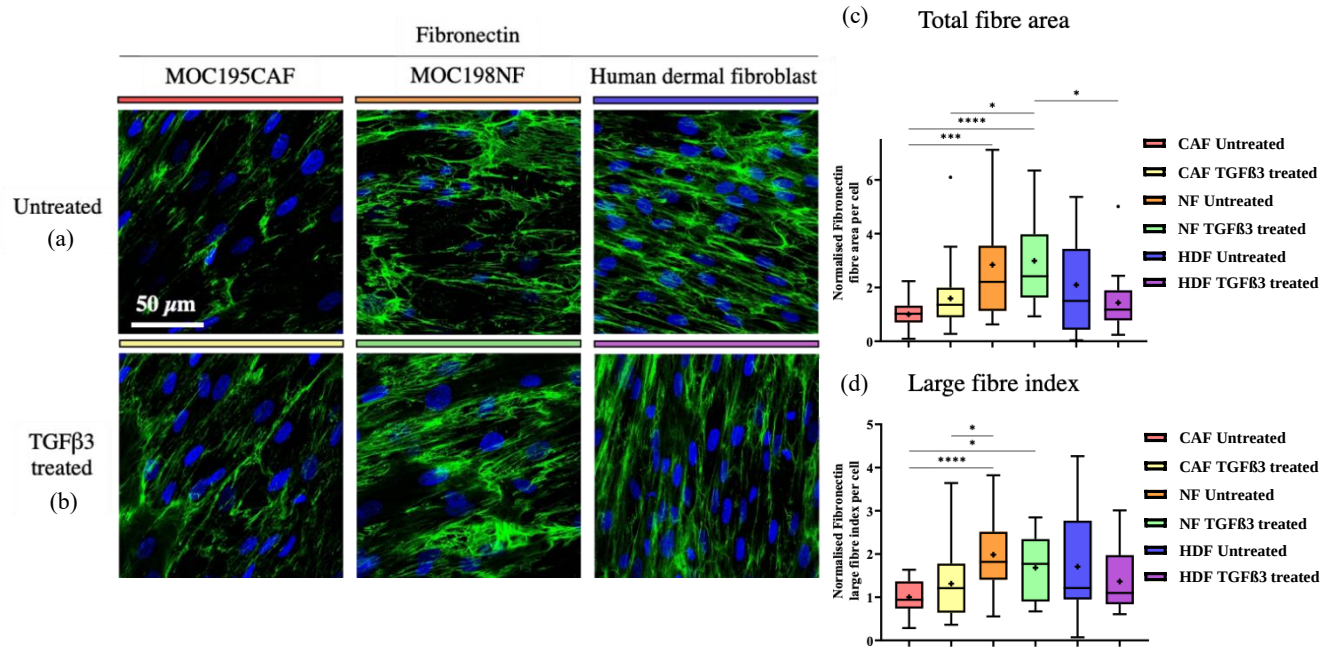

Figure 3.7 – NFs and HDFs assemble more fibronectin than CAFs

*Primary CAFs, NFs and HDFs were immunostained without permeabilisation to detect fibronectin deposition after 10 days in culture, in the presence of ascorbic acid (20 μg.mL^{-1}), and in the presence or absence of TGFβ3 (10 ng.mL^{-1}; n=3). (a) Representative images of fibronectin deposition by untreated treated CAFs, NFs and HDFs. (b) Representative images of fibronectin deposition by TGFβ3 treated CAFs, NFs and HDFs. (c) Quantification of merged data from three biological replicates, and statistical analysis by Kruskal-Wallis test (*p<0.05, ***p<0.001, ****p<0.0001), of total fibronectin fibre area deposited by untreated and TGFβ3 treated CAFs, NFs and HDFs. (d) Quantification of merged data from three biological replicates, and statistical analysis by Kruskal-Wallis test (*p<0.05, ****p<0.0001), of fibronectin large fibre index deposited by untreated and TGFβ3 treated CAFs, NFs and HDFs. All statistically significant results are shown. Nuclei were stained with Hoechst 33342. Scale bar = 50 μm. Maximum intensity projections of z-stacks are shown.*

3.5.5 Collagen XI deposition by CAFs, NFs and HDFs with TGFβ3 treatment

Collagen XI is a minor fibrillar collagen that is thought to have a role in nucleation of collagen I fibrillogenesis, as described previously, whereas versican is a proteoglycan that has several binding partners within the ECM, including collagen I, and as such is believed to play an important role in regulating the overall organisation of complex matrices [96] [344] [345]. Although collagen XI and versican are far less abundant in the HGSOC tumour burdened omentum than collagen I and fibronectin, their general roles in the formation of the ECM, and their increase in abundance in the omentum with tumour progression, suggests they may be of importance in generating an ECM that supports HGSOC tumour development. Furthermore, work by others has demonstrated roles for both collagen XI and versican in supporting OC cell invasion [346] [347].

Previous investigation of collagen XI expression as a CAF biomarker in CAFs, NFs, and HDFs, revealed heterogeneity in its intracellular localisation. All untreated fibroblast types expressed relatively low levels of collagen XI, with expression then elevated by TGFβ3 treatment, such that collagen XI was clearly visible with a reticular, ER-like, localisation in a proportion of cells (Figure 3.3d, 3.3e). However, as well as understanding how the expression levels and intracellular localisation of collagen XI changed with fibroblast activation, it was also important to explore what impact changes in activation state had on the deposition of collagen XI as fibres in the extracellular space. Untreated CAFs, NFs and HDFs deposited comparable amounts of collagen XI, as shown by measurement of total fibre area and large fibre index (Figure 3.8a, 3.8b, 3.8d). Although the large fibre indices measured remained unchanged following treatment of each fibroblast type with TGFβ3, a significant decrease in the total fibre area was observed upon treatment of NFs with TGFβ3 (Figure 3.8b, 3.8c, 3.8d).

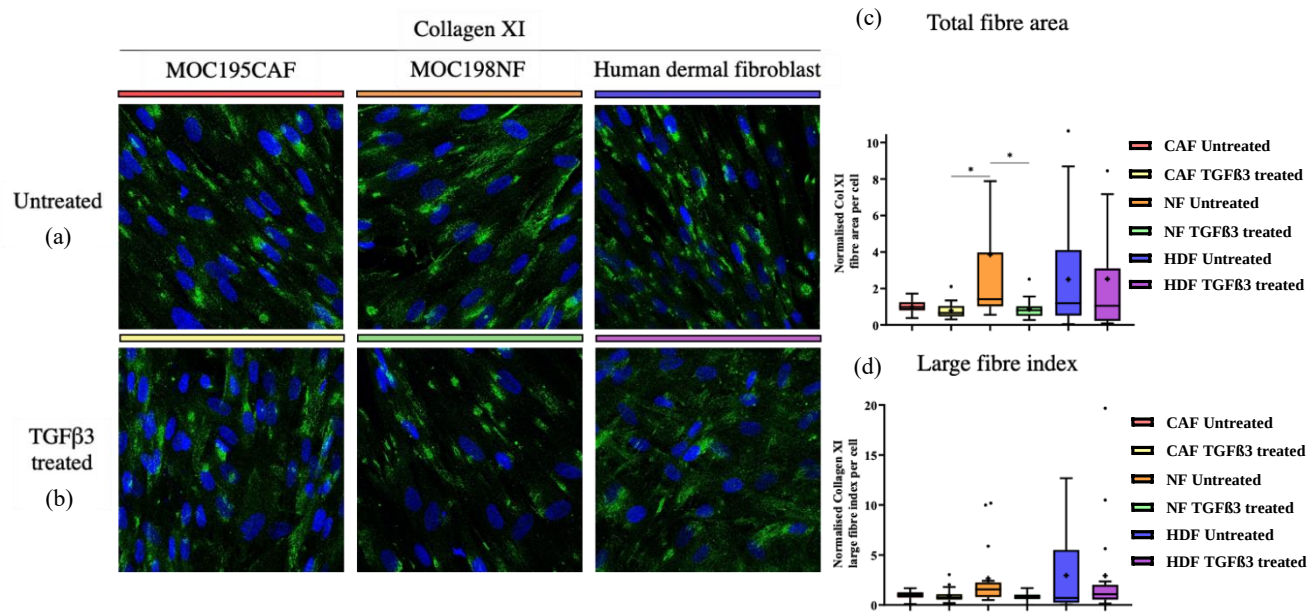

Figure 3.8 – CAFs, NFs and HDFs assemble comparable amounts of collagen XI

*Primary CAFs, NFs and HDFs were immunostained without permeabilisation to detect collagen XI deposition after 10 days in culture, in the presence of ascorbic acid (20 µg.mL^{-1}), and in the presence or absence of TGFβ3 (10 ng.mL^{-1}; n=3). (a) Representative images of collagen XI deposition by untreated treated CAFs, NFs and HDFs. (b) Representative images of collagen XI deposition by TGFβ3 treated CAFs, NFs and HDFs. (c) Quantification of merged data from three biological replicates, and statistical analysis by Kruskal-Wallis test (*p<0.05), of total collagen XI fibre area deposited by untreated and TGFβ3 treated CAFs, NFs and HDFs. (d) Quantification of merged data from three biological replicates, and statistical analysis by Kruskal-Wallis test, of collagen XI large fibre index deposited by untreated and TGFβ3 treated CAFs, NFs and HDFs. All statistically significant results are shown. Nuclei were stained with Hoechst 33342. Scale bar = 50 µm. Maximum intensity projections of z-stacks are shown.*

3.5.6 Versican deposition by CAFs, NFs and HDFs with TGFβ3 treatment

Visualisation of versican deposition by untreated and TGFβ3 treated CAFs, NFs, and HDFs, demonstrated that although versican itself is not fibrillar in nature, a fibre-like localisation in the extracellular space can be observed. This fibrillar localisation has been observed by others, and is likely due to versican accumulating along fibres formed by the many versican-binding partners found within the ECM [348]. In untreated fibroblasts, a significant difference in versican deposition was observed only between NFs and HDFs, where the NFs were more capable of assembling this ECM protein, shown by measurement of total fibre area (Figure 3.9a, 3.9c). TGFβ3 treatment moderately increased the total versican fibre area deposited, however for all fibroblast types, these increases were not statistically significant (Figure 3.9b, 3.9c). A statistically significant increase was however measured in TGFβ3 treated NFs compared to untreated CAFs and HDFs. The large fibre indices measured for all fibroblast types were comparable, with TGFβ3 treatment insufficient to significantly elevate versican deposition by CAFs, NFs, and HDFs (figure 3.9a, 3.9b, 3.9d).

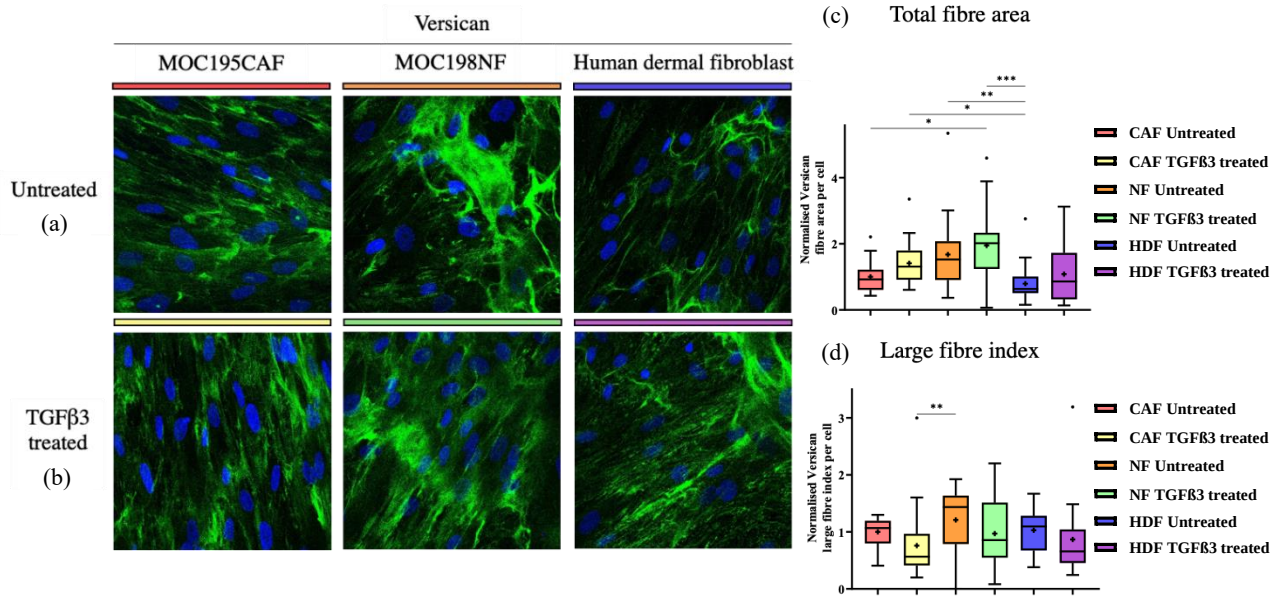

Figure 3.9 – Versican deposition does not correlate with fibroblast activation state

*Primary CAFs, NFs and HDFs were immunostained without permeabilisation to detect versican deposition after 10 days in culture, in the presence of ascorbic acid (20 µg.mL^{-1}), and in the presence or absence of TGFβ3 (10 ng.mL^{-1}; n=3). (a) Representative images of versican deposition by untreated treated CAFs, NFs and HDFs. (b) Representative images of versican deposition by TGFβ3 treated CAFs, NFs and HDFs. (c) Quantification of merged data from three biological replicates, and statistical analysis by Kruskal-Wallis test (*p<0.05, **p<0.01, ***p<0.001), of total versican fibre area deposited by untreated and TGFβ3 treated CAFs, NFs and HDFs. (d) Quantification of merged data from three biological replicates, and statistical analysis by Kruskal-Wallis test (**p<0.01), of versican large fibre index deposited by untreated and TGFβ3 treated CAFs, NFs and HDFs. All statistically significant results are shown. Nuclei were stained with Hoechst 33342. Scale bar = 50 µm. Maximum intensity projections of z-stacks are shown.*

3.6 Invasion assay optimisation with Kuramochi cells and Kuramochi-CAF co-cultures

3.6.1 Overview

The importance of a dense, fibrillar ECM within the TME for the migration and invasion of cancer cells is well documented in the literature. It is known that the formation of a stiff ECM, rich in proteins such as fibronectin and collagen I, plays a key role in cancer metastasis [349] [350] [351] [352] [353]. CAFs are believed to play a crucial part in the assembly and remodelling of ECM within the TME of many different cancer types [354] [355]. For example, CAF-mediated ECM remodelling can generate tracks that permit collective invasion of squamous cell carcinoma cells, ECM stiffening through CAF-secreted cross-linking enzymes can stimulate the invasion of gastric cancer cells, and fibronectin alignment by CAFs promotes prostate cancer cell invasion [356] [357] [358] [359]. In the context of HGSOC, whilst a number of CAF-derived ECM proteins, such as versican, have been shown to stimulate HGSOC cell line invasion, the capacity of HGSOC patient omentum derived CAFs to facilitate HGSOC cell invasion had not been previously investigated [347].

In order to evaluate whether CAFs from the HGSOC omental TME were able to stimulate the invasion of HGSOC cells, two different 3D invasion assays with CAFs and the Kuramochi HGSOC cell line were tested. The Kuramochi cell line was selected for use in invasion assays as work by others in the lab had highlighted their relatively low capacity for invasion when cultured alone in spheroids. Both assays made use of a collagen I hydrogel, and we hypothesised that the CAFs themselves would invade into this gel and remodel the ECM proteins within it, and/or deposit new ECM, in such a way that Kuramochi invasion would then be stimulated. Given the role of ascorbic acid in stimulating collagen I assembly by CAFs, it was included in the growth medium during both invasion assays tested.

3.6.2 Top-down invasion assays

Firstly, the effect of co-culturing Kuramochi cells with CAFs on Kuramochi invasion was evaluated using the top-down invasion assay approach. This involved adding a layer of collagen I hydrogel to the wells of a 96-well imaging plate, followed by the addition of GFP-expressing Kuramochi cells, either as a monoculture, or in co-culture with primary CAFs stained red with the PKH26 dye (Figure 3.10a). In co-cultures, CAFs occupied 25% of the total cell number at the time of cell seeding on to hydrogels. Kuramochi invasion down into the hydrogel was then visualised after 5 and 12 days in culture with confocal microscopy, where Z-sectioning was used to generate 3D reconstructions. Other members of the lab had found that Kuramochi invasion was minimal in the absence of added growth factors, such as EGF. In order to optimise the conditions for this assay, Kuramochi invasion was therefore monitored in the presence or absence of this growth factor. The top-down invasion assay highlighted that even when in co-culture with CAFs, which themselves were able to invade down into the hydrogel, and in the presence of EGF, Kuramochi cells displayed very little capacity for invasion after 5 days (Figure 3.10b). For this reason, cells were maintained in culture on the hydrogel for a longer time period. However, after 12 days, Kuramochi invasion was still not detected, and a considerable reduction in cell number was also observed, suggesting that cell death had occurred (Figure 3.10c). As sufficient invasion was not observed in any of the tested conditions, the 3D reconstructions were not analysed further. These results indicated that, in this type of invasion assay, CAF co-culture with Kuramochi cells did not stimulate cancer cell invasion.

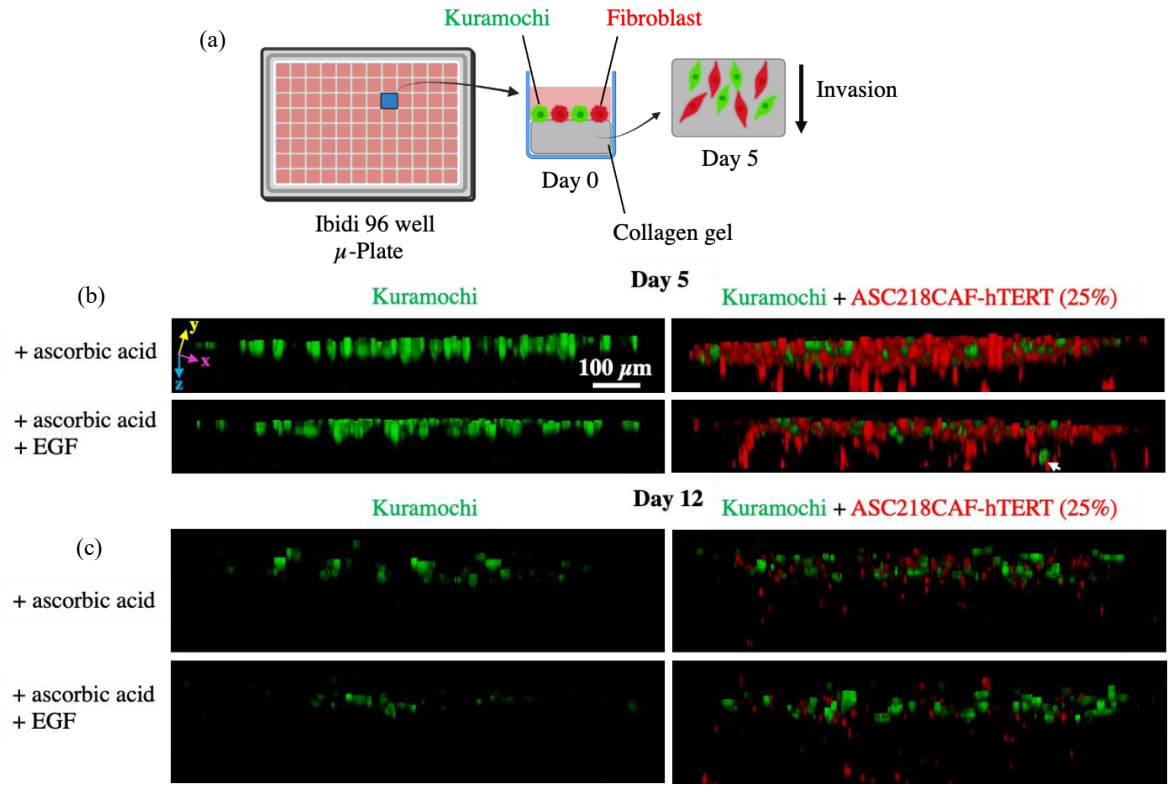

Figure 3.10 – CAFs do not stimulate Kuramochi invasion in top-down invasion assays

GFP-expressing Kuramochi cells, either as a mono-culture or in co-culture with primary CAFs stained red with PKH26, were seeded on to collagen I hydrogels within the wells of a 96-well imaging plate. Invasion in the presence of ascorbic acid (20 μg.mL^{-1}), with EGF present or absent from the RMPI medium, was visualised at day 5 and day 12 by fluorescence microscopy (n=2). (a) Schematic illustrating the top-down invasion assay. (b) Representative 3D reconstructions of Kuramochi and CAF invasion into the collagen I hydrogel at day 5 in the presence or absence of EGF. X, Y and Z axes are shown. White arrow is an example of an invading Kuramochi cell. (c) Representative 3D reconstructions of Kuramochi and CAF invasion into the collagen I hydrogel at day 12 in the presence or absence of EGF. Scale bar = 100 μm.

3.6.3 Spheroid invasion assay overview

The failure of CAFs to facilitate Kuramochi invasion in top-down invasion assays led to the testing and optimisation of the spheroid invasion assay approach. This assay has been used extensively in the study of cancer cell invasion, where cancer cells can be coaxed into forming a 3D spheroid which then becomes surrounded by an ECM-like hydrogel, creating conditions that somewhat mimic those found within a TME [360] [361] [362]. Spheroid invasion assays were carried out by forming spheroids consisting of either a Kuramochi mono-culture, or a Kuramochi-CAF co-culture, using the hanging drop method. A collagen I hydrogel was allowed to polymerise around the spheroids, recapitulating TME conditions where a tumour would be encapsulated by a 3D ECM. Spheroids were then imaged at day 0, where spheroids were inspected to ensure proper formation, and following culture for 4 days in medium containing ascorbic acid, spheroids were imaged to visualise invasion of Kuramochi cells out of the spheroids into the surrounding hydrogel (Figure 3.11a). Spheroid invasion assay data were analysed by measuring the area of cells that had invaded out from the spheroid (Figure 3.11b)

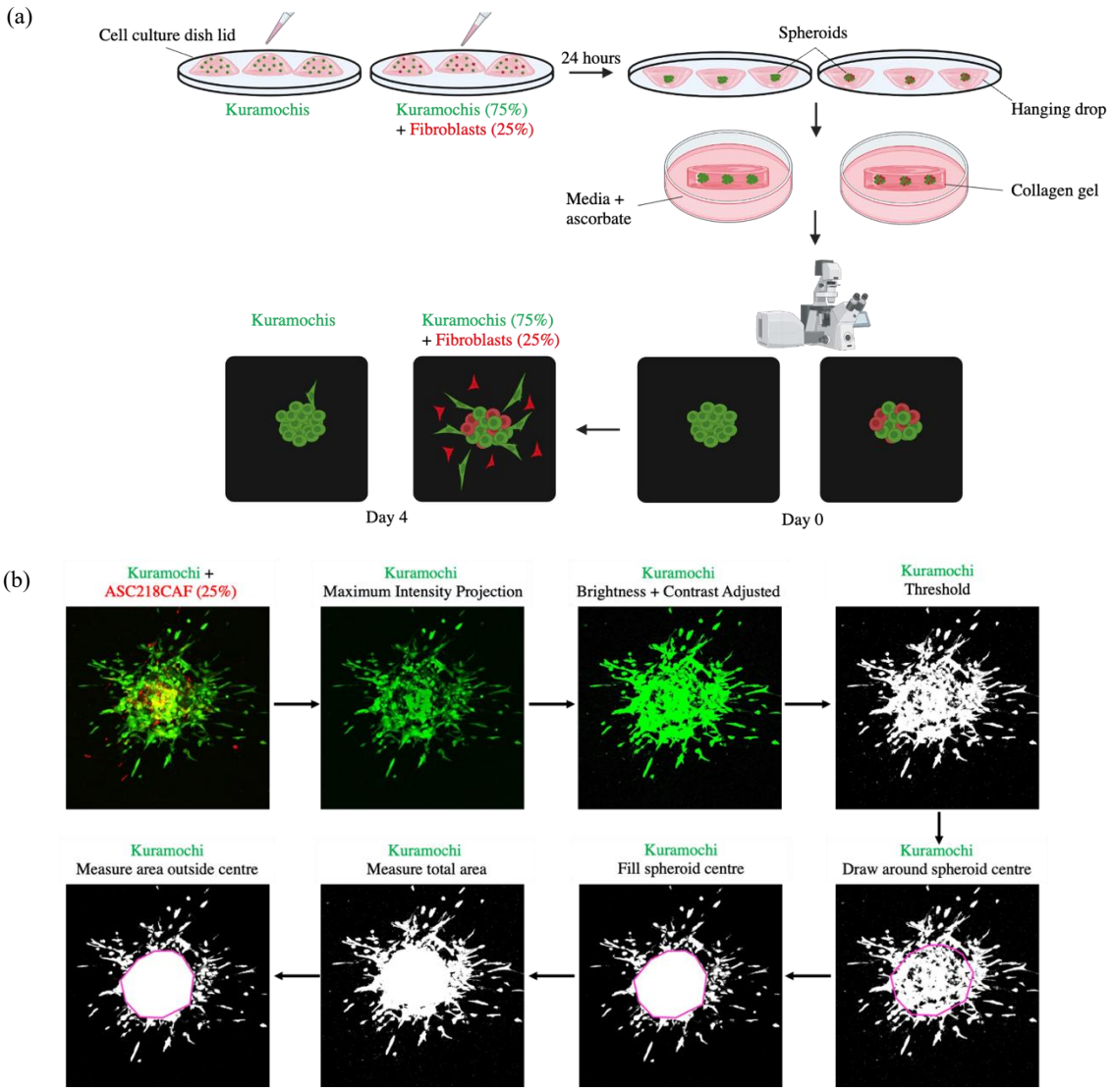

Figure 3.11 – Spheroid invasion assay schematic and image analysis

Spheroids were formed, using the hanging drop method, consisting of either a GFP-expressing Kuramochi cell mono-culture, or Kuramochi-CAF co-culture, where CAFs were stained red with PKH26. Spheroids were embedded into collagen I hydrogels (3 mg.mL^{-1}) and invasion at day 4 was visualised using fluorescence microscopy. (a) Schematic of the spheroid invasion assay protocol. (b) Summary of the spheroid invasion assay image analysis protocol. Images were analysed by firstly generating maximum intensity projections of z-sections from the Kuramochi channel. Images were then enhanced to ensure that all invading cells were clearly visible, and thresholded. The spheroid centre was then approximated and filled to ensure that any gaps in the spheroids central area did not impact upon the total cell area measured that was then measured. Finally, the cell area outside of this spheroid was measured, and invasion was measured as the percentage of invading cells relative to total cell area.

3.6.4 Spheroid invasion assay optimisation

The spheroid invasion assays further demonstrated the relatively limited capacity of Kuramochi mono-cultures to invade. However, in contrast to the top-down invasion approach, co-culture of CAFs with Kuramochi cells resulted in an increase in cancer cell invasion. During the initial optimisation phase of this approach, varying CAF numbers were added to the co-culture spheroids. Due to the lack of Kuramochi invasion observed previously using the top-down invasion assay, it was possible that these cells required EGF and HGF for invasion. These growth factors were therefore initially included in the culture medium. Whilst an increase in Kuramochi invasion was observed out of spheroids in which CAFs occupied 12.5% of the total cell number, this increase was not significant. Co-culture of Kuramochi cells and CAFs in spheroids, where CAFs occupied 25% of the total cell number, was sufficient to yield a significant increase in Kuramochi invasion (Figure 3.12a, 3.12b). In order to further optimise spheroid invasion assay conditions, the effect of including EGF and HGF in the culture medium was evaluated. As expected, EGF and HGF stimulated Kuramochi invasion. However, when CAFs were included in the spheroids, the increase in Kuramochi invasion measured was more statistically significant without these growth factors present (Figure 3.12c, 3.12d, 3.12e, 3.12f). This was likely due to the lower basal level of Kuramochi invasion observed with growth factors absent, allowing any increase in CAF-stimulated Kuramochi invasion to be detected more readily. As anticipated, these results demonstrated the ability of CAFs to enhance cancer cell invasion. Furthermore, these data indicated that the optimal conditions for spheroid invasion assays are those where EGF and HFG are absent from the culture medium, and where CAFs occupy 25% of the total cell number in spheroids.

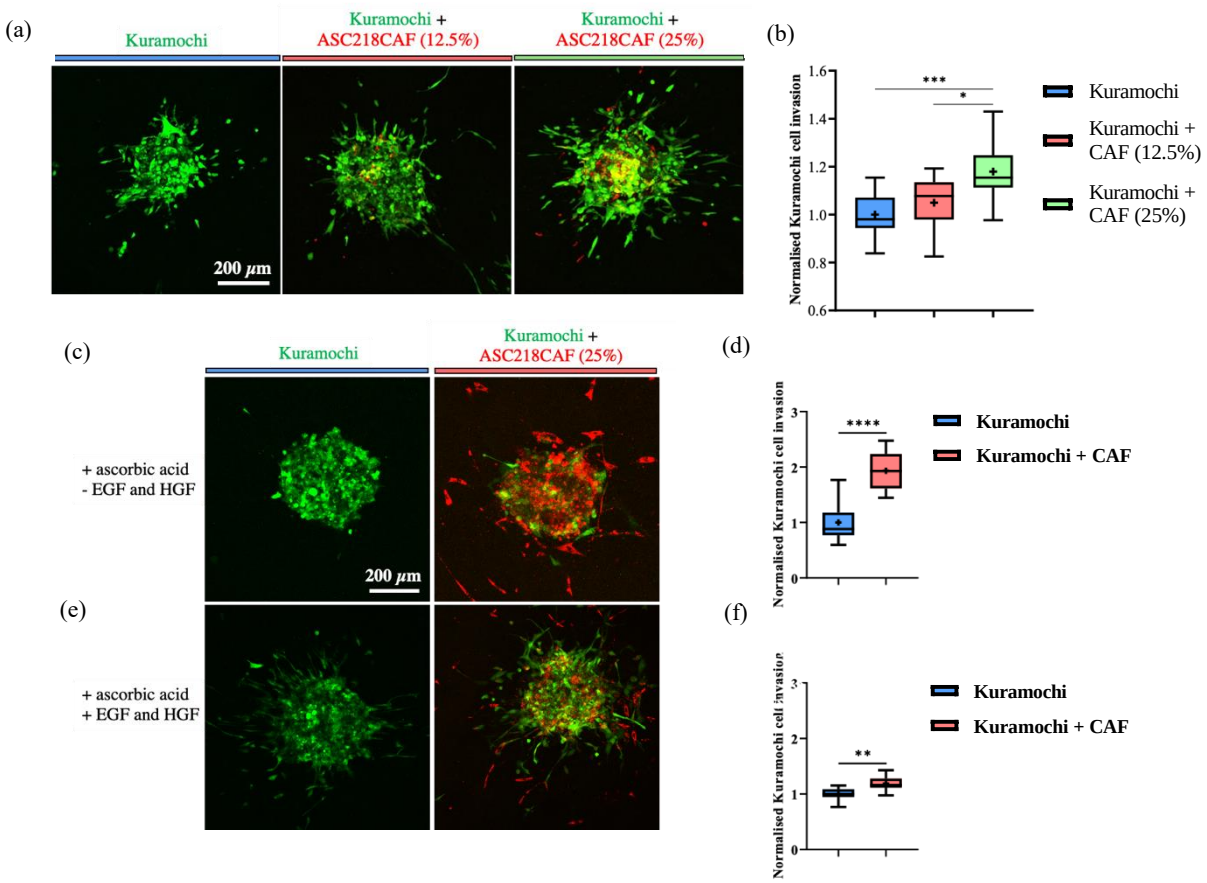

Figure 3.12 – CAFs stimulate the invasion of Kuramochi cells out of spheroids

*Spheroids were formed, using the hanging drop method as described previously, where GFP-expressing Kuramochi cells, and CAFs stained red with PKH26, were included in spheroids. Spheroids were then embedded into a collagen I (3 mg.mL^{-1}) hydrogel, and Kuramochi invasion after 4 days in culture in complete RPMI medium, containing ascorbic acid (20 µg. mL^{-1}, was visualised by fluorescence microscopy. Spheroid invasion assay optimisation was carried out by establishing the effect of CAF numbers within spheroids on Kuramochi invasion, as well the impact of including EGF (30 ng.mL^{-1}) and HGF (100 ng.mL^{-1}) in the growth medium (n=3). (a) Representative images of spheroids consisting of Kuramochis, or Kuramochis and CAFs (ASC218), with CAFs occupying 12.5% or 25% of the total cell number. (b) Quantification of merged data from three biological replicates, and statistical analysis by one-way ANOVA (*p<0.05, ***p<0.001), of Kuramochi invasion out of spheroids. (c) Representative images of spheroids consisting of Kuramochis, or Kuramochis and CAFs (ASC218; 25%). Images were captured after 4 days in culture without EGF and HGF in the growth medium.*

Figure legend continues on the next page.

Figure 3.12 – CAFs stimulate the invasion of Kuramochi cells out of spheroids

*(d) Quantification of merged data from three biological replicates, and statistical analysis by unpaired t-test (****p<0.0001), of Kuramochi invasion out of spheroids in the absence of EGF and HGF. (e) Representative images of spheroids consisting of Kuramochis, or Kuramochis and CAFs (ASC218; 25%). Images were captured after 4 days in culture with EGF and HGF in the growth medium. (f) Quantification of merged data from three biological replicates, and statistical analysis by unpaired t-test (**p<0.01), of Kuramochi invasion out of spheroids, in the presence of EGF and HGF. Normalised Kuramochi invasion values are shown, where the percentage of invading cells for each condition was normalised within each biological replicate by dividing by the average percentage for the Kuramochi monoculture spheroids. All statistically significant results are shown. Scale bars = 200 μm. Maximum intensity projections of z-stacks are shown.*

3.7 Spheroids invasion assays with Kuramochis and CAFs, NFs and HDFs

3.7.1 Overview

Following the optimisation of spheroid invasion assay conditions, it was important to understand the effect of fibroblast activation state on their ability to facilitate the invasion of Kuramochi cells out of the spheroids. To investigate this, 3D spheroid invasion assays were carried out with Kuramochis, either as a mono-culture, or in co-culture with CAFs, NFs or HDFs, where fibroblasts were grown in culture for 4 days prior to spheroid formation in the presence or absence of TGFβ3. Furthermore, in order to explore whether any fibroblast-facilitated invasion of Kuramochi cells was the result of ECM assembly/remodelling, or secretion of soluble factors, spheroid invasion assays with Kuramochi mono-cultures were also performed with culture medium conditioned by either untreated, or TGFβ3 pre-treated, fibroblasts.

3.7.2 Kuramochi-CAF co-culture spheroids

Spheroid invasion assays with Kuramochis and untreated, or TGFβ3 pre-treated, CAFs providing strong evidence in favour of fibroblast activation state impacting upon their capacity to stimulate cancer cell invasion. Alone, Kuramochis displayed a very minimal capacity to invade out of spheroids, and culture medium conditioned by untreated, or TGFβ3 pre-treated, CAFs was not able promote invasion (Figure 3.13a, 3.13b, 3.13d, 3.13f). The data described previously demonstrated that untreated CAFs were able to significantly increase Kuramochi invasion (Figure 3.12), however in these experiments, although untreated CAFs did increase Kuramochi invasion, this difference was not statistically significant (Figure 3.13c, 3.13f). A statistically significant increase in Kuramochi invasion was observed only when TGFβ3 pre-treated CAFs were included in spheroids (Figure 3.13e, 3.13f). These data demonstrated that fibroblast activation state does enhance their ability to stimulate cancer cell invasion as expected, and that the ability of CAFs to aid the invasion of Kuramochi cells is not mediated by secreted factors. Instead, these data suggested that CAFs primarily utilise a different mechanism to support cancer cell invasion, and we hypothesised that this mechanism may be through the assembly/remodelling of ECM. Furthermore, additional evidence supporting the use of TGFβ3 pre-treatment in downstream assays focused on understanding ECM assembly and remodelling by myofibroblast-like CAFs was provided.

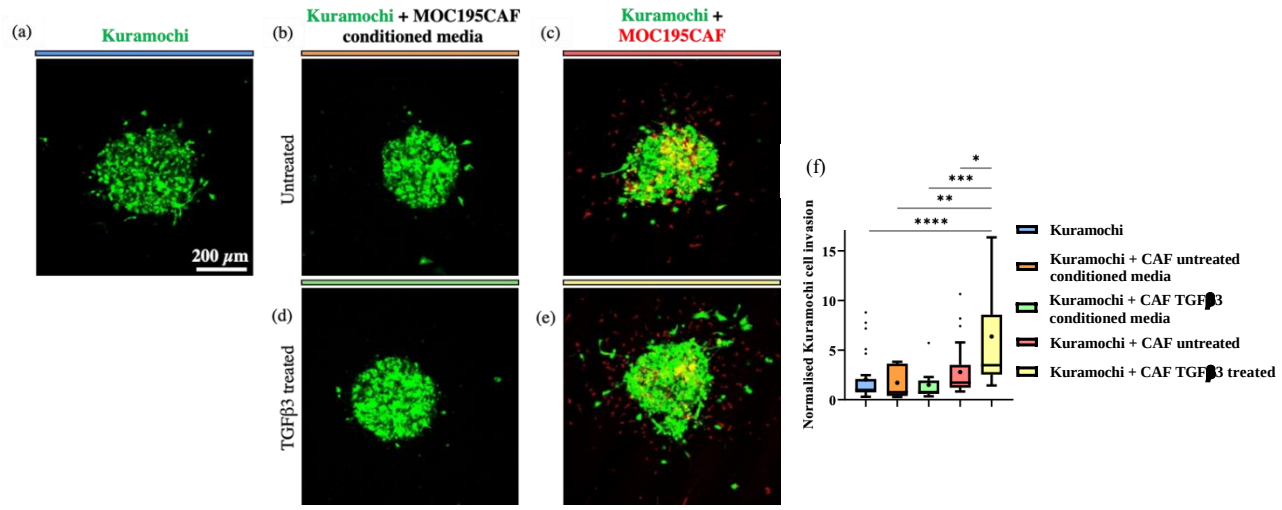

Figure 3.13 – TGFβ3 enhances the CAF-mediated stimulation of Kuramochi invasion

*Spheroids were formed, using the hanging drop method as described previously and embedded into a collagen I (3 mg.mL^{-1}) hydrogel. Spheroids consisted of either a GFP-expressing Kuramochi mono-culture, or a Kuramochi-CAF (MOC195) co-culture, where CAFs were stained red with PKH26. Kuramochi spheroids were cultured in complete RMPI medium, or complete RPMI medium conditioned by untreated, or TGFβ3 (10 ng.mL^{-1}) pre-treated, CAFs. Ascorbic acid was included in the growth medium (20 μg.mL^{-1}). Invasion after 4 days was visualised by fluorescence microscopy (n=3). (a) Representative image of a spheroid consisting of Kuramochi cells. (b) Representative image of a spheroid consisting of Kuramochi cells cultured in RMPI medium conditioned by untreated CAFs (MOC195). (c) Representative image of a spheroid consisting of Kuramochi cells and untreated CAFs (MOC195). (d) Representative image of a spheroid consisting of Kuramochi cells cultured in RMPI medium conditioned by TGFβ3 pre-treated CAFs (MOC195). (e) Representative image of a spheroid consisting of Kuramochi cells and TGFβ3 pre-treated CAFs (MOC195). (f) Quantification of merged data from three biological replicates, and statistical analysis by Kruskal-Wallis test (*p<0.05, **p<0.01, ***p<0.001,****p<0.0001), of Kuramochi invasion out of spheroids when in mono-culture in complete RMPI, or CAF conditioned RMPI, or in co-culture with CAFs. Normalised Kuramochi invasion values are shown, where the percentage of invading cells for each condition was normalised within each biological replicate by dividing by the average percentage for the Kuramochi monoculture spheroids. All statistically significant results are shown. Scale bars = 200 μm. Maximum intensity projections of z-stacks are shown.*

3.7.3 Kuramochi-NF co-culture spheroids

Whereas during these experiments, untreated CAFs were not able to stimulate Kuramochi invasion, untreated NFs were able to do so (Figure 3.14a, 3.14c, 3.14f). This stimulation was then enhanced following pre-treatment of NFs with TGFβ3 (Figure 3.14e, 3.14f). Growth medium conditioned by untreated NFs increased Kuramochi invasion to some extent, however this change was not significant, and TGFβ3 treated NF conditioned medium was not sufficient to stimulate invasion (Figure 3.14b, 3.14d, 3.14f). These results therefore support previous data suggesting that fibroblast activation state influences their capacity to stimulate cancer cell invasion, and that this stimulation of invasion is not through the secretion of soluble factors.

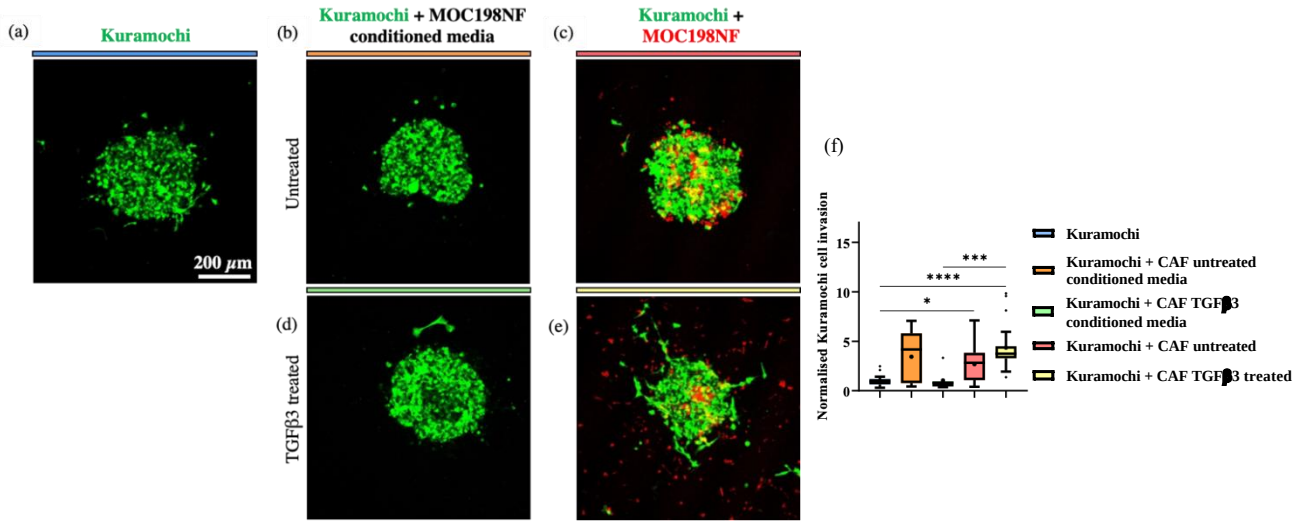

Figure 3.14 – TGFβ3 enhances the NF-mediated stimulation of Kuramochi invasion

*Spheroids were formed, using the hanging drop method as described previously and embedded into a collagen I (3 mg.mL^{-1}) hydrogel. Spheroids consisted of either a GFP-expressing Kuramochi mono-culture, or a Kuramochi-NF (MOC198) co-culture, where NFs were stained red with PKH26. Kuramochi spheroids were cultured in complete RMPI medium, or complete RPMI medium conditioned by untreated, or TGFβ3 (10 ng.mL^{-1}) pre-treated, NFs. Ascorbic acid was included in the growth medium (20 μg.mL^{-1}). Invasion after 4 days was visualised by fluorescence microscopy (n=3). (a) Representative image of a spheroid consisting of Kuramochi cells. (b) Representative image of a spheroid consisting of Kuramochi cells cultured in RMPI medium conditioned by untreated NFs (MOC198). (b) Representative image of a spheroid consisting of Kuramochi cells cultured in RMPI medium conditioned by untreated NFs (MOC198). (c) Representative image of a spheroid consisting of Kuramochi cells and untreated NFs (MOC198). (d) Representative image of a spheroid consisting of Kuramochi cells cultured in RMPI medium conditioned by TGFβ3 pre-treated NFs (MOC198). (e) Representative image of a spheroid consisting of Kuramochi cells and TGFβ3 pre-treated NFs (MOC198). (f) Quantification of merged data from three biological replicates, and statistical analysis by Kruskal-Wallis test (*p<0.05, ***p<0.001,****p<0.0001), of Kuramochi invasion out of spheroids when in mono-culture in complete RMPI, or NF conditioned RMPI, or in co-culture with NFs. Normalised Kuramochi invasion values are shown, where the percentage of invading cells for each condition was normalised within each biological replicate by dividing by the average percentage for the Kuramochi monoculture spheroids. All statistically significant results are shown. Scale bars = 200 μm. Maximum intensity projections of z-stacks are shown.*

3.7.4 Kuramochi-HDF co-culture spheroids

Invasion assays with Kuramochis and untreated, or TGFβ3 treated, HDFs provided interesting results. Whilst fibroblast activation with TGFβ3 treatment of CAFs and NFs elevated their capacity to stimulate Kuramochi invasion, this treatment did not have the same effect on HDFs. Medium conditioned by untreated, or TGFβ3 treated, HDFs did not promote Kuramochi invasion out of spheroids, as was expected given the results generated with CAFs and NFs (Figure 3.15a, 3.15b, 3.15d, 3.15f). Co-culture of Kuramochis with untreated HDFs did not stimulate invasion out of spheroids, and in contrast to the results obtained with CAFs and NFs, TGFβ3 treatment of HDFs was also insufficient to promote Kuramochi invasion (3.15c, 3.15e, 3.15f).

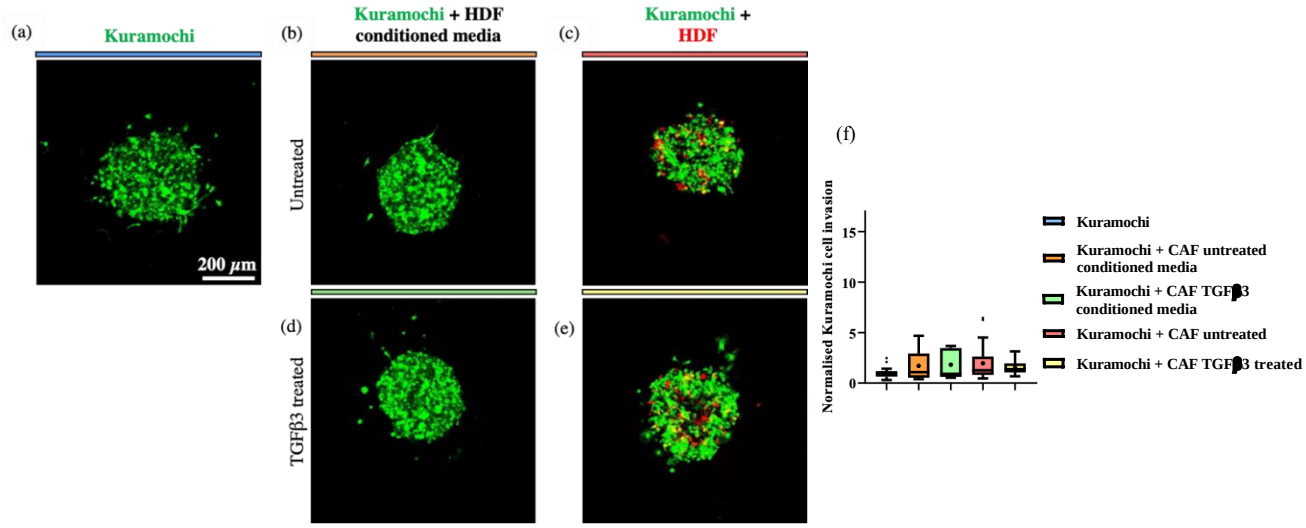

Figure 3.15 – HDFs are unable to facilitate Kuramochi invasion

Spheroids were formed, using the hanging drop method as described previously and embedded into a collagen I (3 mg.mL^{-1}) hydrogel. Spheroids consisted of either a GFP-expressing Kuramochi mono-culture, or a Kuramochi-HDF co-culture, where HDFs were stained red with PKH26. Kuramochi spheroids were cultured in complete RMPI medium, or complete RPMI medium conditioned by untreated, or TGFβ3 (10 ng.mL^{-1}) pre-treated, HDFs. Ascorbic acid was included in the growth medium (20 μg.mL^{-1}). Invasion after 4 days was visualised by fluorescence microscopy (n=3). (a) Representative image of a spheroid consisting of Kuramochi cells. (b) Representative image of a spheroid consisting of Kuramochi cells cultured in RMPI medium conditioned by untreated HDFs. (b) Representative image of a spheroid consisting of Kuramochi cells cultured in RMPI medium conditioned by untreated HDFs. (c) Representative image of a spheroid consisting of Kuramochi cells and untreated HDFs. (d) Representative image of a spheroid consisting of Kuramochi cells cultured in RMPI medium conditioned by TGFβ3 pre-treated HDFs. (e) Representative image of a spheroid consisting of Kuramochi cells and TGFβ3 pre-treated HDFs. (f) Quantification of merged data from three biological replicates, and statistical analysis by Kruskal-Wallis test, of Kuramochi invasion out of spheroids when in mono-culture in complete RMPI, or HDF conditioned RMPI, or in co-culture with HDFs. Normalised Kuramochi invasion values are shown, where the percentage of invading cells for each condition was normalised within each biological replicate by dividing by the average percentage for the Kuramochi monoculture spheroids. All statistically significant results are shown. Scale bars = 200 μm. Maximum intensity projections of z-stacks are shown.

3.8 Collagen gel contraction assays with CAFs, NFs and HDFs

3.8.1 Overview

The findings from spheroid invasion assays suggested that CAF and NF pre-treatment with TGFβ3 enhanced their ability to facilitate cancer cell invasion, and that this effect was not mediated via the secretion of soluble factors. We hypothesised that the observed effect was instead due to changes in their capacity for ECM assembly and/or remodelling. Previous results demonstrated that TGFβ3 treatment activated fibroblasts, increasing their expression of CAF biomarkers, including SMA (Figure 3.2). The remodelling of existing ECM by myofibroblasts is known to depend upon their contractility. As SMA stress fibres are contractile in nature, it was possible an increase in fibroblast contractility was responsible for the enhanced Kuramochi invasion observed when in co-culture with TGFβ3 pre-treated fibroblasts. In order to determine whether the observed differences in the Kuramochi invasion-promoting capacity of fibroblasts in response to TGFβ3 treatment was due to changes in their contractility alone, collagen gel contraction assays were carried out, and contractility was then correlated with their ability to promote invasion.

3.8.2 The effect of TGFβ3 treatment on collagen gel contraction by CAFs, NFs and HDFs

Collagen gel contraction assays with untreated, or TGFβ3 pre-treated, CAFs, NFs and HDFs, were used to determine whether TGFβ3 pre-treatment altered the ability of each fibroblast type to contract collagen gels. When monitoring collagen gel size, gels containing CAFs pre-treated with TGFβ3 became slightly smaller in area over time than those containing untreated CAFs, however this difference was not statistically significant (Figure 3.16a, 3.16b). Furthermore, NF pre-treatment with TGFβ3 did not result in a greater reduction in gel size over 4 days (Figure 3.16c, 3.16d). Similarly, the reduction in the area of gels containing HDFs over the 4-day time period was not impacted by pre-treatment of HDFs with TGFβ3 (Figure 3.16e, 3.16f). This, to some extent, was expected given that this treatment did not render HDFs capable of promoting Kuramochi invasion (Figure 3.15). The inability of TGFβ3 treatment to enhance fibroblast contractility was surprising in that previously, an increase in SMA expression, which is associated with contraction, was observed following this treatment (Figure 3.2). To establish whether fibroblast contractility correlated with their ability to facilitate Kuramochi invasion, Pearson's correlation analysis was used to determine the relationship between data from spheroid invasion assays and collagen gel contraction assays. This analysis revealed that a correlation did not exist between the invasion promoting properties of fibroblasts and their contractility, suggesting that the increase in Kuramochi invasion observed following CAF and NF pre-treatment with TGFβ3 was not due to these fibroblasts gaining contractility (Figure 3.16g).

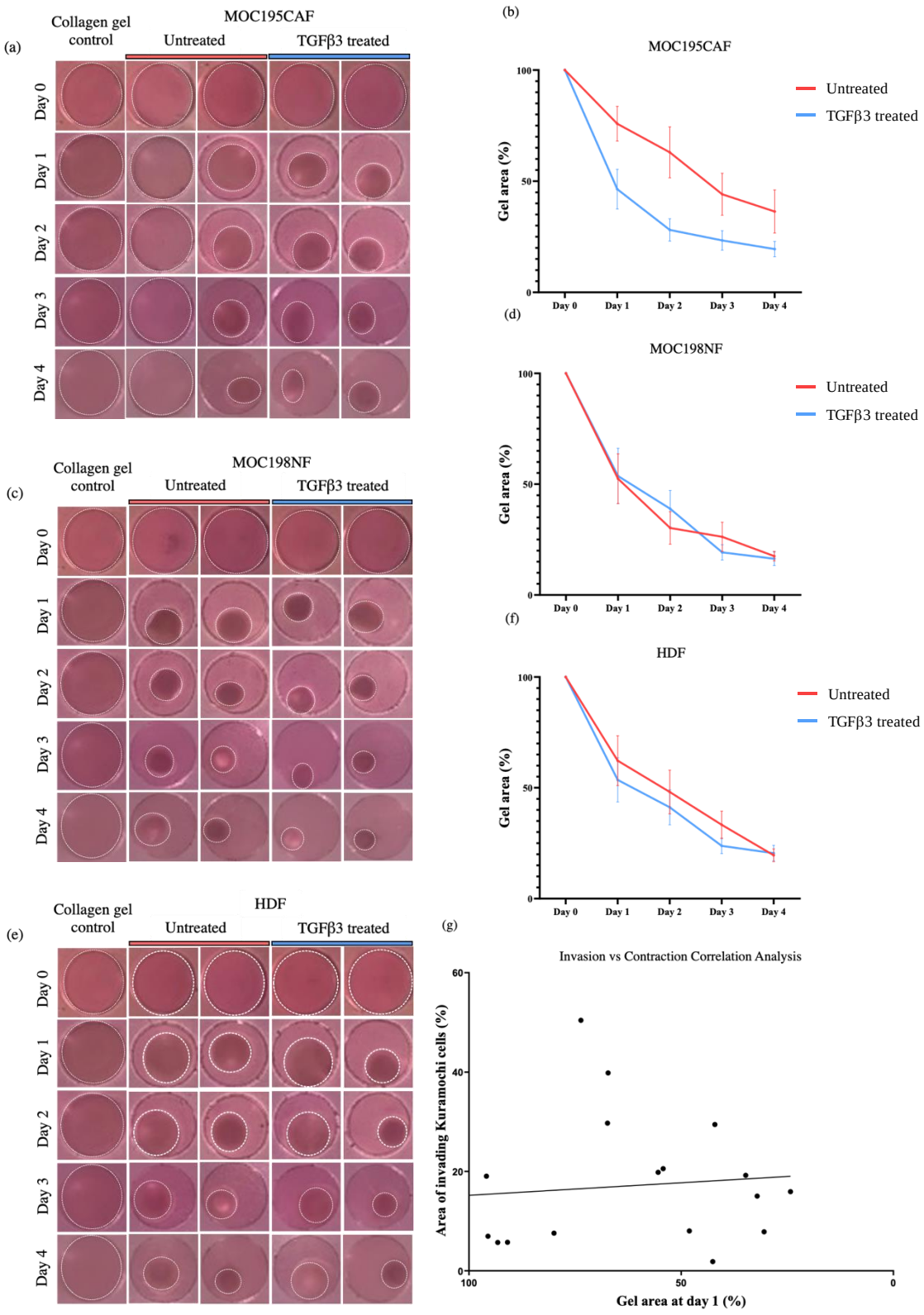

Figure 3.16 – TGFβ3 pre-treatment does not increase fibroblast contractility

Figure legend on the next page.

Figure 3.16 – TGFβ3 pre-treatment does not increase fibroblast contractility

Collagen gel contraction assays were carried out with untreated, or TGFβ3 pre-treated, CAFs, NFs and HDFs present in the gel to determine whether this treatment altered fibroblast contractility (n=4). Fibroblasts were suspended in a collagen I hydrogel mix (2 mg.mL^{-1}), which was allowed to polymerise around them. Images of the gels were captured on days 0, 1, 2, 3 and 4. Fibroblast contractility was calculated by measuring the reduction in gel area over time. (a) Representative images of hydrogels containing untreated, or TGFβ3 pre-treated, CAFs (MOC195), at day 0, 1, 2, 3 and 4. (b) Quantification of merged data from four biological replicates, and statistical analysis by two-way ANOVA, of collagen gel contraction by untreated, or TGFβ3 pre-treated, CAFs (MOC195). (c) Representative images of hydrogels containing untreated, or TGFβ3 pre-treated, NFs (MOC198), at day 0, 1, 2, 3 and 4. (d) Quantification of merged data from four biological replicates, and statistical analysis by two-way ANOVA, of collagen gel contraction by untreated, or TGFβ3 pre-treated, NFs (MOC198). (e) Representative images of hydrogels containing untreated, or TGFβ3 pre-treated, HDFs, at day 0, 1, 2, 3 and 4. (f) Quantification of merged data from four biological replicates, and statistical analysis by two-way ANOVA, of collagen gel contraction by untreated, or TGFβ3 pre-treated, HDFs. (g) Pearson's correlation analysis using all collagen gel contraction assay data and spheroid invasion assay data for CAFs, NFs and HDFs.

3.9 Discussion and conclusions

The results in this chapter demonstrate the characterisation of HGSOC patient omentum derived-CAFs, both in terms of CAF biomarker expression, and capacity for carrying out known CAF functions such as ECM assembly and promoting cancer cell invasion.

3.9.1 Heterogeneity in CAF biomarker expression

The evaluation of CAF biomarker expression revealed that SMA, FAP and collagen XI were expressed homogeneously between all populations of isolated CAFs, however heterogeneity existed in the expression of SMA and collagen XI within each population (Figure 3.1). This heterogeneity was to be expected given that multiple CAF subtypes are thought to exist within a TME, including those which exert either stimulatory or inhibitory effects on tumour development [363]. An explanation for this heterogeneity is that it may reflect the different precursor cell types from which CAFs in the omentum can be derived, as well as the different HGSOC cell-secreted factors involved in reprogramming non-malignant cell types into CAFs [364]. It is likely that inherent differences exist between the CAF-like functions that CAFs derived from different cell types can carry out. For example, NFs and MSCs in the omentum can be reprogrammed into CAFs through HGSOC-cell derived TGFβ, and exosomes, respectively [149] [150]. TGFβ and exosomes secreted by HGSOC cells have been shown to activate TGFβ receptor signalling in these non-malignant cell types to generate CAFs with myofibroblast-like properties. However, the extent of this signalling may differ depending on the factor responsible for its activation. CAFs generated by TGFβ-mediated reprogramming of NFs may be more activated and display higher levels of SMA expression relative to their MSC-derived counterparts. Furthermore, isolation of CAFs from tumour-burdened omentum samples withdraws HGSOC-cell derived factors responsible for maintaining CAF-like phenotypes. The heterogeneity observed here may reflect the extent to which these CAFs were originally activated, and myofibroblast-like in nature, prior to debulking surgery. Those which were initially in close proximity to the tumour would have been exposed to higher concentrations of factors that maintain the CAF phenotype, and may be able to retain this phenotype, and high SMA expression, in culture despite withdrawal of these factors during isolation.

3.9.2 CAF biomarker expression in CAFs, NFs and HDFs with TGFβ3 treatment

The investigation of how fibroblast activation state impacted upon the expression of SMA, FAP and collagen XI, in CAFs, NFs, and HDFs, generated interesting findings. The treatment of all three fibroblast types was sufficient to increase their expression levels of SMA and collagen XI (Figure 3.2, 3.3). These data agree with work carried out by Delaine-Smith et al. highlighting how TGFβ3, as the primary TGFβ isoform secreted by HGSOC cells, is capable of elevating expression of SMA in omental fibroblasts [159]. In addition, and in agreement with these findings, work by others has also demonstrated that treatment of immortalised mesenchymal cells from bone barrow with TGFβ1 was able to elevate expression of the *COL11A1* gene, measured by RT-qPCR [365]. Whilst others have observed relatively low levels of FAP in primary omental fibroblasts, which could then be elevated following TGFβ3 treatment, these findings could not be replicated during this project due to the high basal levels of FAP expression observed prior to TGFβ3 treatment [159].

Surprisingly, although SMA expression in HDFs was low prior to TGFβ3 treatment, CAFs and NFs expressed SMA at moderate and comparable levels (Figure 3.2a). As SMA is an established biomarker of activated, myofibroblast-like CAFs, it was presumed that expression levels would be higher in CAFs relative to NFs. One possible explanation for these similarities in SMA levels, is that SMA expression in the CAFs when grown in culture, may in fact be reduced compared to the levels found in CAFs still present within the omental TME. Isolation of CAFs from the omentum sample, and therefore also from the vicinity of the HGSOC tumour in that sample, would withdraw a whole host of tumour-derived signalling molecules from the CAFs that act to maintain them in a CAF-like state. Alternatively, isolated NFs may instead have increased levels of SMA expression. Work by others has demonstrated the impact of substrate stiffness on fibroblast activation, where growth on a stiffer substrate activates fibroblasts and elevates SMA expression [366]. As NFs were grown on a stiffer substrate in cell culture flasks, compared to a relatively softer substrate found within the omentum, this could have driven them towards a more activated fibroblast state. However, comparing SMA expression between these two fibroblast populations, and the non-omentum derived primary HDFs, suggested that growth on a stiff substrate in culture was insufficient to elevate SMA expression levels to those found in CAFs and NFs (Figure 3.2). These results indicate that growth on a stiff substrate alone is not sufficient to explain the elevated SMA levels detected in NFs. An alternative explanation for the high SMA

expression in NFs, may be due to the patients from which NFs were isolated often having some other form of cancer, such as early-stage endometrial cancer. It is possible that the increased SMA levels were due to the pre-metastatic niche priming that can occur. As in the case of endometrial cancer, changes in the stromal cell composition of the omentum have been shown to occur prior to the arrival of cancer cells, possibly through exosomes that are known to be secreted by endometrial cancer cells [367] [368].

Despite others observing relatively low FAP expression in primary omental CAFs prior to TGFβ3 treatment, FAP expression was high in all three fibroblast types regardless of TGFβ3 treatment [159]. The high basal levels of expression then rendered TGFβ3 incapable of further elevating expression (Figure 3.3). It is possible that NF and HDF growth on the stiff substrate of a cell culture flask may contribute towards their activation and therefore elevated FAP expression levels to some extent. However, a more plausible explanation is that FAP is not as CAF-specific as is suggested in the literature, although it is also possible that the antibody itself may lack specificity, with the absence of a clear plasma membrane localisation supporting this [369]. Others have observed similar staining patterns using this antibody, as well as other antibodies that bind FAP, where localisation at the plasma membrane was not detected [370] [371]. This suggests that a lack of antibody specificity for FAP is not accountable for the staining patterns displayed by CAFs, NFs and HDFs. These results indicate instead that FAP may be a relatively poor CAF biomarker, and that it should be used with caution for the characterisation of omentum derived CAFs in the future.

3.9.3 CAF dependency on ascorbic acid for collagen I biosynthesis

As mentioned previously, the absence of the GLO enzyme in human cells led us to hypothesise that primary omental CAFs required the addition of ascorbic acid for collagen I deposition [341]. However, assessing the dependency of CAFs on ascorbic acid for this process highlighted that, whilst ascorbic acid enhanced collagen I assembly, it was not essential, and CAFs were able to deposit collagen I to some extent in its absence (Figure 3.4). These data confirmed the stimulatory effect of ascorbic acid on collagen I fibrillogenesis by human fibroblasts [372]. However, this finding also raises questions regarding the necessity of ascorbic acid for collagen I synthesis and deposition by human cells. There is a lack of evidence in the literature supporting the existence of pathways in human cells that allow for collagen I synthesis and secretion in the absence of ascorbic acid. It is not yet known whether the ability to deposit collagen I in an ascorbic acid independent manner is specific to CAFs, and further experiments investigating the dependence of CAFs, NFs and HDFs, on ascorbic acid for collagen I assembly will shed light on this.

3.9.4 ECM protein deposition by CAFs, NFs and HDFs with TGFβ3 treatment

Firstly, ECM protein deposition experiments provided additional evidence in support of the heterogeneity that can exist between CAF populations isolated from separate HGSOC patient omentum samples. Despite the TGFβ3 treated CAFs used for the comparison of ECM protein deposition by CAFs, NFs and HDFs (MOC195) being cultured under the same conditions as CAFs used previously to investigate their dependency on ascorbic acid for collagen I deposition (MOC194), noticeable differences in the amount of collagen I deposited were observed. CAFs from isolate MOC195 (Figure 3.6a) were far more competent in collagen I assembly than those from isolate MOC194 (Figure 3.4a, 3.4b, 3.4c), further highlighting the heterogeneity that can exist between CAF populations.

Secondly, it was clear that as well as affecting CAF biomarker expression, fibroblast activation state also impacted upon ECM protein assembly in 2D culture. The measurement of total collagen I fibre area demonstrated that CAFs and NFs were more proficient in collagen I assembly than HDFs regardless of TGFβ3 treatment, despite this treatment elevating SMA expression to comparable levels between each fibroblast type (Figure 3.2, 3.6). This suggested that fibroblast activation, through driving SMA expression via TGFβ3 treatment alone, was insufficient to induce high levels of collagen

I deposition by fibroblasts in 2D. The omentum derived CAFs and NFs likely possess additional properties in their activated state, as well as high SMA expression levels, that allow the excessive deposition of collagen I in the omentum. Delaine-Smith et al. demonstrated that treatment of primary omental fibroblasts with TGFβ3 elevated their deposition of collagen I in 2D culture [159]. However, the data presented in this chapter indicated that treatment of CAFs, NFs, or HDFs, with this growth factor did not increase the amount of collagen deposited under these conditions (Figure 3.6). This finding suggests that despite the activation of CAFs and NFs observed following TGFβ3 treatment, as shown by the increase in SMA expression, they may have already reached their maximum capacity for collagen I fibrillogenesis in 2D culture prior to TGFβ3 addition.

Measuring the large fibre indices of collagen I deposited by CAFs, NFs and HDFs, in the presence or absence of TGFβ3, revealed a significant decrease in the large fibre index of collagen I deposited by HDFs following TGFβ3 treatment. Whilst the large fibre index of the collagen I deposited by CAFs remained constant regardless of TGFβ3 treatment, a decrease in large fibre index, although not statistically significant, was observed following treatment of NFs with this growth factor (Figure 3.6). These findings may allude to how the overall architecture of collagen ECM evolves during the assembly of complex matrices over time. It is possible that thin, but long, collagen I fibres are deposited in the extracellular space initially, such as those assembled by untreated HDFs (Figure 3.6a). This could then be followed by the incorporation of these fibres into a meshwork, such as that assembled by TGFβ3 treated HDFs (Figure 3.6b). These fibres, once incorporated, would evade detection by the ridge detection algorithm, explaining the significant reduction in large fibre index upon HDF treatment with TGFβ3. Subsequently, larger fibres may then be assembled and deposited on top of this meshwork, to generate the type of complex ECM assembled by untreated, or TGFβ3 treated, CAFs and NFs. Future experiments focussed on collagen I assembly by untreated, and TGFβ3 treated, CAFs, NFs and HDFs, over a longer time period, and with multiple time points, should reveal in more detail how the composition of the ECM assembled by these fibroblast types changes over time.

Surprisingly, despite fibronectin levels increasing in the omentum with tumour progression, analysis of fibronectin deposition by CAFs, NFs, and HDFs, revealed that after 10 days in culture, the untreated, and TGFβ3 treated, NFs deposited the most fibronectin, with lower levels deposited by CAFs and HDFs (Figure 3.7) [98]. Importantly, a high total fibronectin fibre area, or large fibre index, does not necessarily correspond to a more stable, mature ECM that is rich in collagen I. For example, during wound healing it is thought that a fibronectin and fibrin rich, provisional ECM is initially formed. This provisional ECM is then thought to mature, via the stimulation of collagen I deposition mediated by fibronectin, followed by the degradation of this fibronectin to allow for the generation of a more stable, collagen I-rich ECM [373] [374]. It is therefore possible that after 10 days in culture, a CAF-derived ECM consisting of relatively low levels of fibronectin may have undergone this maturation process at a faster rate than an ECM that remains rich in fibronectin after this time period. Taking into consideration that a fibronectin-rich, provisional ECM is thought to be replaced by a more mature ECM rich in collagen I, these results, together with the analysis of collagen I deposition by CAFs, may give some insight into how the matrix changes in composition and organisation over time. It is possible that whist the ECM assembled by CAFs after 10 days in culture was relatively low in fibronectin, it may in fact be the most mature ECM assembled by the three fibroblast types. Given that untreated and TGFβ3 treated CAFs were able to assemble large amounts of collagen I (Figure 3.6a, 3.6b), it is possible that the majority of fibronectin assembled by them had already been degraded and replaced with collagen I ECM after 10 days in culture. This is also supported by data from HDFs, which assembled minimal amounts of collagen (Figure 3.6a, 3.6b), but were able to deposit fibronectin with a relatively high total fibre area and large fibre index (Figure 3.7a, 3.7b). However, data from NFs suggests otherwise, where the ECM assembled by these fibroblasts over 10 days in culture contained both high amounts of collagen I and fibronectin (Figure 3.6a, 3.6b, 3.7a, 3.7b). One possible explanation for these findings is that the NFs may have assembled an ECM of intermediate maturity, where whilst large amounts of collagen I are present, the fibronectin rich-provisional ECM has not yet been degraded. Further experiments measuring the deposition of fibronectin, in combination with collagen I, over time, and with multiple time points, will be required to understand in greater detail how the fibrillogenesis of these two major ECM proteins is coordinated by each fibroblast type to assemble complex, mature matrices.

Collagen XI and versican have been implicated previously in the stimulation of ovarian cancer cell invasion, and both are upregulated in HGSOC tumour burdened omentum, with an increase in their levels also correlating with poor prognosis [346] [347] [98]. As a regulator of the nucleation of collagen fibrillogenesis, it is possible that within the HGSOC metastatic TME, high levels of collagen XI may allow CAFs to control ECM assembly, such that HGSOC-supportive matrices are assembled [206] [207] [209]. Although versican has a known role in generating provisional ECMs in a variety of contexts, the increase in versican levels in the omentum with HGSOC progression, and its ability to support OC cell invasion, suggests a more persistent role for versican in the HGSOC TME [348] [375] [376] [347]. For example, its possession of binding sites for various other ECM proteins enables their incorporation into the ECM, enabling ECM maturation, and it may be that high versican levels in the omentum enable the formation of the dense, fibrillar ECM associated with the HGSOC TME [228].

Measuring collagen XI deposition by CAFs, NFs, and HDFs, in the presence or absence of TGFβ3, indicated the amounts of collagen XI deposited by fibroblasts in 2D culture did not correlate with fibroblast activation state (Figure 3.8). A reduction in collagen XI deposition was observed following treatment of NFs with TGFβ3, which was surprising given the increase in collagen XI expression following TGFβ3 treatment observed previously (Figure 3.3d, 3.3e). This may suggest that collagen XI was initially deposited to nucleate collagen I fibrillogenesis, then degraded and replaced by additional collagen I over their time in culture [96]. However, the differences in collagen I assembly between untreated CAFs and HDFs observed previously (Figure 3.6a, 3.6c), together with their comparable levels of collagen XI deposition (Figure 3.8a, 3.8c), instead suggest that collagen XI is not replaced by collagen I in 2D culture. Similarly, the amount of versican deposited also did not correlate with fibroblast activation state (Figure 3.9). An increase in total versican fibre area was measured following treatment of each fibroblast with TGFβ3, however this increase was not statistically significant.

These results therefore somewhat contradict data presented by others, where both collagen XI and versican have been shown to increase in omental abundance with HGSOC progression [98]. However, a possible explanation for these discrepancies is that CAFs likely display different functional capabilities when present in a 3D environment compared to when cultured in 2D. It has been established for some time that many different cell types, including fibroblasts, behave differently depending on whether they are cultured in 2D or in 3D systems [377]. For example, Sung et al. demonstrated that

human mammary fibroblasts, when cultured in 3D, displayed elevated expression levels of a number of factors that stimulate breast cancer cell invasion relative to their expression levels in 2D culture [378]. It is therefore possible that omental CAFs may only deposit large amounts of collagen XI and versican in response to TGFβ3 when cultured in 3D systems that model the microenvironment within the HGSOC TME. Further experiments will be required to investigate how the deposition of collagen XI and versican by CAFs changes in response to activation by TGFβ3 in 3D culture systems.

3.9.5 Spheroid invasion assays

Spheroid invasion assays were used to investigate the ability of fibroblasts to enhance Kuramochi invasion in a 3D culture system. Optimisation of these assays revealed that omentum derived CAFs were able to facilitate the invasion of Kuramochi cells out of spheroids into the surrounding gel. This increase in invasion was most significant when CAFs occupied 25% of the total cell number within spheroids, and when spheroids were cultured in the presence of ascorbic acid, but in the absence of EGF and HGF (Figure 3.12). The treatment of omental CAFs and NFs with TGFβ3 enhanced their ability to facilitate Kuramochi invasion, however, HDFs remained incapable of promoting invasion despite this treatment. These results suggested that, to some extent, fibroblast activation state increases their ability to promote cancer cell invasion, where higher levels of Kuramochi invasion were observed when in co-culture with TGFβ3 pre-treated CAFs, or NFs. However, despite TGFβ3 treated CAFs, NFs and HDFs expressing CAF biomarkers at comparable levels (Figure 3.2, 3.3), differences existed in the ability of these activated fibroblasts to promote Kuramochi invasion. TGFβ3 pre-treated HDFs remained incapable of assisting cancer cell invasion, suggesting that fibroblast activation through TGFβ3 treatment alone is insufficient to drive fibroblast-stimulated cancer cell invasion (Figure 3.15). Omentum derived CAFs and NFs may therefore possess additional properties that allow them to enhance invasion.

Furthermore, carrying out these invasion assays with fibroblast conditioned media clearly demonstrated that the effects of fibroblasts on Kuramochi invasion were not mediated via the secretion of fibroblast-derived soluble factors (Figure 3.13, 3.14, 3.15). This is in contrast to previous results reported in the literature. Media conditioned by myofibroblasts has been shown to stimulate colon cancer cell invasion, and the proliferation, migration, and invasion of the SKOV3 OC cell line was enhanced by ovarian CAF-secreted FGF-1 [379] [380] [381]. These results therefore further highlight the heterogeneity that can exist in CAF behaviour within TMEs of different cancer types, but also within a given cancer type such as OC. However, one possible explanation for the discrepancy between results previously reported in the literature and those obtained in spheroid invasion assays, is that the fibroblasts used were not omentum-derived. Instead, CAFs were isolated from ovarian samples, and it may be that CAFs present within ovarian TME's differ in properties and functional capabilities from those present in the HGSOC omental TME. With ovarian CAFs, whilst also likely able to assemble and remodel ECM, their tumour-promoting properties may rely more heavily on growth factor secretion. In contrast, CAFs within the omentum could primarily use ECM assembly and remodelling to exert their pro-tumourigenic effects.

3.9.6 Collagen gel contraction assays

As the stimulatory effect of TGFβ3 treated CAFs and NFs on Kuramochi invasion was not mediated by the secretion of soluble factors, we hypothesised that these fibroblasts enhanced OC cell invasion through ECM protein assembly/remodelling. It was important to determine whether TGFβ3 treatment rendered CAFs and NFs more capable of supporting Kuramochi invasion through elevating their deposition of new ECM proteins, and/or their ability to contract and remodel existing ECM proteins. To determine whether TGFβ3 treatment enhanced fibroblast contractility, collagen gel contraction assays were carried out, and the relationship between contractility and invasion promoting capacity was investigated.

These assays demonstrated that TGFβ3 treatment of all three fibroblast types did not significantly increase their contractility, and that contractility did not correlate with an increased ability to promote Kuramochi invasion out of spheroids. Although remodelling of existing ECM proteins can occur independently of cell contractility, these data indicate that the way in which omental CAFs predominantly facilitate cancer cell invasion is not through the contraction-mediated pulling/remodelling of the existing ECM. These findings contradict data presented by others demonstrating the importance of contractility in ECM deposition/remodelling by fibroblasts, and in the CAF-mediated facilitation of cancer cell invasion [382] [383]. It is possible that this ability to support OC cell invasion in a contraction-independent manner may be specific to CAFs present in the HGSOC metastatic TME. Additional experiments will be required to determine whether this property is omental CAF-specific, for example collagen gel contraction and spheroid invasion assays with fibroblasts associated with other cancer types may be carried out in the presence or absence of TGFβ3.

As the increased ability of CAFs and NFs to stimulate Kuramochi invasion following TGFβ3 treatment did not correlate with cell contractility, and did not require soluble factor secretion, we hypothesised that these stimulatory effects following fibroblast activation were mediated via the deposition of new ECM proteins, such as collagen I. However, previous analyses of collagen I deposition by CAFs and NFs following TGFβ3 treatment indicated that, in 2D culture, TGFβ3 treatment did not significantly increase collagen I assembly in CAFs and NFs relative to their untreated counterparts. As fibroblasts are known to behave differently depending on whether they are grown in 2D culture or in 3D systems, this may explain these findings [377] [378]. In 2D culture, CAF and NF treatment with TGFβ3 may not stimulate collagen I deposition to the same extent as that when these fibroblasts are cultured in 3D spheroids. Further experiments will be required to investigate how fibroblast activation through TGFβ3 treatment impacts upon ECM protein deposition by CAFs in 3D culture systems.

3.9.7 Summary

To summarise, the results in this chapter indicate that fibroblasts isolated from HGSOC patient omentum samples are CAF-like in nature, where they assemble ECM proteins such as collagen I and fibronectin, and also facilitate cancer cell invasion. TGFβ3 treatment was able to push otherwise heterogeneous CAF populations towards displaying a more homogeneous, myofibroblast-like phenotype, and downstream experiments aiming to investigate the mechanisms of ECM assembly by myofibroblast-like CAFs utilised treatment with this growth factor.

Furthermore, following consideration of the results presented in this chapter, it remained possible that TGFβ3 treated CAFs and NFs stimulated Kuramochi invasion in 3D culture through depositing new ECM proteins, and/or remodelling existing ECM proteins via contraction-independent mechanisms. The remaining experiments carried out during this project aimed to investigate the molecular mechanisms involved in enabling TGFβ3 treated CAFs to deposit and/or remodel ECM proteins in order to support Kuramochi invasion.

Chapter 4: An siRNA screen to identify endocytic recycling regulators required for CAFs to assemble ECM and facilitate HGSOC cell invasion

4.1 Overview

CAFs are known to play a key role within the TMEs of many different cancer types, where they are thought to support a number of the processes required for tumour development, including cancer cell invasion [384] [357]. One aspect of the TME that is believed to impact upon the invasion of cancer cells, and therefore also on metastasis, is the ECM [385]. Whilst many cell types within TMEs can remodel the ECM, for example cancer cells can degrade the ECM via MMP secretion, CAFs are the primary cell type responsible for ECM deposition and remodelling [386] [158].

The mechanisms involved in ECM assembly and remodelling by fibroblasts in a healthy context, such as during development, are understood to some extent. For example, the intra- and extracellular processes involved in the secretion of collagen I and its assembly into fibres have been studied extensively and are now relatively well understood [200]. Furthermore, ECM proteins such as fibronectin, which can interact with other components of the ECM, now have established roles in allowing complex 3D matrices to be generated [220]. However, there are many cellular processes with underappreciated roles in ECM assembly, such as those involved in endocytic recycling. Endocytic recycling pathways and a number of small GTPases that regulate them, have been implicated in ECM assembly in a variety of contexts, including in the vascular morphogenesis that occurs during development [321]. However, the importance of these endocytic recycling pathways, and the small GTPases that regulate them, in ECM assembly and remodelling by CAFs within the microenvironment of different cancers has not yet been investigated.

Once it had been established that primary omental CAFs were capable of firstly facilitating the invasion of Kuramochi cells out of spheroids, and secondly assembling ECM proteins such as collagen I and fibronectin, it was essential to determine which endocytic recycling regulator GTPases were required for CAFs to carry out these functions. In order to investigate the roles of endocytic recycling both in ECM assembly, and in the facilitation of cancer cell invasion by CAFs, an siRNA screening approach was used.

For the siRNA screen, small GTPases implicated in endocytic recycling regulation were grouped according to how closely related they were to one another, based on the Rab family evolutionary tree presented by Klöpper [387]. HGSOC patient derived CAFs, activated by TGFβ3 pre-treatment, were transfected with siRNAs targeting each endocytic recycling regulator GTPase. The mRNA levels of each target GTPase were depleted individually, and in cases where other closely related GTPases of the same sub-family may compensate for target GTPase loss, multiple siRNAs were also used in combination, for example in the case of Rab11a and Rab11b. Following confirmation of GTPase mRNA depletion by RT-qPCR, transfected CAFs were then used in three separate assays. Firstly, spheroid invasion assays with Kuramochi cells were used to determine which GTPases were essential for CAFs to facilitate cancer cell invasion. Secondly, the effect of recycling regulator depletion on the assembly of endogenously synthesised collagen I and fibronectin was investigated using immunofluorescence microscopy. Finally, the requirement of the each GTPase for CAFs to assemble exogenous, fluorophore-labelled, fibronectin into fibres was explored by fluorescence microscopy (Figure 4.1).

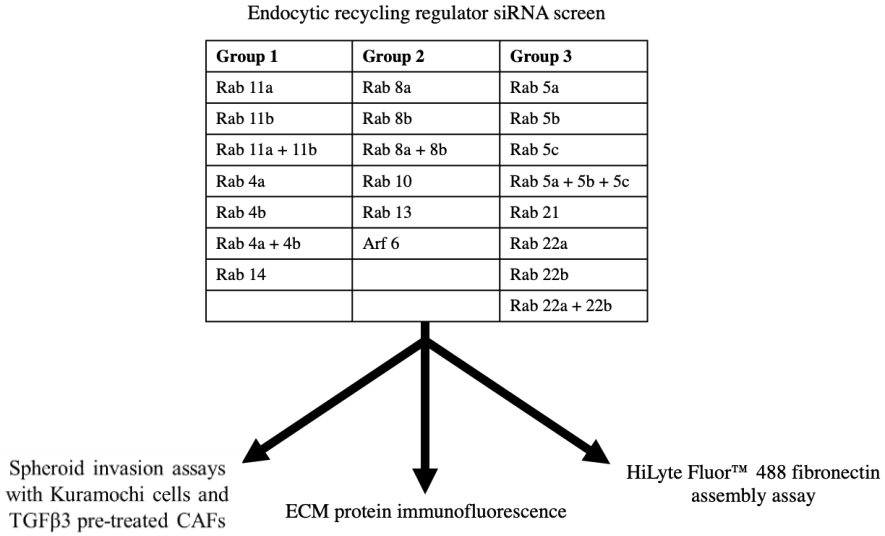

Figure 4.1 – Summary of the endocytic recycling regulator siRNA screening approach

Endocytic recycling regulator GTPases were grouped according to the Rab family evolutionary tree presented by Klöpper [387]. *Each GTPase was depleted individually, or in combination to account for compensation of depleted protein function by closely related proteins. Transfected CAFs were then used in three separate assays: Spheroid invasion with Kuramochi cells, collagen I and fibronectin immunostaining after 10 days in culture, and exogenous fibronectin assembly assays.*

4.2 Measurement of endocytic recycling regulator expression in CAFs

4.2.1 Overview

Human cells express endocytic recycling regulator small GTPases at varying levels [388]. In order to ensure that downstream screening experiments focussed only on those GTPases expressed in primary CAFs, RT-qPCR was used to measure the expression levels of 18 different regulators of endocytic recycling. The expression levels of small GTPases involved in regulating fast recycling, such as Rab4a and Rab4b, and slow recycling, such as Rab11a, Rab11b, and Arf6, were measured. In addition, the expression levels of small GTPases involved in other aspects of endocytic recycling, such as Rab13, Rab21, and Rab5a, Rab5b, and Rab5c, were also measured [389] [390] [391] [392].

4.2.2 Endocytic recycling regulator expression in CAFs

Firstly, the expression of 14 small GTPases was measured in two populations of CAFs isolated from HGSOC patient omentum. In both CAF lines, Rabs 10, 11a, 13 and 14, were the most highly expressed, with Rabs 4a, 4b, 8a, 8b, 11b, 22a, 22b and Arf6, expressed at lower, but measurable, levels. Expression of Rab25 and Rab35 was not detected in either CAF line (Figure 4.2a, 4.2b). Following the initial expression level measurements of these small GTPases in CAFs from patient samples MOC166 and ASC218, the expression levels of Rabs 5a, 5b, 5c and 21 were measured in a CAF line isolated from a third patient sample, MOC195. These data demonstrated that all 4 of these GTPases were expressed in CAFs, with Rab5c expressed at the highest level (Figure 4.2c).

Taken together, these RT-qPCR results indicated that most endocytic recycling regulator GTPases were expressed to some extent by CAFs derived from HGSOC patient omentum samples. In the downstream screening experiments that aimed to determine which recycling regulators were of importance in building the HGSOC metastatic niche, the levels of each of these regulators were depleted. As the expression of Rabs 25 and 35 could not be detected in CAFs, these proteins were not included in downstream experiments.

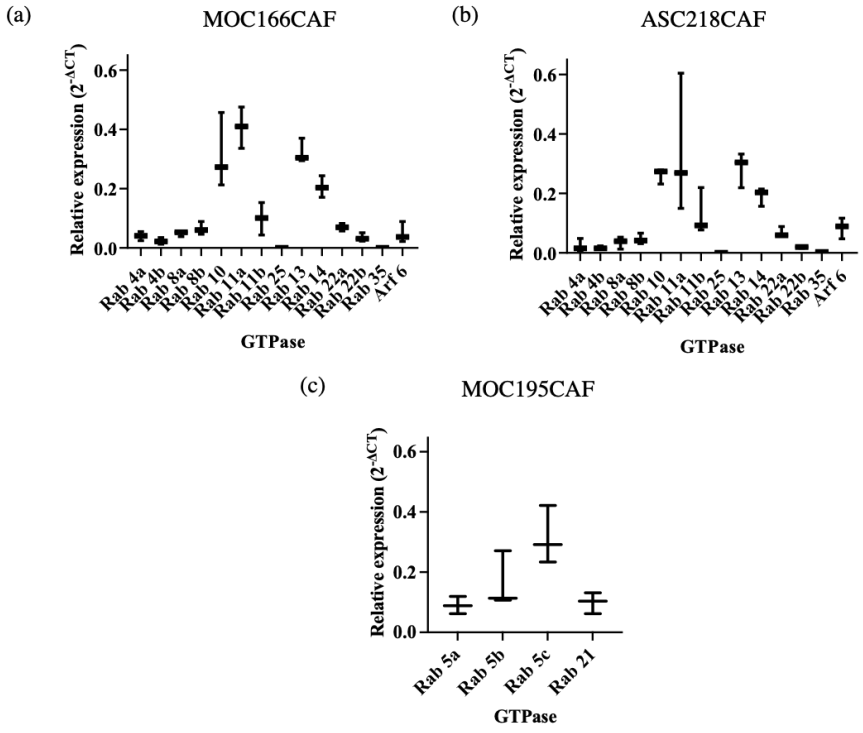

Figure 4.2 – Primary omental CAFs do not express Rab25 or Rab35

RT-qPCR was used to measure the expression levels of 18 different small GTPases implicated in various aspects of endocytic recycling (N = 3). RNA was firstly extracted from CAFs grown in culture for a minimum of 4 days, then the mRNA was converted to cDNA by reverse transcription. qPCR analysis was used to measure expression levels of each small GTPase, and GAPDH, in triplicate. The average expression level of each GTPase, and that of GAPDH, were used to calculate ΔCT values. The relative expression levels were then calculated, where relative expression = $2^{-\Delta CT}$. (a) Relative expression levels of Rabs 4a, 4b, 8a, 8b, 10, 11, 11b, 25, 13, 14, 22a, 22b, 35 and Arf6, in CAFs derived from omentum sample MOC166, from three biological replicates. (b) Relative expression levels of Rabs 4a, 4b, 8a, 8b, 10, 11, 11b, 25, 13, 14, 22a, 22b, 35 and Arf6, in CAFs derived from omentum sample ASC218, from three biological replicates. (c) Relative expression levels of Rabs 5a, 5b, 5c and 21, in CAFs derived from sample MOC195, from three biological replicates.

4.3 Optimisation of gene silencing techniques

4.3.1 Overview

Once it had been established which regulators of endocytic recycling were expressed by omental CAFs, it was essential to identify the most effective method of depleting their levels in order to later determine which of them were required for CAFs to build the metastatic HGSOC TME. Two separate gene silencing techniques were tested: CRISPR-cas9 and RNAi.

4.3.2 CRISPR-Cas9

With the aim of generating a collection of primary CAF lines in which each recycling regulator GTPases had been knocked out, the LentiCRISPR version of CRISPR-cas9 technology was tested by trialling the capacity of a Rab11a targeting guide RNA (Rab11a-gRNA) to deplete protein levels. Following the transduction of CAFs either with the empty Lenti-CRISPRv2 vector, or with this vector containing a sequence encoding the Rab11a-gRNA (Rab11a-LentiCRISPRv2), CAFs were subjected to selection with puromycin for at least one week. Importantly, due to the slow growth rate of primary fibroblasts, it was decided that transduced cells would not be clonally expanded. It was highly unlikely that a single cell would give rise to a population of a large enough size for use in downstream experiments, and as such, cells remained as a mixed population. The levels of the Rab11a protein present in each CAF population were then assessed by western blotting 1 day after the selection period. As expected, a clear reduction in the levels of Rab11a was observed in CAFs transduced with Rab11a-LentiCRISPRv2 relative to those transduced with the empty vector (Figure 4.3a). However, unfortunately, the assessment of Rab11a protein levels 14 days after the selection period revealed that Rab11a levels in CAFs transduced with Rab11 a-LentiCRISPRv2 were comparable to those transduced with the empty vector (Figure 4.3b). These results suggested that whilst this gene silencing technique may have led to a relatively significant reduction in the levels of Rab11a in CAFs initially, this reduction was not maintained over time in culture. It was likely that due to cells remaining as a mixed population, transduced cells were outcompeted and outgrown by their non-transduced counterparts over time, resulting in a population which overall expressed Rab11a at normal levels.

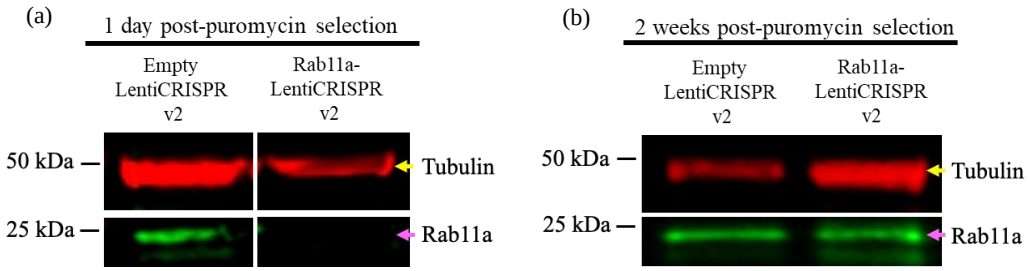

Figure 4.3 – CRISPR-cas9 technology was ineffective in Rab11a gene silencing

The effectiveness of using CRISPR-cas9 technology to silence Rab11a expression was tested by firstly cloning a Rab11a-gRNA encoding sequence into the Lenti-CRISPRv2 vector. The empty vector, and the vector containing Rab11a-gRNA, were used to transfect HEK293T cells. The viral particles generated following this transfection were used to transduce CAFs (MOC195), and transduced cells were selected for using puromycin (0.75 µg.mL^{-1}) treatment for 7-8 days. The levels of the Rab11a protein were assessed by western blotting using anti-Rab11a (Rab11a MW = 25 kDa; magenta arrow indicates Rab11a band) and anti-α-tubulin (Tubulin MW = 50 kDa; yellow arrow indicates Tubulin band) antibodies. (a) Western blot from one biological replicate showing Rab11a and α-tubulin protein levels in CAFs (MOC195) transduced with the empty Lenti-CRISPRv2 vector, or Rab11a-LentiCRISPRv2, 1 day after the puromycin selection period (images shown from non-adjacent lanes on the same western blot). (b) Western blot from one biological replicate showing Rab11a and α-tubulin protein levels in CAFs (MOC195) transduced with the empty Lenti-CRISPRv2 vector, or Rab11a-LentiCRISPRv2, 14 days after the puromycin selection period.

4.3.3 RNAi optimisation

Following the failure of CRISPR-cas9 to generate a mixed population of CAFs in which Rab11a protein levels were reduced, the RNAi approach of gene silencing was tested using siRNA. To initially test this approach, CAFs were transfected with siRNAs targeting Rab11a or Rab11b. Due to the problems that can be encountered when attempting to transfect primary cells, transfection of these siRNAs into primary CAFs was carried out using either Lipofectamine™ 2000 (lipofectamine) or Fuse-It-siRNA (fuse-it) transfection reagents [393]. Whilst both reagents operate via the formation of liposomes that encapsulate siRNA, they differ in their method of entry into the cell. Whereas lipofectamine uses endocytosis to enter, Fuse-It-siRNA enters via membrane fusion. Furthermore, the efficiency of transfection and subsequent knockdown by these siRNAs was also tested in HDFs, which were in included as a non-omental, primary cell control. Protein levels following transfection were assessed by western blotting on day 5 and day 10 post-transfection. As the downstream ECM assembly and spheroid invasion assays would be carried out over time frames ranging from 5 to 11 days, it was essential to ensure that gene silencing by these siRNAs was maintained over the majority of this period.

It was expected that primary CAFs and HDFs would be difficult to transfect with lipofectamine, given the levels of toxicity that are generally believed to be associated with this reagent [394]. However, lipofectamine was, in fact, very effective in depleting the levels of both Rab11a and Rab11b in CAFs and HDFs. Clearly visible reductions in the levels of both Rab11 isoforms were observed at day 5, and levels remained reduced at day 10 post-transfection (Figure 4.4a, 4.4b). Fuse-it on the other hand, despite the low levels of toxicity associated with this reagent, was less effective in reducing the levels of Rab11a and Rab11b in both CAFs and HDFs. When protein levels were assessed on day 5, Rab11a and Rab11b levels in cells transfected with their corresponding siRNAs were reduced relative to those in cells transfected with a non-silencing control siRNA (NS siRNA). However, at day 10 post-transfection, the levels of both Rab11 isoforms were comparable to those in cells transfected with the NS siRNA (Figure 4.4a, 4.4b)

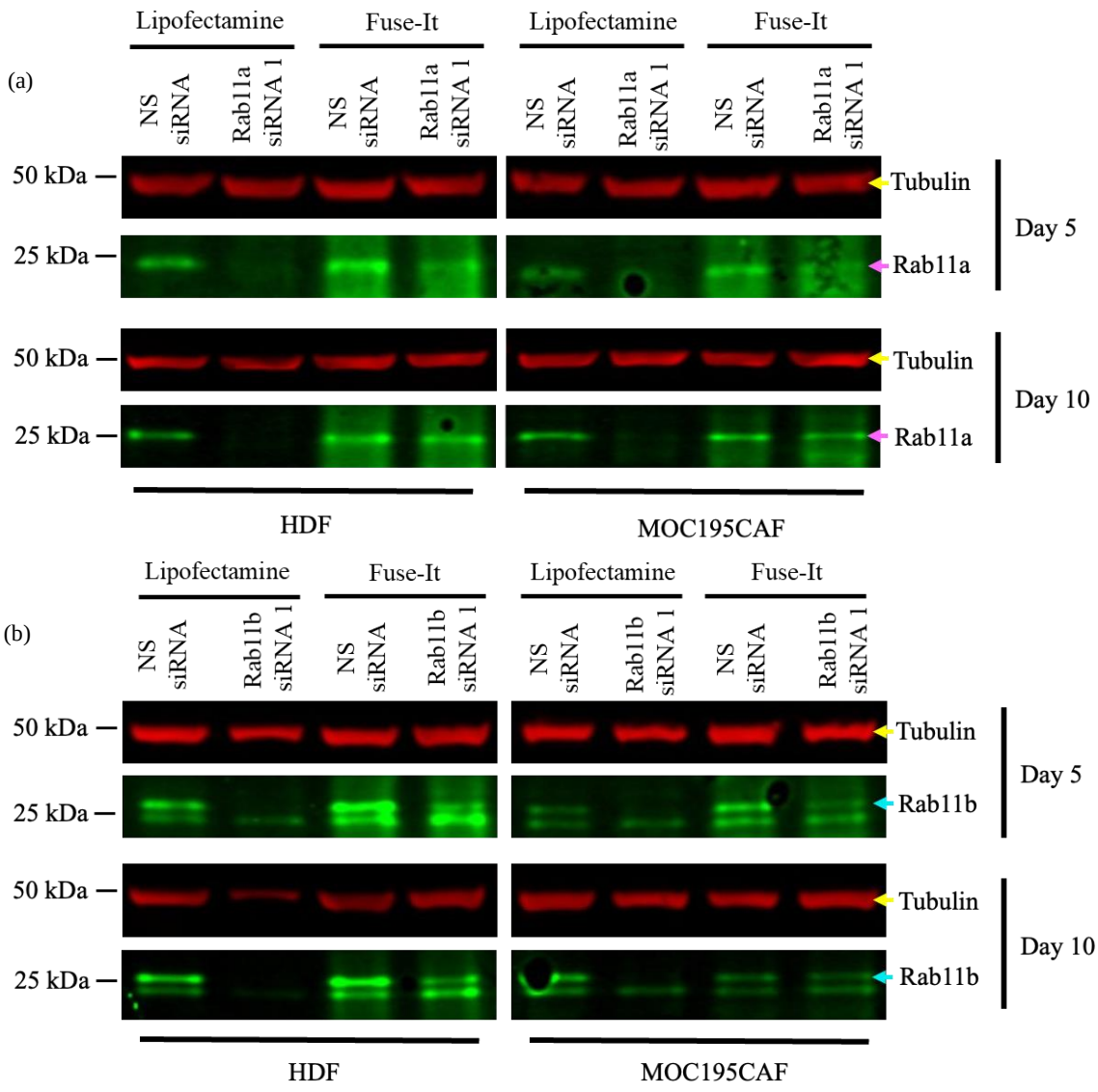

Figure 4.4 – Rab11a and Rab11b protein levels can be depleted for 10 days using Lipofectamine™ 2000

CAFs (MOC195) and HDFs were transfected either with the NS siRNA, or siRNA targeting Rab11a (Rab11a siRNA 1) or Rab11b (Rab11b siRNA 1; 80 nM), using either lipofectamine or fuse-it transfection reagents. Cell lysates were collected at day 5 and day 10 post-transfection, and western blotting with anti-Rab11a (Rab11a MW = 25 kDa; magenta arrow indicates Rab11a band), anti-Rab11b (Rab11b MW = 25 kDa, cyan arrow indicates Rab11b band), and anti-α-tubulin (Tubulin MW = 50 kDa; yellow arrow indicates Tubulin band), was used to evaluate knockdown efficiencies (N = 1). Anti-Rab11b recognises both Rab11 isoforms, the larger MW band corresponds to Rab11b.

Figure legend continues on the next page.

Figure 4.4– Rab11a and Rab11b protein levels can be depleted for 10 days using Lipofectamine™ 2000

(a) Western blot from one biological replicate highlighting that Rab11a depletion is more efficient when using lipofectamine compared with fuse-it, demonstrated by reduced protein levels in lysates collected from cells transfected with Rab11a siRNA 1 at day 5 and day 10 post-transfection, compared with those transfected with NS siRNA. (b) Western blot from one biological replicate highlighting that Rab11b depletion is more efficient when using lipofectamine compared with fuse-it, demonstrated by reduced protein levels in lysates collected from cells transfected with Rab11b siRNA 1 at day 5 and day 10 post-transfection, compared with those transfected with NS siRNA.

4.3.4 Efficiency of endocytic recycling regulator depletion with siRNA

The results obtained during the optimisation of protein level depletion strategies suggested that the use of siRNA, transfected into cells with lipofectamine, was the most efficient method of achieving a significant depletion in the levels of Rab11a, or Rab11b, for a minimum of 10 days. In order to confirm that the levels of all endocytic recycling regulators of interest could be depleted to a similar extent using this technique, primary omental CAFs were transfected with siRNA oligos targeting each small GTPase. For each GTPase of interest, the efficiencies of 2-3 different siRNA oligos in depleting protein levels were tested, including that for second siRNA oligos targeting Rab11a and Rab11b, with mRNA levels measured via RT-qPCR at day 2 and day 8 post-transfection. It was important to ensure that for each small GTPase, at least 2 different siRNA oligos were able to efficiently reduce protein levels, as any positive results in downstream screening experiments with one siRNA oligo (siRNA 1) would require validation using a second siRNA oligo (siRNA 2) against the same target. The testing of all siRNA oligos targeting each recycling regulator revealed that all were capable of depleting the mRNA levels of their corresponding targets. RT-qPCR demonstrated that the mRNA levels of each GTPase in cells transfected with GTPase targeting siRNA oligos were reduced at day 2 relative to cells transfected with the NS siRNA. These levels then remained reduced in cells at day 8 post-transfection (Figure 4.5). Per target, the two siRNA oligos that were most effective in depleting target protein levels were then taken forward for use in downstream screening experiments.

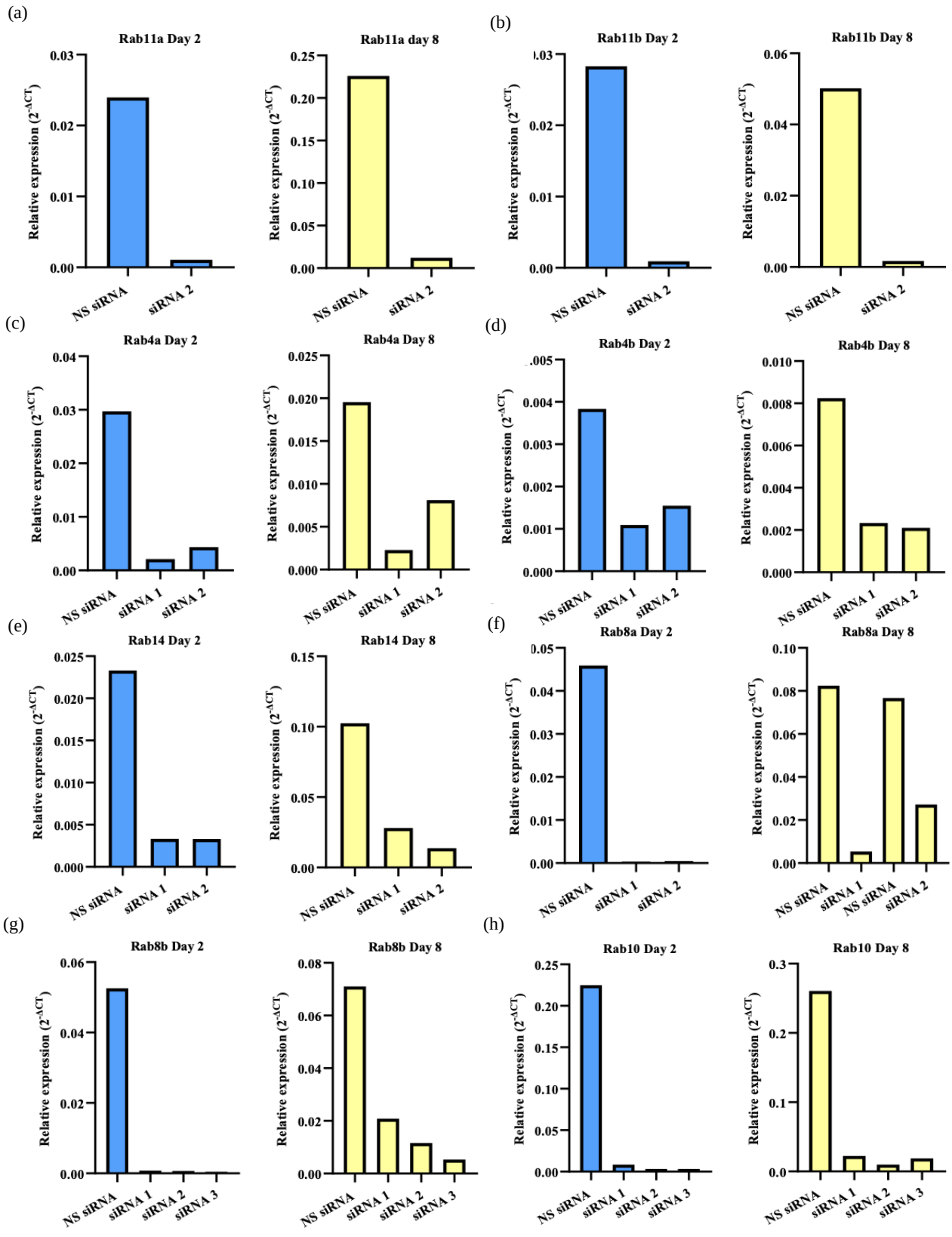

Figure 4.5 – Lipofectamine transfection of all siRNA oligos tested was sufficient to reduce mRNA levels each endocytic recycling regulator at day 2 and day 8 post-transfection

Figure continues on the next page.

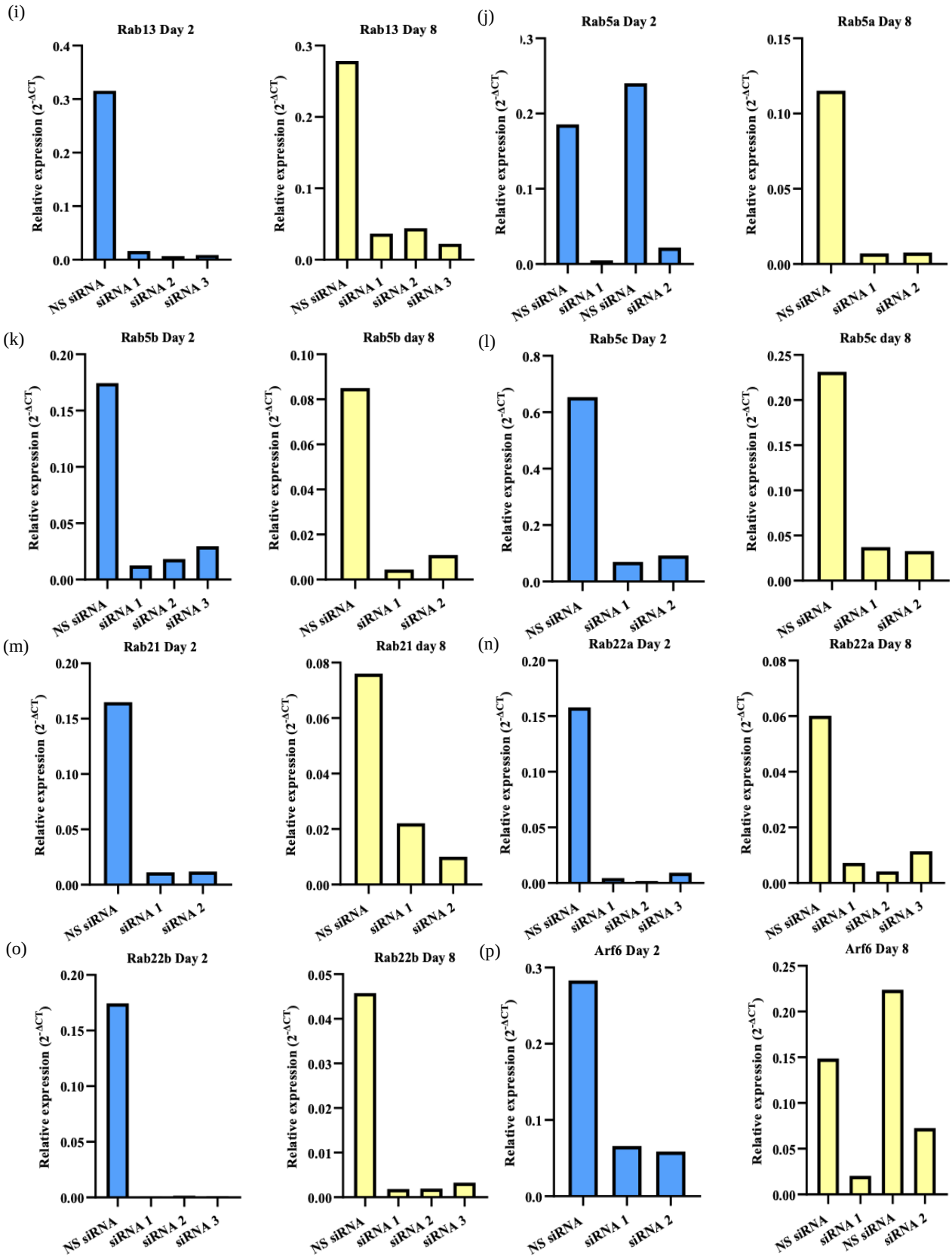

Figure 4.5 – Lipofectamine transfection of all siRNA oligos tested was sufficient to reduce mRNA levels each endocytic recycling regulator at day 2 and day 8 post-transfection

Figure legend on the next page.

Figure 4.5 – Lipofectamine transfection of all siRNA oligos tested was sufficient to reduce mRNA levels each endocytic recycling regulator at day 2 and day 8 post-transfection

CAFs (MOC195), pre-treated with TGFβ3 (10 ng.mL^{-1}) were transfected either with the NS siRNA, or siRNA targeting each endocytic recycling regulator GTPase (80 nM). Per GTPase , the efficiency of knockdown after separately transfecting CAFs with a minimum of 2 different siRNAs oligos was tested (N = 1). RNA was extracted from CAFs at day 2 and day 8 post-transfection, and the mRNA was converted to cDNA by reverse transcription. The expression levels of each endocytic recycling regulator, and GAPDH, were measured in triplicate by RT-qPCR. ΔCT values were calculated for each GTPase, and relative expression values relative to GAPDH expression, were calculated as described previously. Relative expression levels are shown for each GTPase, at day 2 and day 8 post-transfection, in CAFs transfected with NS siRNA, or one of the following GTPase targeting siRNA oligos: (a) Rab11a siRNA 2. (b) Rab11b siRNA 2. (c) Rab4a siRNA 1 or Rab4a siRNA 2. (d) Rab4b siRNA 1 or Rab4b siRNA 2. (e) Rab14 siRNA 1 or Rab14 siRNA 2. (f) Rab8a siRNA 1 or Rab8a siRNA 2. (g) Rab8b siRNA 1, Rab8b siRNA 2 or Rab8b siRNA 3. (h) Rab10 siRNA 1, Rab10 siRNA 2 or Rab10 siRNA 3. (i) Rab13 siRNA 1, Rab13 siRNA 2 or Rab13 siRNA 3. (j) Rab5a siRNA 1 or Rab5a siRNA 2. (k) Rab5b siRNA 1, Rab5b siRNA 2 or Rab5b siRNA 3. (l) Rab5c siRNA 1 or Rab5c siRNA 2. (m) Rab21 siRNA 1 or Rab21 siRNA 2. (n) Rab22a siRNA 1, Rab22a siRNA 2 or Rab22a siRNA 3. (o) Rab22b siRNA 1, Rab22b siRNA 2 or Rab22b siRNA 3. (p) Arf6 siRNA 1 or Arf6 siRNA 2.

4.4 Endocytic recycling influences the ability of CAFs to support HGSOC cell invasion

4.4.1 Group 1 small GTPases

As work carried out previously by others had implicated Rab11 isoforms in ECM assembly, to begin investigating the impact of depleting group 1 GTPases on the ability of TGFβ3 pre-treated CAFs to support the invasion of OC cells, Rab11a and Rab11b were firstly depleted in CAFs, both individually and in combination [321]. As expected, based on results observed previously, Kuramochi cells without CAFs present in the spheroid were largely incapable of invading into the surrounding collagen I hydrogel (Figure 4.6a, 4.6f). Co-culture of CAFs transfected with the NS siRNA was able to significantly stimulate the invasion of Kuramochi cells out of spheroids (Figure 4.6a, 4.6b, 4.6f, 4.6g). Following the transfection of CAFs with siRNA oligos targeting either Rab11a, Rab11b, or both in combination, CAFs remained competent in facilitating Kuramochi invasion. Relative to spheroids consisting only of Kuramochi cells, significant increases in Kuramochi invasion were observed, with the levels of invasion measured being comparable with those observed with NS siRNA-transfected CAFs (Figure 4.6). These results suggest that omental CAFs do not utilise Rab11 isoforms to support OC invasion in 3D.

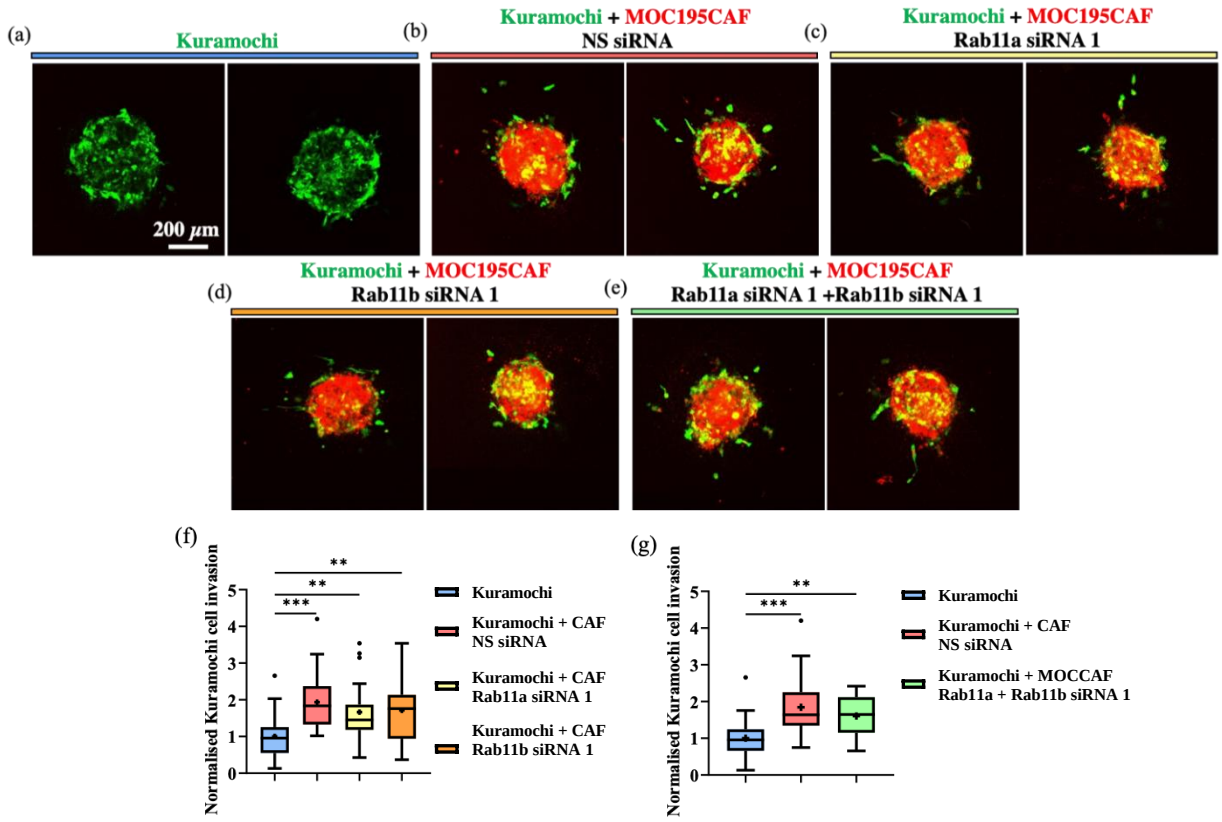

Figure 4.6 – CAFs do not require Rab11a or Rab11b to facilitate Kuramochi cell invasion

*Spheroids were formed, using the hanging drop method as described previously and embedded into a collagen I (3 mg.mL^{-1}) hydrogel. Spheroids consisted of either a GFP-expressing Kuramochi cell mono-culture, or a Kuramochi-CAF (MOC195) co-culture, treated for a minimum of 4 days, and transfected with siRNA (80 nM total) one day prior to inclusion in spheroids. Ascorbic acid was included in the growth medium (20 μg.mL^{-1}). Invasion after 4 days was visualised by fluorescence microscopy (N = 3). Representative images are shown of spheroids consisting of Kuramochi cells (a), or Kuramochi cells in co-culture with CAFs pre-transfected with NS siRNA (b), Rab11a siRNA 1 (c), Rab11b siRNA 1 (d), or Rab11a siRNA 1 + Rab11b siRNA 1 (e). (f) Quantification of merged data from three biological replicates, and statistical analysis by Kruskal-Wallis test (**p<0.01, ***p<0.001), of Kuramochi invasion out of spheroids consisting of Kuramochi cells as a mono-culture, or in co-culture with CAFs pre-transfected with NS, Rab11a siRNA 1 or Rab11b siRNA 1.*

Figure legend continues on the next page.

Figure 4.6–CAFs do not require Rab11a or Rab11b to facilitate Kuramochi cell invasion

*(g) Quantification of merged data from three biological replicates, and statistical analysis by Kruskal-Wallis test (**p<0.01, ***p<0.001), of Kuramochi invasion out of spheroids consisting of Kuramochi cells as a mono-culture, or in co-culture with CAFs pre-transfected with NS siRNA or Rab11a siRNA 1 + Rab11b siRNA 1. Normalised Kuramochi invasion values are shown, where the percentage of invading cells for each spheroid was normalised within each biological replicate by dividing by the average percentage for the Kuramochi monoculture spheroids. All statistically significant results are shown. Scale bar = 200 μm. Maximum intensity projections of z-stacks are shown.*

Next, the remaining small GTPases in group 1 were depleted in CAFs by transfection with siRNA, and transfected CAFs were co-cultured in spheroids with Kuramochi cells. As expected, CAFs transfected with the NS siRNA were able to significantly increase Kuramochi invasion when present in spheroids (Figure 4.7a, 4.7b, 4.7g). Whilst, like Rab11 and Rab11b, depleting Rab4a or Rab4b in CAFs did not affect their ability to support Kuramochi invasion, the depletion of Rab14, or Rab4a and Rab4b in combination, significantly reduced the CAF-mediated stimulation of Kuramochi invasion (Figure 4.7). These results suggested that endocytic recycling regulated by Rab14 was required for CAFs to facilitate Kuramochi invasion. Furthermore, these results suggested that Rab4a and Rab4b were also involved, and as a significant decrease in Kuramochi invasion was observed only when both Rab4 isoforms were depleted in CAFs , Rab4a was likely able to compensate for Rab4b when it's levels were depleted, and vice versa. However, data described here were obtained by depleting each recycling regulator with one siRNA oligo, and in CAFs isolated from one HGSOC patient omentum sample (MOC194). It was therefore possible that any significant results could have been observed due a non-specific effect of the siRNA, or they may have been specific to the CAFs obtained from that particular patient. As such, it was essential to later validate these statistically significant findings.

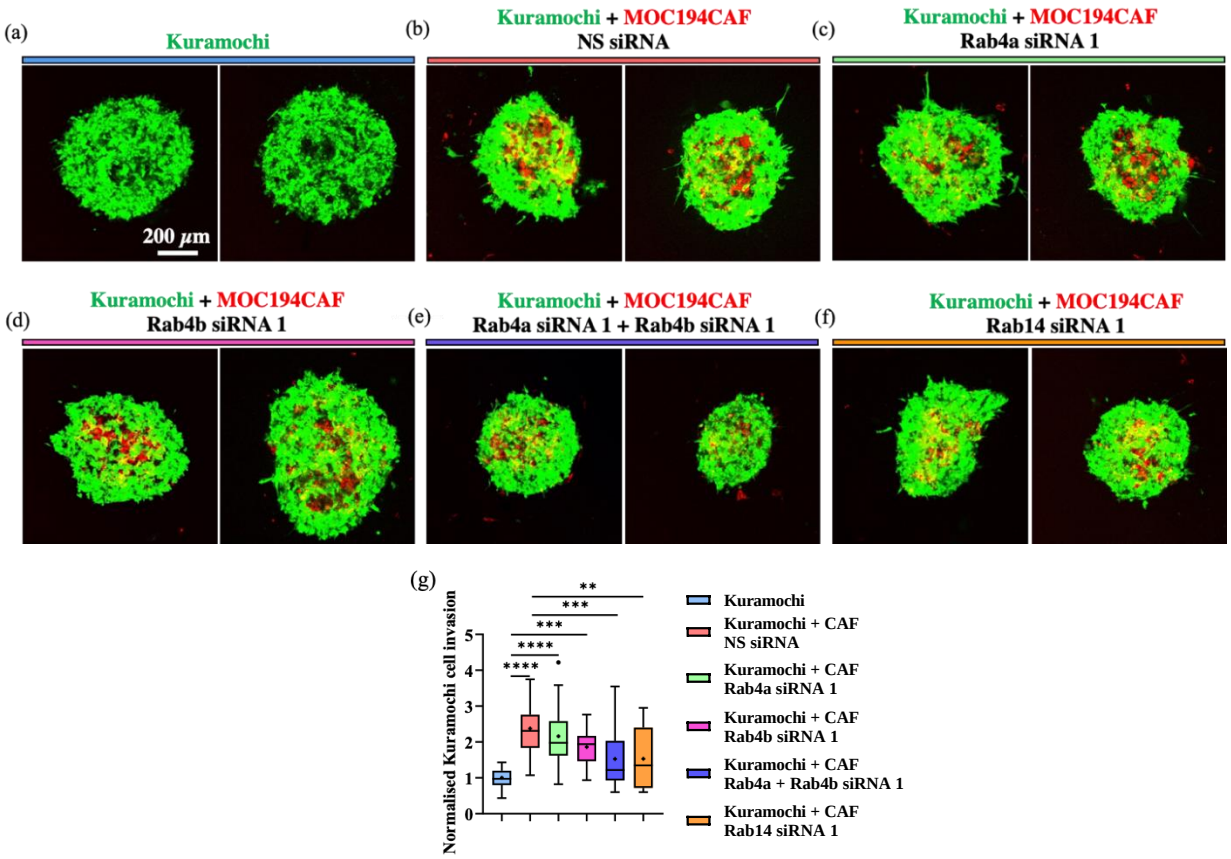

Figure 4.7 – Depletion of Rab4a + Rab4b, or Rab14 significantly reduces the CAF-mediated stimulation of Kuramochi invasion out of spheroids

Spheroids were formed, using the hanging drop method as described previously and embedded into a collagen I (3 mg.mL^{-1}) hydrogel. Spheroids consisted of either a GFP-expressing Kuramochi cell mono-culture, or a Kuramochi-CAF (MOC194) co-culture, where CAFs were stained red with PKH26. All CAFs were TGFβ3 (10 ng.mL^{-1}) pre-treated for a minimum of 4 days, and transfected with siRNA (80 nM total) one day prior to inclusion in spheroids. Ascorbic acid was included in the growth medium (20 μg.mL^{-1}). Invasion after 4 days was visualised by fluorescence microscopy (N = 3). Representative images are shown of spheroids consisting of Kuramochi cells (a), or Kuramochi cells in co-culture with CAFs pre-transfected with NS siRNA (b), Rab4a siRNA 1 (c), Rab4b siRNA 1 (d), Rab4a siRNA 1 + Rab4b siRNA 1 (e), or Rab14 siRNA 1 (f).

Figure legend on the next page.

Figure 4.7– Depletion of Rab4a + Rab4b, or Rab14 significantly reduces the CAF-mediated stimulation of Kuramochi invasion out of spheroids

*(g) Quantification of merged data from three biological replicates, and statistical analysis by one-way ANOVA (**p<0.01, ***p<0.001, ****p<0.0001), of Kuramochi invasion out of spheroids consisting of Kuramochi cells as a mono-culture, or in co-culture with CAFs pre-transfected with siRNA. Normalised Kuramochi invasion values are shown, where the percentage of invading cells for each spheroid was normalised within each biological replicate by dividing by the average percentage for the Kuramochi monoculture spheroids. All statistically significant results are shown. Scale bar = 200 μm. Maximum intensity projections of z-stacks are shown.*

4.4.2 Group 2 and 3 small GTPases

Prior to the validation of results obtained from spheroid invasion assays with CAFs transfected with group 1 GTPase targeting-siRNAs, these assays were first carried out with CAFs pre-transfected with siRNAs targeting regulators classified into groups 2 or 3. When depleting group 2 small GTPases, CAFs pre-transfected with the NS siRNA were able to significantly increase the invasion of the Kuramochi cells out of spheroids (Figure 4.8a, 4.8b). Within this group, the depletion of Rab8a, Rab8b, Rab8a + Rab8b in combination, Rab10 or Rab13 in CAFs, did not significantly reduce their capacity to promote Kuramochi invasion relative to that observed with CAFs pre-transfected with the NS siRNA (Figure 4.8). The only GTPase classified into group 2 that, when depleted in CAFs, resulted in a significant reduction in their ability to stimulate Kuramochi invasion, was Arf6 (Figure 4.8h, 4.8i). These results indicated that whilst the majority of the GTPases classified into group 2 were not involved in the facilitation of cancer cell invasion by CAFs, Arf6 was required. As in the case of the significant results observed with group 1 GTPases, this significant decrease in invasion upon Arf6 depletion would later have to be validated with a second siRNA, in CAFs isolated from a second HGSOC patient.

In contrast to groups 1 and 2, the depletion of each of the GTPases classified into group 3 did not significantly alter the capacity of CAFs to support Kuramochi invasion. A significant increase in Kuramochi invasion was observed upon co-culture with CAFs pre-transfected with the NS siRNA. However, CAFs in which Rab5a, Rab5b, Rab5c, Rab5a + Rab5b + Rab5c in combination, Rab21, Rab22a, Rab22b, or Rab22a + Rab22b in combination, had been depleted, were still capable of supporting the invasion of Kuramochi cells out of spheroids. This suggested that these endocytic recycling regulators are not required for CAFs to facilitate this process (Figure 4.9).

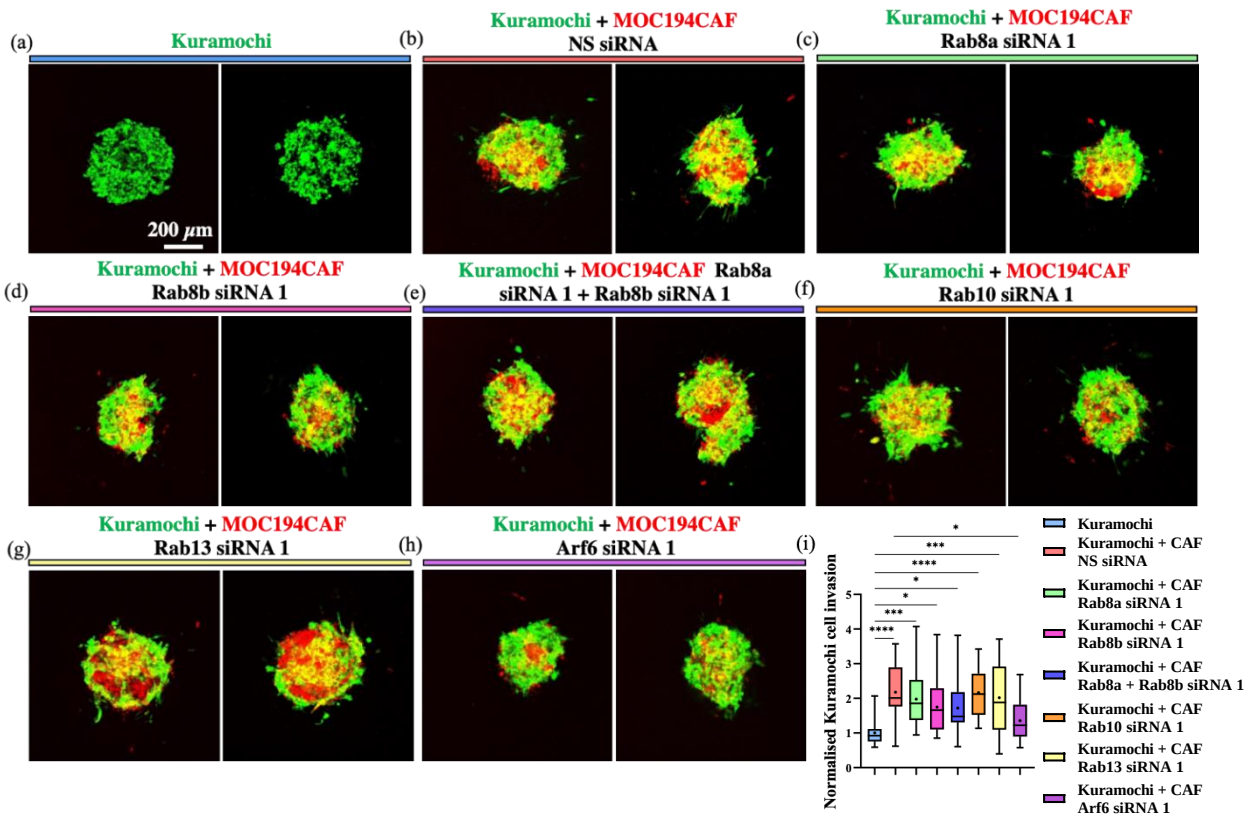

Figure 4.8 – Depletion of Arf6 significantly reduces the CAF-mediated stimulation of Kuramochi invasion out of spheroids

Spheroids were formed, using the hanging drop method as described previously and embedded into a collagen I (3 mg.mL^{-1}) hydrogel. Spheroids consisted of either a GFP-expressing Kuramochi cell mono-culture, or a Kuramochi-CAF (MOC194) co-culture, where CAFs were stained red with PKH26. All CAFs were TGFβ3 (10 ng.mL^{-1}) pre-treated for a minimum of 4 days, and transfected with siRNA (80 nM total) one day prior to inclusion in spheroids. Ascorbic acid was included in the growth medium (20 μg.mL^{-1}).

Figure legend continues on the next page.

Figure 4.8– Depletion of Arf6 significantly reduces the CAF-mediated stimulation of Kuramochi invasion out of spheroids

*Invasion after 4 days was visualised by fluorescence microscopy (N = 3). Representative images are shown of spheroids consisting of Kuramochi cells (a), or Kuramochi cells in co-culture with CAFs pre-transfected with NS siRNA (b), Rab8a siRNA 1 (c), Rab8b siRNA 1 (d), Rab8a siRNA 1 + Rab8b siRNA 1 (e), Rab10 siRNA 1 (f), Rab13 siRNA 1 (g), or Arf6 siRNA 1 (h). (i) Quantification of merged data from three biological replicates, and statistical analysis by Kruskal-Wallis test (*p<0.05, ***p<0.001, ****p<0.0001), of Kuramochi invasion out of spheroids consisting of Kuramochi cells as a mono-culture, or in co-culture with CAFs pre-transfected with siRNA. Normalised Kuramochi invasion values are shown, where the percentage of invading cells for each spheroid was normalised within each biological replicate by dividing by the average percentage for the Kuramochi monoculture spheroids. All statistically significant results are shown. Scale bar = 200 μm. Maximum intensity projections of z-stacks are shown.*

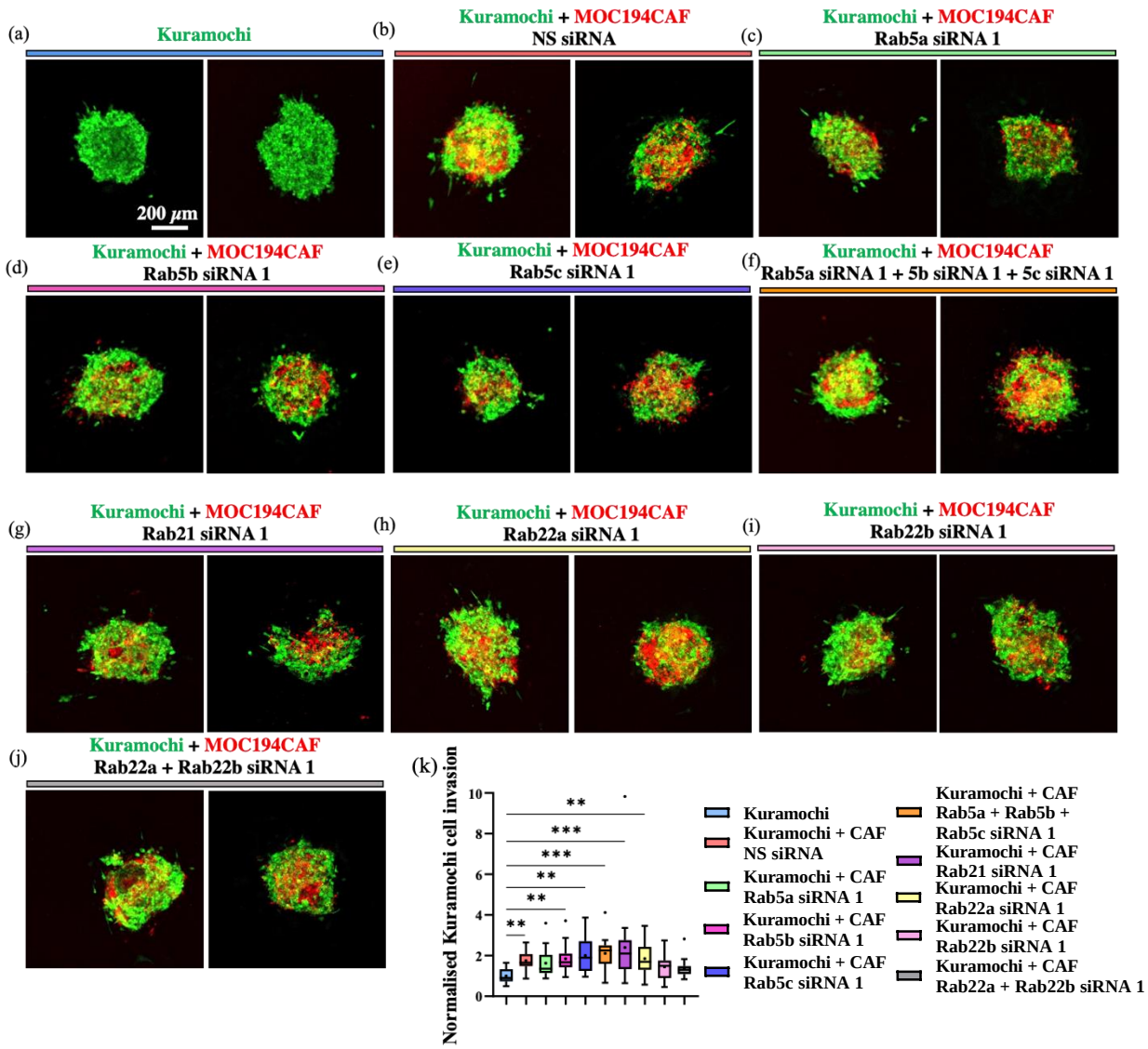

Figure 4.9 – Group 3 GTPase depletion in CAFs does not significantly reduce Kuramochi invasion

Spheroids were formed, using the hanging drop method as described previously and embedded into a collagen I (3 mg.mL^{-1}) hydrogel. Spheroids consisted of either a GFP-expressing Kuramochi cell mono-culture, or a Kuramochi-CAF (MOC194) co-culture, where CAFs were stained red with PKH26. All CAFs were TGFβ3 (10 ng.mL^{-1}) pre-treated for a minimum of 4 days, and transfected with siRNA (80 nM total) one day prior to inclusion in spheroids. Ascorbic acid was included in the growth medium (20 μg.mL^{-1}). Invasion after 4 days was visualised by fluorescence microscopy (N = 3).

Figure legend continues on the next page.

Figure 4.9 – Group 3 GTPase depletion in CAFs does not significantly reduce Kuramochi invasion

*Representative images are shown of spheroids consisting of Kuramochi cells (a), or Kuramochi cells in co-culture with CAFs pre-transfected with NS siRNA (b), Rab5a siRNA 1 (c), Rab5b siRNA 1 (d), Rab5c siRNA 1 (e), Rab5a siRNA 1 + Rab8b siRNA 1 + Rab5c siRNA 1 (f), Rab21 siRNA 1 (g), Rab22a siRNA 1 (h), Rab22b siRNA 1 (i), or Rab22a siRNA 1 + Rab22b siRNA 1 (j). (k) Quantification of merged data from three biological replicates, and statistical analysis by Kruskal-Wallis test (**p<0.01, ***p<0.001), of Kuramochi invasion out of spheroids consisting of Kuramochi cells as a mono-culture, or in co-culture with CAFs pre-transfected with siRNA. Normalised Kuramochi invasion values are shown, where the percentage of invading cells for each spheroid was normalised within each biological replicate by dividing by the average percentage for the Kuramochi monoculture spheroids. All statistically significant results are shown. Scale bar = 200 μm. Maximum intensity projections of z-stacks are shown.*

4.4.3 Validation

The results from the initial round of screening with siRNA oligos targeting each GTPase in CAFs isolated from a HGSOC patient (either MOC194 or MOC195), indicated that Arf6, Rab14, and Rab4a + Rab4b, may be required for CAFs to support OC cell invasion. In order to ensure that the significant differences in Kuramochi invasion observed when using these siRNAs were not due to non-specific, off-target effects, it was crucial that results were validated by carrying out additional spheroid invasion assays using different siRNA oligos that targeted these GTPases. Furthermore, to ensure that the CAF phenotypes were not specific to CAFs isolated from a single patient, CAFs isolated from a second patient were used for validation. When validating the previous findings, depletion of Rab14 with siRNA 2 in CAFs did not alter their ability to support Kuramochi invasion relative to CAFs pre-transfected with the NS siRNA (Figure 4.10b, 4.10d, 4.10f). In contrast, pre-transfection of CAFs with Rab4a siRNA 2 + Rab4b siRNA 2 in combination, or Arf6 siRNA 2, was sufficient to reduce Kuramochi invasion relative to that observed in the presence of NS siRNA pre-transfected CAFs, validating previous results for these GTPases (Figure 4.10c, 4.10e, 4.10f). These data suggest that Rab4 isoforms, as well as Arf6, play a role in enabling CAFs to support HGSOC cell invasion in the metastatic TME.

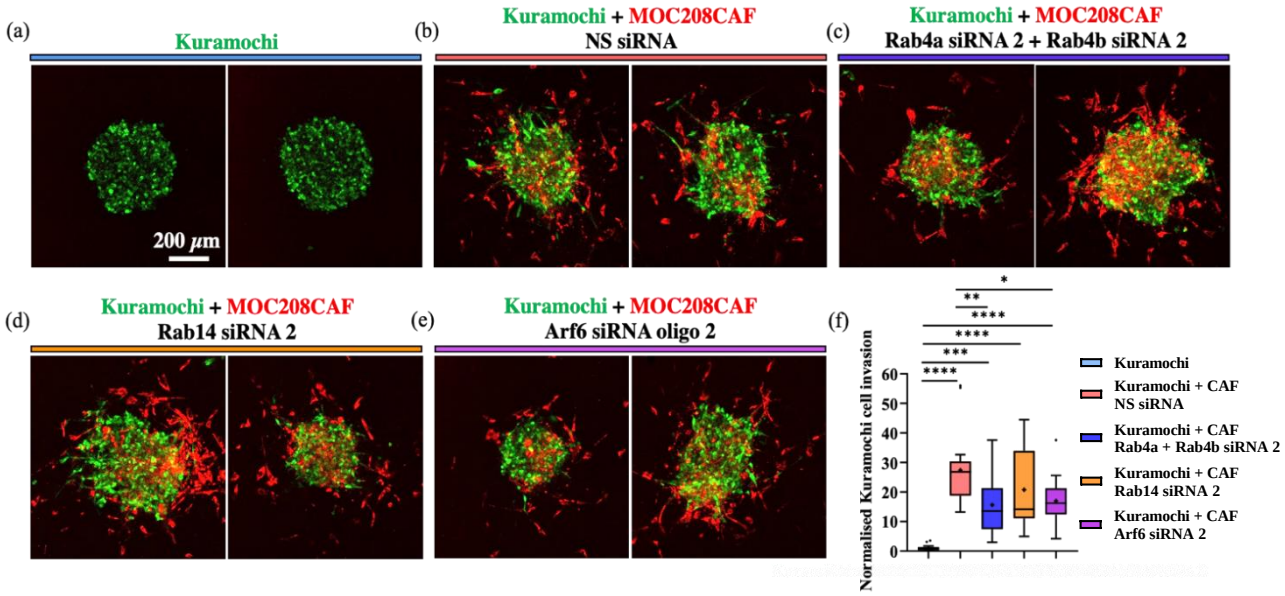

Figure 4.10 – Depletion of Rab4a + 4b, or Arf6, significantly reduces the stimulation of Kuramochi invasion out of spheroids by a second CAF line

*Spheroids were formed, using the hanging drop method as described previously and embedded into a collagen I (3 mg.mL^{-1}) hydrogel. Spheroids consisted of either a GFP-expressing Kuramochi cell mono-culture, or a Kuramochi-CAF (MOC208) co-culture, where CAFs were stained red with PKH26. All CAFs were TGFβ3 (10 ng.mL^{-1}) pre-treated for a minimum of 4 days, and transfected with siRNA (80 nM total) one day prior to inclusion in spheroids. Ascorbic acid was included in the growth medium (20 μg.mL^{-1}). Invasion after 4 days was visualised by fluorescence microscopy (N = 3). Representative images are shown of spheroids consisting of Kuramochi cells (a), or Kuramochi cells in co-culture with CAFs pre-transfected with NS siRNA (b), Rab4a siRNA 2 + Rab4b siRNA 2 (c), Rab14 siRNA 2 (d), or Arf6 siRNA 2 (e). (f) Quantification of merged data from three biological replicates, and statistical analysis by Kruskal-Wallis test (*p<0.05, **p<0.01, ***p<0.001, ****p<0.0001), of Kuramochi invasion out of spheroids consisting of Kuramochi cells as a mono-culture, or in co-culture with CAFs pre-transfected with siRNA. Normalised Kuramochi invasion values are shown, where the percentage of invading cells for each spheroid was normalised within each biological replicate by dividing by the average percentage for the Kuramochi monoculture spheroids. All statistically significant results are shown. Scale bar = 200 μm. Maximum intensity projections of z-stacks are shown.*

4.4.4 The effect of endocytic recycling regulator depletion on CAF proliferation, invasion and contractility

As well as validating the spheroid invasion assay results, it was also critical to evaluate the effect of depleting Rab4a + Rab4b, Rab14, or Arf6, on CAF proliferation, as a decrease in proliferation following siRNA transfection would confound any validated findings. In order to evaluate the proliferative capacity of CAFs following siRNA transfection, EdU labelling assays were carried out. Compared to CAFs transfected with NS siRNA, depletion of neither Rab4a + Rab4b, Rab14, or Arf6, significantly altered CAF proliferation (Figure 4.11). These results indicated that transfecting CAFs with these siRNAs did not impact upon proliferation, and suggested that the behaviours of CAFs observed previously following siRNA treatment were not the result of alterations in their proliferation rate.

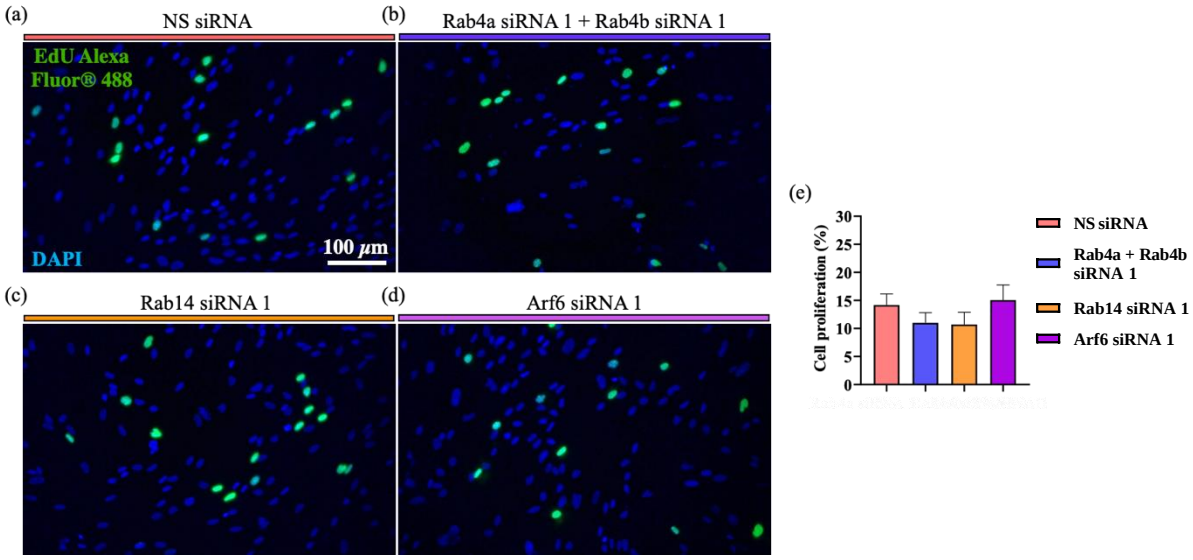

Figure 4.11 – Depletion of Rab4a + 4b, Rab14 ,or Arf6, does not significantly alter CAF proliferation

CAFs (MOC194) were transfected with NS siRNA, Rab4a siRNA 1 + Rab4b siRNA 1, Rab14 siRNA 1, or Arf6 siRNA 1, and grown in culture for 5 days in the presence of TGFβ3 (10 ng.mL^{-1}). EdU Alexa Fluor 488 was then added to label proliferative cells and nuclei were stained with Hoechst 33342. Fluorescence microscopy was used to visualise cells, a minimum of 150 cells per condition were counted, and the percentage of proliferating cells was calculated (N = 3). Representative images from three biological replicates are shown for cells transfected with NS siRNA (a), Rab4a siRNA 1 + Rab4b siRNA 1 (b), Rab14 siRNA 1 (c), or Arf6 siRNA 1 (d). (e) Quantification of merged data from three biological replicates, and statistical analysis by one-way ANOVA, of CAF proliferation following siRNA transfection. Scale bar = 200 μm. Images from a single z-plane are shown.

It was essential to ensure that the validated spheroid invasion assay results when Rab4a, Rab4b, or Arf6, were depleted, were not due to the depletion of these GTPases somehow impeding the ability of the CAFs to invade themselves. To investigate this, the images obtained during the validation with CAFs isolated from patient MOC208 were re-analysed to measure CAF invasion. This analysis highlighted that depletion of Rab4a + Rab4b in combination, or Arf6, did not alter the ability of CAFs to invade, suggesting that these regulators allow CAFs to support Kuramochi invasion via a different mechanism, for example in possibly regulating ECM assembly/remodelling (Figure 4.12).

To determine whether the inability of Rab4a + Rab4b, or Arf6, depleted CAFs to support Kuramochi invasion was due to a reduction in their ability to remodel pre-existing collagen fibres ECM through cell contraction, collagen gel contraction assays were carried out. Following siRNA transfection, CAFs were embedded into collagen I hydrogels and gel contraction was monitored over 2 days as described previously. These assays revealed that CAF contractility remained unimpaired following depletion of Rab4a + Rab4b, or Arf6 (Figure 4.12e, 4.12f, 4.12g). These results therefore indicate that the reduced ability of CAFs to support Kuramochi invasion following depletion of these GTPases was not the result of them becoming less contractile. Furthermore, this suggests that Rab4a + Rab4b, or Arf6, depletion does not impede on the cell contraction mediated-remodelling of pre-existing collagen fibres.

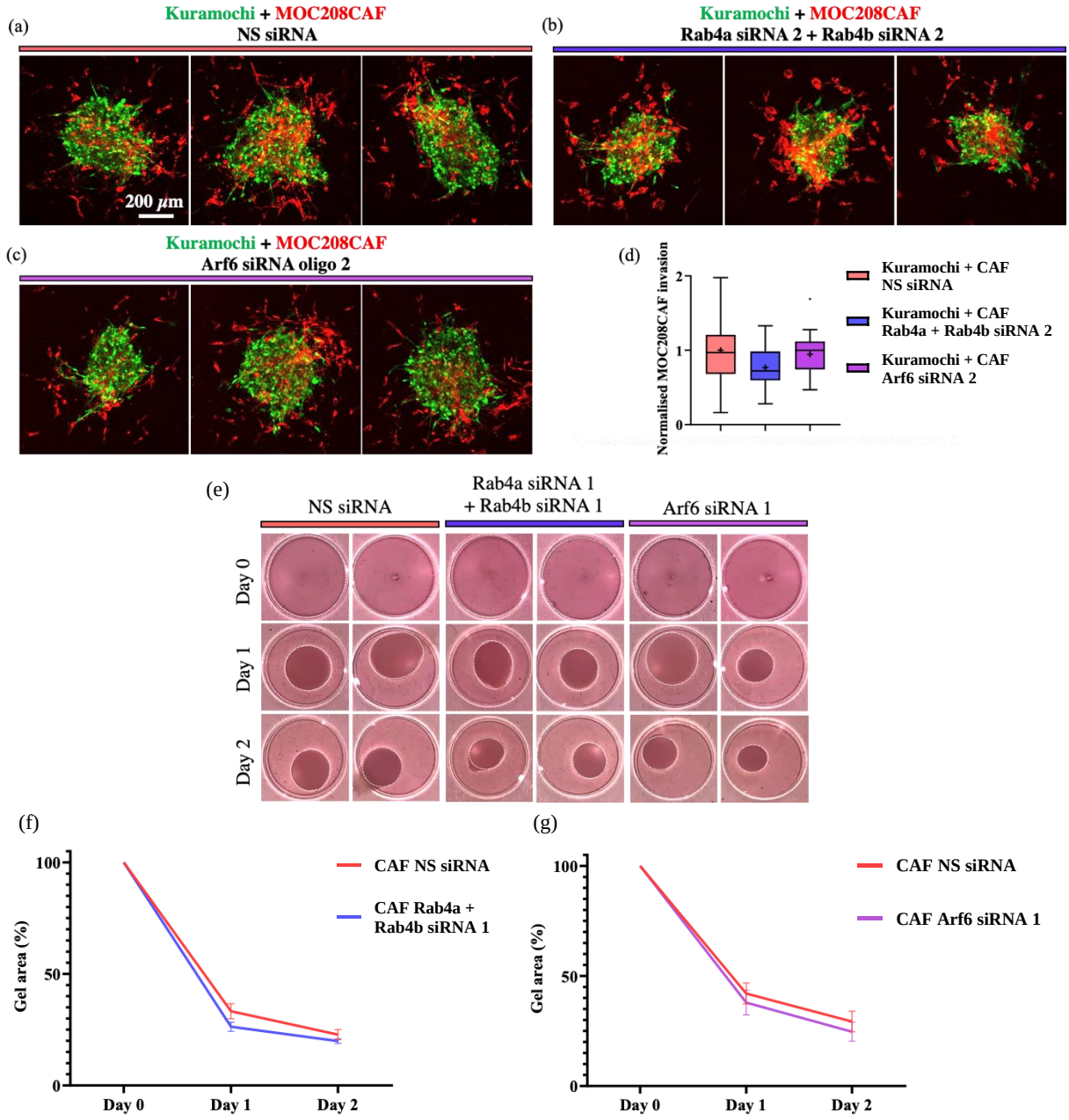

Figure 4.12 – Depletion of Rab4a + 4b, or Arf6, does not significantly alter CAF invasion or collagen gel contraction

Using the data displayed in the previous figure (Figure 4.10), the invasion of the fibroblasts themselves out of the spheroids following pre-transfection with NS siRNA, Rab4a siRNA 2 + 4b siRNA 2, or Arf6 siRNA 2, and co-culture with Kuramochi cells, was measured. Invasion after 4 days was visualised by fluorescence microscopy (N = 3). Representative images are shown of spheroids consisting of CAFs (MOC208) pre-transfected with NS siRNA (a), Rab4a siRNA 2 + Rab4b siRNA 2 (b), or Arf6 siRNA 2 (c).

Figure legend continues on the next page.

Figure 4.12 – Depletion of Rab4a + 4b, or Arf6, does not significantly alter CAF invasion or collagen gel contraction

(d) Quantification of merged data from three biological replicates, and statistical analysis by one-way ANOVA, of CAF invasion out of Kuramochi-CAF co-culture spheroids following pre-transfection of CAFs with siRNA. Normalised CAF invasion values are shown, where the percentage of invading cells for each spheroid was normalised within each biological replicate by dividing by the average percentage for the NS siRNA spheroids. Scale bar = 200 μm. Maximum intensity projections of z-stacks are shown. Figure legend continues on the next page. Collagen gel contraction assays were carried out as described previously by embedding CAFs pre-transfected with the NS siRNA, or siRNA oligos targeting Rab4a + Rab4b, or Arf6 (e; N = 3). Representative images from a single biological replicate including both Rab4a + 4b, and Arf6, are shown. Quantification of merged data from three biological replicates, and statistical analysis by two-way ANOVA, of collagen gel contraction by Rab4a + Rab4b (f) or Arf6 (g), depleted CAFs. .

4.5 Endogenous fibronectin deposition by CAFs does not require endocytic recycling

4.5.1 Overview

Spheroid invasion assay data suggested that omental CAFs required endocytic recycling, regulated by Rab4 isoforms and Arf6, to support the invasion of OC cells. However, it was not clear exactly how depleting the levels of recycling regulator GTPases in CAFs was interfering with their ability to facilitate Kuramochi invasion. We hypothesised that depleting the levels of these GTPases perturbed the ability to CAFs to efficiently assemble/remodel ECM proteins, which in turn rendered the ECM in the spheroid vicinity less suitable for Kuramochi cells to invade through. To assess the dependence of TGFβ3 pre-treated CAFs on endocytic recycling for ECM protein assembly in 2D culture, the effect of depleting each GTPase on the deposition of fibronectin was investigated. CAFs in which recycling regulator GTPases had been depleted were seeded on to coverslips and cultured for 10 days in the presence of both ascorbic acid and TGFβ3. Extracellular fibronectin was then immunostained, without cell permeabilisation, and visualised by confocal microscopy.

4.5.2 Group 1 small GTPases

As previous work by others had implicated Rab11 isoforms in the assembly of fibronectin, in particular Rab11b, it was expected that depletion of Rab11a, Rab11b, or both, would reduce fibronectin fibrillogenesis by CAFs [321]. However, depleting Rab11a or Rab11b individually in CAFs isolated from patient sample MOC195 did not impact upon their ability to assemble fibronectin fibres (Figure 4.13a, 4.13b, 4.13c, 4.13e). Depleting Rab11a and Rab11b in combination in CAFs from patient sample MOC195 surprisingly resulted in a significant increase in the deposition of fibronectin, in contrast to what was expected based on data reported previously in the literature (Figure 4.13d, 4.13e). This result however could not be validated in CAFs from a second patient sample, MOC194, using Rab11a siRNA 2 and Rab11b siRNA 2, where a significant decrease in fibronectin deposition was observed following GTPase depletion (Figure 4,13g, 4.13h). This may suggest that CAFs isolated from different patients may use endocytic recycling regulators to different extents for the assembly of fibronectin, however an alternative possibility is that these opposing results may be due to non-specific, off-target effects of each siRNA. Rab4 has also been implicated in fibronectin assembly, in particular during the branching of endothelial vessels [320]. However, depletion of Rab4 isoforms, or any of the remaining small GTPases classified into group 1 did not significantly impact upon the deposition of fibronectin by CAFs (Figure 4.14).

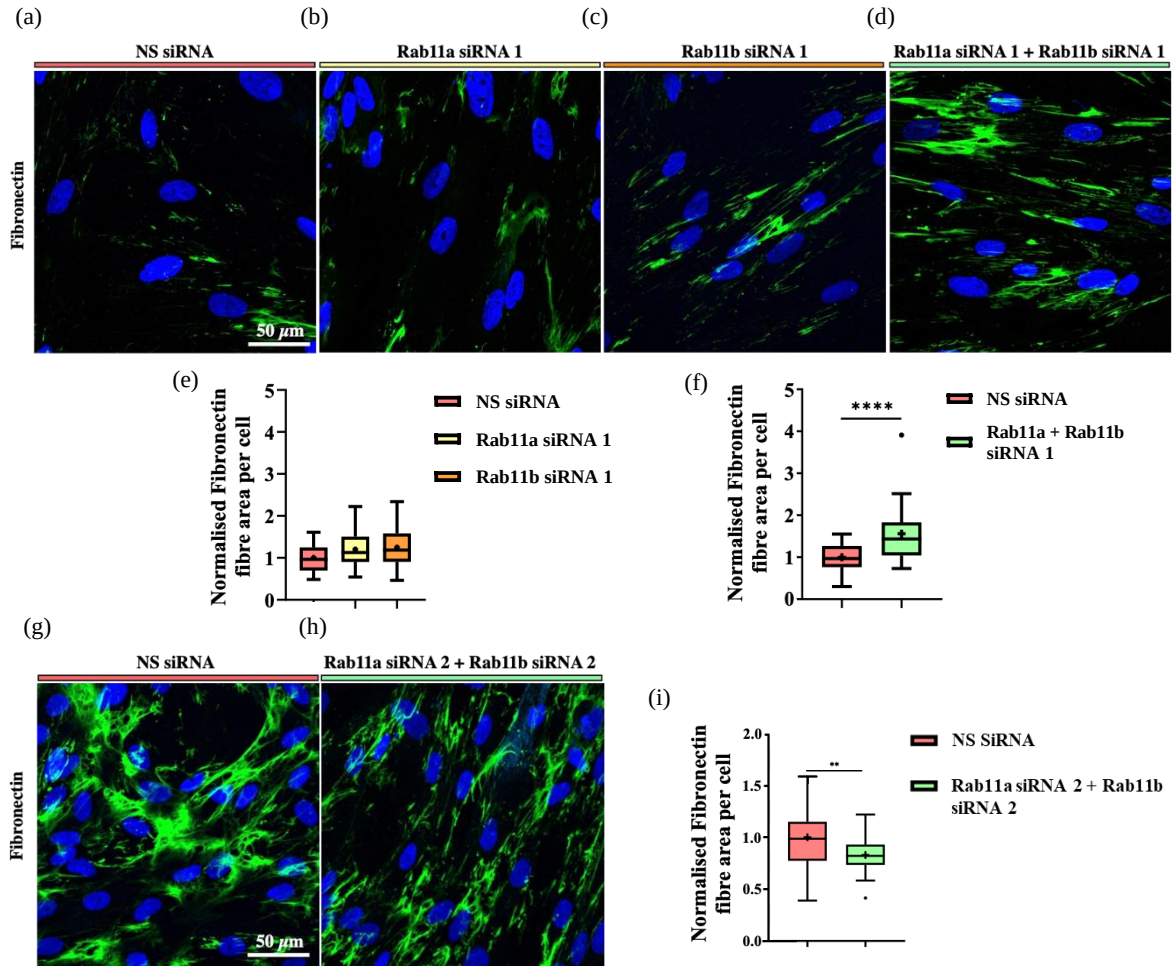

Figure 4.13 – Depletion of Rab11a, 11b, or both 11a and 11b, does not alter fibronectin deposition by CAFs

*Primary CAFs (MOC195) were pre-transfected with either the NS siRNA, or recycling regulator targeting siRNA oligos, then seeded on to coverslips and cultured for 10 days in the presence of TGFβ3 (10 ng.mL^{-1}) and ascorbic acid (20 µg.mL^{-1}). Fibronectin was immunostained and visualised by fluorescence microscopy (N = 3). Representative images from three biological replicates are shown, where CAFs (MOC195) were pre-transfected with the NS siRNA (a), Rab11a siRNA 1 (b), Rab11b siRNA 1 (c), or Rab11a siRNA 1+ Rab11b siRNA 1 (d). Merged data from three biological replicates of fibronectin deposition by CAFs (MOC195) following depletion of Rab11a or Rab11b (e), or Rab11a and Rab11b together (f), was quantified and statistically analysed by one-way ANOVA (****p<0.0001). Statistically significant results were then validated using a second siRNA oligo against the target GTPase in a second CAF line (MOC194).*

Figure legend continues on the next page.

Figure 4.13 – Depletion of Rab11a, 11b, or both 11a and 11b, does not alter fibronectin deposition by CAFs

*Representative images from three biological replicates are shown, where CAFs (MOC194) were pre-transfected with the NS siRNA (g), or Rab11a siRNA 2 + Rab11b siRNA 2 (h). Merged data from three biological replicates of fibronectin deposition by CAFs (MOC194) following Rab11a + Rab11b depletion (i) was quantified and statistically analysed by unpaired t-test (**p<0.01). Normalised fibronectin fibre area values are sown, where the fibre area for each image was normalised within each biological replicate by dividing by the average fibre area for the NS siRNA condition. All statistically significant results are shown. Nuclei were stained with Hoechst 33342. Scale bar = 50 μm. Maximum intensity projections of z-stacks are shown.*

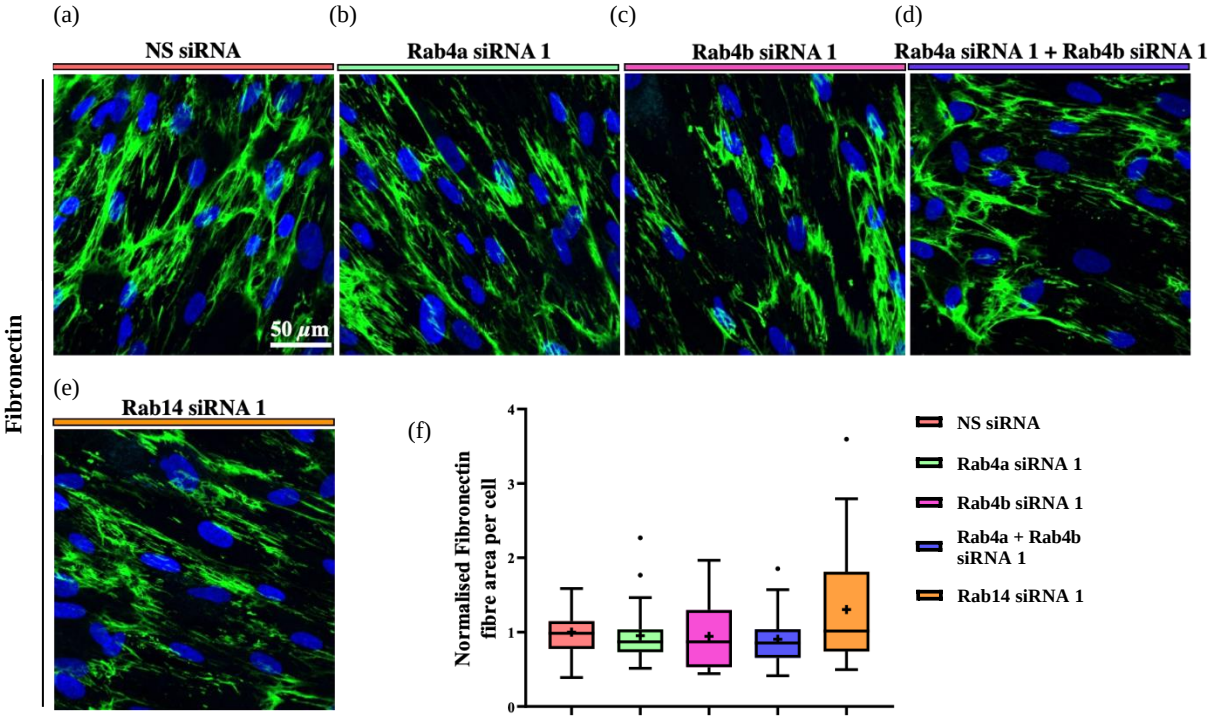

Figure 4.14 – Fibronectin deposition is not regulated by group 1 small GTPases

Primary CAFs (MOC194) were pre-transfected with either the NS siRNA, or recycling regulator targeting siRNA oligos, then seeded on to coverslips and cultured for 10 days in the presence of TGFβ3 (10 ng.mL^{-1}) and ascorbic acid (20 μg.mL^{-1}). Fibronectin was immunostained and visualised by fluorescence microscopy (N = 3).

Figure legend continues on the next page.

Figure 4.14 – Fibronectin deposition is not regulated by group 1 small GTPases

Representative images from three biological replicates are shown, where CAFs (MOC194) were pre-transfected with the NS siRNA (a), Rab4a siRNA 1 (b) , Rab4b siRNA 1 (c), Rab4a siRNA 1 + Rab4b siRNA 1 in combination (d), or Rab14 siRNA 1 (e). Merged data from three biological replicates of fibronectin deposition by CAFs (MOC194) following siRNA transfection was quantified and statistically analysed by Kruskal-Wallis test. Normalised fibronectin fibre area values are sown, where the fibre area for each image was normalised within each biological replicate by dividing by the average fibre area for the NS siRNA condition. All statistically significant results are shown. Nuclei were stained with Hoechst 33342. Scale bar = 50 μm. Maximum intensity projections of z-stacks are shown.

4.5.3 Group 2 and 3 small GTPases

Recycling regulator GTPases classified into groups 2 and 3 were also depleted in CAFs, and the effect of depletion on CAF ability to deposit fibronectin was evaluated. The depletion of each group 2 small GTPase in CAFs from patient sample MOC194 did not result in a significant defect in fibronectin deposition (Figure 4.15). Similarly, group 3 small GTPase depletion also did not impact upon this process (Figure 4.16). Whilst Rab5c depletion with siRNA 1 in CAFs from sample MOC194 resulted in a significant decrease in fibronectin deposition (Figure 4.16a, 4.16d, 4.16j), this result could not be validated with siRNA 2 in CAFs from sample MOC195 (Figure 4.16k, 4.16l, 4.16m).

Taken together, these data suggest that the endocytic recycling regulators classified into groups 1, 3, or 3 do not influence the deposition of endogenous fibronectin as fibres in the extracellular space by omental CAFs.

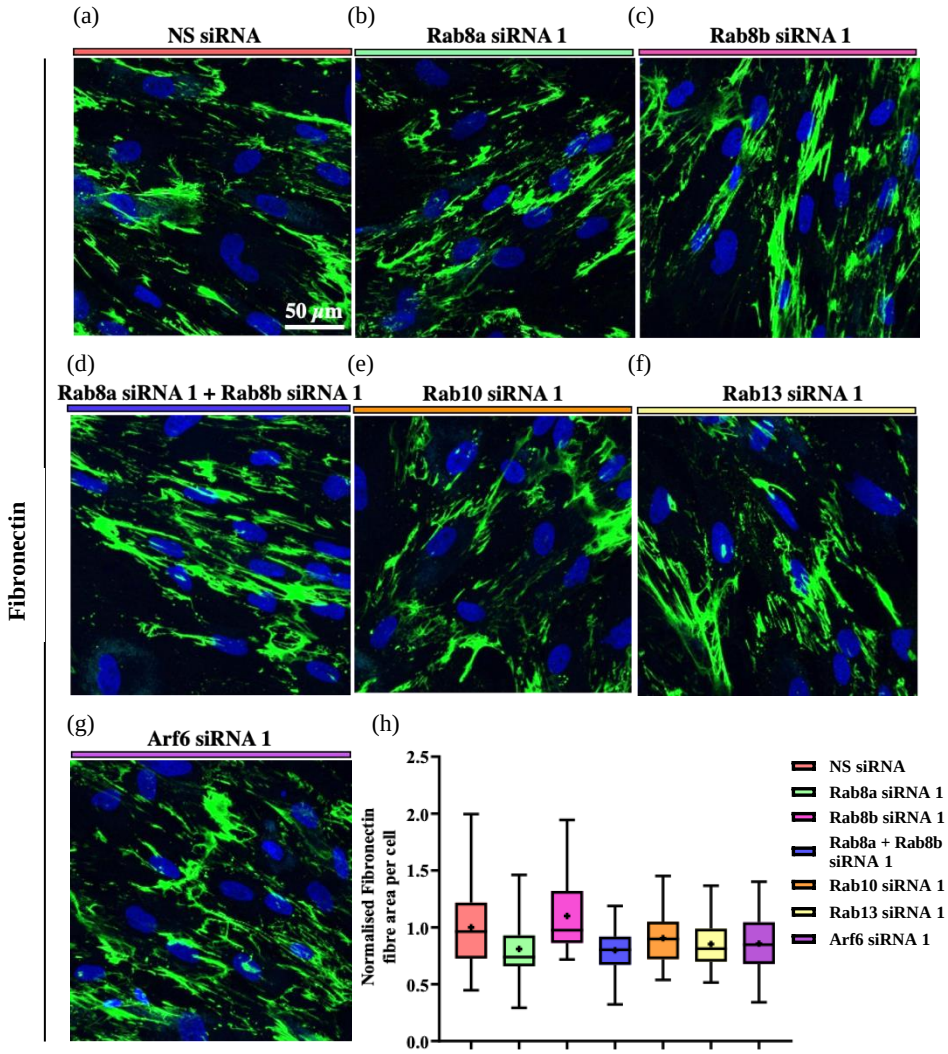

Figure 4.15 – Fibronectin deposition is not regulated by group 2 small GTPases

Primary CAFs (MOC194) were pre-transfected with either the NS siRNA, or recycling regulator targeting siRNA oligos, then seeded on to coverslips and cultured for 10 days in the presence of TGFβ3 (10 ng.mL^{-1}) and ascorbic acid (20 µg.mL^{-1}). Fibronectin was immunostained and visualised by fluorescence microscopy (N = 3). Representative images from three biological replicates are shown, where CAFs (MOC194) were pre-transfected with NS siRNA (a), Rab8a siRNA 1 (b), Rab8b siRNA 1 (c), Rab8a siRNA 1 + Rab8b siRNA 1 in combination (d), Rab10 siRNA 1 (e), Rab13 siRNA 1 (f), or Arf6 siRNA 1 (g). Merged data from three biological replicates of fibronectin deposition by CAFs (MOC194) following siRNA transfection was quantified and statistically analysed by Kruskal-Wallis test. Normalised fibronectin fibre area values are sown, where the fibre area for each image was normalised within each biological replicate by dividing by the average fibre area for the NS siRNA condition. All statistically significant results are shown. Nuclei were stained with Hoechst 33342. Scale bar = 50 µm. Maximum intensity projections of z-stacks are shown.

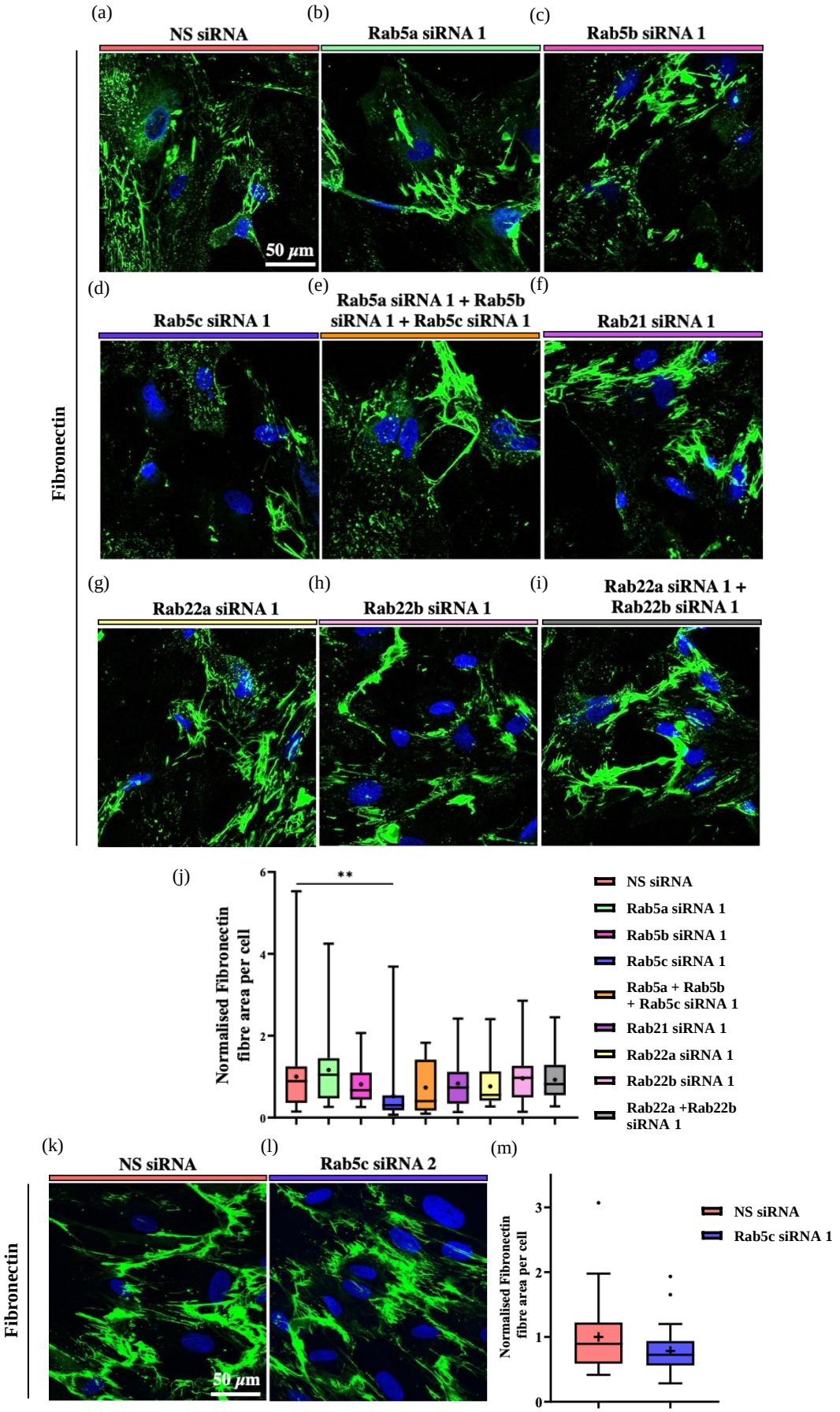

Figure 4.16 – Fibronectin deposition is not regulated by group 3 small GTPases

Figure legend on the next page.

Figure 4.16 – Fibronectin deposition is not regulated by group 3 small GTPases

*Primary CAFs (MOC194) were pre-transfected with either the NS siRNA, or recycling regulator targeting siRNA oligos, then seeded on to coverslips and cultured for 10 days in the presence of TGFβ3 (10 ng.mL^{-1}) and ascorbic acid (20 μg.mL^{-1}). Fibronectin was immunostained and visualised by fluorescence microscopy (N = 3). Representative images from three biological replicates are shown, where CAFs (MOC194) were pre-transfected with NS siRNA (a), Rab5a siRNA 1 (b), Rab5b siRNA 1 (c), Rab5c siRNA 1 (d), Rab5a siRNA 1 + Rab5b siRNA 1 + Rab5c siRNA 1 in combination (e), Rab21 siRNA 1 (f), Rab22a siRNA 1 (g), Rab22b siRNA 1 (h), or Rab22a siRNA 1 + Rab22b siRNA 1 in combination (i). (j) Merged data from three biological replicates of fibronectin deposition by CAFs (MOC194) following siRNA transfection was quantified and statistically analysed by Kruskal-Wallis test (**p<0.01). Statistically significant results were then validated using a second siRNA oligo against the target GTPase in a second CAF line (MOC195). Representative images from three biological replicates are shown, where CAFs (MOC195) were pre-transfected with the NS siRNA (k), or Rab5c siRNA 2 (l). Merged data from three biological replicates of fibronectin deposition by CAFs (MOC195) following Rab5c depletion (m) was quantified and statistically analysed by Mann-Whitney test. Normalised fibronectin fibre area values are sown, where the fibre area for each image was normalised within each biological replicate by dividing by the average fibre area for the NS siRNA condition. All statistically significant results are shown. Nuclei were stained with Hoechst 33342. Scale bar = 50 μm. Maximum intensity projections of z-stacks are shown.*

4.6 Exogenous fibronectin assembly is regulated by endocytic recycling

4.6.1 Overview

The level of fibronectin fibril formation was often found to be variable between CAFs within individual samples and could depend upon a number of factors, including the ability of cells to synthesise, or remodel, fibronectin. To simplify the analysis, the role of these recycling regulator GTPases in the assembly of exogeneous fluorophore labelled fibronectin into fibres was investigated. The aim of these assays was to elucidate whether endocytic recycling, whilst not being required for the synthesises and deposition of endogenous fibronectin by omental CAFs, was involved in assembling fibronectin dimers which were already present in the extracellular space into fibres. Following CAF TGFβ3 pre-treatment, and pre-transfection with siRNAs targeting recycling regulator GTPases, exogenous fibronectin was added. As this fibronectin is only visible by fluorescence microscopy after it has been assembled into fibres, fibronectin assembly could be observed over time by fixing CAFs at time points of 5-, 15-, 30- and 60-minutes post-fibronectin addition.

4.6.2 Exogenous fibronectin assembly analysis by ridge detection

The assembly of exogenous fibronectin by CAFs was measured using the ridge detection algorithm described previously. However, whereas in previous experiments only large fibres were detected, with a minimum width of 10 pixels and a minimum length of 70 pixels, the minimum line length was reduced to 5 pixels in order to detect exogenous fibronectin fibres of all sizes such that the fibre index could be calculated (Figure 4.17).

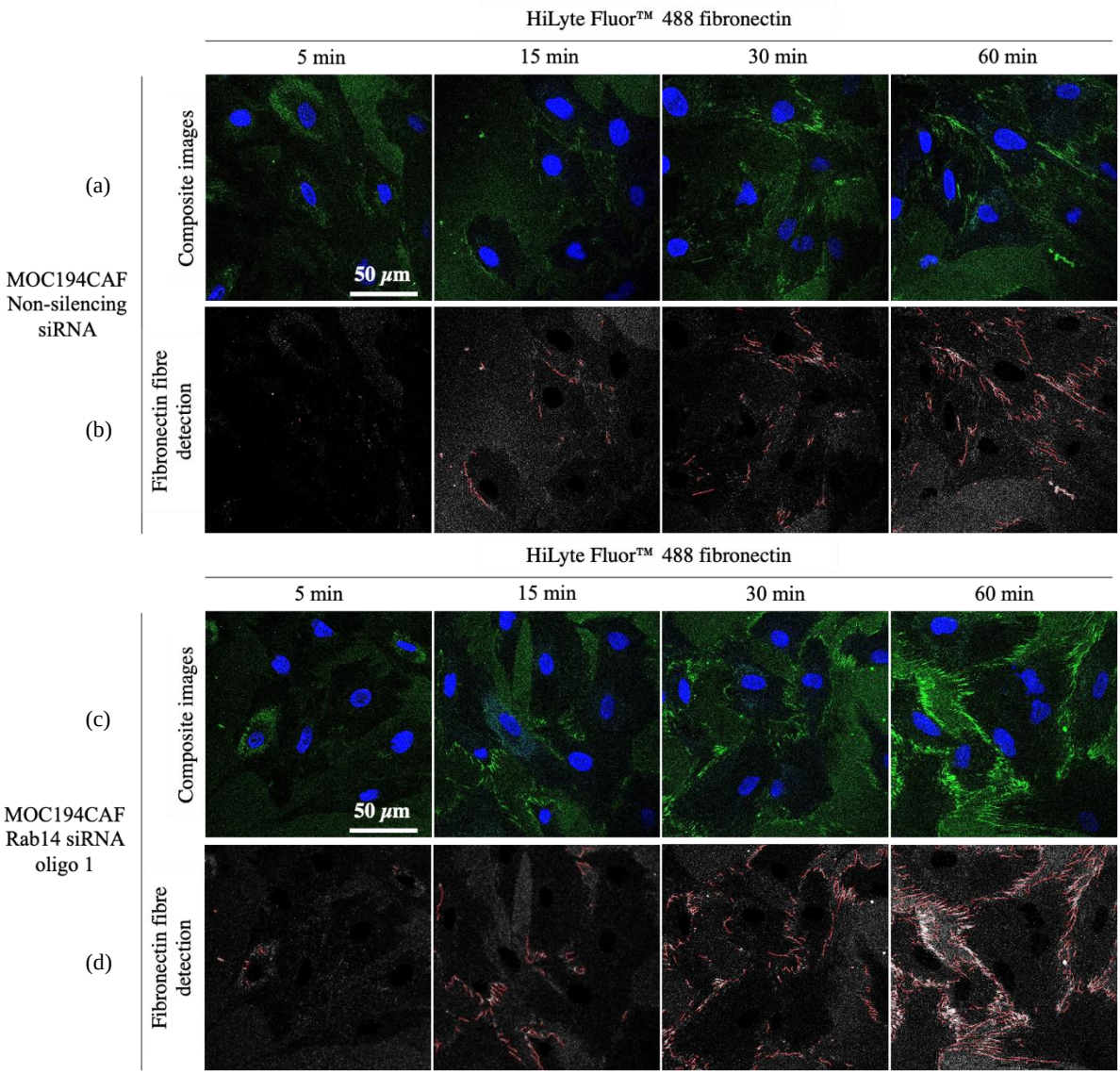

Figure 4.17 – The assembly of exogenous fibronectin was analysed by calculating fibre indices using the ridge detection algorithm

Following TGFβ3 (10 ng.mL^{-1}) pre-treatment and siRNA transfection, CAFs were seeded in to 96-well imaging plates. After cell attachment, exogenous fibronectin was added to each well (5 μg.mL^{-1}) and cells were fixed after 5-, 15-, 30- or 60-minutes. Assembled fibronectin was visualised by fluorescence microscopy, where a single z-plane was captured at 10 positions for each condition. The ridge detection algorithm was then used to calculate the fibre index for each image by detecting fibres with a minimum line width of 10 pixels and a minimum length of 5 pixels. All measured values were normalised to cell number for each image. Example composite images for CAFs (MOC194) transfected with NS siRNA (a), or Rab14 siRNA 1 (c), are shown at each time point, together with their corresponding example greyscale ridge detection images, (b) and (d) respectively, where detected fibres are shown in red. Nuclei were stained with Hoechst 33342.

4.6.3 Group 1 small GTPases

Initially, the impact of depleting Rab11a, Rab11b, or both isoforms in combination, on exogenous fibronectin assembly by CAFs was evaluated. Despite the depletion of Rab11a and Rab11b, individually, having no impact on exogenous fibronectin assembly by CAFs from patient MOC194, the depletion of both Rab11 isoforms together significantly elevated the ability of these CAFs to assemble exogenous fibronectin, with higher fibre indices measured at the 15- and 30-minute time points (Figure 4.18a, 4.18b). This result was then validated using Rab11a siRNA 2 and Rab11b siRNA 2 in CAFs from patient MOC195 , where larger fibre indices were measured at the 5- and 60-minute time points (Figure 4.18c). Surprisingly, the depletion of all other small GTPases classified into group 1, in CAFs from patient MOC194, also lead to a significant increase in exogenous fibronectin assembly. Larger fibronectin fibre indices were measured following depletion of Rab4a, Rab4b, Rab4a + Rab4b in combination, or Rab14, at the 15- and 60-minute time points (Figure 4.17, 4.18d). Example images demonstrating higher fibronectin assembly following Rab14 depletion in CAFs from patient MOC194 are shown (Figure 4.17). However, only the significant increase in fibre index measured following Rab14 depletion could be validated in CAFs from patient MOC195. The depletion of Rab14 with siRNA 2 in CAFs from a second patient resulted in a significantly larger fibre index measured at the 30-minute time point (Figure 4.18e).

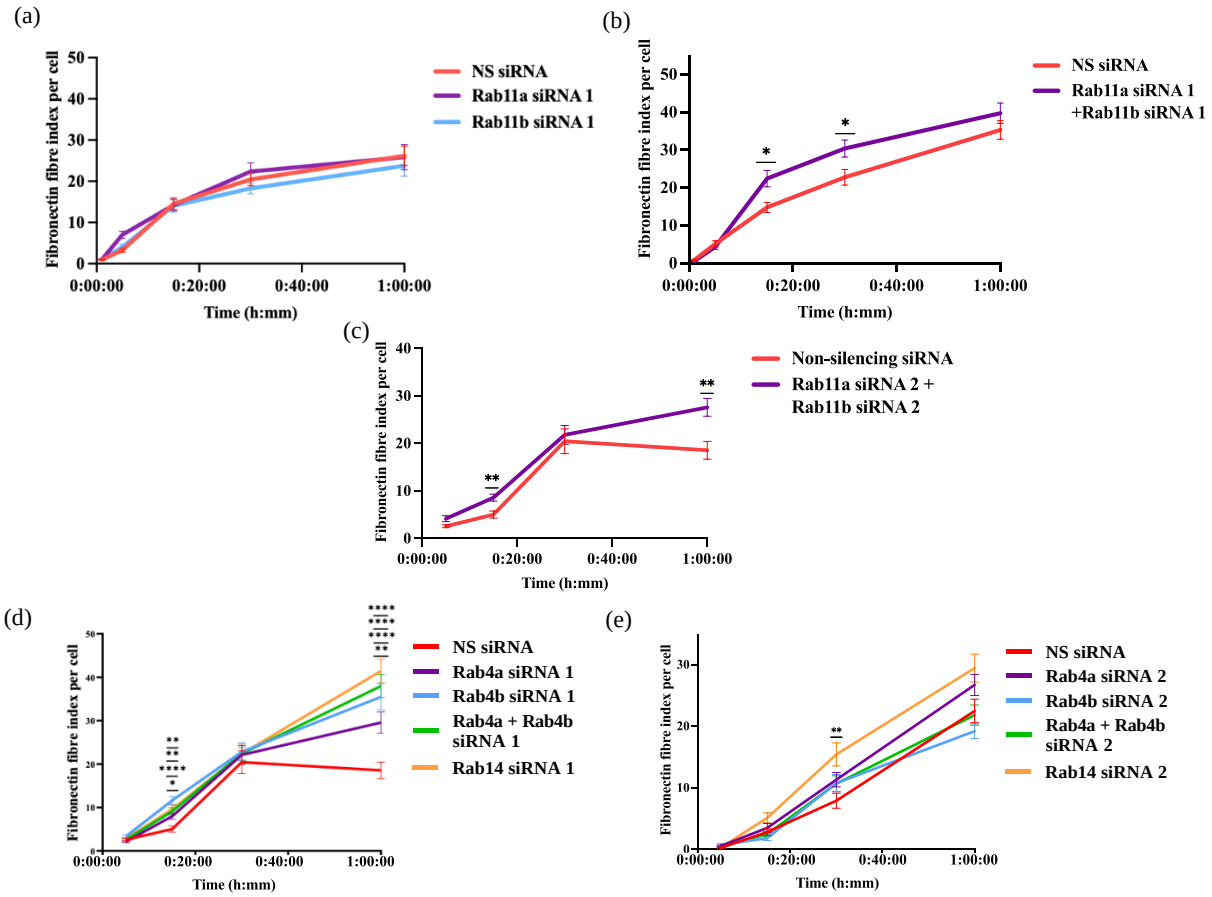

Figure 4.18 – Multiple group 1 small GTPases influence assembly of exogenous fibronectin by CAFs

*CAFs (MOC195 or MOC194) were pre-treated with TGFβ3 (10 ng.mL^{-1}), then transfected with the NS siRNA, or recycling regulator targeting siRNAs. CAFs were seeded into 96-well imaging dishes, and after cell attachment, exogenous fibronectin was added (5 µg.mL^{-1}) and cells were fixed after 5-, 15-, 30- or 60-minutes. Fluorescence microscopy was used to capture a single z-section at 10 different positions per condition, and the ridge detection algorithm was used to calculate the fibre index for each image as described previously, which was then normalised to cell number (N = 3). (a) Quantification, and statistical analysis, of fibre index for fibronectin assembled by CAFs (MOC194) transfected with NS siRNA, Rab11a siRNA 1, or Rab11b siRNA 1. (b) Quantification, and statistical analysis (*p<0.5), of fibre index for fibronectin assembled by CAFs (MOC194) transfected with NS siRNA, or Rab11a siRNA 1 + Rab11b siRNA 1.*

Figure legend continues on the next page.

Figure 4.18 – Multiple group 1 small GTPases influence assembly of exogenous fibronectin by CAFs

*(c) Quantification, and statistical analysis (**p<0.01), of fibre index for fibronectin assembled by CAFs (MOC195) transfected with NS siRNA, or Rab11a siRNA 2 + Rab11b siRNA 2. (d) Quantification, and statistical analysis (*p<0.05, **p<0.01, ****p<0.0001), of fibre index for fibronectin assembled by CAFs (MOC195) transfected with NS siRNA, Rab4a siRNA 1, Rab4b siRNA 1, Rab4a siRNA 1 + Rab4b siRNA 1, or Rab14 siRNA 1. (e) Quantification, and statistical analysis (**p<0.01), of fibre index for fibronectin assembled by CAFs (MOC195) transfected with NS siRNA, Rab4a siRNA 2, Rab4b siRNA 2, Rab4a siRNA 2 + Rab4b siRNA 2, or Rab14 siRNA 2. All statistical analyses were carried out by two-way ANOVA. All statistically significant results are shown.*

4.6.4 Group 2 and 3 small GTPases

Similar to the endocytic recycling regulators classified into group 1, groups 2 and 3 also contained a number of small GTPases that when depleted led to significant increases in the fibronectin fibre indices measured. Within group 2, depletion of Rab8a or Arf6 in CAFs from patient MOC194 resulted in significantly higher levels of fibronectin assembly at the 60-minute time point (Figure 4.19c, 4.19d). Example images demonstrating higher fibronectin assembly following Arf6 depletion are shown (Figure 4.19a, 4.19b). These finding were then validated in CAFs from patient MOC195 using Rab8a siRNA 2, or Arf6 siRNA 2, where significantly higher fibronectin fibre indices were measured at the 30-minute time point (Figure 4.19e). Within group 3, depletion of multiple small GTPases significantly increased the capacity of CAFs from patient sample MOC194 to assemble exogenous fibronectin. Higher fibre indices were measured at the 15-minute time point following depletion of Rab5b, Rab5c, Rab5a + Rab5b + Rab5c, Rab21, or Rab22a. In addition, higher fibre indices were measured at the 30- and 60-minute time points following Rab5a + Rab5b + Rab5c, or Rab22a depletion, with Rab21 depletion also leading to a higher fibre index measured at the 60-minute time point (Figure 4.20c, 4.20d). Example images demonstrating the enhanced ability of CAFs from patient MOC194 to assemble exogenous fibronectin following Rab22a depletion are shown (Figure 4.20a, 4.20b). These results for Rab5c, Rab21, Rab22a, and Rab22b, could then be validated in CAFs from patient MOC195, where higher fibre indices were measured at the 30-minute timepoint following depletion of these GTPases. Furthermore, Rab5c depletion also lead to a higher fibre index measured at the 60-minute timepoint.

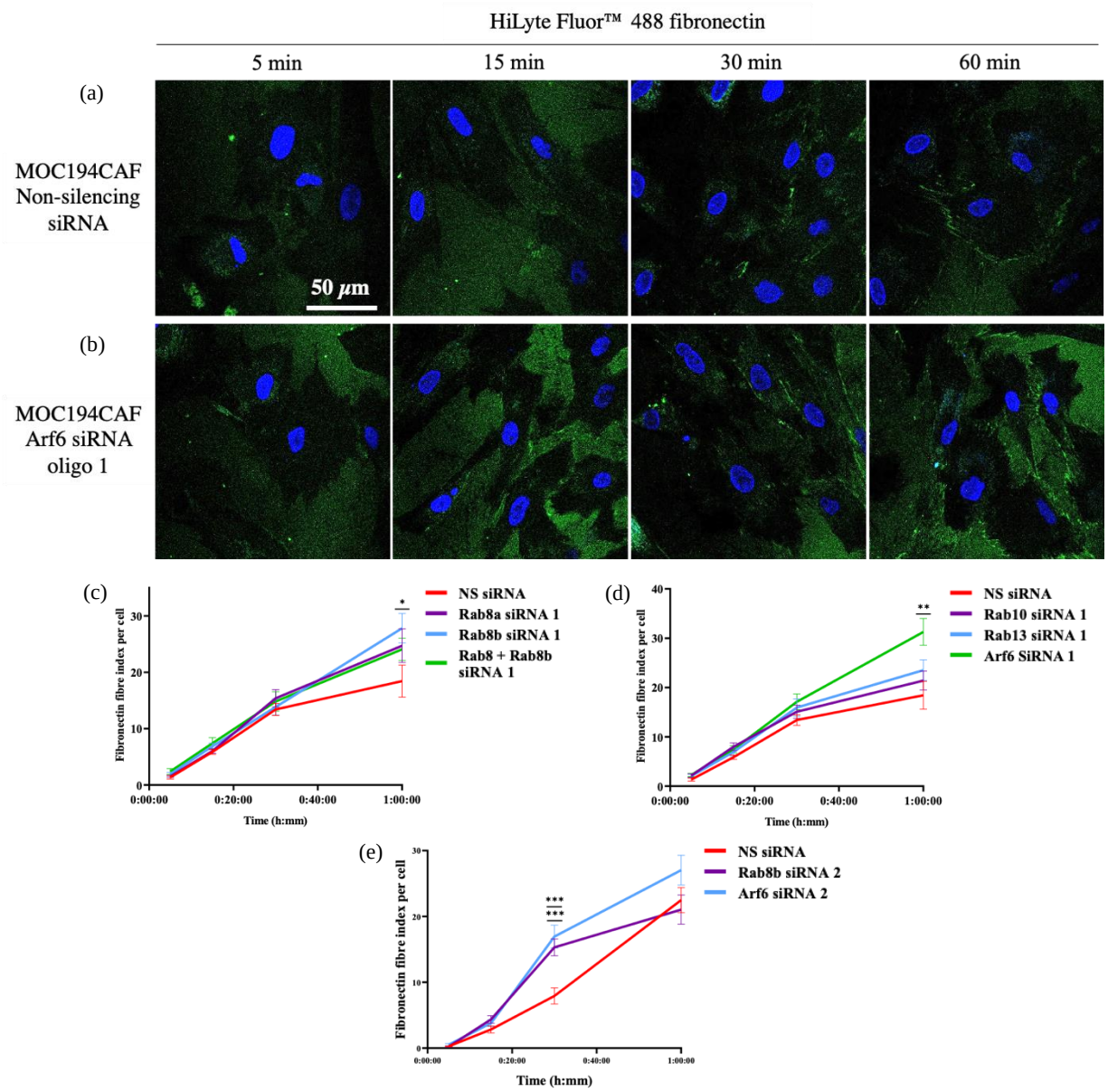

Figure 4.19 – Rab8a and Arf6 influence the assembly of exogenous fibronectin by CAFs

*Exogenous fibronectin assembly assays were carried out with CAFs (MOC194 or MOC195) transfected with recycling regulator GTPase targeting siRNAs as described previously (N = 3). Example composite images for CAFs (MOC194) transfected with NS siRNA (a) or Arf6 siRNA 1 (b) are shown at each time point. (c) Quantification, and statistical analysis (*p<0.05), of fibre index for fibronectin assembled by CAFs (MOC194) transfected with NS siRNA, Rab8a siRNA 1, Rab8b siRNA 1, or Rab8a siRNA 1 + Rab8b siRNA 1.*

Figure legend continues on the next page.

Figure 4.19 – Rab8a and Arf6 influence the assembly of exogenous fibronectin by CAFs

*(d) Quantification, and statistical analysis (**p<0.01), of fibre index for fibronectin assembled by CAFs (MOC194) transfected with NS siRNA, Rab10a siRNA 1, Rab13 siRNA 1, or Arf6 siRNA 1. (e) Quantification, and statistical analysis (***p<0.001), of fibre index for fibronectin assembled by CAFs (MOC195) transfected with NS siRNA, Rab8b siRNA 2, or Arf6 siRNA 2. All statistical analyses were carried out by two-way ANOVA. All statistically significant results are shown.*

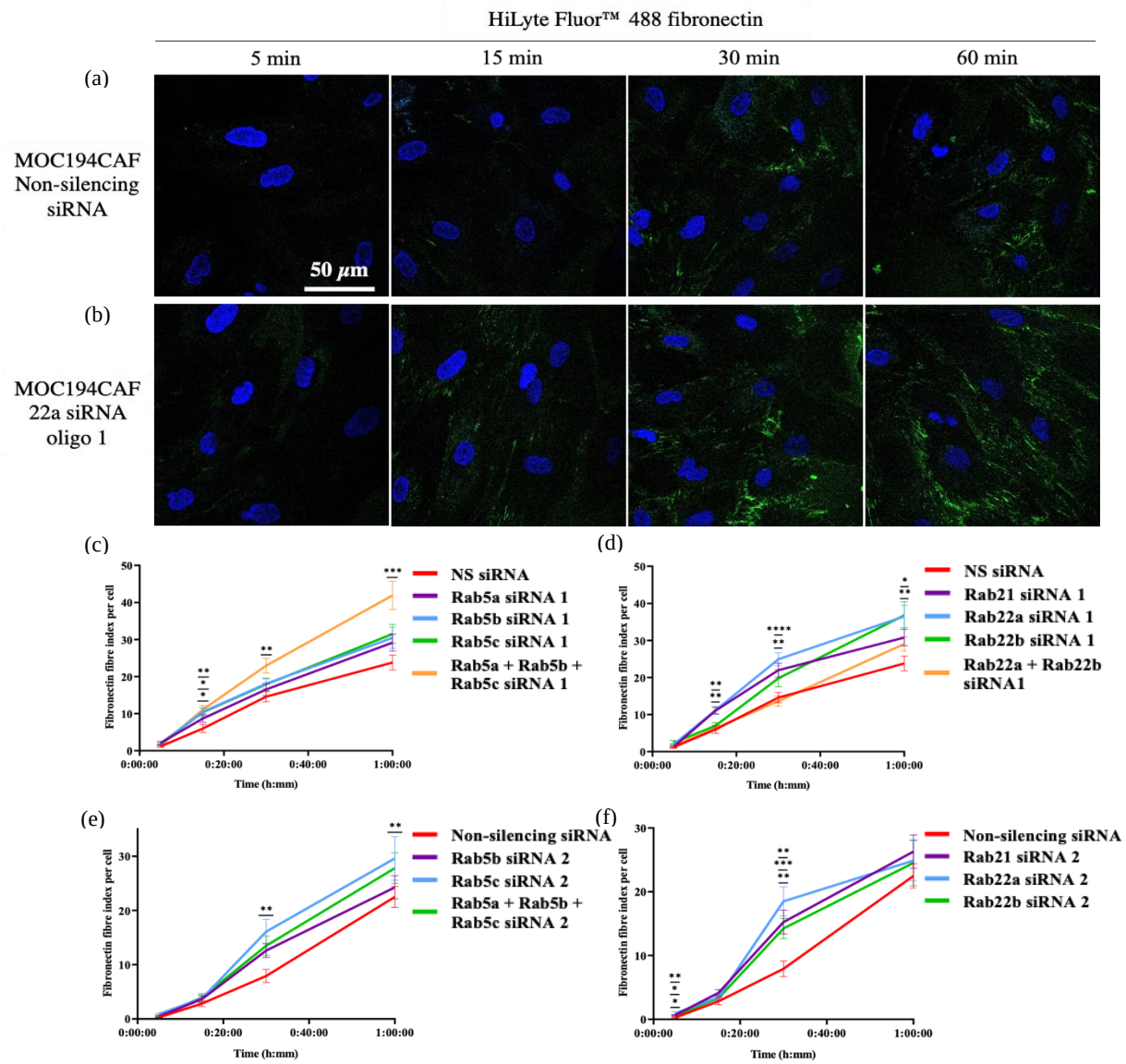

Figure 4.20 – Rab5c, Rab21, Rab22a and Rab22b influence the assembly of exogenous fibronectin by CAFs

*Exogenous fibronectin assembly assays were carried out with CAFs (MOC194 or MOC195) transfected with recycling regulator GTPase targeting siRNAs as described previously (N = 3). Example composite images for CAFs (MOC194) transfected with NS siRNA (a) or Rab22a siRNA 1 (b) are shown at each time point. (c) Quantification, and statistical analysis (*p<0.05, **p<0.01, ***p<0.001), of fibre index for fibronectin assembled by CAFs (MOC194) transfected with NS siRNA, Rab5a siRNA 1, Rab5b siRNA 1, Rab5c siRNA 1, or Rab5a siRNA 1 + Rab5b siRNA 1 + Rab5c siRNA 1.*

Figure legend continues on the page.

Figure 4.20 – Rab5c, Rab21, Rab22a and Rab22b influence the assembly of exogenous fibronectin by CAFs

*(d) Quantification, and statistical analysis (*p<0.05,**p<0.01, ****p<0.0001), of fibre index for fibronectin assembled by CAFs (MOC194) transfected with NS siRNA, Rab21 siRNA 1, Rab22a siRNA 1, Rab22b siRNA 1, or Rab22a siRNA 1 + Rab22b siRNA 1. (e) Quantification, and statistical analysis (**p<0.01), of fibre index for fibronectin assembled by CAFs (MOC195) transfected with NS siRNA, Rab5b siRNA 2, Rab5c siRNA 2, or Rab5a siRNA 2 + Rab5b siRNA 2+ Rab5c siRNA 2. (f) Quantification, and statistical analysis (*p<0.05, **p<0.01, ***p<0.001), of fibre index for fibronectin assembled by CAFs (MOC195) transfected with NS siRNA, Rab21 siRNA 2, Rab22a siRNA 2, or Rab22b siRNA 2. All statistical analyses were carried out by two-way ANOVA. All statistically significant results are shown.*

4.7 Collagen I deposition requires endocytic recycling

4.7.1 Overview

As with fibronectin, collagen I is also abundant within the HGSOC omental TME, and is known to play roles in facilitating cancer cell invasion and growth [98] [395] [396]. Therefore, in addition to evaluating the impact of depleting recycling regulator GTPases in CAFs on their ability to deposit endogenous fibronectin, and to assemble exogenous fibronectin, the role of each GTPase in collagen I assembly by CAFs in 2D culture was also investigated. In contrast to fibronectin, where several Rab GTPases have been implicated in regulating its assembly by a number of cell types, none of the recycling regulator GTPases depleted during this siRNA screen had previously been associated with regulating collagen I deposition.

4.7.2 Group 1 GTPases

To begin investigating the role of each recycling regulator GTPase in collagen I fibrillogenesis, Rab11a and Rab11b were depleted in CAFs from patient MOC195, both individually and in combination, and the effect of doing so on their ability to assemble collagen I in 2D was assessed by immunofluorescence microscopy. CAFs in which Rab11a, or Rab11b, had been depleted were able to assemble collagen I at a level comparable to that observed when CAFs were transfected with the NS siRNA (Figure 4.21a, 4.21b, 4.21c, 4.21e). Depletion of both Rab11 isoforms in combination in CAFs from patient MOC195 resulted in a significant increase in collagen I deposition, where a higher total fibre area was measured relative to CAFs transfected with the NS siRNA (Figure 4.21d, 4.21f). However, this result could not be validated in CAFs from patient MOC194, where instead a significant decrease in collagen I deposition was measured following depletion of both Rab11 isoforms (Figure 4.21g, 4.21h, 4.21i). Interestingly, these patterns of collagen I deposition in CAFs from patient MOC194 and MOC195 following Rab11a and Rab11b depletion were also observed in the deposition of fibronectin (Figure 4.13). As may be the case with fibronectin deposition, the opposite collagen I assembly capacities following GTPase depletion displayed by the CAFs from these two patients could indicate that they utilise different small GTPases to varying extents to assemble collagen I. However, it is also possible that the opposite results observed are due to off target effects of each siRNA used to deplete GTPase levels.

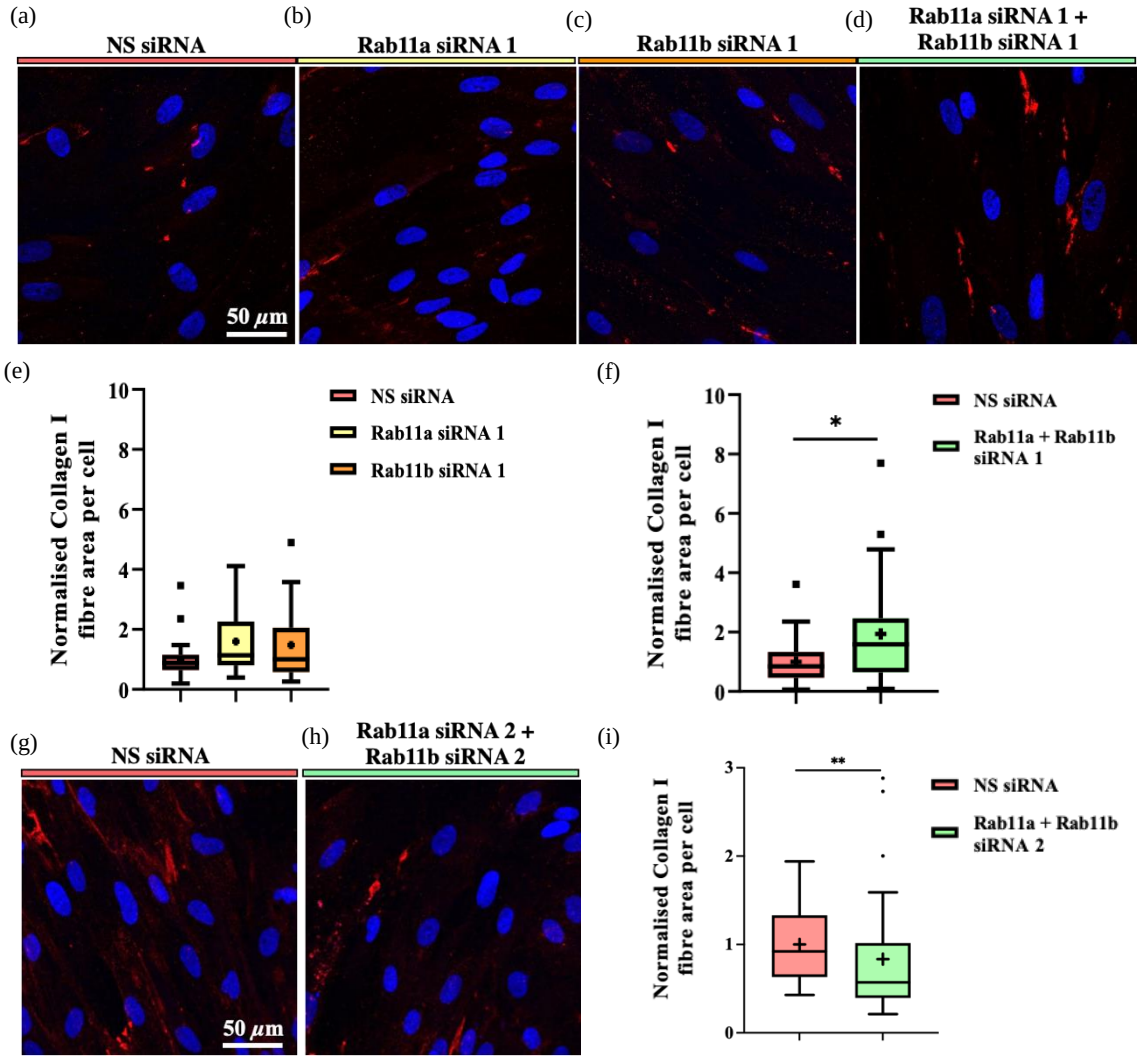

Figure 4.21 – CAFs do not require Rab11a or Rab11b to deposit collagen I

*Primary CAFs (MOC195) were pre-transfected with either the NS siRNA, or recycling regulator targeting siRNA oligos, then seeded on to coverslips and cultured for 10 days in the presence of TGFβ3 (10 ng.mL^{-1}) and ascorbic acid (20 μg.mL^{-1}). Collagen I was immunostained and visualised by fluorescence microscopy (N = 3). Representative images from three biological replicates are shown, where CAFs (MOC195) were pre-transfected with the NS siRNA (a), Rab11a siRNA 1 (b), Rab11b siRNA 1 (c), or Rab11a siRNA 1+ Rab11b siRNA 1 (d). Merged data from three biological replicates of collagen I deposition by CAFs (MOC195) following depletion of Rab11a or Rab11b (e), or Rab11a and Rab11b together (f), was quantified and statistically analysed by one-way ANOVA (*p<0.05). Statistically significant results were then validated using a second siRNA oligo against the target GTPase in a second CAF line (MOC194). Representative images from three biological replicates are shown, where CAFs (MOC194) were pre-transfected with the NS siRNA (g), or Rab11a siRNA 2 + Rab11b siRNA 2 (h).*

Figure legend on the next page.

Figure 4.21 – CAFs do not require Rab11a or Rab11b to deposit collagen I

*Merged data from three biological replicates of collagen I deposition by CAFs (MOC194) following Rab11a + Rab11b depletion (i) was quantified and statistically analysed by Mann-Whitney test (**p<0.01). Normalised collagen I fibre area values are sown, where the fibre area for each image was normalised within each biological replicate by dividing by the average fibre area for the NS siRNA condition. All statistically significant results are shown. Nuclei were stained with Hoechst 33342. Scale bar = 50 μm. Maximum intensity projections of z-stacks are shown.*

The depletion of the remaining small GTPases classified into group 1 in CAFs from patient MOC194 indicated that Rab4b, Rab4a + Rab4b in combination, and Rab14, may be involved in regulating collagen I deposition, where significant reductions in total collagen fibre area were measured (Figure 4.22). However, during the validation of these findings, only the depletion of Rab14 with siRNA 2 in CAFs from patient MOC194 resulted in collagen I assembly defects (Figure 4.22j, 4.22k). These results suggest that of the small GTPases classified into group 1, only Rab14 is essential for collagen I fibrillogenesis by omental CAFs in the HGSOC TME.

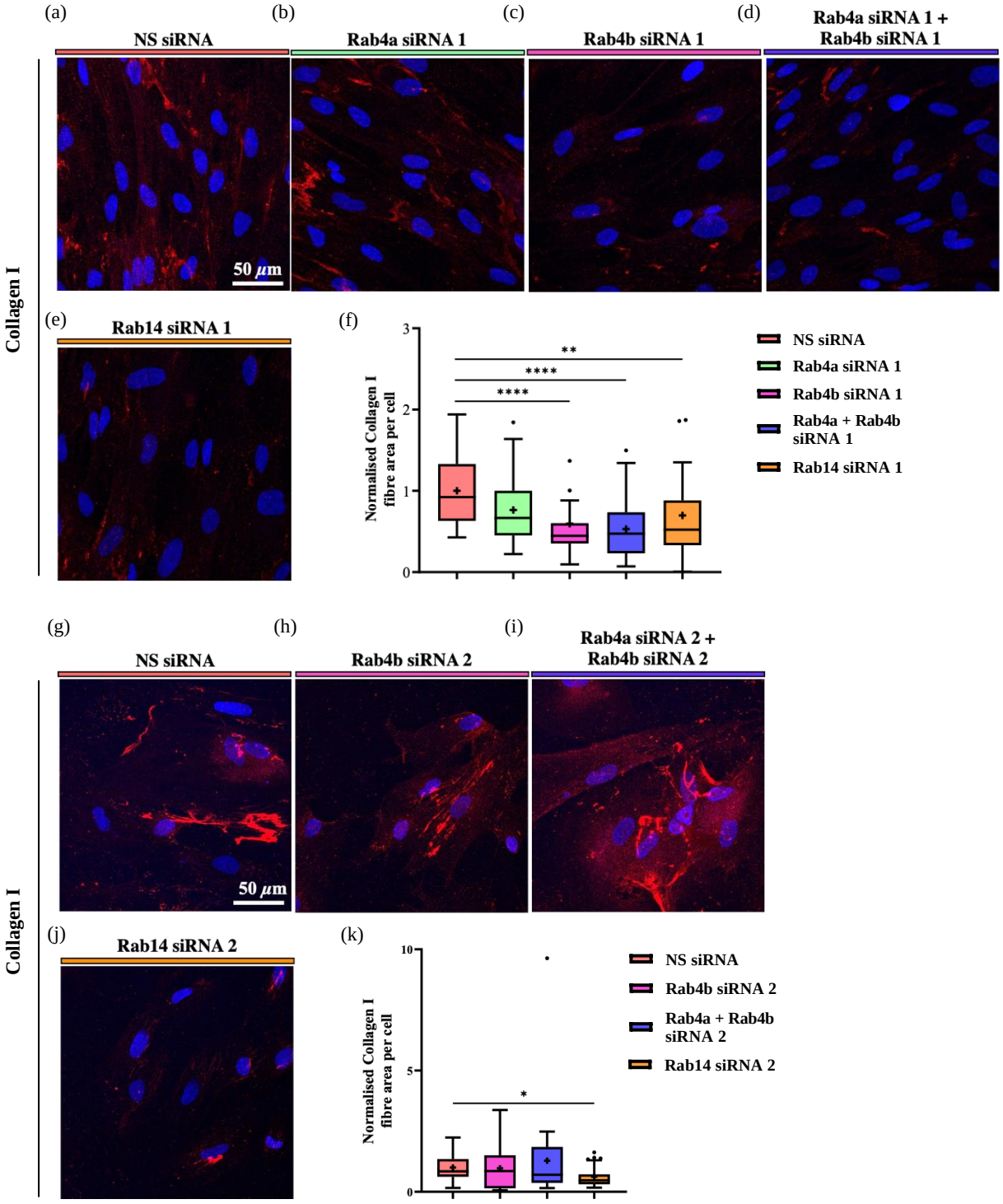

Figure 4.22 – Rab14 is required for the deposition of collagen I omental CAFs

Primary CAFs (MOC194) were pre-transfected with either the NS siRNA, or recycling regulator targeting siRNA oligos, then seeded on to coverslips and cultured for 10 days in the presence of TGFβ3 (10 ng.mL^{-1}) and ascorbic acid (20 μg.mL^{-1}). Collagen I was immunostained and visualised by fluorescence microscopy (N = 3).

Figure legend continues on the next page.

*Representative images from three biological replicates are shown, where CAFs (MOC194) were pre-transfected with the NS siRNA (a), Rab4a siRNA 1 (b) , Rab4b siRNA 1 (c), Rab4a siRNA 1 + Rab4b siRNA 1 in combination (d), or Rab14 siRNA 1 (e). Merged data from three biological replicates of collagen I deposition by CAFs (MOC194) following siRNA transfection was quantified and statistically analysed by Kruskal-Wallis test (**p<0.01, ****p<0.0001). Statistically significant results were then validated using a second siRNA oligo against the target GTPase in a second CAF line (MOC195). Representative images from three biological replicates are shown, where CAFs (MOC195) were pre-transfected with the NS siRNA (g), Rab4b siRNA 2, Rab4a siRNA 2 + Rab4b siRNA 2, or Rab14 siRNA 2 (h). Merged data from three biological replicates of collagen I deposition by CAFs (MOC195) following Rab11a + Rab11b depletion (i) was quantified and statistically analysed by Kruskal-Wallis (*p<0.01). Normalised collagen I fibre area values are sown, where the fibre area for each image was normalised within each biological replicate by dividing by the average fibre area for the NS siRNA condition. All statistically significant results are shown. Nuclei were stained with Hoechst 33342. Scale bar = 50 μm. Maximum intensity projections of z-stacks are shown.*

4.7.3 Group 2 and 3 small GTPases

Similarly, the depletion of multiple recycling regulators classified into group 2 in CAFs from patient MOC194 resulted in defects in their ability to deposit collagen I. Significant reductions in the total collagen I fibre area were measured following depletion of Rab8a + Rab8b in combination, Rab10, Rab13, and Arf6 (Figure 4.23). When these group 2 recycling regulators were then depleted in CAFs from patient MOC195, only pre-transfection of CAFs with Arf6 siRNA 2 resulted in a significant reduction in the total collagen I fibre area measured, with collagen I deposition following Rab8a + Rab8b, Rab10, or Rab13 depletion remaining unaffected (Figure 4.23n, 4.23o). These data therefore suggest that of the recycling regulators classified into group 2, only Arf6 influences the assembly of collagen I fibres in 2D by omental CAFs.

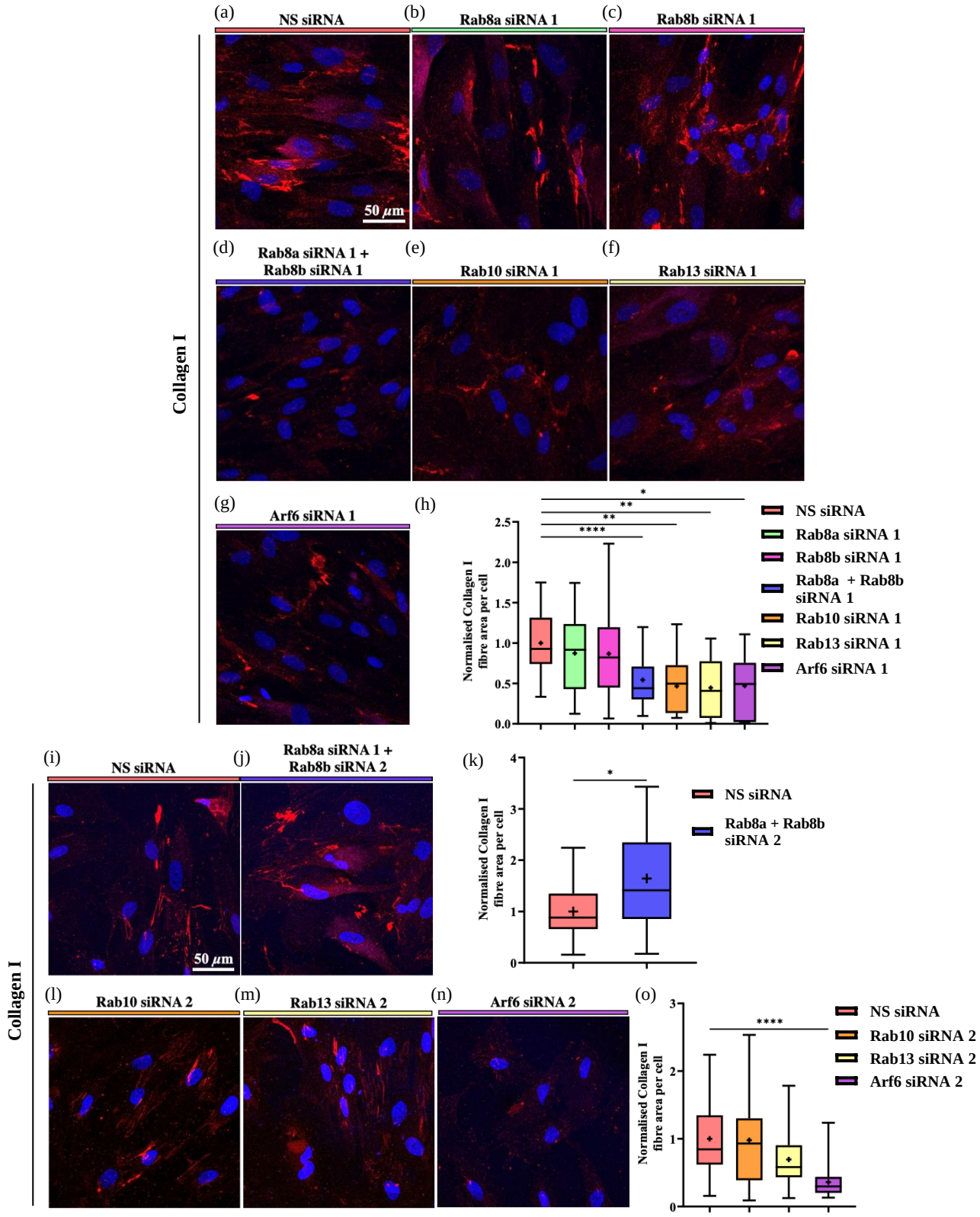

Figure 4.23 – Arf6 is required for the deposition of collagen I omental CAFs

Figure legend on the next page.

Figure 4.23 – Arf6 is required for the deposition of collagen I omental CAFs

*Primary CAFs (MOC194) were pre-transfected with either the NS siRNA, or recycling regulator targeting siRNA oligos, then seeded on to coverslips and cultured for 10 days in the presence of TGFβ3 (10 ng.mL^{-1}) and ascorbic acid (20 µg.mL^{-1}). Collagen I was immunostained and visualised by fluorescence microscopy (N = 3). Representative images from three biological replicates are shown, where CAFs (MOC194) were pre-transfected with the NS siRNA (a), Rab8a siRNA 1 (b), Rab8b siRNA 1 (c), Rab8a siRNA 1 + Rab8b siRNA 1 in combination (d), Rab10 siRNA 1 (e), Rab13 siRNA 1 (f), or Arf6 siRNA 1 (g). (h) Merged data from three biological replicates of collagen I deposition by CAFs (MOC194) following siRNA transfection was quantified and statistically analysed by Kruskal-Wallis test (*p<0.05, **p<0.01, ****p<0.0001). Statistically significant results were then validated using a second siRNA oligo against the target GTPase in a second CAF line (MOC195). Representative images from three biological replicates are shown, where CAFs (MOC195) were pre-transfected with the NS siRNA (i), Rab8a siRNA 2 + Rab8b siRNA 2 (j), Rab10 siRNA 2 (l), Rab13 siRNA 2 (m), or Arf6 siRNA 2 (n). Merged data from three biological replicates of collagen I deposition by CAFs (MOC195) following siRNA transfection was quantified and statistically analysed by Mann-Whitney test (*p<0.01; k), or by Kruskal-Wallis test (****p<0.0001, o). Normalised collagen I fibre area values are sown, where the fibre area for each image was normalised within each biological replicate by dividing by the average fibre area for the NS siRNA condition. All statistically significant results are shown. Nuclei were stained with Hoechst 33342. Scale bar = 50 µm. Maximum intensity projections of z-stacks are shown.*

In contrast to groups 1 and 2 that each contained a recycling regulator required for collagen I assembly by CAFs, depletion of any of the small GTPases classified into 3 suggested that none have a role in regulating collagen I deposition. CAFs from patient MOC194 remained capable of depositing collagen I in the extracellular space following depletion of Rab5a, Rab5b and Rab5c, all Rab5 isoforms in combination, Rab21, Rab22a, Rab22b, and both Rab22 isoforms in combination (Figure 4.24).

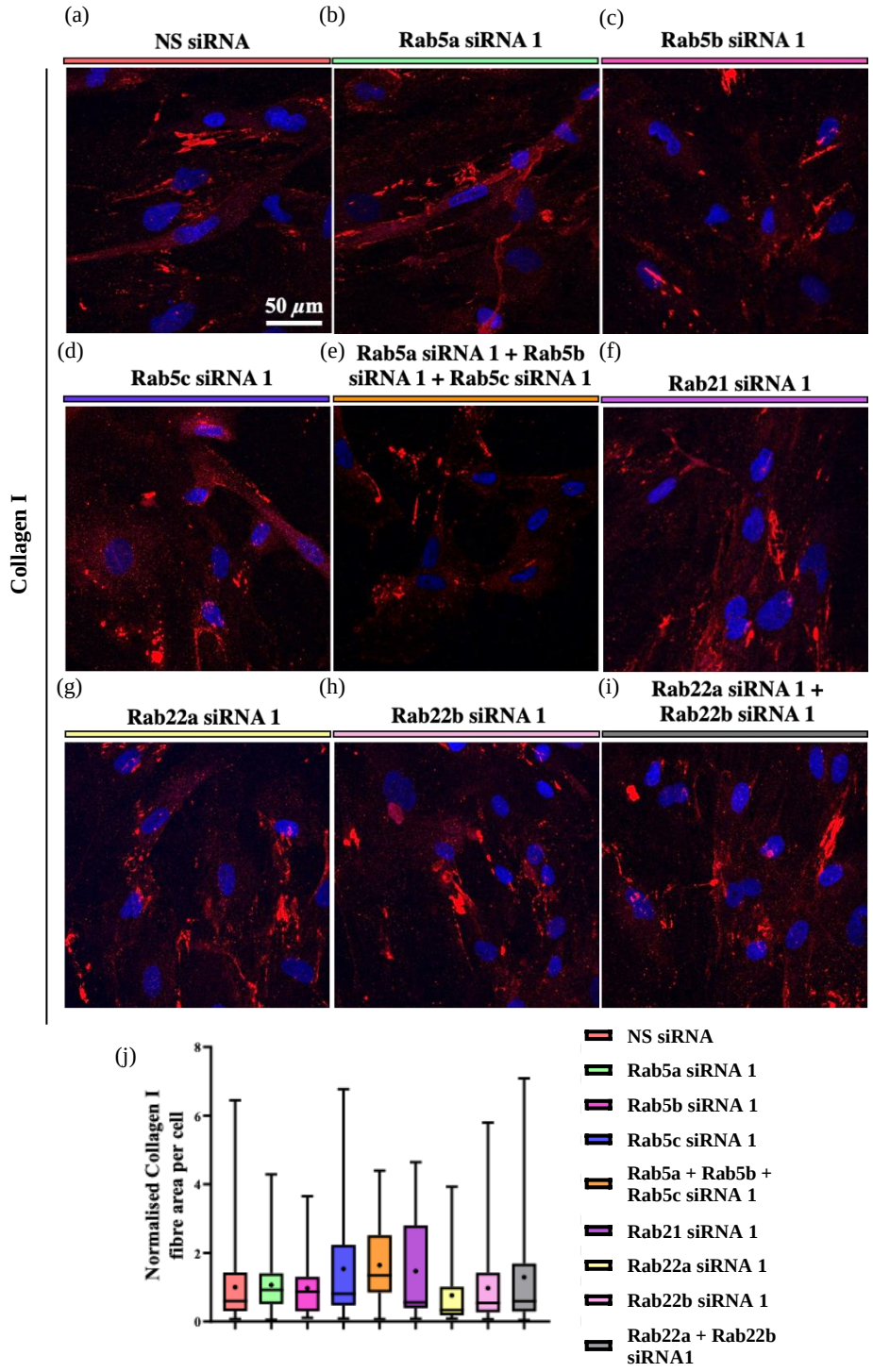

Figure 4.24 – Collagen I deposition is not regulated by group 3 small GTPases

Primary CAFs (MOC194) were pre-transfected with either the NS siRNA, or recycling regulator targeting siRNA oligos, then seeded on to coverslips and cultured for 10 days in the presence of TGFβ3 (10 ng.mL^{-1}) and ascorbic acid (20 μg.mL^{-1}). Collagen I was immunostained and visualised by fluorescence microscopy (N = 3).

Figure legend continues on the next page.

Figure 4.24 – Collagen I deposition is not regulated by group 3 small GTPases

*Representative images from three biological replicates are shown, where CAFs (MOC194) were pre-transfected with the NS siRNA (a), Rab5a siRNA 1 (b), Rab5b siRNA 1 (c), Rab5c siRNA 1 (d), Rab5a siRNA 1 + Rab5b siRNA 1 + Rab5c siRNA 1 in combination (e), Rab21 siRNA 1 (f), Rab22a siRNA 1 (g), Rab22b siRNA 1 (h), or Rab22a siRNA 1 + Rab22b siRNA 1 in combination (i). (j) Merged data from three biological replicates of collagen I deposition by CAFs (MOC194) following siRNA transfection was quantified and statistically analysed by Kruskal-Wallis test (**p<0.01). Normalised collagen I fibre area values are sown, where the fibre area for each image was normalised within each biological replicate by dividing by the average fibre area for the NS siRNA condition. All statistically significant results are shown. Nuclei were stained* with *Hoechst 33342. Scale bar = 50 μm. Maximum intensity projections of z-stacks are shown.*

These data therefore indicate that, of the recycling regulators depleted during this siRNA screen, only Rab14 and Arf6 were required for CAFs from across HGSOC patients to assemble collagen I ECM in 2D. Interestingly, Arf6 was also required for CAFs to facilitate the invasion of Kuramochi cells during 3D spheroid invasion assays, suggesting that defects in collagen I deposition/remodelling could underlie why CAFs in which Arf6 has been depleted display a limited capacity to support Kuramochi invasion in 3D (Figure 4.10). However, the reduction in Kuramochi invasion following Rab14 depletion could not be validated in a second CAF isolate with a second siRNA. This suggested that an inability to deposit new collagen I fibres in 2D alone, was not sufficient to cause defects in the HGSOC cell invasion-promoting capacity of CAFs in 3D. Furthermore, the depletion of Rab4a + Rab4b in CAFs from patients MOC194 and MOC208 reduced their ability to promote Kuramochi invasion, however only in CAFs from patient MOC194 did depletion of these regulators result in collagen I deposition defects in 2D. This indicated that the limited ability of CAFs to support Kuramochi invasion following depletion of Rab4a and Rab4b in combination was likely not the result of impaired collagen I fibre deposition.

4.8 Second-harmonic generation (SHG) microscopy to visualise the organisation of collagen around spheroids

4.8.1 Overview

The data obtained during the siRNA screen suggested that Arf6 depletion in CAFs may reduce their capacity for supporting Kuramochi invasion through causing defects in their ability to deposit new collagen I fibres. However, considering the ECM deposition and spheroid invasion assay results following Rab4a + Rab4b, or Rab14 depletion, this indicated that alternative mechanisms may also be important for CAFs to support invasion in 3D.

It is possible that only Arf6 is required for collagen I deposition by CAFs both in 2D and 3D, whereas Rab14, and Rab4 isoforms, are required for the deposition of new collagen I fibres only in 2D, and 3D culture, respectively. However, as during the invasion assays spheroids were embedded in a collagen I hydrogel, it was unclear how defective collagen I deposition by CAFs, for example following Arf6 depletion, would result in such a significant reduction in their capacity for supporting cancer cell invasion. We hypothesised that the reduced Kuramochi invasion observed following GTPase depletion, may be due to them having a role in regulating collagen ECM remodelling. Data described previously indicated that depletion of either Arf6, or Rab4 isoforms, did not alter cell contractility. We therefore also hypothesised that any observed ECM remodelling defects caused by Rab4 isoform or Arf6 depletion, were due to these GTPases having an involvement in contraction-independent ECM remodelling mechanisms.

In order to investigate whether depletion of Rab4a + Rab4b, Rab14, or Arf6, resulted in differences in collagen ECM organisation in the vicinity of spheroids, second-harmonic generation microscopy was used. This microscopy technique generates contrast through the interaction of light with structures that do not possess a centre of symmetry (non-centrosymmetric). Very few structures in biology are non-centrosymmetric, however collagen is one is them. Using multiphoton microscopy, a second harmonic signal can be generated from tissues rich in collagen, allowing the organisation of that collagen to be visualised, where larger collagen fibres give rise to a stronger signal [397]. This technique therefore allowed for the imaging of collagen organisation around Kuramochi and CAF co-culture spheroids following depletion of Rab4a + Rab4, Rab14, or Arf6 in CAFs.

4.8.2 SHG microscopy on collagen gels following small GTPase depletion

When comparing the structure of collagen around spheroids consisting only of Kuramochi cells with that surrounding Kuramochi and CAF (MOC208) co-culture spheroids, where CAFs had been transfected with the NS siRNA, clear differences were observed. The collagen around Kuramochi monoculture spheroids consistently adopted a cross-hatched organisation, where defined, unbundled fibres were observed crossing over one-another (Figure 4.25a). In contrast, the arrangement of collagen in the vicinity of Kuramochi and CAF co-culture spheroids following transfection with the NS siRNA was consistently more bundled, generating a meshwork of collagen where individual fibres were more difficult to resolve (Figure 4.25b). Whilst, in some cases, the collagen around spheroids appeared bundled into a meshwork arrangement similar to that observed following transfection with the NS siRNA, this bundling was less consistent. The collagen in the vicinity of many spheroids following depletion of these GTPases, particularly in the case of Arf6, was more cross-hatched with minimal bundling, suggesting that these GTPases may be involved in regulating ECM remodelling by CAFs (Figure 4.25c, 4.25e). It was suspected that the ability of CAFs to remodel the collagen in this way, may in part be responsible for their invasion promoting properties, and visualisation of the collagen around spheroids following Rab14 depletion provided evidence in favour of this. The collagen surrounding spheroids containing Rab14 depleted CAFs was mostly bundled, and in a similar arrangement to that observed following NS siRNA transfection, which was expected as a role for Rab14 in the facilitation of Kuramochi invasion by CAFs could not be validated previously (Figure 4.25d).

4.8.3 SHG microscopy image analysis method

Prior to validating these findings in CAFs isolated from a different patient with second siRNA oligos targeting these GTPases, a method for analysing the arrangement of collagen in the spheroid vicinity was developed. As the presence or absence of collagen bundling around the spheroids correlated with the invasion of Kuramochi cells into the hydrogel, the aim of this analysis was to measure collagen bundling. Due to the fact that collagen fibres were more defined in the absence of bundling, the ridge detection algorithm could be used to detect fibres with a minimum line width of 10 pixels and a minimum line length of 150 pixels. This enabled large fibre indices to be measured, where a large fibre index corresponded to minimal collagen bundling (Figure 4.25f). This analysis revealed that the arrangement of the collagen surrounding spheroids where Rab4a + Rab4b, or Arf6 had been depleted in CAFs from patient MOC208, had a higher large fibre index than those where CAFs had been transfected with the NS siRNA (Figure 4.25g). Although the differences in fibre index were not statistically significant, these results did suggest that depletion of Rab4a + Rab4b, or Arf6, may reduce the ability of CAFs to support Kuramochi invasion through perturbing their ECM remodelling capabilities.

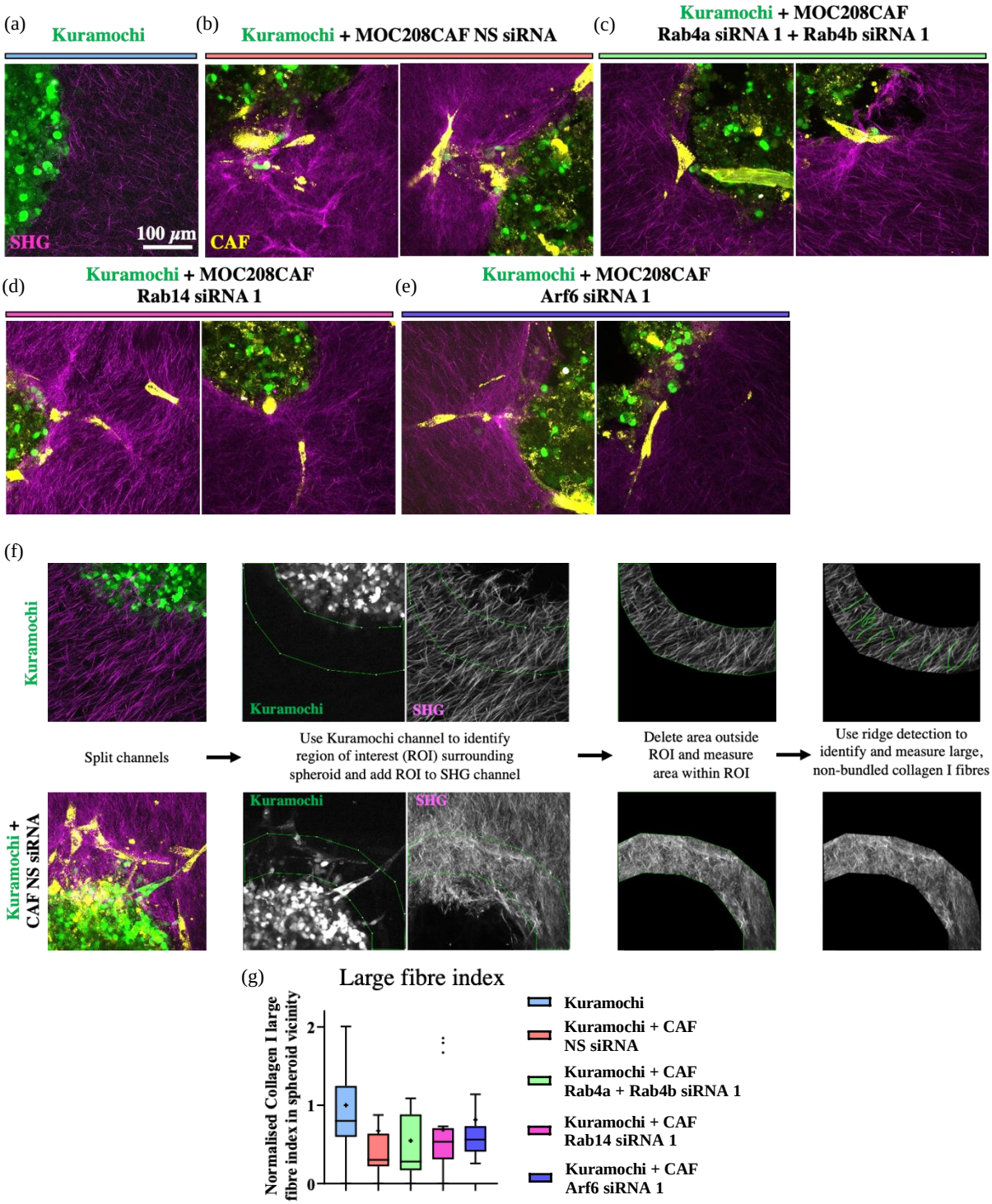

Figure 4.25 – CAFs remodel collagen in the vicinity of spheroids

CAFs (MOC208) were pre-transfected with either the NS siRNA, or siRNA oligos targeting recycling regulator GTPases. Spheroids were formed as described previously, consisting of GFP-expressing Kuramochi cells either as a mono-culture, or in co-culture with CAFs, where CAFs were stained red with PKH26 (shown as yellow in images).

Figure legend continues on the next page.

Figure 4.25 – CAFs remodel collagen in the vicinity of spheroids

After 4 days within the collagen hydrogel, Spheroids were fixed in PFA (4%), and the organisation of the collagen surrounding spheroids was then visualised by SHG microscopy using a multiphoton microscope (SHG signal shown in magenta; N = 3). Representative images of spheroids consisting of Kuramochi cells as a monoculture (a), or in co-culture with CAFs pre-transfected with the NS siRNA (b), Rab4a siRNA 1 + Rab4b siRNA 1 (c), Rab14 siRNA 1 (d), or Arf6 siRNA 1 (e). (f) Collagen organisation within the spheroid vicinity was analysed using the ridge detection algorithm (Minimum line width = 10 pixels, minimum line length = 150 pixels) to generate a large fibre index around each spheroid. (g) Merged data from three biological replicates of large fibre index in the area surrounding spheroids was quantified and statistically analysed by Kruskal-Wallis test. Normalised large fibre indices are shown, where the large fibre index for each image was normalised within each biological replicate by dividing by the average large fibre index of the Kuramochi mono-culture spheroids. All statistically significant results are shown. Scale bar = 100 μm. Maximum intensity projections of z-stacks are shown.

4.8.4 SHG microscopy validation

To validate these findings, and to ensure that these differences in collagen ECM bundling around the spheroids were not due to off-target effects of the siRNA oligos, Rab4a + Rab4b, Rab14, or Arf6, were depleted in CAFs using different siRNA oligos against these GTPases. Unfortunately, at the time of carrying out these experiments, only CAFs from patient MOC208 were available for use in spheroid invasion assays and SHG microscopy. Nevertheless, depletion of these GTPases with the second siRNA oligos generated similar results to those observed previously. CAFs transfected with the NS siRNA were capable of bundling collagen, resulting in a significantly lower large fibre index measured relative to that measured when Kuramochi cells alone were present in spheroids (Figure 4.26a, 4.26b, 4.26f). Similar to the collagen organisation around spheroids observed previously, transfection of CAFs with Rab4a siRNA 2 + Rab4b siRNA 2, or Arf6 siRNA 2, resulted in a reduction in collagen bundling, particularly in the case of Arf6, and a corresponding increase in the large fibre indices measured (Figure 4.26c, 4.26e, 4.26f). Furthermore, following depletion of Rab14 with siRNA 2, collagen bundling by CAFs was more extensive relative to those in which Rab4a + Rab4b, or Arf6, had been depleted, however the differences in large fibre indices measured between these conditions was not as great as that observed previously (Figure 4.26d, 4.26f)

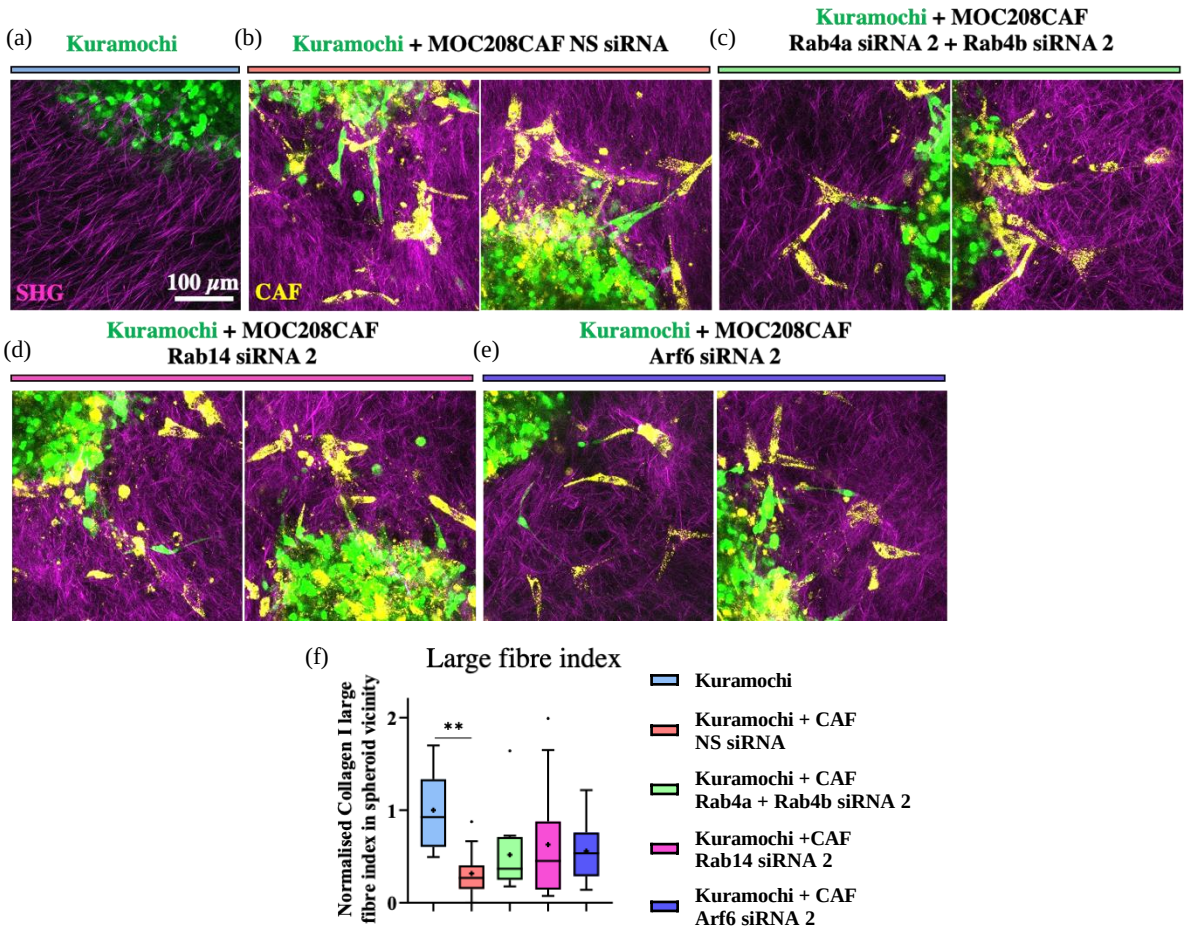

Figure 4.26 – Arf6 depletion in CAFs impairs collagen remodelling in the spheroid vicinity

*CAFs (MOC208) were pre-transfected with either the NS siRNA, or the second siRNA oligos targeting recycling regulator GTPases. Spheroids were formed, fixed in PFA (4%) 4 days after embedding into the collagen hydrogel, and the collagen organisation around spheroids was visualised by SHG microscopy as described previously (N = 3). Representative images of spheroids consisting of Kuramochi cells as a monoculture (a), or in co-culture with CAFs pre-transfected with the NS siRNA (b), Rab4a siRNA 2 + Rab4b siRNA 2 (c), Rab14 siRNA 2 (d), or Arf6 siRNA 2 (e). (f) Merged data from three biological replicates of large fibre index in the area surrounding spheroids was quantified and statistically analysed by Kruskal-Wallis test (**p<0.01). Normalised large fibre indices are shown, where the large fibre index for each image was normalised within each biological replicate by dividing by the average large fibre index of the Kuramochi mono-culture spheroids. All statistically significant results are shown. Scale bar = 100 μm. Maximum intensity projections of z-stacks are shown.*

4.9 Discussion and conclusions

The results in this chapter demonstrate the identification of endocytic recycling regulators that are required for HGSOC patient derived CAFs to support the invasion of Kuramochi cells and to assemble/remodel collagen I ECM.

4.9.1 Endocytic recycling is required for CAFs to support HGSOC cell invasion in 3D

Following RT-qPCR analysis to measure expression levels of each recycling regulator GTPase, an siRNA screen was used to identify which of them were required firstly for CAFs to support Kuramochi invasion in spheroid invasion assays. Work by others has highlighted Rab11b, Rab4a, and Rab10, as being required for the assembly of ECM proteins, such as fibronectin in the case of Rab4 and Rab11 isoforms, by various cell types [321] [320] [318] [319]. Furthermore, others have demonstrated the importance of MT1-MMP, which is recycled in a Rab8, Rab14, Rab22a, and Arf6 regulated manner, in ECM protein deposition and remodelling [324] [323] [299]. Given the role of the ECM in supporting the invasion of many different cancer cell types, we hypothesised that depletion of these GTPases and/or others would impair the capacity of CAFs to support Kuramochi invasion through perturbing recycling pathways involved in ECM assembly [150].

Spheroid invasion assays revealed that depletion of Rab4a + Rab4b, Rab14, or Arf6, in CAFs from patient MOC194 reduced their capacity for facilitating the invasion of Kuramochi cells (Figure 4.7, 4.8). During validation of these results using CAFs from patient MOC208, only the depletion of Rab4a + Rab4b, or Arf6, resulted in defects in their capacity to support Kuramochi invasion, with invasion after Rab14 depletion remaining similar to that observed following NS siRNA transfection (Figure 4.10). A possible explanation for these findings is that given the heterogeneity that is known to exist between CAFs within cancer types, it may be expected that CAFs from different HGSOC patient omentum samples may primarily depend upon different endocytic recycling regulators to promote cancer cell invasion. The CAFs from isolate MOC194 may rely more heavily on Rab14 to support cancer cell invasion than those from isolate MOC208. Further spheroid invasion experiments, where Rab14 siRNA 2 is used to pre-transfect CAFs from isolate MOC194, will be required to determine whether these CAFs require Rab14 to support invasion more so than those from other HGSOC patients.

The depletion of Rab4a + Rab4b, or Arf6, did not alter CAF proliferation rates, their ability to invade out of spheroids themselves, or their ability to contract collagen hydrogels (Figure 4.11, 4.12). These findings, together with spheroid invasion assay data, highlight Rab4a, Rab4b, and Arf6, as having important roles in regulating the endocytic recycling pathways in CAFs across different HGSOC patients to support OC cell invasion. Furthermore, as cell contractility remained unaltered following Rab4a + Rab4b, or Arf6 depletion, these data indicate that the observed defects in the support of Kuramochi invasion by CAFs were not the result of impaired contraction-mediated remodelling of pre-existing ECM proteins.

Arf6 has been implicated in the regulation of cancer cell invasion, where it has been shown that Arf6 localises to invadopodia of breast cancer cells, allowing the ECM to be degraded such that cells can migrate through it [398]. However, the involvement of Arf6 in the support of tumour development by CAFs had not previously been investigated. The siRNA screen results presented here therefore demonstrate a novel role for Arf6 in cancer metastasis, where this GTPase is required for omental CAFs to support HGSOC cell invasion.

4.9.2 Heterogeneity in the invasive capacity of CAFs

Following the use of CAFs isolated from patient MOC208 in spheroid invasion assays, it became clear that heterogeneity can exist in the ability of the CAFs themselves to invade out from the spheroid into the surrounding gel. The CAFs from patient MOC208 were far more invasive compared to the CAFs transfected with the siRNA oligos previously, including those isolated from MOC194 and MOC195 (Figure 4.6, 4.7, 4.10). Furthermore, it also became evident that the invasive capacity of CAFs can change over time. During the initial spheroid invasion assays carried out, CAFs isolated from patient MOC195 were more invasive themselves, than when CAFs from this patient were used during the siRNA screen (Figure 3.13). This firstly suggests that CAFs from different patients are not all equally invasive, and secondly that CAF age (the number of passages in culture) can impact upon their ability to invade. Considering all of the spheroid invasion assay data obtained, CAFs were still capable of facilitating Kuramochi invasion regardless of whether they themselves were able to migrate a significant distance away from the spheroid. Presumably, even when minimal CAF invasion had occurred, they were still able to locally deposit and remodel ECM in the vicinity of the spheroid which may have in turn enabled Kuramochi invasion.

4.9.3 Omental CAFs do not require endocytic recycling for endogenous fibronectin deposition in 2D

A dense, fibrillar ECM, rich in fibronectin, is common in the TMEs of many different cancer types, with this ECM protein known to promote a number of processes required for malignant cell growth, including proliferation, invasion, and angiogenesis [399]. As mentioned previously, a number of endocytic recycling regulators have been implicated in controlling fibronectin assembly by cell types other than CAFs [320] [321]. It was therefore important to understand which of them were required for fibronectin fibrillogenesis by CAFs in 2D, in order to gain an understanding of how these recycling regulators may function for CAFs to support HGSOC cell invasion in the TME.

Exploring the impact of recycling regulator depletion on fibronectin deposition in 2D generated surprising results. Only the depletion of Rab11a + Rab11b in CAFs from patient MOC195, and that of Rab5c in CAFs from patient MOC194, was sufficient to impair fibronectin deposition, however these results could not be validated in CAFs from other isolates (Figure 4.15, 4.16). These results suggested that the small GTPases depleted during this screen are largely not required for the assembly of endogenous fibronectin by CAFs in the omentum. As discussed previously, it is possible that the opposite phenotypes observed upon Rab11a + Rab11b depletion in CAFs from isolates MOC195 and MOC194, may be due to non-specific effects of each siRNA. However, an alternative explanation is that CAFs from different patient samples utilise each GTPase to varying extents. Whereas CAFs from sample MOC195 could rely more heavily on Rab11a and Rab11b for fibronectin assembly, CAFs from sample MOC194 may upregulate a different small GTPase capable of recycling fibronectin binding integrins in response to Rab11 isoform depletion, which would result in the elevated levels of fibronectin deposition observed (Figure 4.13). One candidate GTPase that may have been upregulated in these circumstances is Rab4a, however depletion of Rab4 isoforms in CAFs from sample MOC194, either individually, or in combination, did not alter fibronectin deposition (Figure 4.14) [320]. Nevertheless, it is also important to consider the possibility that the impact of depleting a specific recycling GTPase involved in fibronectin assembly, may be compensated for by an alternative, functionally redundant GTPase, such that fibronectin fibrillogenesis can occur. Further experiments aiming to explore the impact of depleting small GTPases in different combinations on fibronectin fibrillogenesis by CAFs, with a specific focus on simultaneously depleting those GTPases which may be functionally redundant, will therefore be required to investigate this possibility,

These data contrast work presented by others in the literature, highlighting roles for several recycling regulator GTPases, including those which control the fast and the slow recycling pathways, in fibronectin fibrillogenesis [321] [320] [318]. However, it is likely that different cell types will utilise different mechanisms to deposit ECM proteins and assemble them into more complex matrices. For example, whilst Rab4a and Rab11b regulated endocytic recycling may be essential for endothelial cells to assemble fibronectin during remodelling of the vasculature, CAFs such as those found in the HGSOC metastatic TME may not rely as heavily on endocytic recycling for fibronectin deposition.

These findings, together with results from the spheroid invasion assays, also imply that the deposition of fibronectin by CAFs is not a contributing factor towards their capacity for supporting OC cell invasion. Given that fibronectin levels in the omentum increase with HGSOC progression, it remains unclear what function fibronectin plays in the metastatic TME. [98]. However, as discussed in the previous chapter, these findings may allude to the differences in behaviour displayed by cells depending on whether they are cultured in 2D or in 3D systems. Whilst depletion of each recycling regulator GTPase may not impair fibronectin fibrillogenesis in 2D, it is possible that these recycling pathways are required only for fibronectin assembly by CAFs cultured in 3D. Further work will be required to firstly determine the importance of fibronectin in the CAF-mediated facilitation of HGSOC cell invasion in 3D, and secondly to understand the role of endocytic recycling in fibronectin deposition by CAFs in a 3D environment similar to that found in the omentum. This may initially be investigated by carrying out spheroid invasion assays with Kuramochi cells in co-culture with CAFs in which fibronectin levels have been depleted, for example through the use of siRNA. Should fibronectin deposition be required for CAFs to support Kuramochi invasion in this 3D system, the impact of recycling regulator depletion on fibronectin fibrillogenesis in 3D could then be investigated. This may be carried out through fluorescently tagging endogenous fibronectin and monitoring changes in its deposition following small GTPase depletion.

4.9.4 Endocytic recycling regulates exogenous fibronectin assembly CAFs in 2D

It was expected that small GTPase depletion would either not give rise to defects in exogenous fibronectin assembly, or alternatively, based on results reported in the literature, we expected a decrease in fibronectin assembly following the depletion of GTPases such as Rab11b and Rab4a [321] [320]. In contrast, depletion of Rab11a, Rab11b, Rab14, Rab8b, Arf6, Rab5c, Rab21, Rab22a and Rab22b, resulted in an increased capacity of CAFs from isolates MOC194 and MOC195 to assemble exogenous fibronectin (Figure 4.18, 4.19, 4.20).

Considering these data, together with the finding that endocytic recycling did not influence endogenous fibronectin assembly, this suggests roles for several small GTPases in regulating the assembly of fibronectin dimers, which are already present in the extracellular space, into fibrils. However, it is not yet clear how these GTPases regulate this assembly. It is known that reciprocal relationships exist between the trafficking itineraries of certain integrins, such as αvβ3 and α5β1 [400]. Inhibition of an integrins return to the plasma membrane after endocytosis can enhance recycling of an alternative integrin, leading to changes in cell behaviour. For example, the importance of reciprocal integrin trafficking has been demonstrated in regulating cell migration. Perturbation of direct αvβ3 integrin recycling, and therefore also the downstream signalling events associated with this integrin, was shown to elevate α5β1 levels at the cell surface resulting in random, rather than persistent, cell migration [400]. Furthermore, it has been shown that Arf6 has a role in regulating α5β1 and αvβ3 integrin levels at the cell surface, where Arf6 activity, and therefore also the relative cell surface levels of these integrins, can be regulated by syndecan-4 in response to ECM engagement [401]. It is therefore possible that the depletion of specific small GTPases in CAFs may elevate their capacity to assemble exogenous fibronectin through stimulating the activity of alternative recycling regulators. These alternative GTPases could recycle a fibronectin binding integrin more efficiently, leading to enhanced fibrillogenesis. An alternative explanation could be that given the significant increases in exogenous fibronectin assembly observed following depletion of specific recycling regulators, these GTPases may play an inhibitory role in regulating this process. It could be that they act to prevent the incorporation of free-floating, unbound, fibronectin dimers into fibres, which may ensure that fibronectin dimers secreted by the CAFs can be bound immediately following secretion, allowing control over where fibronectin fibrillogenesis takes place.

4.9.5 Endocytic recycling regulates collagen I deposition by CAFs in 2D

Evaluating the impact of recycling regulator depletion on collagen I deposition by CAFs revealed roles for Rab14 and Arf6 in regulating this process. In CAFs from patient MOC194, the depletion of several small GTPases reduced their deposition of collagen I, however only the depletion of Rab14, or Arf6, in CAFs from patient MOC195 was sufficient to produce similar results (Figure 4.22, 4.23, 4.24). Taken together, these results suggest that Rab14 and Arf6 are involved in regulating collagen I fibrillogenesis in CAFs across HGSOC patients.

Both Rab14 and Arf6 have been implicated in regulating the recycling of MT1-MMP, which itself is thought to cleave fibronectin at fibripositor sites to release collagen fibrils from the cell surface, such that collagen fibres can be assembled [323] [324] [299]. It is therefore possible that the way in which these GTPases regulate collagen fibrillogenesis in omental CAFs is through controlling the recycling of MT1-MMP. However, Rab8 and Rab22a have also been highlighted as regulators of MT1-MMP recycling, and depletion of either of these GTPases did not impair collagen I deposition by CAFs. Although it is not yet clear whether Rab8, Rab14, Rab22a, and Arf6 control MT1-MMP recycling in CAFs, these data may suggest that changes in MT1-MMP recycling alone are insufficient to disrupt their deposition of collagen I.

Additional experiments will be required to understand whether each of these GTPases regulate MT1-MMP recycling in CAFs from HGSOC patients, and also to investigate whether MT1-MMP recycling influences collagen I assembly in these cells. This may be investigated initially by fluorophore-tagging each GTPase together with MT1-MMP, followed by the using live-cell imaging to visualise whether the trafficking/recycling of MT1-MMP is coordinated by Rab8, Rab14, Rab22a, and/or Arf6. Should only Rab14 and Arf6 colocalise with MT1-MMP during trafficking, this would suggest a regulatory role for these GTPases in MT1-MMP recycling, and would also indicate that MT1-MMP may influence collagen I deposition by CAFs. The importance of this recycling for the assembly of collagen I could then be investigated by depleting MT1-MMP in CAFs and evaluating the impact of this on their ability to deposit collagen I fibres.

Arf6 depleted CAFs also displayed a reduced capacity for supporting Kuramochi invasion, and it may be that the defects in collagen I deposition are responsible for their inability to facilitate invasion, however it is not yet clear whether a direct link exists between these two phenotypes. Experiments aiming to explore the effect of collagen I depletion in CAFs on their ability to enhance Kuramochi invasion will be required to investigate the link between the assembly of collagen I and the support of cancer cell invasion.

4.9.6 Endocytic recycling regulates contraction-independent collagen remodelling by CAFs in 3D

Following the findings from spheroid invasion and collagen gel contraction assays, we hypothesised that CAFs may remodel collagen ECM in the vicinity of spheroids, via a mechanism that does not require cell contractility but may involve Rab4a, Rab4b, and Arf6, allowing for Kuramochi invasion to be stimulated. SHG microscopy was used to observe the organisation of collagen in the area surrounding spheroids, and revealed differences between the organisation of the collagen ECM surrounding spheroids consisting of Kuramochi cells as a monoculture or Kuramochi-CAF co-cultures. NS siRNA transfected CAFs were consistently able to efficiently remodel and bundle the collagen ECM, with this bundling then less consistent in the vicinity of spheroids formed with Rab4a + Rab4b, or Arf6 depleted CAFs. These results indicate that one of the ways in which omental CAFs can support the invasion of Kuramochi cells out of spheroids may be through their ability to remodel ECM. Interestingly, similar differences in collagen organisation have been observed by others following the examination of the collagen structure between healthy and tumour burdened human ovary samples [402]. Nadiarnykh et al. observed defined fibres of collagen in a cross-hatched arrangement in healthy ovarian samples, whereas in tumour burdened samples, collagen fibres were poorly defined and bundled together to create a meshwork. Considering their findings, together with the SHG microscopy data presented here, it is possible that the differences in collagen organisation they observed were the result of ovarian CAF-mediated ECM remodelling. It is therefore also likely that HGSOC-associated CAFs in the omentum remodel collagen to create a similar meshwork, rendering the structure of the ECM more suitable for HGSOC cell invasion and omentum colonisation.

In addition, the SHG microscopy data also suggested that Rab4a + Rab4b, and Arf6 were involved in the remodelling of collagen by CAFs, which allowed them to support cancer cell invasion. As cell contractility was unimpaired following depletion of these recycling regulators, this remodelling likely occurs via a mechanism that is not dependent on cell contraction. In the case of Arf6, defects in collagen ECM remodelling by CAFs in which this GTPase has been depleted may be linked to their reduced capacity to deposit new collagen I as fibres.

It is possible that in some cases, CAFs may require the synthesis of pericellular collagen in order for them to interact with and remodel collagen fibres which are already present in the extracellular space. However, it is important to consider that all collagen fibres in the spheroid vicinity, that are large enough, will produce a signal by SHG microscopy, including those which are CAF-derived. Therefore, the meshworks of bundled collagen assembled by CAFs likely consist not only of the collagen polymerised to form the hydrogel, but also collagen that CAFs have secreted and assembled into fibres. The larger fibre indices, and therefore reduced levels of collagen bundling measured by Arf6 depleted CAFs, could simply be the result of these CAFs lacking the ability to efficiently assemble their own endogenous collagen into fibres. Alternatively, it is possible that Arf6 depletion impairs ECM remodelling through a mechanism independent of collagen I deposition. For example, given the known role of Arf6 in MT1-MMP recycling, and the importance of this MMP in ECM remodelling, the observed defects in remodelling following Arf6 depletion may be the result of impaired MT1-MMP recycling [324] [299]. The importance of MT1-MMP in the remodelling of the ECM that surrounds spheroids by CAFs may be investigated by firstly depleting MT1-MMP levels in CAFs using siRNA prior to their inclusion in co-culture spheroids, followed by SHG microscopy to visualise any potential defects in collagen bundling/remodelling.

4.9.7 Summary

To summarise, the results in this chapter indicate that myofibroblast-like CAFs within the omental TME of HGSOC tumours utilise small GTPases, and the endocytic recycling pathways that they regulate, to assemble/remodel ECM and to support cancer cell invasion. Rab4a + Rab4b, and Arf6, were identified as key regulators of endocytic recycling required for CAFs to facilitate Kuramochi invasion, and in addition to their requirement for Arf6, CAFs also displayed a dependence on Rab14 for the assembly of endogenous collagen I. However, the precise mechanisms by which Rab14 and Arf6 regulate recycling to control the deposition of collagen I were not yet clear.

Chapter 5: Investigating the regulation of collagen I assembly by Arf6 and Rab14

5.1 Overview

Whilst it was clear that HGSOC patient omentum derived CAFs required Arf6 and Rab14 to deposit collagen I ECM, the mechanisms by which these GTPases were regulating this process were not yet clear. There are a variety of possible means by which Rab14 and Arf6 could regulate collagen I deposition, for example through controlling the secretion or recycling of collagen itself, the recycling of collagen binding integrins, or the recycling of enzymes that are thought to be required for collagen I assembly, such as MT1-MMP [323] [324] [299]. To begin investigating these possibilities, experiments were carried out aiming to investigate the influence of Rab14 and Arf6 on collagen I secretion and recycling.

Previous work by Chang et al. demonstrated that collagen I secretion and assembly into fibres by mouse tail tendon fibroblasts (iTTF) was controlled by the circadian clock [403]. Proteins such as TANGO1, and the VPS33B subunit of the CHEVI membrane tethering complex, were shown to be rhythmically expressed to enable collagen secretion and assembly to be controlled in this way, with this regulation being of importance for collagen homeostasis in tissue.

Fibripositors are specialised plasma membrane invaginations, or protrusions, involved in collagen fibril formation [195]. They have been identified in cell types such as tendon fibroblasts, and are generated following collagen-carrier fusion with the plasma membrane in order for secretion and fibril assembly to occur [194] [195]. The transport of collagen into fibripositors requires non-muscle myosin II, and the release of assembled collagen fibrils from these sites at the cell surface requires MT1-MMP mediated cleavage of fibronectin [324]. Chang et al. also demonstrated that collagen assembly by iTTF cells requires both the secretion of soluble collagen I monomers into the extracellular space, as well as the endocytosis and recycling of a proportion of these monomers back to specific fibripositor sites for fibrillogenesis [325]. It was proposed that this recycling allows cells to gain control over where the initiation of collagen I fibrillogenesis takes place. Furthermore, VPS33B, together with α11 integrin, a known collagen-binding integrin subunit, were identified as key regulators of this recycling process [305]. Depletion of VPS33B with siRNA was shown to elevate collagen I monomer levels in conditioned media, whereas its overexpression resulted in a reduction in these levels,

suggesting VPS33B acted either as a negative regulator of secretion, or a positive regulator of endocytosis and/or recycling. Analysis of exogenous collagen uptake following VPS33B knockout, or overexpression, indicated that endocytosis was not regulated by VPS33B. Instead, it was proposed that VPS33B regulates collagen I monomer recycling for fibrillogenesis, as VPS33B knockout cells displayed a reduced capacity for assembling collagen I fibrils following exogenous collagen uptake and re-seeding on to coverslips. It was also demonstrated that VPS33B interacted with collagen I during its recycling after endocytosis through the use of a split GFP system. Finally, reduced levels of integrin α11 at the cell surface following VPS33B knockout suggested that the regulation of collagen I fibrillogenesis via this mechanism by VPS33B may be mediated by integrin α11. Depletion of this integrin subunit elevated internalisation of exogenous collagen I, which indicated a role for integrin α11 in the recycling of collagen I, rather than in endocytosis after secretion [325]. Considering these findings, together with data presented in the previous chapter, we aimed to investigate the mechanisms of Rab14- and Arf6-regulated collagen I fibrillogenesis in more detail. Similar experimental approaches to those described by Chang et al. were utilised to determine whether Rab14 and Arf6 regulated aspects of this collagen I monomer secretion, internalisation, and recycling pathway to influence fibrillogenesis by CAFs.

To investigate whether the depletion of Rab14 or Arf6 resulted in defects in the assembly of collagen I through altering the secretion of collagen I monomers, SDS-PAGE with western blotting was used to detect collagen I present in media conditioned by omental CAFs following siRNA transfection. To then evaluate the impact of Rab14 or Arf6 depletion on the internalisation of collagen I, flow cytometry was used to measure the percentage of CAFs that had endocytosed exogenous Cy3-tagged rat tail collagen I (Cy3-Col I) after treatment for 1 hour and trypsinisation to remove cell surface-bound collagen. A proportion of trypsinised cells following exogenous collagen treatment were subsequently re-seeded on to coverslips and cultured for 48 hours in the presence of ascorbic acid, and Cy3-Col I that had been recycled and deposited as fibres in the extracellular space was visualised by fluorescence microscopy. In order to further understand the role of Arf6 in collagen I recycling and fibrillogenesis, live-cell fluorescence microscopy was used with CAFs overexpressing Arf6-mNeonGreen (Arf6-mNG). These cells were treated with Cy3-Col I, and the localisation of Arf6 during of the assembly of collagen into fibres was visualised.

Previous work by Pearce et al. highlighted a number of proteins, such as fibronectin, collagen XI, and versican, that increase in abundance in the omentum with HGSOC progression using a multi-omics approach [98]. In order to identify additional ECM proteins that increase in omental abundance during HGSOC progression, and therefore may be of importance for HGSOC tumour development, we used mass spectrometry to compare the ECM protein composition between omentum samples with varying disease extents. Heathy samples were collected from patients that did not have HGSOC, whereas uninvolved samples and diseased samples were collected from HGSOC patients. The uninvolved sample group included samples from patients where metastasis to the omentum had not yet occurred, and also samples collected from the region of tumour-burdened omentum located away from the tumour. Importantly, previous analyses carried out by others to identify proteins that increase in omental abundance with HGSOC progression, compared the ECM protein composition between diseased and uninvolved sample types only. Through the inclusion of healthy samples from non-HGSOC patients in our analysis, we aimed to identify additional proteins with increases in their levels associated with HGSOC progression. Furthermore, pre-metastatic niche priming is thought to occur in HGSOC, where changes in non-malignant cell behaviour can take place prior to colonisation of the omentum by disseminated HGSOC cells [404]. By comparing the ECM protein composition between healthy and uninvolved omentum samples, we also aimed to determine whether changes in the ECM can occur in the omentum prior to metastasis.

5.2 Analysis of collagen I monomer secretion following Arf6 and Rab14 depletion

To begin investigating the mechanisms by which Rab14 and Arf6 regulate collagen I assembly by omental CAFs, the impact of depleting these small GTPases on collagen I monomer secretion was assessed.

Following transfection of TGFβ3 treated CAFs with the NS siRNA, or siRNA oligos targeting Arf6, or Rab14, CAFs were grown in culture for 72 hours. The conditioned media was then collected, and SDS-PAGE followed by western blotting was then used to detect secreted collagen I monomers. This analysis revealed that depletion of Rab14, or Arf6, in CAFs, did not impair their ability to secrete soluble collagen I monomers into the extracellular space (Figure 5.1a, 5.1b, 5.1c). Comparable levels of collagen I were detected in conditioned media between all three conditions, across three biological replicates. This therefore suggested that the way in which Rab14 and Arf6 regulate collagen I fibrillogenesis, is not through controlling the initial secretion of soluble collagen I monomers into the extracellular space.

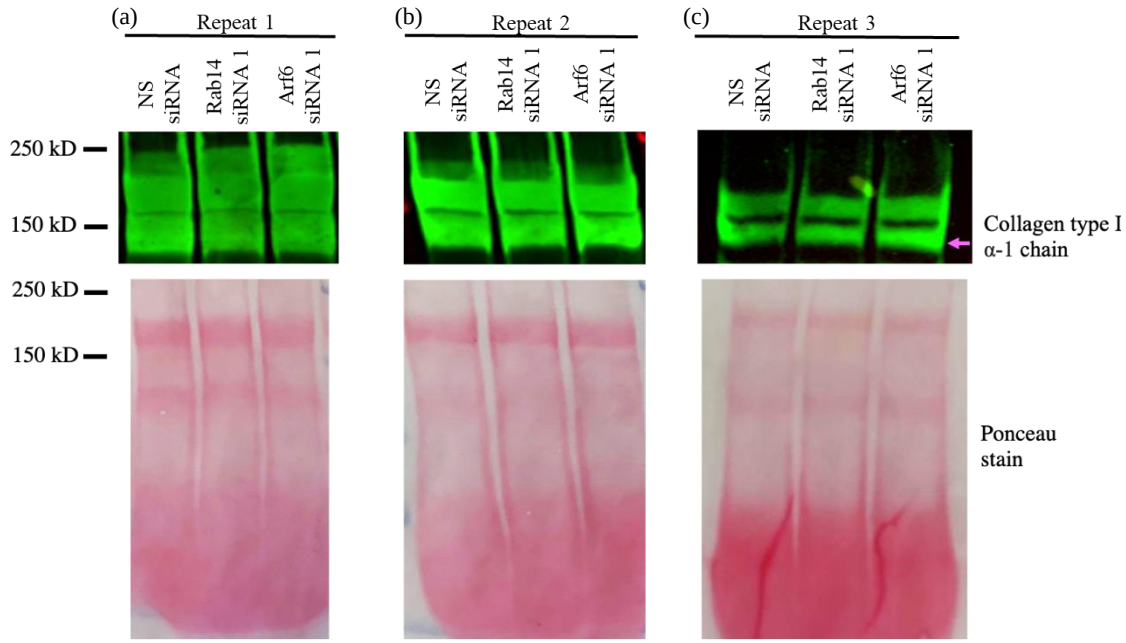

Figure 5.1 – Depletion of Arf6, or Rab14, does not impact upon collagen I monomer secretion by CAFs

Primary CAFs (MOC194), pre-treated with TGFβ3 (10 ng.mL^{-1}), were transfected with the NS siRNA, Rab14 siRNA 1, or Arf6 siRNA 1, then seeded into cell culture dishes the following day at a density of 50,000 cells per mL. Cells were grown in culture for 72 hours in the presence of TGFβ3 and ascorbic acid (20 μg mL^{-1}), and the conditioned media was collected and analysed by SDS-PAGE and western blotting with anti-collagen I (collagen type I α-1 MW = 136.5 kDa; magenta arrow) and Ponceau S staining solution (N = 3). Western blots and corresponding Ponceau stained membranes from biological replicates 1 (a), 2 (b) and 3 (c).

5.3 Arf6 regulates exogenous collagen recycling for deposition after endocytosis

5.3.1 Overview

As Arf6, or Rab14, depletion did not alter the secretion of collagen I by CAFs, it was possible that the impaired collagen I fibrillogenesis following the depletion of these GTPases observed previously was the result of defects in collagen I monomer trafficking to fibripositor sites after internalisation. In order to evaluate the effect of Rab14 or Arf6 depletion on the internalisation and recycling of collagen I, collagen I uptake and deposition assays were carried out with exogenous Cy3-Col I (Figure 5.2). These assays were carried by adding Cy3-Col I to CAFs pre-transfected with siRNA, for 1 hour, followed by trypsinisation to cleave any Cy3-Col I away from the cell surface. CAFs were then either subjected to flow cytometric analysis, or re-seeded on to coverslips. Flow cytometry was used to measure the percentage of cells that had internalised Cy3-Col I after the 1 hour treatment (Figure 5.2b, 5.2c), and cells seeded on to coverslips were grown in culture for 48 hours in the presence of ascorbic acid, then the Cy3-Col I that was deposited as fibres after recycling was visualised by fluorescence microscopy (Figure 5.2d, 5.2e).

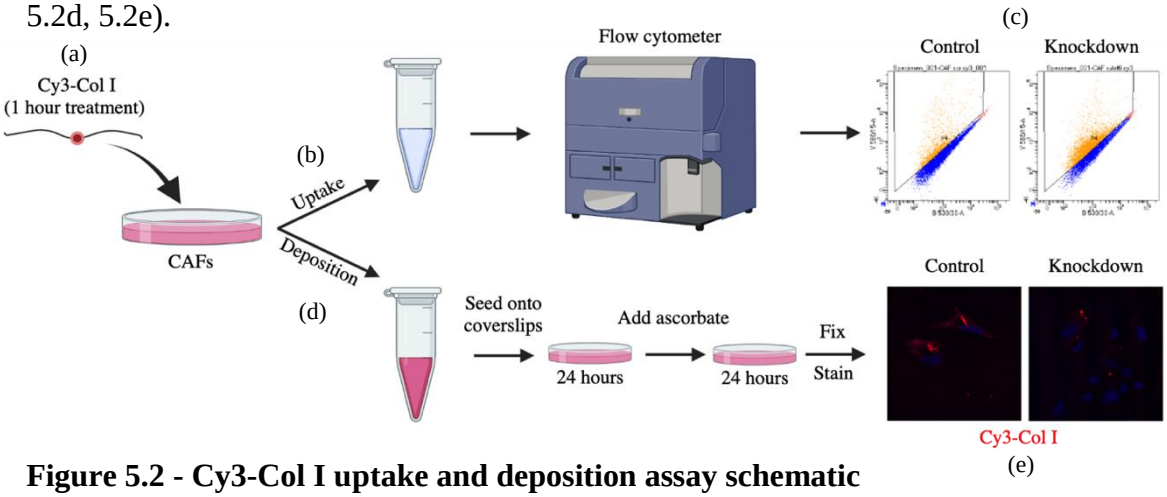

Figure 5.2 - Cy3-Col I uptake and deposition assay schematic

Following TGFβ3 (10 ng.mL^{-1}) pre-treatment, and transfection with either the NS siRNA, or siRNAs targeting Rab14, or Arf6, primary CAFs, at a density of 40,000 cells per mL, were treated with Cy3-Col I (10 µg.mL^{-1}) for 1 hour (a). CAFs were trypsinised, and around 30% of cells were resuspended in PBS for flow cytometry analysis (b, c). The remaining cells were seeded on to coverslips and grown for 24 hours, after which time ascorbic acid (20 µg mL^{-1}) was added to the culture medium (d). Cells were grown for an additional 24 hours, followed by PFA (4%) fixation and visualisation of recycled Cy3-Col I deposited as fibres by fluorescence microscopy (e).

5.3.2 Measurement of Cy3-Col I uptake by flow cytometry

The use of flow cytometry to measure the percentage of cells that were positive for internalised Cy3-Col, revealed that a larger percentage of cells had internalised this collagen following transfection with Arf6 siRNA 1, or Rab14 siRNA 1. In CAFs isolated from patient sample MOC194, approximately 30% of cells were positive for internalised Cy3-Col I after transfection with the NS siRNA (Figure 5.3a). The depletion of Rab14 increased the percentage of positive cells to approximately 40%, whereas that of Arf6 increased this value further to approximately 50% (Figure 5.3b, 5.3c). Although depletion of either small GTPase in CAFs from sample MOC194 resulted in a clear increase in Cy3-Col I internalisation, only that for Arf6 was statistically significant (5.3d). These increases in the percentage of positive cells following Rab14 or Arf6 depletion were then validated in CAFs from patient sample MOC195 with Rab14 siRNA 2 and Arf6 siRNA 2. The percentage of CAFs from patient MOC195 that had internalised Cy3-Col I following NS siRNA transfection was approximately 73%, and this percentage was then elevated to approximately 86%, and 90%, following depletion of Rab14, or Arf6, respectively (Figure 5.3e, 5.3f, 5.3g, 5.3h). Interestingly, these percentages measured with CAFs from patient MOC195 were far greater than those measured with CAFs from patient MOC194, further demonstrating the heterogeneity that can exist between CAFs derived from different patients. Although increases in the percentage of cells that had internalised Cy3-Col I following Rab14 or Arf6 depletion were observed, these increases were not statistically significant. However, this was likely due to the high basal level of internalisation observed following NS siRNA transfection. These results taken together suggest that depletion of Rab14 or Arf6 increases the amount of Cy3-Col I present in cells after 1 hour, but it was not yet clear whether these increases were the result of more efficient internalisation, defects in collagen recycling, or impaired collagen degradation.

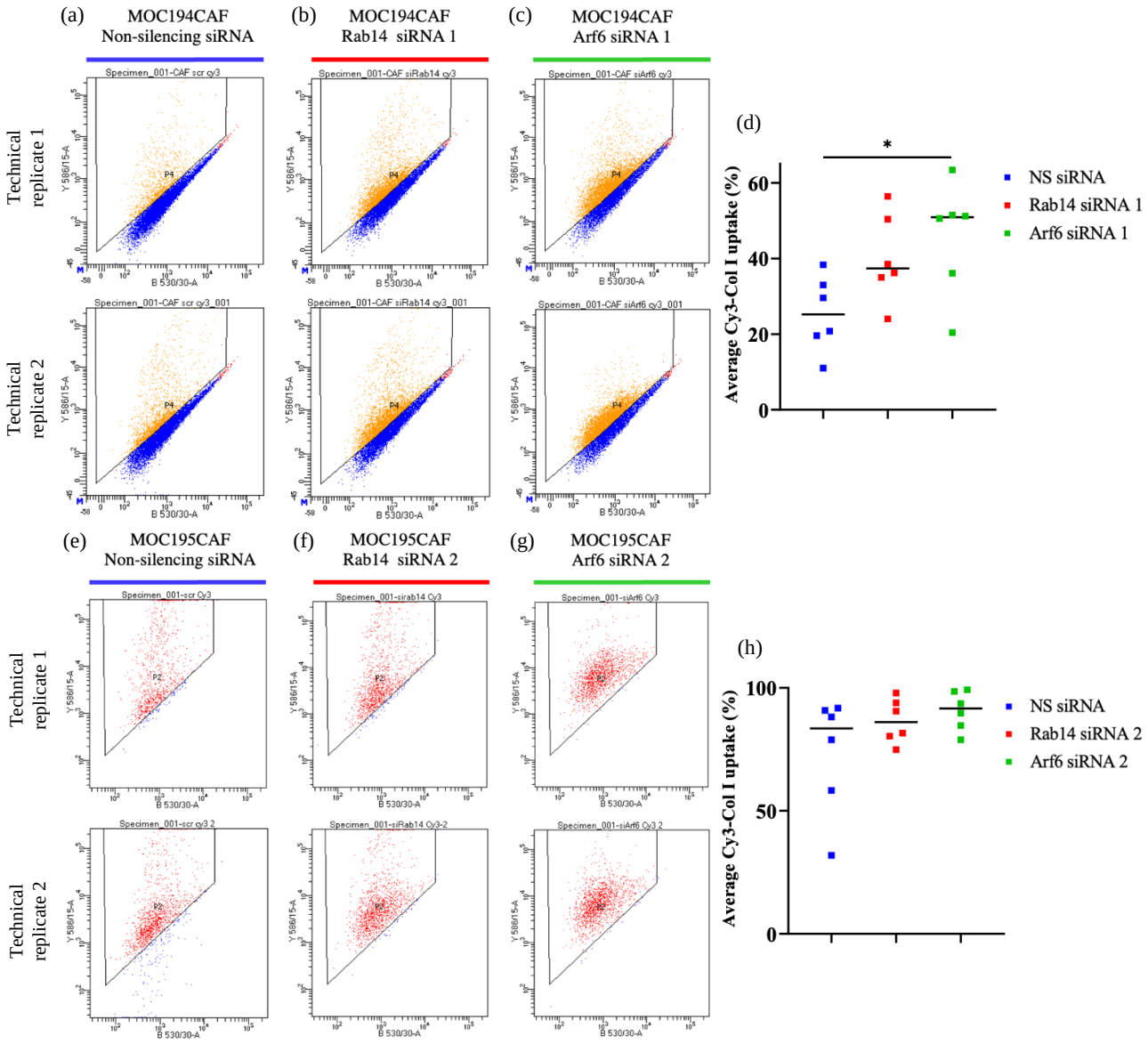

Figure 5.3 - Depletion Rab14 or Arf6 in CAFs increases Cy3-Col I uptake

Primary CAFs, pre-treated with TGFβ3 (10 ng.mL^{-1}), were treated with Cy3-Col I for 1 hour, one day after transfection with either the NS siRNA, or siRNAs targeting Rab14 or Arf6, as described previously. Cells were trypsinised and prepared for flow cytometry by resuspension in PBS. Each condition was carried out in duplicate within each biological replicate. Non-treated cells were used to establish the background level of fluorescence, allowing only cells positive for Cy3-Col I to be measured by flow cytometry (N = 3). Representative dot plots are shown from one biological replicate, where CAFs from patient MOC194 were transfected with the NS siRNA (a), Rab14 siRNA 1 (b), or Arf6 siRNA 1 (c) and subjected to flow cytometric analysis. P4 (orange) indicates cells positive for Cy3-Col I.

Figure legend continues on the next page.

Figure 5.3 Depletion Rab14 or Arf6 in CAFs increases Cy3-Col I uptake

*(d) Quantification of merged data from three biological replicates, and statistical analysis by Kruskal-Wallis test (*p<0.05), of the average percentage of cells positive for Cy3-Col I. Representative dot plots are shown from one biological replicate, where CAFs from patient MOC195 were transfected with the NS siRNA (e), Rab14 siRNA 2 (f), or Arf6 siRNA 2 (g) and subjected to flow cytometric analysis. P2 (red) indicates cells positive for Cy3-Col I. (h) Quantification of merged data from three biological replicates, and statistical analysis by Kruskal-Wallis test, of the average percentage of cells positive for Cy3-Col I. All statistically significant results are shown.*

5.3.3 Recycling and deposition of internalised Cy3-Col I by CAFs is influenced by Arf6

To determine whether the increase in Cy3-Col I positive cells following depletion of Rab14 or Arf6 was due to defects in their ability to recycle and deposit internalised Cy3-Col I as fibres, trypsinised cells were re-seeded on to coverslips. After ascorbic acid addition for 24 hours, Cy3-Col I deposited as fibres in the extracellular space was visualised and measured 48 hours after re-seeding. CAFs isolated from patient MOC194 were less capable of recycling the internalised Cy3-Col I and assembling it into fibres following the depletion of either Rab14 or Arf6. A statistically significant reduction in Cy3-Col I fibre area was measured in all three biological replicates with CAFs transfected with Rab14 siRNA 1, or Arf6 siRNA, relative to those transfected with the NS siRNA (Figure 5.4). Furthermore, combining the data from each replicate revealed that the reduction was more statistically significant following Rab14 depletion than for Arf6 (Figure 5.4m). Surprisingly, when validating these findings with Rab14 siRNA 2 and Arf6 siRNA 2 in CAFs from isolate MOC195, merging the data from each biological replicate highlighted that only the depletion of Arf6 impaired their ability to recycle the internalised Cy3-Col I and assemble it into fibres after (Figure 5.5). Furthermore, a larger amount of Cy3-Col I was detected as fibres in the NS siRNA transfected CAFs from patient MOC195 relative to those from patient MOC194, which may be accounted for by the elevated levels of Cy3-Col I internalisation measured with isolate MOC195 CAFs. These data suggest that endocytic recycling, regulated in particular by Arf6, influences the deposition of collagen I as fibres following endocytosis.

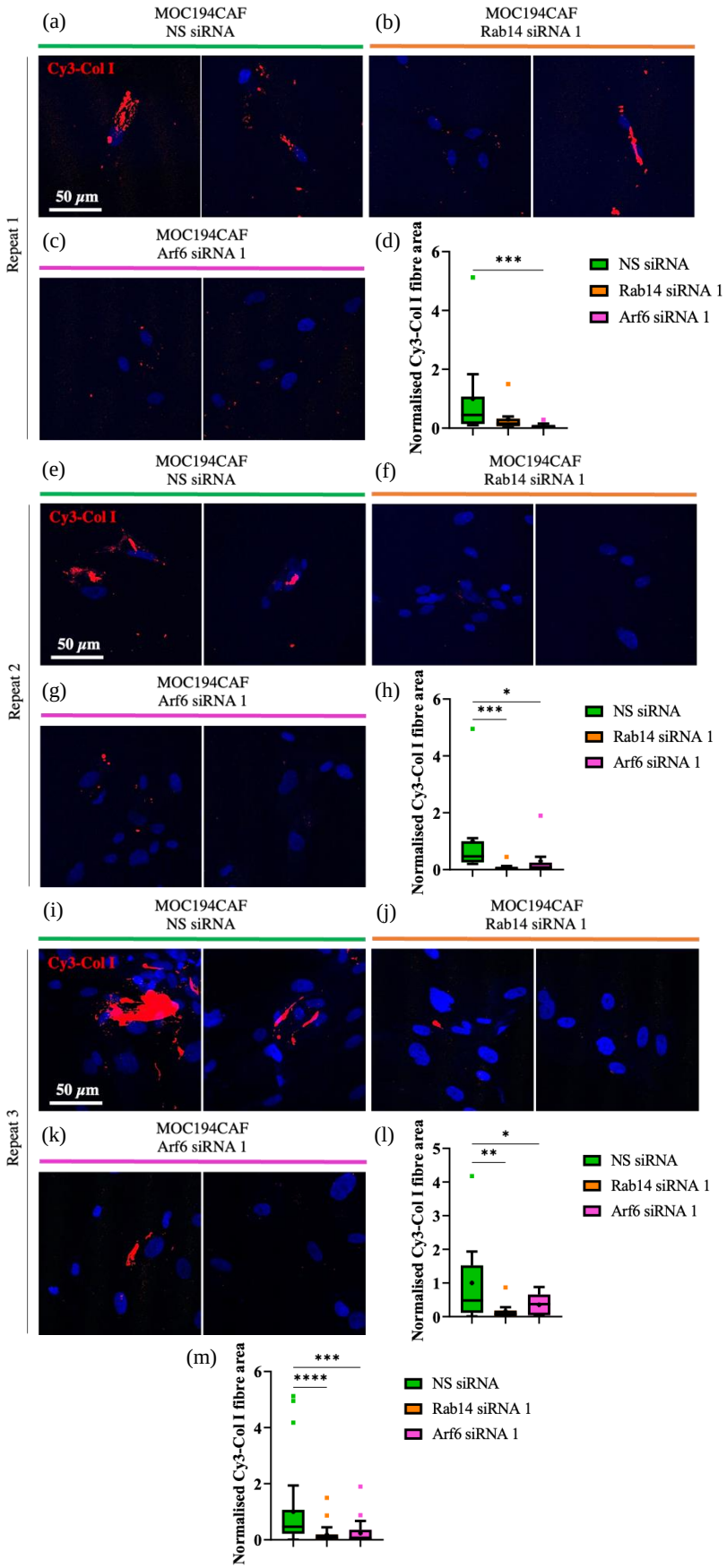

Figure 5.4 - Recycling and deposition of Cy3-Col I after uptake by CAFs (MOC194) is impaired by Arf6 or Rab14 depletion

Figure legend on the next page.

Figure 5.4 Recycling and deposition of Cy3-Col I after uptake by CAFs (MOC194) is impaired by Arf6 or Rab14 depletion

*Primary CAFs (MOC194), pre-treated with TGFβ3 (10 ng.mL^{-1}), were treated with Cy3-Col I for 1 hour, one day after transfection with either the NS siRNA, Rab14 siRNA 1, or Arf6 siRNA 1, as described previously. Cells were trypsinised to cleave any collagen bound to the cell surface, then re-seeded on to coverslips. After 24 hours, ascorbic acid (20 μg mL^{-1}) was added for an additional 24 hours, after which time cells were fixed in PFA (4%) and recycled and deposited Cy3-Col I was visualised by fluorescence microscopy (N = 3). Each condition was carried out in duplicate within each biological replicate. Representative images from biological replicates 1, 2, and 3, of Cy3-Col I deposition by CAFs transfected with the NS siRNA (a, e, i), Rab14 siRNA 1 (b, f, j), or Arf6 siRNA 1 (c, g, k), are shown. (d, h, l) Quantification, and statistical analysis by Kruskal-Wallis test (*p<0.05, **0.01, ***p<0.001), of Cy3-Col I deposition by CAFs from biological replicates 1 (d), 2 (h), and 3 (l). (m) Quantification of merged data from three biological replicates, and statistical analysis by Kruskal-Wallis test (***p<0.001, ****p<0.0001), of Cy3-Col I deposition by CAFs (MOC194). Normalised Cy3-Col I fibre area values are sown, where the fibre area for each image was normalised within each biological replicate by dividing by the average fibre area for the NS siRNA condition. All statistically significant results are shown. Nuclei were stained with Hoechst 33342. Scale bar = 50 μm. Maximum intensity projections of z-stacks are shown*

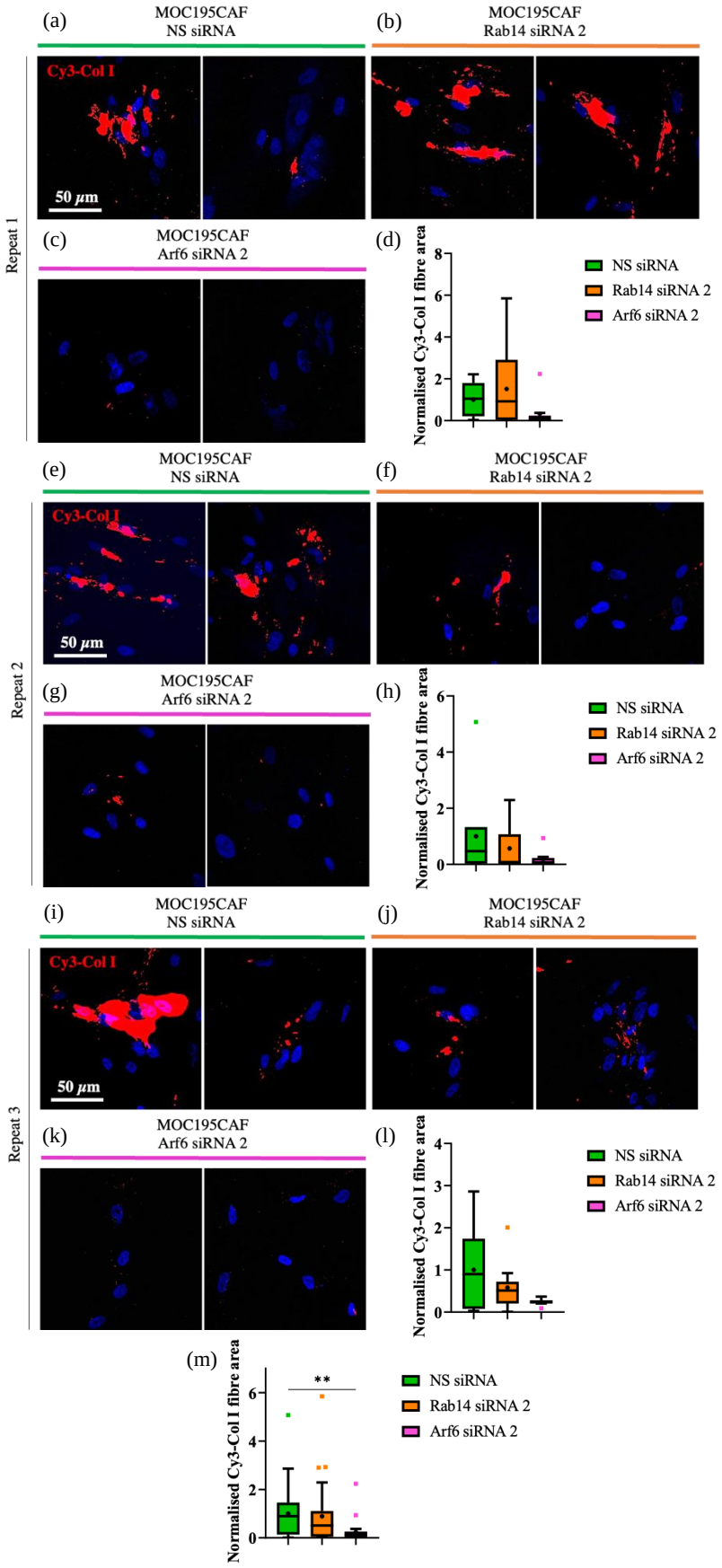

Figure 5.5 - Recycling and deposition of Cy3-Col I after uptake by CAFs (MOC195) is impaired by depletion of Arf6 only

Figure legend on the next page.

Figure 5.5 Recycling and deposition of Cy3-Col I after uptake by CAFs (MOC195) is impaired by depletion of Arf6 only

*Primary CAFs (MOC195), pre-treated with TGFβ3 (10 ng.mL^{-1}), were treated with Cy3-Col I for 1 hour, one day after transfection with either the NS siRNA, Rab14 siRNA 2, or Arf6 siRNA 2, as described previously. Cells were trypsinised, re-seeded on to coverslips, treated with ascorbic acid, and imaged by fluorescence microscopy as described previously (N = 3). Each condition was carried out in duplicate within each biological replicate. Representative images from biological replicates 1, 2, and 3, of Cy3-Col I deposition by CAFs transfected with the NS siRNA (a, e, i), Rab14 siRNA 2 (b, f, j), or Arf6 siRNA 2 (c, g, k), are shown. (d, h, l) Quantification, and statistical analysis by Kruskal-Wallis test, of Cy3-Col I deposition by CAFs from biological replicates 1 (d), 2 (h), and 3 (l). (m) Quantification of merged data from three biological replicates, and statistical analysis by Kruskal-Wallis test (**p<0.01), of Cy3-Col I deposition by CAFs (MOC195). Normalised Cy3-Col I fibre area values are sown, where the fibre area for each image was normalised within each biological replicate by dividing by the average fibre area for the NS siRNA condition. All statistically significant results are shown. Nuclei were stained with Hoechst 33342. Scale bar = 50 μm. Maximum intensity projections of z-stacks are shown*

5.4 Live-cell imaging of Cy3-Col 1 uptake and assembly with Arf6-mNG expressing CAFs

5.4.1 Overview

Although omental CAFs had demonstrated an ability to internalise and recycle Cy3-Col I after trypsinisation, others have shown that trypsinisation itself can significantly increase cell permeability [405]. It was therefore possible that the endocytosis of Cy3-Col I observed previously was the result of trypsin-mediated cleavage of cell surface proteins. In order to determine whether CAFs were capable of Cy3-Col I endocytosis in a trypsin-independent manner, live-cell fluorescence microscopy was used to visualise uptake in live cells. Furthermore, these live-cell imaging experiments were carried out in CAFs overexpressing mNeon-Green (mNG) or Arf6-mNG through lentiviral transduction in order to begin investigating how Arf6 regulates collagen I deposition after internalisation.

Importantly, experiments were carried out with transduced cells that were not subjected to FACS. We found that sorting these primary cells in this way hindered their growth following sorting. Transduced cells therefore remained as a mixed population in culture with non-transduced cells, and only cells overexpressing either mNG, or Arf6-mNG, at an intermediate level, were visualised by fluorescence microscopy.

5.4.2 Live-cell imaging of trypsin-independent Cy3-Col I endocytosis by CAFs

Cy3-Col I was added directly to the culture medium of TGFβ3 pre-treated CAFs overexpressing Arf6-mNG, and uptake by cells was imaged immediately over approximately 2-3 hours. In order to evaluate whether CAFs were capable of internalising Cy3-Col I without trypsin treatment, 3D reconstructions of time-lapses were generated. Firstly, this revealed that, even in the absence of trypsin, CAFs were capable of internalising collagen, suggesting that collagen endocytosis is trypsin-independent (Figure 5.6). In the snapshots of a representative time-lapse shown in figure 5.6, a Cy3-Col I positive structure can be observed in the extracellular space, either free-floating or possibly bound to the neighbouring cell which is not overexpressing Arf6-mNG, until t = 55 minutes. At t = 64 minutes, this Cy3-Col I structure is then bound by the Arf6-mNG overexpressing cell, and internalised. Over the remainder of the time lapse, this collagen is then trafficked throughout the cell, possibly to a site where fibrillogenesis can occur. Furthermore, a co-localisation between Arf6-mNG and the site at which the Cy3-Col I was endocytosed was not observed. Taken together, these data firstly suggest that collagen I endocytosis by CAFs is trypsin independent. Furthermore, considering that Arf6-mNG did not co-localise with sites of Cy3-Col I endocytosis, together with the finding that Arf6 depletion increases Cy3-Col I internalisation, these data strongly imply that Arf6 does not regulate the endocytic pathways involved in collagen I uptake.

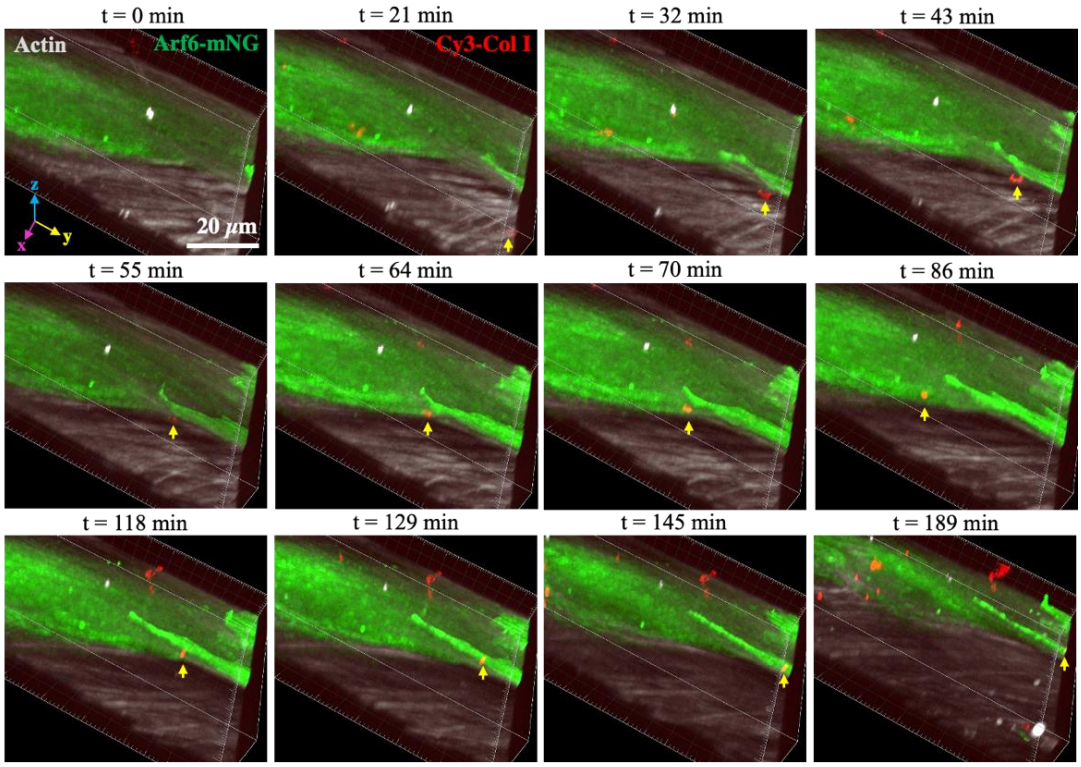

Figure 5.6 - Uptake of Cy3-Col I by CAFs is trypsin independent, and Arf6-mNG does not co-localise with sites of Cy3-Col I endocytosis

Primary CAFs (MOC195) overexpressing Arf6-mNG (green) were pre-treated with TGFβ3 (10 ng.mL^{-1}) as described previously, then seeded into glass-bottomed dishes for 24 hours. The following day, cells were stained with CellMask™ deep red actin tracking stain (grey) to allow for non-transduced cells to also be visualised. Cy3-Col I (10 µg.mL^{-1}; red) was then added directly to the cell culture medium, and Cy3-Col I uptake was imaged immediately by spinning disk confocal fluorescence microscopy for 2-3 hours (N = 3). Snapshots from a 3D reconstruction of a representative time-lapse are shown. The yellow arrow indicates an internalised Cy3-Col I positive structure. Scale bar = 20 μm. Maximum intensity projections of z-stacks are shown.

5.4.3 Live-cell imaging of Arf6 and collagen I fibrillogenesis

Following the observation that Arf6-mNG did not co-localise with sites of Cy3-Col I internalisation, and therefore was likely not involved in regulating this endocytic process, we hypothesised that Arf6 may regulate the recycling of internalised Cy3-Col I to sites of collagen I fibrillogenesis. This was investigated by live-cell imaging, with the aim being to visualise a co-localisation between Arf6-mNG and sites at which endocytosed collagen I was assembled following recycling.

Live-cell imaging of Cy3-Col I added to CAFs overexpressing Arf6-mNG demonstrated that Arf6 co-localised with sites of Cy3-Col I fibrillogenesis, whereas in control cells, mNG did not co-localise with assembled Cy3-Col 1 fibres (Figure 5.7a, 5.67, 5.7c, 5.7d). Arf6-mNG expressing CAFs were observed assembling Cy3-Col 1 into a branched network, and visualisation of single z-sections suggested that Arf6-mNG was located within, or just beneath the plasma membrane (Figure 5.7c). The generation of maximum intensity projection of 4 z-sections at each time point then revealed that above the Cy3-Col I branch points at which Arf6-mNG was localised, Cy3-Col I was assembled into more elaborate structures over time, with networks extending away from the cell surface (Figure 5.7d, 5.7e).

Although Arf6-mNG was located within the same z-section as the Cy3-Col I branch point, it was not clear whether Arf6 was located within the plasma membrane, or just beneath the plasma membranes inner leaflet. Furthermore, it was not yet clear whether Arf6 localised to sites of collagen I assembly prior to the initiation of fibrillogenesis, or whether its localisation to these sites occurred after this process had been initiated. To understand the dynamics of the localisation of Arf6 to sites of Cy3-Col I fibrillogenesis in greater detail, 3D reconstructions of time-lapse images were generated. These reconstructions firstly revealed that in CAFs overexpressing Arf6-mNG, large Arf6 positive structures existed prior to the initiation of Cy3-Col I fibrillogenesis (Figure 5.7f). Secondly, visualising the localisation of Arf6, Cy3-Col I, and actin, from a side-on view indicated that large Arf6 positive structures sit just beneath the cortical actin, at the site where Cy3-Col I is being assembled, and it is possible that these Arf6 positive structures correspond to recycling endosomes (Figure 5.7g).

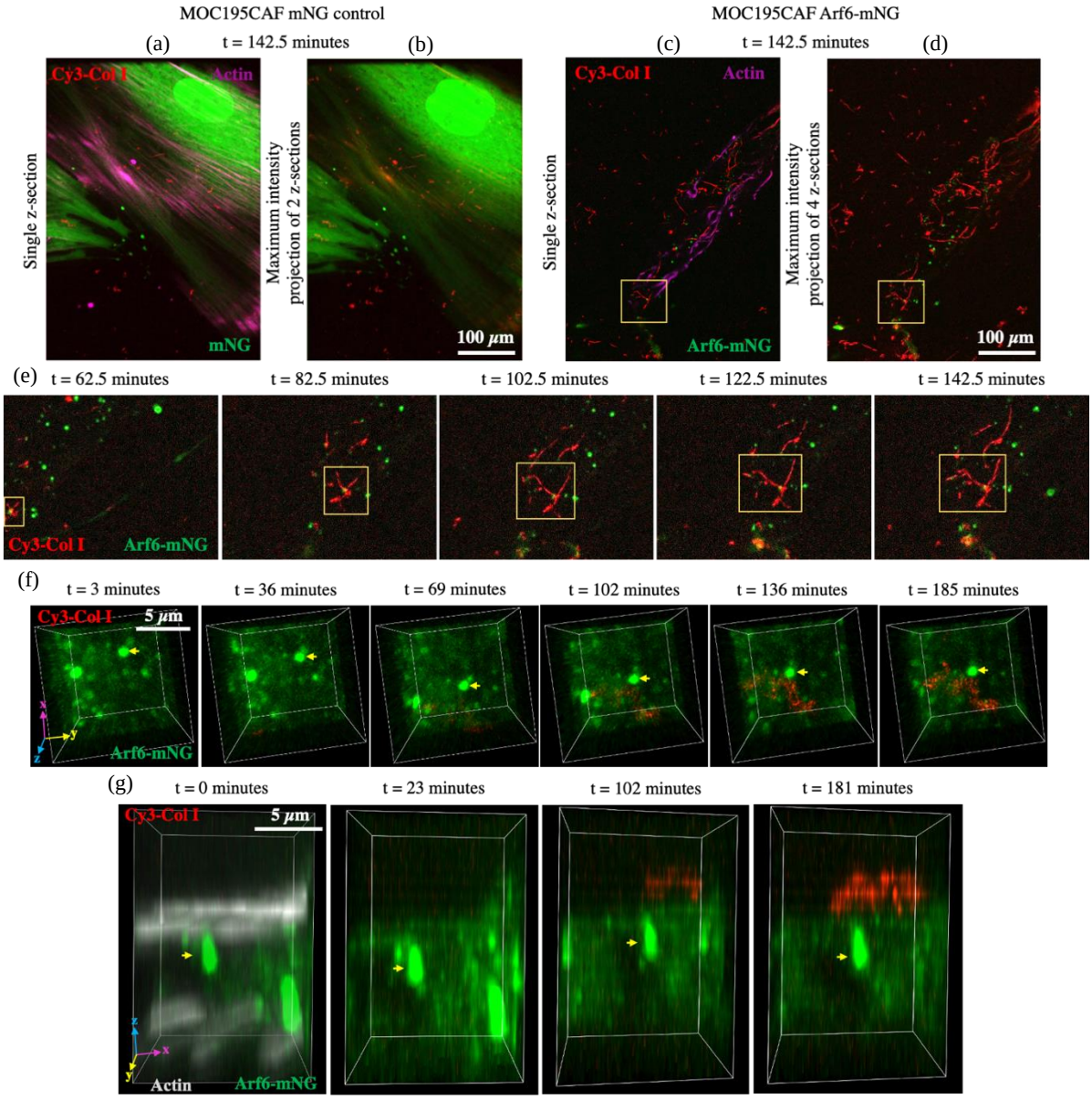

Figure 5.7 - Arf6-mNG localises to sites of Cy3-Col I fibrillogenesis in CAFs

Primary CAFs (MOC195) overexpressing mNG (green), or Arf6-mNG (green), were pre-treated with TGFβ3 (10 ng.mL^{-1}), then seeded into glass-bottomed dishes for 24 hours, and the actin (grey) was stained as described previously. Cy3-Col I (10 μg.mL^{-1}; red) was then added directly to the cell culture medium, and Cy3-Col I uptake and assembly was imaged immediately by spinning disk confocal fluorescence microscopy for 2-3 hours (N = 3). Snapshots at t = 142.5 minutes from time lapse imaging of Cy3-Col I assembly by CAFs overexpressing mNG (a, b), or Arf6-mNG (c, d). Either single z-sections (a, c), or maximum intensity projections of 4 z-sections (b, d) are shown. The actin stain has been omitted from (b) and (d).

Figure legend continues on the next page.

Figure 5.7 Arf6-mNG localises to sites of Cy3-Col I fibrillogenesis in CAFs

Scale bar = 100 μm. (e) Zoomed in snapshots from a time lapse showing Arf6-mNG co-localisation with Cy3-Col I assembly. The yellow boxes indicate the region where Arf6-mNG co-localises with a Cy3-Col I branch point (c, d, e). Top-down (f) and side-on (g) views of 3D reconstructions from time-lapse imaging showing co-localisation of Arf6-mNG with a Cy3-Col I fibre in CAFs. Yellow arrows indicate an Arf6-mNG positive structure that co-localises with Cy3-Col I. (g) Actin stain is shown only at t = 0 minutes. Scale bar = 5 μm.

5.5 Analysis of HGSOC patient omentum sample ECM protein composition by mass spectrometry

5.5.1 Overview

Previous work by others has identified a number of proteins that increase in abundance in tumour burdened omentum with HGSOC progression, including collagen I, fibronectin, collagen XI, versican, and COMP [98]. However, by comparing the ECM protein composition between diseased and uninvolved omentum samples only, any differences in ECM composition that exist between diseased and healthy omentum could not be identified. In order to identify additional changes in ECM protein composition in the omentum with HGSOC progression, we used mass spectrometry to analyse the ECM composition in healthy, uninvolved, and diseased patient omentum samples. The diseased omentum samples used during this analysis were isolated from HGSOC patients, and were collected from the region of the omentum where the tumour was located, whereas healthy omentum samples were isolated from patients that did not have HGSOC. Uninvolved samples were also isolated from HGSOC patients, with this group including samples that were either collected from non-tumour burdened omentum, or from regions of tumour-burdened omentum located away from the tumour. In addition, by comparing the ECM composition between healthy and uninvolved omentum samples, we also aimed to identify changes that may occur in the omental ECM prior to the arrival of disseminated HGSOC cells in the omentum, in order to investigate whether pre-metastatic niche priming occurs.

5.5.2 ECM protein enrichment from HGSOC patient omentum

Healthy, uninvolved, and diseased omentum samples, of which there were 5, 4, and 6, respectively, were homogenised using a pestle and mortar and ECM proteins were enriched via a series of centrifugations and incubations in various buffers. Furthermore, the uninvolved and diseased sample categories contained 3 pairs of matched samples (MOC109, MOC126 and MOC169) with the aim of identifying differences in ECM protein composition that existed between distinct regions of tumour burdened omentum (Figure 5.8a). The success of ECM protein enrichment from omentum samples was evaluated through SDS-PAGE and western blotting using anti-fibronectin and anti-tubulin antibodies as ECM and cytosolic protein markers respectively. For all samples, western blot analysis indicated that ECM proteins had been enriched during the protocol, without enriching cytosolic proteins (Figure 5.8b). The resulting ECM protein pellets generated by this enrichment were then prepared for mass spectrometry by in-gel digestion, and the protein composition of each sample was analysed by mass spectrometry. This analysis firstly revealed that approximately 10% of the proteins within each sample were matrisome proteins, with the remaining proteins being cytosolic (Figure 5.8c). Although this value was lower than expected given that ECM protein enrichment was carried out, this result indicated that the enrichment was consistent between samples.

(a)

Healthy	Uninvolved	Diseased
MOC158	MOC109	MOC109
MOC159	MOC111	MOC124
MOC164	MOC126	MOC126
MOC165	MOC169	MOC127
MOC167		MOC160
		MOC169

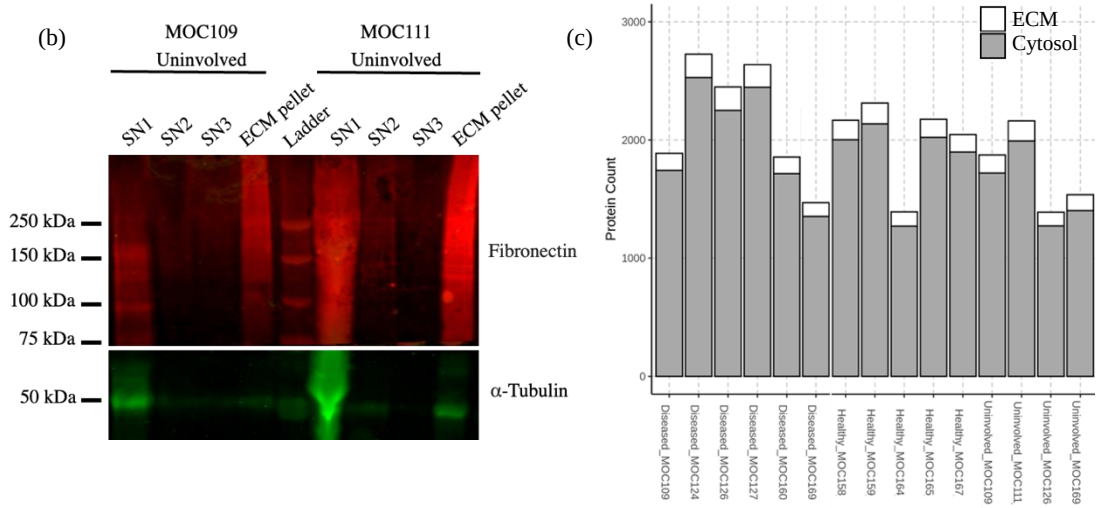

Figure 5.8 – ECM proteins were enriched from healthy, uninvolved and diseased omentum patient samples for analysis by mass spectrometry

Diseased, uninvolved, and healthy omentum samples, obtained from patients undergoing debulking surgery, and homogenised. ECM proteins were enriched (a). The success of the enrichment was evaluated by SDS-PAGE and western blotting, with anti-fibronectin (MW = 220 kDa) as an ECM protein marker, and anti-tubulin (MW = 50 kDa) as a cytosolic protein marker. Representative blots from two omentum samples, MOC109 and MOC111, are shown (b). The ECM protein composition of each omentum sample was analysed by mass spectrometry, and quantified in house using MaxQuant and MSqRob software. This analysis revealed that approximately 10% of the proteins within each sample were matrisome proteins (c).

5.5.3 Significant changes in ECM composition between samples

During the analysis of the mass spectrometry data generated, 4 separate comparisons were carried out to identify ECM proteins that increased in abundance with disease progression: diseased vs healthy, diseased vs uninvolved (all samples included), diseased vs uninvolved (matched samples only), and healthy vs uninvolved. Comparing enriched ECM proteins between diseased and healthy omentum samples revealed that versican was the only protein with significantly (q-value < 0.05) altered levels between these samples, where an increase was measured in diseased samples (Figure 5.9a). This finding therefore supports data reported by others where versican increases in abundance in the omentum with disease progression [98]. Comparing the ECM protein composition between diseased and uninvolved samples, where all samples within these categories were included, highlighted a number of proteins with significantly altered levels between these sample types. Adipocyte enhancer binding protein 1 (AEBP1), versican, collagen VIII and prolargin, were all significantly more abundant in diseased samples (Figure 5.9b). The comparison of matched omentum samples between these two sample types highlighted that vitronectin and agrin were present at higher levels in the regions of these tumour-burdened samples where the tumours were located, compared to sites away from the tumours. A statistically significant increase was also measured in coagulation factor IX (F9) in diseased samples relative to matched uninvolved samples, however this was ignored due to the expected variability in the amount of blood that remained in samples following processing (Figure 5.9c). Interestingly, the comparison between healthy and uninvolved omentum samples did not generate any statistically significant results, indicating that changes in ECM composition do not occur prior to HGSOC cell colonisation of the omentum, and suggesting that pre-metastatic niche priming does not occur (Figure 5.9d). Comparing the ECM composition between diseased and uninvolved omentum where all samples, or only matched samples, were included, also highlighted a number of ECM proteins that decreased in abundance with disease progression. However, as only those proteins that increased in abundance with disease progression were of interest during this analysis, these proteins were ignored and will be omitted from downstream experiments (Figure 5.9c, 5.9e).

(a)

Diseased vs Healthy (q<0.05)

Protein name	Fold change	q-value
Versican core protein	2.6	0.0321

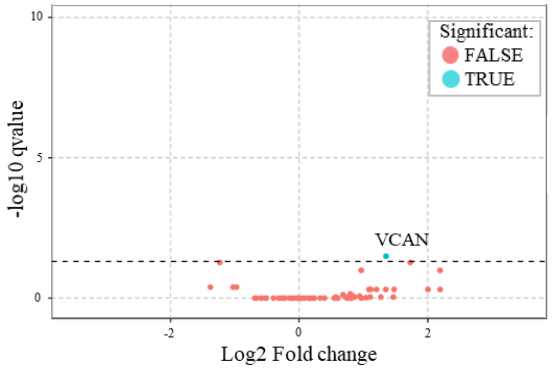

(b)

Diseased vs Uninvolved (q<0.05)

Protein name	Fold change	q-value
Adipocyte enhancer binding protein 1	5.1	0.006
Versican core protein	2.4	0.0153
Collagen alpha-1 (VIII) chain	10.2	0.0191
Prolargin (PRELP)	1.6	0.0432

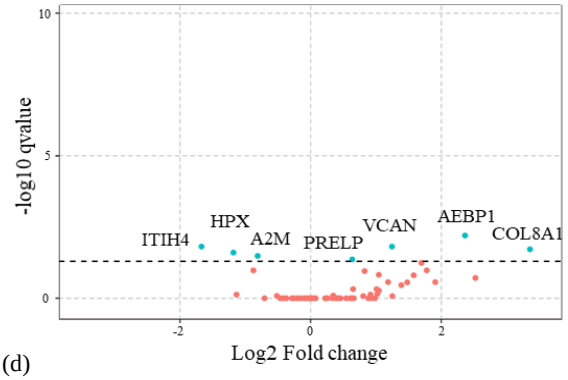

(c)

Diseased vs Uninvolved
Matched Samples (q<0.05)

Protein name	Fold change	q-value
Agrin	9.4	$2.36x10^{-7}$
Vitronectin	2.7	0.0006

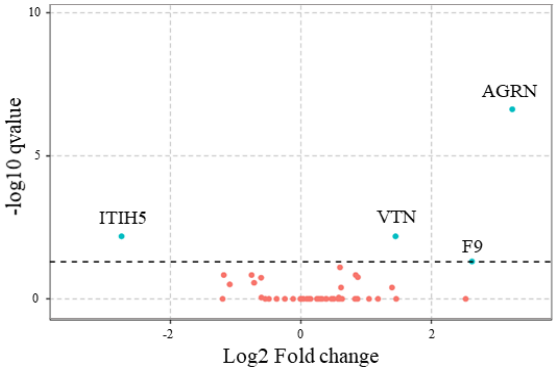

(d)

Uninvolved vs Healthy (q<0.05)

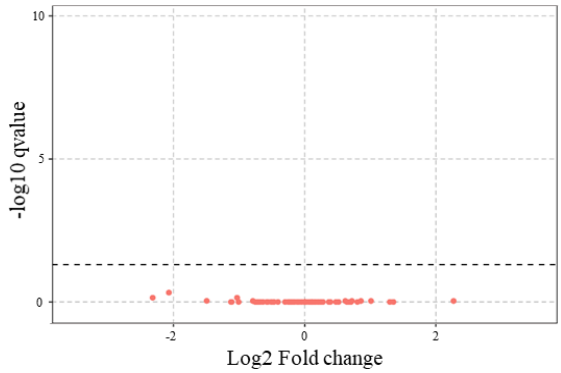

(e)

Diseased vs Healthy (q<0.15)

Protein name	Fold change	q-value
Latent-transforming growth factor beta-binding protein-2	3.3	0.0539
Fibulin-2	2	0.1028
Adipocyte enhancer binding protein 1	4.6	0.1028
Protein S100-P	14.1	0.1116

(f)

Diseased vs Uninvolved (q<0.15)

Protein name	Fold change	q-value
Hyaluronan-binding protein 2	3.2	0.0572
Vitronectin	3.4	0.1052

(g)

Diseased vs Uninvolved
Matched Samples (q<0.15)

Protein name	Fold change	q-value
Versican core protein	1.8	0.1464

Figure 5.9 The ECM protein composition in the omentum changes with disease progression

Following ECM protein enrichment from patient omentum samples, the ECM protein composition was compared between each sample group. Q-values were generated by correcting p-values for multiple testing, where a q-value of < 0.05 indicates a statistically significant difference in abundance, and a q-value of <0.015 indicates a near-statistically significant difference in abundance, between sample groups.

Figure legend continues on the next page.

Figure 5.9 The ECM protein composition in the omentum changes with disease progression

Significant (a) and near-significant (e) results generated by comparing diseased and healthy omentum sample ECM compositions are shown with the corresponding PCA plot. Significant (b) and near-significant (f) results generated by comparing diseased and uninvolved omentum sample ECM compositions are shown with the corresponding PCA plot, where all samples within these groups were included. Significant (c) and near-significant (g) results generated by comparing diseased and uninvolved omentum sample ECM compositions are shown with the corresponding PCA plot, where only matched samples within these groups were included. Results generated by comparing uninvolved and healthy omentum sample ECM compositions are shown with the corresponding PCA plot (d).

5.5.4 Near-significant changes in ECM composition between samples

Although all samples were analysed by mass spectrometry at the same time, an underlying variance existed between them, firstly because they were collected from different patients, and secondly because the ECM protein enrichment was not carried out simultaneously for all samples. It was therefore reasonable to also consider certain other ECM proteins for follow up analyses together with those proteins with significantly altered levels. Additional proteins were selected based on their implication in cancer progression from the literature, and also based on whether near-significant (q-value < 0.15) fold changes of +/-75% existed in their levels between omentum sample types [406] [407] [408] [409] [410] [411]. A number of proteins met these criteria, including fibulin-2, which was present at higher levels in diseased compared to healthy samples, vitronectin, which was more abundant in diseased compared to uninvolved samples, and versican, which was detected at higher levels in diseased samples relative to matched uninvolved samples (Figure 5.9e, 5.9f, 5.9g). Surprisingly, the comparison of healthy and uninvolved samples also did not highlight any ECM proteins with near-significant alterations in their levels between these sample types. This therefore further suggests that the omental ECM pre-metastatic niche is not primed prior to the arrival of HGSOC cells.

5.6 Discussion and conclusions

The results in this chapter provide further insight into the role of Arf6 in the assembly of collagen I ECM by omental CAFs. The data presented indicates that Arf6 regulates this process, at least in part, through controlling the deposition of internalised and recycled collagen I monomers as fibrils. Furthermore, the comparison of ECM protein composition between healthy omentum samples, and samples obtained from patients at varying stages of HGSOC progression highlighted a number of proteins that become more abundant with disease extent.

5.6.1 Collagen I internalisation by CAFs is enhanced following Arf6 depletion

The data presented in chapter 4 demonstrate that CAFs require Arf6, and Rab14, for the assembly of collagen I ECM in 2D. Furthermore, depletion of Arf6 in CAFs was sufficient to impair the ability of CAFs to facilitate Kuramochi cell invasion from spheroids, possibly through defective collagen ECM remodelling capabilities. Chang et al. had demonstrated previously that in order for mouse tail tendon fibroblasts to assemble collagen I, soluble collagen I monomers must first be secreted, then internalised and recycled back to the plasma membrane. It was proposed that assembling collagen via this mechanism enables cells to gain a degree of control over where collagen I fibrillogenesis is initiated [325]. Evaluating the impact of Arf6, and Rab14, depletion in CAFs on collagen I monomer secretion suggested that these small GTPases do not regulate collagen I assembly through controlling its secretion. By measuring the uptake of Cy3-Col I in Arf6 or Rab14 depleted cells after a 1 hour treatment, it was evident that a higher percentage of CAFs were positive for Cy3-Col I following depletion of Arf6 in CAF isolates from two HGSOC patients (Figure 5.3).

5.6.2 Arf6 influences the recycling and deposition of endocytosed collagen I

Following Cy3-Col I uptake assays, it was essential to determine whether the elevated uptake of collagen by Arf6 depleted CAFs was due to recycling defects. Seeding Cy3-Col I treated CAFs on to coverslips revealed that Arf6 depleted CAFs displayed a reduced ability to recycle and deposit internalised collagen I as fibres in the extracellular space (Figure 5.4, 5.5). Whilst Rab14 depletion with siRNA 1 in CAFs from patient MOC194 impaired their ability to recycle and deposit internalised collagen, this result could not be validated in CAFs from patient MOC195. These results demonstrate a clear role for Arf6 in regulating the deposition of internalised and recycled collagen I such that fibrillogenesis can occur. This recycling may allow internalised collagen monomers to be trafficked to specific sites, such as fibripositors, for the initiation of collagen I fibrillogenesis, and the impaired collagen recycling following Arf6 depletion may explain the defects in collagen I deposition by CAFs observed during the siRNA screen preventing in the previous chapter.

5.6.3 Mechanisms of collagen I endocytosis

Despite the detection of Cy3-Col I within CAFs after trypsinisation by flow cytometry, and the observation that this internalisation can occur independently of trypsinisation, it is not yet clear how CAFs endocytose collagen in this manner such that it can be recycled and deposited as fibres (Figure 5.3, 5.6). Given that collagen monomers are approximately 300 nm in length, the most likely mechanism of internalisation is macropinocytosis, as these monomers are too large to be internalised by mechanisms such as clathrin- or caveolae-mediated endocytosis [412] [413]. Others have demonstrated that cell types such as pancreatic ductal adenocarcinoma cells, and stellate cells in the liver can endocytose collagen via macropinocytosis, which is thought to either enable survival following nutrient deprivation, or to allow changes in microenvironment to be sensed, respectively [414] [415]. As mentioned previously, this endocytosis mechanism was previously thought to only occur non-specifically, however it has become clear that membrane protein sorting into sites of macropinocytosis can occur [253] [254]. In addition, work by others has highlighted that during growth-factor induced fibroblast cell migration, integrins can be endocytosed via macropinocytosis and trafficked to specific sites for focal adhesion formation at the leading edge [416]. This therefore opens up the possibility of omental CAFs utilising macropinocytosis for the specific internalisation of collagen-bound integrins. For example, the engagement of integrins such as α1β1 and α2β1 with secreted collagen monomers at the cell surface, could result in their specific internalisation via macropinocytosis, followed by the trafficking of these integrins and their bound collagen to specific sites for collagen fibrillogenesis [417] [418] [419].

5.6.4 Arf6 does not regulate collagen I endocytosis

A role for Arf6 in macropinocytosis has already been established by others. It is thought to be active at the plasma membrane at sites where internalisation via this mechanism takes place, and to also be required for the recycling of internalised membrane back to the cell surface [420] [421]. However, data presented in this chapter indicate that Arf6 does not regulated the endocytosis of collagen, as internalised Cy3-Col I levels were higher following Arf6 depletion, and Arf6-mNG did not localise to sites of Cy3-Col I endocytosis (Figure 5.3, 5.6). The mechanisms utilised by CAFs to endocytose collagen I therefore remain unclear. As Arf6 does not influence Cy3-Col I internalisation, this may indicate that macropinocytosis is not involved in collagen uptake by CAFs. However, it is possible that macropinocytosis is not regulated by identical sets of small GTPases in all cell types. Whilst Arf6 may be required for cell types, such as fibrosarcoma cells, to internalise macromolecules by macropinocytosis, Arf6 may not regulate this process in CAFs such as those found within the HGSOC metastatic TME [421]. Further experiments will be required to determine the mechanism utilised by CAFs for collagen internalisation. Compounds that inhibit macropinocytosis, clathrin- or caveolae-mediated endocytosis, may be used prior to measuring collagen uptake by CAFs using flow cytometry in order to develop an understanding of how large collagen monomers can be internalised.

5.6.5 Arf6 co-localises with sites of collagen I fibrillogenesis

Live-cell fluorescence microscopy also revealed that Arf6 localised to sites of collagen I fibrillogenesis in omental CAFs overexpressing Arf6-mNG, and provided additional evidence in support of a role for Arf6 in the recycling of endocytosed collagen I such that it can be incorporated into fibres. Arf6 was consistently found near the branch point of Cy3-Col I networks as they were assembled, with this branch point likely corresponding to the site of fibrillogenesis initiation. It is not clear whether this localisation occurs due to Arf6 overexpression, and further experiments aiming to visualise the localisation of fluorophore tagged-endogenous Arf6 should determine whether this co-localisation occurs if Arf6 is expressed at endogenous levels. It is also not yet clear whether collagen I fibre assembly by this mechanism involves only the incorporation of endocytosed and recycled collagen I monomers, or whether monomers which have not been internalised, and are present within the extracellular space, are incorporated as well. Interestingly, although cells were often observed moving somewhat during the time-lapse, as indicated by the actin staining, the localisation of Arf6-mNG to these branch points remained constant. This suggested that Arf6 positive structures may be either located within the plasma membrane, or somehow anchored to the membrane at sites of Cy3-Col I fibrillogenesis. Furthermore, as these live-cell imaging experiments were carried out in the absence of ascorbic acid, assembly of collagen I fibres via this mechanism is ascorbic acid independent. This may be expected, as in human cells ascorbic acid is involved only in stabilising pro-collagen chains within the ER such that triple-helical structures can form prior to secretion [188].

5.6.6 Regulation of collagen I recycling for fibrillogenesis by Arf6

The generation of 3D reconstructions indicated that large Arf6 positive structures, possibly corresponding to recycling endosomes, were localised just beneath the plasma membrane at sites of collagen assembly (Figure 5.7). However, at the resolution obtained through the use of spinning disk confocal microscopy, individual vesicular carriers containing internalised Cy3-Col I could not be observed trafficking towards sites of collagen I fibrillogenesis. Whilst these data, and those previously described, implicate Arf6 in the regulation of collagen I recycling for fibrillogenesis, exactly how Arf6 regulates the deposition of collagen following endocytosis is not yet clear. It is possible that Arf6 regulates the recycling of endocytosed collagen directly, where it may influence the trafficking of collagen monomer-bound integrins, ensuring that their recycling is targeted to sites of fibrillogenesis initiation. For example, Arf6 is known to control the recycling of the β1 integrin subunit, which is found within a number of collagen-binding integrins, such as α1β1, α2β1, and α11β1 [417] [419]. Furthermore, as described previously, Chang et al. demonstrated the role of the α11 integrin subunit in the recycling and deposition of endocytosed collagen monomers as fibrils by mouse tail tendon fibroblasts. It is therefore possible that Arf6 influences the deposition of internalised collagen I monomers by CAFs through regulating α11β1 integrin recycling [325].

However, an alternative possibility is that Arf6 instead regulates the trafficking/recycling of other cargoes that may be required for assembling collagen into fibres. Another candidate cargo that could be recycled by Arf6 for this purpose is MT1-MMP. As mentioned in the previous chapter, MT1-MMP is known to be involved in the cleavage of fibronectin to release collagen fibrils from the cell surface at fibripositors, and is also known to be recycled in an Arf6 dependant manner [299] [324]. Further experiments that firstly utilise super-resolution live-cell imaging microscopy should reveal in greater detail how the trafficking itineraries of Arf6 and internalised collagen I are coordinated with one another. It will be important to determine whether Arf6 itself localises to these vesicles, or whether it remains situated on larger endosomal structures through which Cy3-Col I vesicles are trafficked. Secondly, it may become evident that Arf6 does not directly regulate collagen I recycling, but instead regulates fibrillogenesis after endocytosis via influencing the recycling of alternative cargoes. Subsequent experiments will therefore also aim to identify other cargoes which are both recycled in an Arf6-dependant manner, and required for collagen I assembly following endocytosis, for example through the use of proximity labelling techniques such as BioID [422] [291].

5.6.7 Identification of additional ECM proteins which increase in omental abundance with HGSOC progression

Finally, mass spectrometry was also used to identify other ECM proteins that increased in abundance in the omentum with HGSOC progression. Through comparing the ECM protein composition between healthy, uninvolved, and diseased, omentum samples, a number of ECM proteins were identified that were present at higher levels in diseased samples relative to those that were healthy or uninvolved (Figure 5.9). As well as highlighting proteins that others had previously found to become more abundant in the omentum with disease progression, such as versican, this analysis also indicated a number of additional ECM proteins that may be of importance in the HGSOC metastatic niche, such as vitronectin, collagen VIII, and prolargin [98].

AEBP1 has been highlighted as an oncogene in a variety of different cancer types, including colorectal and breast cancers, where it is thought to have roles in regulating processes such as invasion, proliferation and apoptosis [408] [423] [424]. Interestingly, AEBP1 is also believed to play a role in fibroblast proliferation, myofibroblast differentiation, and collagen assembly/remodelling [425] [426, 427]. In addition, studies in ovarian cancer mouse models have shown that the levels of this protein within extracellular vesicles, isolated from ascites present in the peritoneal cavity, increase with disease progression [426]. Whilst these studies demonstrated that HGSOC cells can produce extracellular vesicles containing AEBP1, it is not yet clear whether omental CAFs are capable of secreting this protein. However, given that others have shown AEBP1 is highly expressed in CAFs associated with colon adenocarcinoma, and that high AEBP1 expression correlates with fibroblast activation, it is likely that CAFs in the omentum are also capable of its synthesis and secretion [428].

Collagen VIII is considered a non-fibrillar collagen, where instead it is thought to form unique hexagonal networks [429]. Although the function of collagen VIII remains relatively poorly understood, it is believed to be of particular importance during remodelling of the vasculature, where its expression levels become elevated in vascular smooth muscle cells following vascular damage [430]. Furthermore, collagen VIII levels in serum are upregulated in a number of cancer types, including ovarian and breast, and it is thought that collagen VIII plays a role in the angiogenesis that occurs within the TME of these cancer types [431]. Although in cancers such as hepatocellular carcinoma, an upregulation of collagen VIII in the cancer cells themselves has been demonstrated, it is not yet apparent whether CAFs can secrete this ECM protein [432]. In order to understand the roles of AEBP1 and collagen VIII in the HGSOC metastatic niche, further experiments aiming to evaluate their expression in CAFs, and the impact of their depletion of CAF and cancer cell behaviour, will be required.

Prolargin is a proteoglycan that in heathy tissue functions to bind collagen to the basement membrane [433]. Surprisingly, although our analyses revealed that prolargin was more abundant in diseased omentum samples relative to uninvolved samples, prolargin is described in the literature as a tumour suppressor gene in a number of cancer types [434] [435]. Furthermore, in hepatocellular carcinoma, subsets of CAFs that function as suppressors of tumour development have been shown to do so through the secretion of prolargin [436]. It is therefore unclear whether the prolargin within the HGSOC metastatic niche is CAF-derived, and further work will be required to further understand this, as well as the role of prolargin in the HGSOC TME. One possibility is that in the omentum, prolargin has a more oncogenic function, and it has been demonstrated that the N-terminal region of this protein can bind proteoglycans on the cell surface of fibroblasts to enhance their interaction with the ECM [437]. It may be that prolargin, either secreted by CAFs, other stromal cells, or HGSOC cells themselves, can facilitate the remodelling of the ECM by CAFs in a manner that supports HGSOC tumour progression.

The comparison of ECM composition between matched diseased and uninvolved omentum samples indicated that the tumour burdened region of these samples contained significantly higher levels of agrin and vitronectin, both of which have been previously linked with cancer progression. Agrin is a proteoglycan that, in healthy tissues, is thought to be of particular importance in the formation of neuromuscular junctions, where it primarily functions to bind laminin and to act as a link between the cell surface and the basement membrane [438]. However, in the context of cancer, a number of pro-tumourigenic roles have been highlighted. For example, in rectal cancer, agrin has been shown to stimulate cancer cell migration, invasion and proliferation, and an upregulation in its expression is associated with poor prognosis, however exactly how it functions to promote these processes is not yet understood [439]. In addition, agrin is thought to also play a role in stimulating angiogenesis in the microenvironment of hepatocellular carcinoma tumours, and it has been shown that activated stellate cells within this TME contribute towards its secretion [438] [440].

In contrast to proteins such as collagen and fibronectin, which act primarily in a structural capacity within the ECM, vitronectin is believed to carry out its roles through interacting with other ECM proteins, cell-surface receptors such as integrins, and other secreted factors including proteases and cytokines [441]. A number of pro-tumourigenic functions of vitronectin have been highlighted by others, and it is thought that vitronectin stimulates the invasion of a variety of different cancer cell types via integrin binding, whilst also promoting angiogenesis within TMEs [442]. Although tumour promoting functions of vitronectin have been demonstrated in the context of a number of cancer types, including breast cancer and glioblastoma, its involvement in the metastasis of HGSOC cells to the omentum is not yet clear [411] [443]. It has however been shown that mesothelial cell-secreted vitronectin has a stimulatory effect on OC cell line invasion, and that during OC metastasis, the MMP-2 mediated cleavage of vitronectin facilitates OC cell attachment to the peritoneum and omentum [444] [445]. It may be that the role of vitronectin within the HGSOC omental TME is limited to facilitating the initial attachment and implantation of cells on to the omentum. However, it is also possible that it may have other roles following implantation, such as assisting with HGSOC cell invasion into the omentum, as well as in other processes such as allowing angiogenesis to occur in the TME. It is not clear whether CAFs in the omentum are capable of secreting and assembling agrin and vitronectin.

Although immunohistochemical staining of HGSOC omentum sample sections will be required to validate these findings, these data, in combination with data available in the literature, suggest that the identified proteins may play important tumourigenic roles within the HGSOC metastatic TME. Although these additional ECM proteins have been implicated in the progression of other cancer types, their role in the HGSOC metastatic niche has not yet been investigated. Further experiments will therefore be required to firstly determine whether CAFs in the omentum are responsible for the synthesis and assembly of these proteins, and secondly to understand the functions of these proteins in supporting HGSOC tumour development.

5.6.8 Changes in omental ECM composition do not occur prior to HGSOC cell arrival

Pre-metastatic niche priming is a feature shared across many different cancer types, including OC, but also others such as cancer of the prostate or lung [404] [446] [447]. It can occur via mechanisms such as exosome secretion, or the secretion of other tumour-derived factors, which function to drive initial changes in stromal cell behaviour within secondary organs such that the environment within these organs is more suited to support secondary tumour formation [448]. Changes in ECM protein composition are known to occur within secondary sites prior to the arrival of DTCs in a number of cancer types [449]. For example, studies in mice have demonstrated that exosomes derived from pancreatic cancer cells can stimulate fibronectin production in the liver [450]. Whilst changes in stromal cell behaviour in the omentum have been shown to occur before DTC colonisation, such as resident macrophage reprogramming to generate TAMs, whether or not pre-metastatic changes in omental ECM composition occur had not previously been investigated [119].

Somewhat surprisingly, the comparison of ECM protein composition between healthy and uninvolved omentum samples did not highlight any proteins with levels that were altered significantly, or near-significantly, between these sample types (Figure 5.9c). These data suggested that the changes in stromal ECM composition in the omentum do not occur prior to colonisation by metastatic HGSOC cells. However, it is possible that whilst large scale changes in ECM protein abundance may not occur until DTCs colonise the omentum, smaller scale changes may occur which renders the pre-metastatic TME more suitable for secondary HGSOC tumour development. It will be interesting to evaluate the capacity of HGSOC cell lines, and primary HGSOC cells, to produce exosomes and other secreted factors which may alter CAF behaviour to stimulate excessive ECM protein deposition. This may be carried out through isolating exosomes from HGSOC cells, and investigating the impact of CAF exposure to these exosomes on the assembly of ECM proteins such as collagen I and fibronectin.

5.6.9 Summary

To summarise, the results presented in this chapter demonstrate that Arf6 controls the assembly of collagen I by CAFs in the omentum through regulating its deposition as fibres following endocytosis and recycling. A number of ECM proteins were also identified as becoming more abundant in the omentum with HGSOC progression, including vitronectin, prolargin and collagen VIII. These proteins may be of importance in the colonisation of the omentum by disseminated HGSOC cells and additional experiments should reveal whether these ECM proteins are produced by CAFs, and also whether they have a role in stimulating processes such as HGSOC cell invasion.

Chapter 6: Discussion

6.1 Overview and results summary

The colonisation of the omentum by disseminated HGSOC cells, and the subsequent formation of secondary tumours, is a crucial step in HGSOC progression and is largely responsible for the high mortality rate associated with this disease. HGSOC cells within the peritoneal cavity preferentially colonise the omentum, and their tendency to do so is the result of this organ providing a specific set of conditions, which together create a microenvironment that supports tumour development [46]. One property of this TME that is thought to be of particular importance in supporting the growth, proliferation, and invasion of HGSOC cells, is the synthesis and assembly of a dense, fibrillar ECM by CAFs [150] [151]. Given the role of the ECM in driving HGSOC progression in the omentum, it is essential to understand the molecular mechanisms involved in ECM production by CAFs in greater detail, such that new therapies aiming to prevent or minimise metastasis to the omentum may be developed.

Although endocytic recycling pathways and a number of small GTPases involved in their regulation have been previously implicated in ECM assembly by cell types such as endothelial cells, the role of endocytic recycling in the assembly of ECM by CAFs, such that HGSOC cell invasion can be supported in the omentum, remains poorly understood [318] [321] [323]. This project therefore aimed to investigate the role of endocytic recycling pathways, and their regulator small GTPases, in the assembly of an invasion supportive ECM by CAFs isolated from HGSOC patient omentum samples, and a summary of results is presented in figure 6.1. To develop an understanding of how endocytic recycling regulators were involved in the synthesis of this type of ECM by omental CAFs, the work conducted during this project included:

- The characterisation of CAFs isolated from HGSOC patient omentum samples, in terms of their CAF biomarker expression, and their ability to generate an ECM that supported Kuramochi invasion.
- An endocytic recycling regulator siRNA screen which highlighted Rab4a + Rab4b, and Arf6, as being essential for the facilitation of Kuramochi invasion by CAFs in 3D, and Arf6 and Rab14 as being required for the assembly of collagen I ECM in 2D.

- Exogenous collagen I uptake and deposition assays that indicated a role for Arf6 in the regulation of collagen I assembly through influencing its deposition following endocytosis and recycling, such that it could be trafficked to specific sites for fibrillogenesis to take place.
- Live-cell imaging of Arf6-mNG expressing CAFs following Cy3-Col I treatment, which demonstrated that Arf6 co-localised to sites of Cy3-Col I fibrillogenesis, and that large Arf6 positive structures were located near the inner leaflet of the plasma membrane at sites of Cy3-Col I assembly.
- A compositional analysis by mass spectrometry of ECM proteins in healthy, uninvolved, and diseased omentum samples which, as well as providing evidence in support of data reported by others, highlighted a number of additional proteins that may be of importance within the HGSOC metastatic TME.

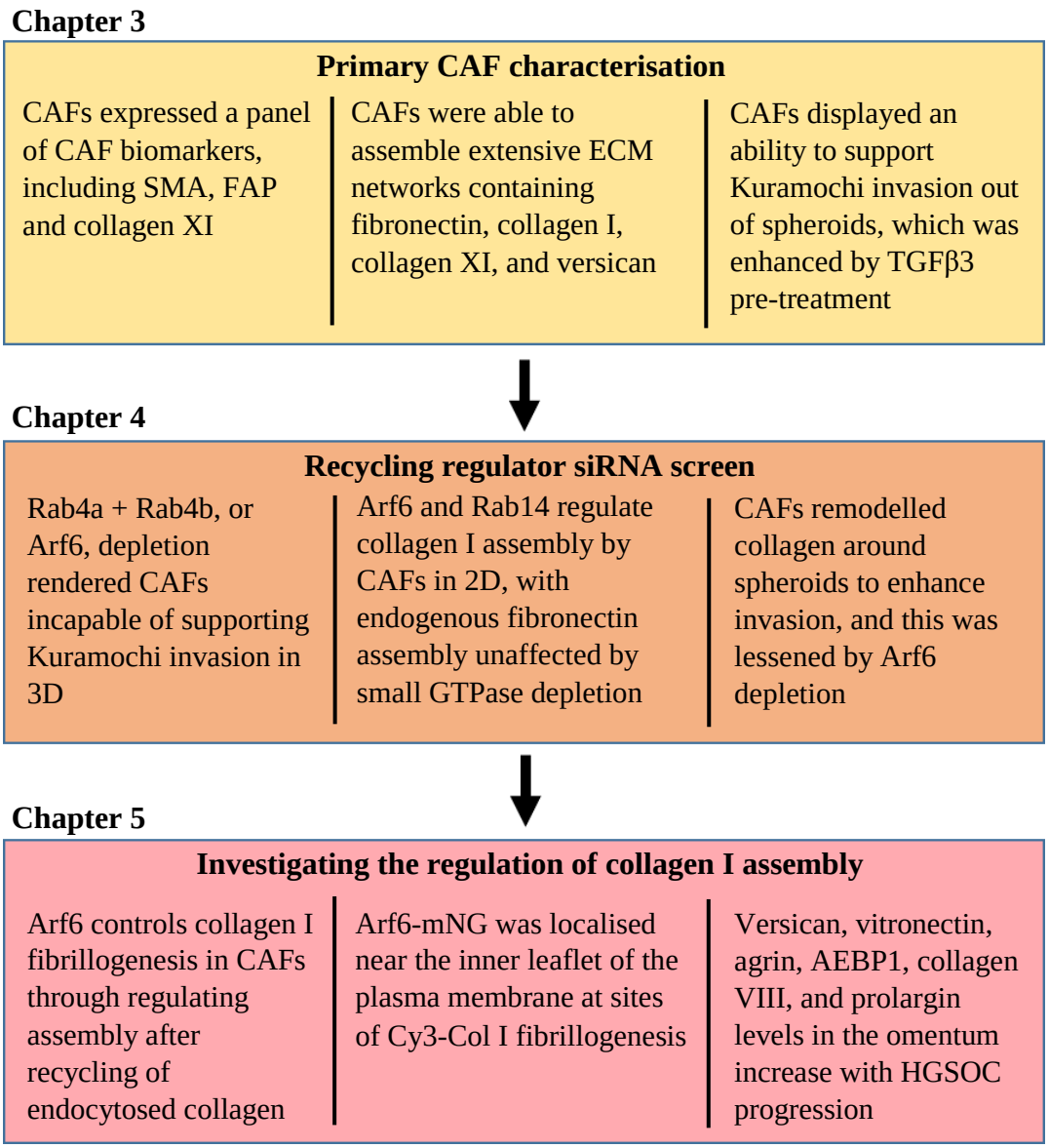

Figure 6.1 - Results summary

The findings presented in chapter 3 (yellow) demonstrated the characterisation of primary omental CAF isolates, in terms of their CAF biomarker expression, and their capacity to carry out CAF-associated functions. The siRNA screening results presented in chapter 4 highlighted a number of recycling regulator GTPases as being of importance in enabling CAFs to support HGSOC cell invasion and/or to assemble/remodel ECM proteins. Finally, the results presented in chapter 5 provided evidence in support of a role for Arf6 in collagen I assembly, where this GTPase was shown to influence the deposition of collagen I as fibres in the extracellular space following endocytosis and recycling. In addition mass spectrometry analysis of omental ECM protein composition between omentum samples of varying HGSOC disease extents, highlighted a number of proteins that increase in abundance with disease progression.

6.2 CAF heterogeneity within the HGSOC TME

6.2.1 Overview

The importance of the TME in the progression of many different cancer types has been established for a number of years, and a great deal of research has focussed on developing our understanding of the interplay between cancer cells and the cellular, and non-cellular, components within microenvironments [451]. Of the cellular components, CAFs are believed to play a crucial role in promoting tumour progression through ECM assembly and remodelling, growth factor secretion, and contributing towards immune evasion and chemoresistance [150] [151] [452] [453]. However, it has become increasingly evident that a great deal of heterogeneity can exist between CAFs, both across cancer types, and also within a given cancer type [329]. It is now known that CAF sub-populations can possess tumour-suppressive properties, for example through the secretion of soluble factors, and exosomes containing microRNAs [84]. If CAFs in the omentum are to be targeted with the aim of suppressing their tumour-promoting functions to inhibit HGSOC metastasis, a better understanding of CAF heterogeneity in the omentum will be crucial to ensure that tumour-suppressive CAF subpopulations remain unaffected.

6.2.2 CAF biomarkers in the characterisation of isolated CAF subpopulations

The biomarkers that have conventionally been used to isolate, identify, and characterise CAFs in the past include, but are not limited to, SMA, FAP, FSP-1 and vimentin [86]. The use of many different CAF biomarkers has become controversial in recent years, primarily due to their overall lack of specificity, and at present, there is no single biomarker that is capable of specifically identifying all CAF subpopulations [454]. The effectiveness of using these biomarkers is dictated firstly by what the aim of their use is, and secondly by which CAF subpopulation is of interest. Myofibroblasts, and likely tumour-promoting, subpopulations of CAFs, can be identified based on high levels of SMA and FAP expression, and Pearce et al. have demonstrated that high expression of SMA and FAP by CAFs in the omentum correlated with HGSOC disease extent. However, subpopulations of CAFs that function in a tumour-suppressive manner are more difficult to identify using biomarker staining, and additional work focussed on identifying biomarkers specific for these CAFs will be required for their identification.

During this project, the primary goal of using immunofluorescence to stain SMA and FAP, as well as collagen XI, in CAFs, was to confirm that myofibroblast-like CAFs had indeed been successfully isolated from HGSOC tumour burdened omentum samples. The HGSOC cells initially present within these samples were expected to be negative for biomarkers such as SMA and FAP. As such, their use in this way was sufficient for ensuring each isolated population of cells mostly consisted of CAFs, and that the HGSOC cells had either been outgrown by the CAFs, or that they had been removed through differential trypsinisation. Using these biomarkers also allowed for some information to be obtained regarding the level of heterogeneity present in samples. During this project, when staining CAFs isolated from diseased omentum samples for SMA, FAP, and collagen XI, it was clear that a degree of heterogeneity existed (Figure 3.1). Whilst the FAP staining pattern was homogeneous, suggesting that all cells present were CAF-like in nature, not all cells expressed SMA and collagen XI to a similar extent, possibly indicating differences in the activation state between cells (Figure 3.2, 3.3). As only an average of 35% of CAFs from diseased omentum samples were positive for large SMA stress fibres, it was possible that during the isolation process, CAFs had become less activated through the withdrawal of HGSOC-tumour derived secreted factors, such as TGFβ isoforms. In order to ensure that activated, myofibroblast-like CAFs were used for the identification of recycling regulators required for ECM generation, we utilised TGFβ3 treatment to activate primary CAFs, and to reduce the level of heterogeneity present in the sample (Figure 3.2. 3.3). The use of this treatment to activate primary CAFs has been carried out by others, and Delaine-Smith et al were able to use TGFβ3 to activate omental CAFs to increase their deposition of ECM proteins, including fibronectin, collagen I, collagen XI, COMP, and versican [159].

6.2.3 Investigating CAF heterogeneity with single-cell RNA sequencing

To fully understand CAF heterogeneity in the HGSOC TME, and to investigate how all CAF subpopulations within the HGSOC TME function, and contribute towards, or supress tumour development, techniques other than the use of biomarker staining are required. One such technique that has been used in recent years to characterise individual subpopulations of primary CAFs within samples, is single-cell RNA sequencing (scRNA-seq) [455]. This technique enables transcriptomes to be analysed with single-cell resolution, and has revolutionised our understanding of how complex the heterogeneity is that exists between CAF subpopulations within TMEs of different cancer types [456] [457]. CAF heterogeneity has been analysed by scRNA-seq in a number of cancer types, including pancreatic and breast cancers [458] [459]. Whilst this technique has been used to identify distinct immune cell populations within the HGSOC TME in the omentum, an investigation into omental CAF heterogeneity has not yet been carried out [460]. Furthermore, this technique has limitations, for example whilst it has the potential to provide information regarding heterogeneity in CAF gene expression, it is well established that transcript and protein levels often do not correlate [461]. Nevertheless, this technique will be vital to understand CAF heterogeneity in the omentum in greater depth, and to ensure that strategies aiming to target CAFs therapeutically are focussed only on those responsible for stimulating HGSOC development

6.2.4 Functional assays for CAF characterisation

Given the lack of biomarkers capable of identifying specific subpopulations of isolated CAFs, it has become clear that functional analyses of CAF behaviour are required for proper characterisation [462]. It was therefore essential that during this project, CAFs were not only characterised based on biomarker expression, but also on their ability to carry out CAF-associated functions of interest. In combination with the analysis of CAF biomarker expression by CAFs, NFs, and non-omental HDFs, functional assays aiming to assess the capacity of these fibroblasts to assemble ECM and to support Kuramochi invasion revealed interesting results.

Although differences in CAF biomarker expression were initially observed between CAFs, NFs, and HDFs prior to TGFβ3 treatment, treatment with this growth factor resulted in each biomarker being detected at comparable levels between each fibroblast type (Figure 3.2, 3.3). However, similar CAF biomarker expression levels did not correlate with CAF behaviour during the functional assays carried out. Firstly, clear differences were observed in the capacity of these fibroblasts to assemble collagen I fibres, where HDFs were less able to do so compared to CAFs and NFs (Figure 3.6). Furthermore, despite TGFβ3 pre-treatment of CAFs and NFs rendering them significantly more competent at facilitating Kuramochi invasion out of spheroids, HDFs remained incapable of doing so, despite the high levels of SMA expression following TGFβ3 treatment detected previously (Figure 3.13, 3.14, 3.15). This suggests that high expression of SMA, FAP, and collagen XI alone, is not necessarily always sufficient for activated fibroblasts to be able to carry out tumour-promoting functions. Furthermore, omentum-derived CAFs and NFs may possess additional properties that enable them to support HGSOC tumour development following activation with TGFβ3.

6.3 Endocytic recycling in generating the HGSOC TME

6.3.1 Overview

The role of endocytic recycling in the assembly of ECM by various normal cell types had been demonstrated by others. A number of Rab GTPases have been implicated in the control of ECM assembly, including Rab10 in protein secretion to generate basement membrane, as well as Rab4a and Rab11b in fibronectin fibrillogenesis by endothelial cells during branching of the vasculature [318] [320] [321]. Several cargo proteins which are recycled in a Rab GTPase-dependant manor have also been highlighted as having roles in the assembly of ECM, including α5β1 integrin in fibronectin fibrillogenesis, and MT1-MMP in collagen I fibrillogenesis [321] [324]. However, until recently, it was not clear whether the internalisation and recycling of ECM proteins themselves was of importance in their assembly to generate fibres. Chang et al. demonstrated that mouse tendon fibroblasts can endocytose secreted collagen I monomers and recycle them to specific sites for fibrillogenesis, and regulators of this recycling were also identified [325].

The results obtained during this project highlighted a number of endocytic recycling regulators as being required for CAFs to contribute towards generating a HGSOC-supportive TME in the omentum. Through the using an siRNA screening approach, omental CAFs displayed a dependency on Rab4a, Rab4b, and Arf6, to facilitate Kuramochi cell invasion in 3D, and as well as Arf6, Rab14 was also required for the deposition of collagen I fibres in 2D (Figure 4.7, 4.8, 4.10, 4.22, 4.23). Exogenous collagen I uptake and deposition assays, combined with live-cell fluorescence microscopy, revealed that Arf6 localised to sites of collagen I assembly, and that Arf6 functioned in controlling collagen I assembly through regulating the deposition of internalised and recycled collagen (Figure 5.3, 5.4, 5.5, 5.7).

6.3.2 Rab4a and Rab4b in the support of HGSOC invasion by CAFs

Depletion of Rab4a + Rab4b in combination in CAFs isolated from two HGSOC patient omentum samples was sufficient to impair their capacity for supporting Kuramochi invasion (Figure 4.7, 4.10). However, although depletion of these GTPases resulted in fewer collagen I fibres deposited by CAFs from isolate MOC194, this result could not be validated in CAFs from patient MOC195 (Figure 4.22). This suggested that whilst Rab4a and Rab4b are utilised by omental CAFs to support HGSOC invasion within the omentum, the stimulatory effect of endocytic recycling regulated by these GTPases is likely not exerted through controlling collagen I deposition. Work by others had demonstrated the involvement of Rab4a in fibronectin fibrillogenesis. However, the siRNA screening data indicate that neither Rab4 isoform was required for fibronectin assembly by omental CAFs (Figure 4.14). Although SHG microscopy revealed that depletion of Rab4a and Rab4b in CAFs isolated from patient MOC208 impaired collagen I remodelling in the vicinity of spheroids to some extent, this was not consistent (Figure 4.25, 4.26). It is therefore not clear how Rab4a- and Rab4b-regulated endocytic recycling enables CAFs to support HGSOC invasion. One possibility is that Rab4 isoforms may influence ECM assembly by CAFs in 3D more so than in 2D, however they may also be required for the assembly of other ECM components involved in facilitating HGSOC invasion. For example, CAF-secreted versican has been shown to enhance OC cell invasion, and further experiments aiming to investigate how Rab4 isoform depletion impacts the assembly of such proteins may provide information regarding how these GTPases enable CAFs to support invasion [347].

6.3.3 Arf6 in collagen I assembly and remodelling

CAFs displayed a requirement for Arf6 in order to assemble collagen I, and Cy3-Col I uptake and deposition assays indicated that the role of Arf6 in regulating this process was through controlling the deposition of collagen I following endocytosis and recycling (Figure 6.2). A co-localisation between Arf6-mNG and sites of Cy3-Col I fibrillogenesis was observed by live-cell fluorescence microscopy, where Arf6 localised just beneath the plasma membranes inner leaflet (Figure 5.7). However, exactly how Arf6 regulates endocytic recycling such that internalised collagen can be deposited as fibres is not yet clear.

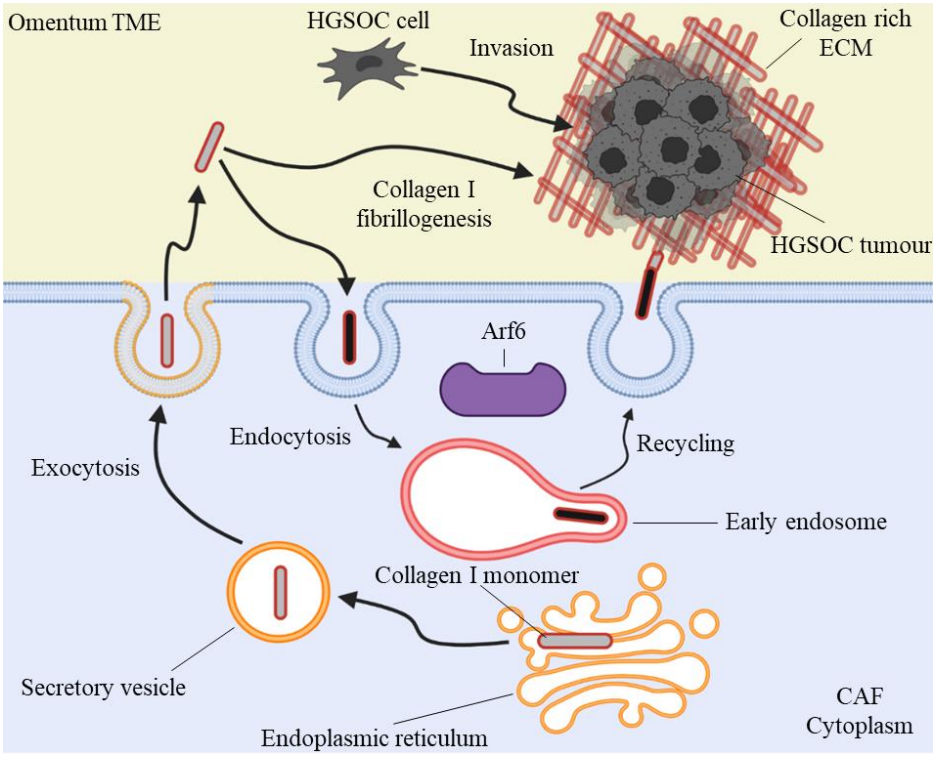

Figure 6.2 - Proposed model of Arf6-regulated recycling in the support of HGSOC invasion by CAFs in the omentum.

Taking the findings from this research project into consideration, we propose that Arf6 functions as a critical regulator of ECM generation by CAFs in the omentum. Arf6-regulated endocytic recycling influences the assembly and remodelling of collagen I through regulating its deposition as fibrils following internalisation. The assembly/remodelling of collagen via a mechanism that firstly requires collagen I monomer secretion, followed by collagen endocytosis and recycling, plays a key role in constructing an ECM microenvironment that supports HGSOC cell invasion. Arf6 may therefore contribute towards colonisation of the omentum by metastatic HGSOC cells, and has the potential to serve a target for chemotherapeutic intervention in the treatment of HGSOC.

The molecular mechanism involved in the internalisation and recycling of collagen I monomers by CAFs have not yet been investigated in detail, however the increase in Cy-Col I internalisation following Arf6 depletion suggests that this GTPase does not regulate collagen endocytosis (Figure 5.3). Arf6 could regulate the recycling of internalised collagen directly, where it may traffic with collagen I positive vesicles to guide them towards sites at the plasma membrane for fibrillogenesis. This may be investigated using the split GFP approach described by Chang et al., where they were able to demonstrate that VSP33B trafficked with vesicles containing endocytosed collagen I monomers [325].

Should Arf6 operate in this manner, it is unlikely that a direct interaction, between Arf6 and collagen I exists during these membrane trafficking events. Instead, Arf6 localised to the surface of endosomal or vesicular structures may interact with other cargos which themselves interact with endocytosed collagen I monomers. Possible candidates that act as a bridge between Arf6 and collagen I are the integrin family of cell-adhesion receptors. Arf6 is known to interact with, and to regulate the recycling of, the β1 integrin subunit, and several integrin dimers containing this subunit have been shown to bind collagens in a variety of cell types, including α1β1, α2β1, α10β1 and α11β1 [417] [418] [419]. Arf6 may therefore regulate collagen I recycling through its interactions with β1 subunit containing integrins. However it is also possible that Arf6 does not directly influence collagen I recycling, but instead may regulate the recycling of alternative cargoes that function in collagen fibrillogenesis. As mentioned previously, an alternative candidate cargo is MT1-MMP, which can be recycled in an Arf6 dependant manner, and is known to have a role in ECM remodelling and the release of collagen I fibrils from the cell surface at fibripositors [299] [324].

In order to investigate the mechanisms of Arf6 regulated recycling in collagen I deposition, we aim to firstly determine whether Arf6 influences MT1-MMP recycling in CAFs, and secondly to evaluate the impact of MT1-MMP depletion in CAFs on their ECM remodelling/collagen I deposition capabilities. Furthermore, to identify near-neighbour cargoes and recycling machineries which associate with Arf6 in CAFs, we will use the BioID proximity labelling technique [422] [291]. This technique is particularly useful for identifying interactors of recycling regulator GTPases, as transient associations with regulators, such as GEFs and GAPs, and effector proteins, are often crucial for the regulation of endocytic recycling [463] [464]. The use of BioID may therefore highlight specific Arf6-associated cargoes, such as integrins, which could interact with collagen I during its recycling and enable Arf6 to influence its trafficking for fibrillogenesis, as well as other effector proteins that enable Arf6 to regulate this process.

6.4 More complex models to study CAFs in the HGSOC TME

6.4.1 Overview

As described in chapter 1, there is a complex interplay between the different non-malignant cell types within TMEs of many cancer types, including that of HGSOC. It is known that whilst the cell-cell communication that occurs between stromal cells, such as CAFs, and the tumour with which they are associated is essential for tumourigenesis, the interactions that occur between different stromal cells is also vital for tumour progression [55]. In the context of CAFs, constant multi-directional cross-talk occurs with other stromal cells, which not only contributes towards the tumour-promoting capacity of these other cells, but also maintains CAFs in a state capable of facilitating malignant cell growth, proliferation, survival and invasion [79] [80] [81] [82] [83].

During this project, CAFs were studied either as a mono-culture in 2D, or in co-culture with the Kuramochi cell line in 3D invasion assays. Although these experiments generated interesting results demonstrating how CAFs may function to stimulate HGSOC cell invasion through ECM protein synthesis and remodelling, it is important to consider the impact of other stromal cells on CAF behaviour in this context. In order to investigate how CAFs operate to support HGSOC metastasis in the omentum in a more physiologically relevant context, there is a need to study CAF function in the presence of other stromal cells, such as white adipocytes, and the various immune cell types present in the omentum. Furthermore, to fully understand the mechanisms by which CAFs support HGSOC tumour development in the omentum, it is essential to investigate CAF behaviour *in vivo*, for example in animal models of HGSOC.

6.4.2 White adipocytes

As white adipocytes are the most abundant cell within the omentum, an understanding of how CAFs assemble and remodel ECM to modulate the invasive capacity of HGSOC cells in an adipocyte rich environment is vital. Whilst the results produced during this project indicated a role for Arf6 in the regulation of collagen I deposition and remodelling by CAFs to facilitate HGSOC cell invasion, the relevance of this mechanism in the omentum is not yet clear. It is possible that the regulation of ECM assembly and remodelling through endocytic recycling in CAFs is impacted by the tri-directional cross-talk which likely occurs between CAFs, HGSOC cells, and white adipocytes in the omentum. Delaine-Smith et al. have developed a tri-culture model which includes HGSOC cells, primary CAFs, and primary omental white adipocytes. In this model, CAFs were able to efficiently assemble ECM proteins such as fibronectin, collagen I, fibronectin, and versican, proving that it can be used to study CAF behaviour in an environment that more accurately recapitulates the complex interactions which occur in the omental TME. We hypothesise that Arf6 plays a role in the assembly of ECM by CAFs in the omentum, and we aim to utilise a similar tri-culture model to determine the importance of Arf6 in collagen I deposition and remodelling within a more physiological relevant setting.

6.4.3 Immune cells

The cell-cell interactions between CAFs and the various immune cells present in TMEs are known to be of great importance in tumour progression. CAFs in the omentum are capable of secreting factors, such as CXCL12 and CSF-1, which recruit tumour-promoting TAMs displaying an M2 phenotype to the TME [160]. Furthermore, their secretion of additional factors, including IL-6, supports the generation of an immunosuppressive environment by stimulating Treg cell proliferation and survival [161]. Furthermore, the cross-talk between CAFs and immune cells in the omentum is bidirectional. For example, Treg cells have been shown to secrete PDGFA which enhances the growth of CAFs [139]. Given the ability of immune cells to modulate CAF behaviour in the omentum, it will be important to investigate how endocytic recycling controls ECM assembly and remodelling by CAFs in the presence of immune cells.

A possible approach to study the impact of immune cells on CAF function is to generate tri-culture spheroids consisting of Kuramochi cells, CAFs, and an immune cell type such as primary TAMs. Similar work by others has demonstrated how the inclusion of immune cells in 3D culture systems of fibroblasts and non-small cell lung cancer cells was sufficient to enhance MMP secretion and ECM protein deposition [465]. It will therefore be interesting to monitor whether immune cells, such as HGSOC patient derived TAMs, are capable of altering the dependence of CAFs on Arf6 for supporting Kuramochi invasion out of spheroids.

6.4.4 Animal models

Models that incorporate other stromal cells will enable CAF behaviour, and the importance of Arf6 in ECM assembly, to be studied in a more physiologically relevant setting. However, given the complexity of the many different interactions occurring between each cell type in the HGSOC TME, the ultimate aim is to investigate the importance of Arf6 for HGSOC metastasis in animal models. Genetically engineered mouse models have been used extensively to study the metastasis of various cancer types, including HGSOC, and mouse models of HGSOC can be generated through the expression of known oncogenic mutations associated with the disease in the ovary, or in the fallopian tube [466] [467]. In addition, metastatic HGSOC mouse models can be produced through intra-peritoneal injection of HGSOC cells derived from mice, or humans. Omental metastases were detected in a number of mouse models generated in this manner, and analyses of their TME revealed similarities with that found within human HGSOC patient derived omentum [468].

With regards to modulating CAF function within the omentum of HGSOC mouse models, one approach that maybe used is the Cre/Lox system. Mo et al. recently demonstrated how this method can be used to generate mice in which a protein of interest has been knocked out specifically in stromal fibroblasts [469]. They were able to highlight a role for their protein of interest, YAP1, in enabling OC cells to communicate with stromal fibroblasts through exosome secretion. A similar approach may therefore be used to investigate the importance of Arf6 in HGSOC metastasis *in vivo*, where mice could be generated with Arf6 knocked out specifically in CAFs within the omental stroma.

6.5 Conclusions and future directions

The work carried out during this project highlights Arf6-regulated endocytic recycling as an important controller of collagen I assembly and remodelling by activated, myofibroblast-like, CAFs which enables the support of cancer cell invasion in the HGSOC metastatic TME. In addition, the comparison of ECM protein composition between healthy, uninvolved, and diseased, omentum samples highlighted several proteins which may be of importance in supporting metastatic HGSOC tumour development. As discussed previously, there a number of additional experiments which may be carried out to investigate these findings in greater detail, and those which will be prioritised are as follows:

- As MT1-MMP has been implicated in collagen I fibrillogenesis and is thought to undergo recycling in an Arf6-regulated manner, ECM deposition assays, and spheroid invasion assays together with SHG microscopy, will be carried out following MT1-MMP depletion to investigate the potential role of this cargo in generating ECM in the omental TME.

- BioID will be used to identify key Arf6 regulators, such as GEFs and GAPs, which control its activity in CAFs, as well as Arf6-associated cargoes and effector proteins that may enable Arf6 to influence ECM assembly and remodelling in the HGSOC metastatic TME.

- It will be essential to investigate the importance Arf6-regulated recycling in CAFs during HGSOC metastasis in a system that more accurately recapitulates the environment found within the omentum. Initially, tri-culture systems will be set up consisting of CAFs, HGSOC cells, and either white adipocytes or immune cell types such as TAMs. The impact of Arf6 depletion on ECM assembly/remodelling will be evaluated, together with the influence of these other non-malignant cell types on the Arf6-mediated facilitation of OC cell line invasion. Following on from this, Arf6 function in CAFs may also be investigated in mouse models of HGSOC through generating Arf6 knockout CAFs specifically in the stroma of the omentum as described previously. Furthermore, others have demonstrated how the Arf6 inhibitor, NAV-2729, can hinder uveal melanoma tumourigenesis in mouse models via injection into the peritoneum, and we may utilise a similar approach to target Arf6 function in the HGSOC omental stroma [470].

- Whilst a number of ECM proteins were identified using mass spectrometry as increasing in omental abundance with HGSOC progression, the functions of these proteins in the TME, and the role of CAFs in their synthesis and assembly, have not yet been investigated. The expression levels of proteins such as vitronectin, agrin, AEBP1, collagen VIII, and prolargin, will firstly be measured in CAF isolates. The impact of depleting these proteins on the facilitation of HGSOC cell invasion by CAFs will then be investigated, together with the influence of endocytic recycling pathways on their synthesis and deposition in the extracellular space.

The necessity of Arf6-regulated endocytic recycling for CAFs to support HGSOC metastasis opens up the possibility of chemotherapeutically interfering with Arf6 function in the omentum as a means of preventing, or minimising, HGSOC colonisation. Furthermore, Arf6 has also been shown to be involved in cell invasion, both in normal and malignant cells, suggesting that targeting Arf6 in the omentum has the potential to obstruct the pro-tumourigenic properties of both the cancer cells and the non-malignant stromal cells to prevent metastasis [471] [472] [473].

However, an issue that is often encountered during attempts to target either individual ECM components in the TME, or their synthesis, is that healthy, non-tumour burdened tissues can also be effected [109]. Given that Arf6-regulated endocytic recycling is also involved in the cellular processes which occur in healthy tissue, including normal cell migration, cytokinesis, and endothelial cell adhesion, impairing Arf6 function *in vivo* may result in non-desirable off-target effects [474]. It will therefore be essential to determine the impact of Arf6 inhibition on normal cell behaviour, both in cell culture systems and in model organisms. Furthermore, the use of BioID may allow the identification of other protein machineries that associate with Arf6 and enable it to regulate collagen I assembly and remodelling by CAFs, but are not as essential as Arf6 for normal cell function, and may therefore serve as more suitable targets for chemotherapeutic intervention [422] [291].

References

[1] J Ferlay et al, “Cancer statistics for the year 2020: An overview,” *International Journal of Cancer ,* vol. 149, no. 4, pp. 778-789, 2021.

[2] SH Hassanpur & M Dehghani, “Review of cancer from perspective of molecular,” *Journal of Cancer Research and Practice,* vol. 4, no. 4, pp. 127-129, 2017.

[3] D. Hanahan, “Hallmarks of Cancer: New Dimensions,” *Cancer Discovery,* vol. 12, no. 1, pp. 31-46, 2022.

[4] BM Reid et al, “Epidemiology of ovarian cancer: a review,” *Cnacer Biology & Medicine ,* vol. 14, no. 1, pp. 9-32, 2017.

[5] Z Khazaei et al, “Worldwide incidence and mortality of ovarian cancer and Human Development Index (HDI): GLOBOCAN sources and methods 2018,” *Journal of Preventive Medicine and Hygiene ,* vol. 62, no. 1, pp. E174-184, 2021.

[6] J Huang et al, “Worldwide Burden, Risk Factors, and Temporal Trends of Ovarian Cancer: A Global Study,” *Cancers,* vol. 14, no. 9, 2022.

[7] S Yeoh et al, “Trends in the overall survival rates in women with advanced ovarian cancer in a single tertiary centre in New Zealand,” *Obstetrics & Gynaecology ,* vol. 59, no. 6, pp. 861-866, 2019.

[8] GC Jayson et al, “Ovarian cancer,” *The Lancet,* vol. 384, no. 9951, pp. 1376-1388, 2014.

[9] LS Lino-Silva, “Ovarian carcinoma: pathology review with an emphasis in their molecular characteristics,” *Chinese Clinical Oncology,* vol. 9, no. 4, 2020.

[10] K Gajjar et al, “Symptoms and Risk Factors of Ovarian Cancer: A Survey in Primary Care,” *ISRN Obstetrics and Gynecology ,* vol. 2012, 2012.

[11] MA Roett et al, “Ovarian Cancer: An overview,” *American Family Physician ,* vol. 80, no. 6, pp. 609-616, 2009.

[12] KR Cho et al, “Ovarian cancer,” *Annual Review of Pathology: Mechanisms of Disease,* vol. 4, pp. 287-313, 2009.

[13] MA Lisio et al, “High-Grade Serous Ovarian Cancer: Basic Sciences, Clinical and Therapeutic Standpoints,” *International Journal of Molecular Sciences ,* vol. 20, no. 4, p. 952, 2019.

[14] M Koshiyama et al, “Subtypes of Ovarian Cancer and Ovarian Cancer Screening,” *Diagnostics (Basel),* vol. 7, no. 1, p. 12, 2017.

[15] M Tuna et al, “Clinical relevance of TP53 hotspot mutations in high-grade serous ovarian cancers,” *Genetics and Genomics ,* vol. 122, pp. 405-412, 2019.

[16] MH Sohn et al, “Classification of High-Grade Serous Ovarian Carcinoma by Epithelial-to-Mesenchymal Transition Signature and Homologous Recombination Repair Genes,” *Genes (Basel),* vol. 12, no. 7, p. 1103, 2021.

[17] K Lohmussaar et al, “Assessing the origin of high-grade serous ovarian cancer using CRISPR-modification of mouse organoids,” *Nature Communications ,* vol. 11, p. 2660, 2020.

[18] J Kim et al, “Cell Origins of High-Grade Serous Ovarian Cancer,” *Cancers (Basel),* vol. 10, no. 11, p. 433, 2018.

[19] SE Bachert et al, “Serous Tubal Intraepithelial Carcinoma: A Concise Review for the Practicing Pathologist and Clinician,” *Diagnostics (Basel),* vol. 10, no. 1, p. 102, 2020.

[20] GO Chong et al, “Incidental Serous Tubal Intraepithelial Carcinoma that Developed into Primary Peritoneal Serous Carcinoma in a Patient without BRCA Mutation,” *American Journal of Case Reports,* vol. 21, pp. e921146-1–e921146-4, 2020.

[21] SI Labidi-Galy et al, “High grade serous ovarian carcinomas originate in the fallopian tube,” *Nature Communications,* vol. 8, p. 1093, 2017.

[22] NG Alkema et al, “Studying platinum sensitivity and resistance in high-grade serous ovarian cancer: Different models for different questions,” *Drug Resistance Updates ,* vol. 24, pp. 55-69, 2016.

[23] KC Kurnit et al, “Updates and New Options in Advanced Epithelial Ovarian Cancer Treatment,” *Obstetrics and Gynecology,* vol. 137, no. 1, pp. 108-121, 2021.

[24] FT Unger et al, “DNA damage induced by cis- and carboplatin as indicator for in vitro sensitivity of ovarian carcinoma cells,” *BMC Cancer ,* vol. 9, p. 359, 2009.

[25] NT Bound et al, “Improving PARP inhibitor efficacy in high-grade serous ovarian carcinoma: A focus on the immune system,” *Frontiers in Genetics,* vol. 13, p. 886170, 2022.

[26] G Damia et al, “Platinum Resistance in Ovarian Cancer: Role of DNA Repair,” *Cancers (Basel),* vol. 11, no. 1, p. 119, 2019.

[27] PA Konstantinopoulos et al, “PARP Inhibitors for Ovarian Cancer: Current Indications, Future Combinations, and Novel Assets in Development to Target DNA Damage Repair,” *American Society of Clinical Oncology Educational Book ,* vol. 40, p. e116, 2020.

[28] T Foo et al, “PARP inhibitors in ovarian cancer: An overview of the practice-changing trials,” *Genes Chromosomes and Cancer,* vol. 60, no. 5, pp. 385-397, 2020.

[29] T. C. G. A. R. Network, “Integrated Genomic Analyses of Ovarian Carcinoma,” *Nature,* vol. 474, no. 7353, pp. 609-615, 2011.

[30] F Pepe et al, “BRCA1/2 NGS Somatic Testing in Clinical Practice: A Short Report,” *Genes,* vol. 12, no. 12, p. 1917, 2021.

[31] L Biegala et al, “PARP inhibitor resistance in ovarian cancer: Underlying mechanisms and therapeutic approaches targeting the ATR/CHK1 pathway,” *Biochemica et Biophysica Acta - Reviews on Cancer ,* vol. 1876, no. 2, p. 188633, 2021.

[32] S. Irani, “Emerging insights into the biology of metastasis: A review article,” *Iranian Journal of Basic Medical Sciences,* vol. 22, no. 8, pp. 883-847, 2019.

[33] KW Hunter et al, “Mechanisms of metastasis,” *Breast Cancer Research ,* vol. 10, p. S2, 2008.

[34] SPH Chiang et al, “Tumor cell intravasation,” *American Journal of Cell Physiology ,* vol. 311, no. 1, pp. C1-C14, 2016.

[35] K Ganesh et al, “Targeting metastatic cancer,” *Nature Medicine,* vol. 27, no. 1, pp. 34-44, 2021.

[36] NV Krakhmal et al, “Cancer Invasion: Patterns and Mechanisms,” *Acta Naturae,* vol. 7, no. 2, pp. 17-28, 2015.

[37] JS Wu et al, “Plasticity of cancer cell invasion: Patterns and mechanisms,” *Translational Oncology ,* vol. 1, no. 100899, p. 14, 2021.

[38] Y Yang et al, “An emerging tumor invasion mechanism about the collective cell migration,” *American Journal of Translational Research ,* vol. 11, no. 9, pp. 5301-5312, 2019.

[39] MB Chen et al, “Mechanisms of tumor cell extravasation in an in vitro microvascular network platform,” *Integrative Biology,* vol. 5, no. 10, pp. 1262-1271, 2013.

[40] TA Martin et al, “Cancer Invasion and Metastasis: Molecular and Cellular Perspective,” *Metastatic Cancer: Clinical and Biological Perspectives,* 2013.

[41] J Fares et al, “Molecular principles of metastasis: a hallmark of cancer revisited,” *Nature ,* vol. 5, p. 28, 2020.

[42] H Lusk et al, “Models for measuring metabolic chemical changes in the metastasis of high grade serous ovarian cancer: Fallopian tube, ovary, and omentum,” *Molecular Omics,* vol. 17, no. 6, pp. 819-832, 2021.

[43] E lengyel, “Ovarian Cancer Development and Metastasis,” *The American Journal of Pathology ,* vol. 177, no. 3, pp. 1053-1064, 2010.

[44] I Konishi et al, “Peritoneal dissemination of highgrade serous ovarian cancer: pivotal roles of chromosomal instability and epigenetic dynamics,” *Journal of Gynecologic Oncology,* vol. 33, no. 5, p. e83, 2022.

[45] SJ Ritch et al, “The metastatic capacity of high-grade serous ovarian cancer cells changes along disease progression: inhibition by mifepristone,” *Cancer Cell International,* vol. 22, p. 397, 2022.

[46] T Motohara et al, “An evolving story of the metastatic voyage of ovarian cancer cells: cellular and molecular orchestration of the adipose-rich metastatic microenvironment,” *Oncogene,* vol. 38, no. 16, pp. 2885-2898, 2019.

[47] W Chen et al, “Organotropism: new insights into molecular mechanisms of breast cancer metastasis,” *NPJ Precision Oncology,* p. 42, 2018.

[48] K. Mortezaee, “Organ tropism in solid tumor metastasis: an updated review,” *Future Oncology,* vol. 17, no. 15, pp. 1943-1961, 2021.

[49] TL Yeung et al, “Cellular and molecular processes in ovarian cancer metastasis. A Review in the Theme: Cell and Molecular Processes in Cancer Metastasis,” *American Journal of Physiology: Cell Physiology ,* vol. 309, no. 7, pp. C444-456, 2015.

[50] I. K, “ellular basis of omentum activation and expansion revealed by single-cell RNA sequencing using a parabiosis model,” *Scientific Reports,* vol. 11, 2021.

[51] HC Gusky et al, “Omentum and bone marrow: how adipocyte-rich organs create tumour microenvironments conducive for metastatic progression,” *Obesity Reviews ,* vol. 17, no. 11, pp. 1015-1029, 2016.

[52] H. N. a. D. Montell, “Ovarian Cancer Metastasis: Integrating insights from disparate model organisms,” *Nature Reviews Cancer ,* vol. 5, pp. 355-366, 2005.

[53] M. J. a. W. Jin, “The updated landscape of tumor microenvironment and drug repurposing,” *Signal Transduction and Targeted Therapy,* vol. 5, p. 166, 2020.

[54] L Bejarano et al, “Therapeutic Targeting of the Tumor Microenvironment,” *Cancer Discovery,* vol. 11, no. 4, pp. 933-959, 2021.

[55] A Bozyk et al, “Tumor Microenvironment—A Short Review of Cellular and Interaction Diversity,” *Biology (Basel),* vol. 11, no. 6, p. 929, 2022.

[56] H Gonzalez et al, “Roles of the immune system in cancer: from tumor initiation to metastatic progression,” *Genes and Development ,* vol. 32, no. 19-20, pp. 1267-1284, 2018.

[57] X Lei et al, “Immune cells within the tumor microenvironment: Biological functions and roles in cancer immunotherapy,” *Cancer Letters,* vol. 470, pp. 126-133, 2020.

[58] F Galli et al, “Relevance of immune cell and tumor microenvironment imaging in the new era of immunotherapy,” *Journal of Experimental and Clinical Cancer Research ,* vol. 39, p. 89, 2020.

[59] SM Downes-Canner et al, “B Cell Function in the Tumor Microenvironment,” *Annual Reviews of Immunology ,* vol. 40, pp. 169-193, 2022.

[60] NB Hao et al, “Macrophages in Tumor Microenvironments and the Progression of Tumors,” *Clinical and Developmental Immunology,* vol. 2012, p. 948098, 2012.

[61] P Dumont et al, “Expression of galectin-3 in the tumor immune response in colon cancer,” *Laboratory Investigations ,* vol. 88, no. 8, pp. 896-906, 2008.

[62] J Liu et al, “New insights into M1/M2 macrophages: key modulators in cancer progression,” *Cancer Cell International ,* no. 21, p. 389, 2021.

[63] Y Chen et al, “Tumor-associated macrophages: an accomplice in solid tumor progression,” *Journal of Biomedical Science ,* no. 28, p. 78, 2019.

[64] H Raskov et al, “Cancer-Associated Fibroblasts and Tumor-Associated Macrophages in Cancer and Cancer Immunotherapy,” *Frontiers in Oncology,* vol. 11, p. 668731, 2021.

[65] G Bergers & LE Benjamin, “Tumorigenesis and the angiogenic switch,” *Nature Reviews Cancer ,* vol. 3, pp. 401-410, 2003.

[66] L Moserle et al, “The angiogenic switch: implications in the regulation of tumor dormancy,” *Current Molecular Medicine,* vol. 9, no. 8, pp. 935-941, 2009.

[67] DR Bielenberg & BR Zetter, “The Contribution of Angiogenesis to the Process of Metastasis,” *Cancer Journal ,* vol. 21, no. 4, pp. 267-273, 2015.

[68] MD Palma et al, “Microenvironmental regulation of tumour angiogenesis,” *Nature,* vol. 17, pp. 457-474, 2017.

[69] J Linares et al, “Determinants and Functions of CAFs Secretome During Cancer Progression and Therapy,” *Frontiers in Cell and Developmental Biology,* vol. 8, p. 621070, 2021.

[70] B Huang et al, “Cancer-Associated Fibroblasts Promote Angiogenesis of Hepatocellular Carcinoma by VEGF-Mediated EZH2/VASH1 Pathway,” *Technology in Cancer Research and Treatment ,* vol. 18, p. 1533033819879905., 2019.

[71] T Yang et al, “Down-regulation of KLF5 in cancer-associated fibroblasts inhibit gastric cancer cells progression by CCL5/CCR5 axis,” *Cancer Biology and Therapy ,* vol. 18, no. 10, pp. 806-815, 2017.

[72] M Plikus, “Fibroblasts: origins, definitions, and functions in health and disease,” *Cell ,* vol. 184, no. 15, pp. 3852-3872, 2022.

[73] MD Lynch et al, “Fibroblast heterogeneity: implications for human disease,” *The Journal of Clinical Investigation ,* vol. 128, no. 1, pp. 26-35, 2018.

[74] P Pakshir et al, “The myofibroblast at a glance,” *Journal of Cell Science ,* vol. 133, no. 13, 2020.

[75] AA Fitzgerald et al, “The role of fibroblast activation protein in health and malignancy,” *Cancer and Metastasis Reviews ,* vol. 39, no. 3, pp. 783-803, 2020.

[76] T Liu et al, “Cancer-associated fibroblasts: an emerging target of anti-cancer immunotherapy,” *Journal of Hematology and Oncology ,* vol. 12, no. 86, 2019.

[77] Y Chen et al, “Clinical and therapeutic relevance of cancer-associated fibroblasts,” *Nature Reviews Clinical Oncology,* vol. 18, pp. 792-804, 2021.

[78] FT Wang et al, “Cancer-associated fibroblast regulation of tumor neo-angiogenesis as a therapeutic target in cancer,” *Oncology Letters,* vol. 17, no. 3, pp. 3055-3065, 2019.

[79] E Sahai et al, “A framework for advancing our understanding of cancer-associated fibroblasts,” *Nature,* vol. 20, pp. 174-186, 2020.

[80] MW Pickup et al, “The extracellular matrix modulates the hallmarks of cancer,” *EMBO Reports,* vol. 15, pp. 1243-1253, 2014.

[81] E Henke et al, “Extracellular Matrix in the Tumor Microenvironment and Its Impact on Cancer Therapy,” *Frontiers in Molecular Biosciences,* vol. 6, p. 160, 2020.

[82] A Chakravarthy et al, “TGF-β-associated extracellular matrix genes link cancer-associated fibroblasts to immune evasion and immunotherapy failure,” *Nature Communications,* vol. 9, no. 1, p. 4692, 2018.

[83] I Aserbi et al, “Human breast cancer invasion and aggression correlates with ECM stiffening and immune cell infiltration.,” *Integrative Biology,* vol. 7, pp. 1120-1134, 2015.

[84] Z Whang et al, “Cancer-Associated Fibroblasts Suppress Cancer Development: The Other Side of the Coin,” *Frontiers in Cell and Developmental Biology,* vol. 9, p. 613534, 2021.

[85] BC Ozdemir et al, “Depletion of Carcinoma-Associated Fibroblasts and Fibrosis Induces Immunosuppression and Accelerates Pancreas Cancer with Diminished Survival,” *Cancer Cell,* vol. 25, no. 6, pp. 719-734, 2015.

[86] C Han et al, “Biomarkers for cancer-associated fibroblasts,” *Biomarker Research ,* vol. 8, no. 64, 2020.

[87] M Nurmik et al, “In search of definitions: Cancer-associated fibroblasts and their markers,” *International Journal of Cancer,* vol. 146, no. 4, pp. 895-905, 2019.

[88] RS Joshi et al, “The Role of Cancer-Associated Fibroblasts in Tumor Progression,” *Cancers ,* vol. 13, no. 6, p. 1399, 2021.

[89] Q Yao et al, “CLIC4 mediates TGF-beta1-induced fibroblast-to-myofibroblast transdifferentiation in ovarian cancer,” *Oncology Reports ,* vol. 22, no. 3, pp. 541-548, 2009.

[90] M Li et al, “High expression of fibroblast activation protein (FAP) predicts poor outcome in high-grade serous ovarian cancer,” *BMC Cancer ,* vol. 20, no. 1, p. 1032, 2020.

[91] R Bughda et al, “Fibroblast Activation Protein (FAP)-Targeted CAR-T Cells: Launching an Attack on Tumor Stroma,” *ImmunoTargets and Therapy,* vol. 10, pp. 313-323, 2021.

[92] D Lai et al, “Fibroblast activation protein regulates tumor-associated fibroblasts and epithelial ovarian cancer cells,” *International Journal of Oncology ,* vol. 41, no. 2, pp. 541-550, 2012.

[93] Strutz F et al, “Identification and Characterization of a Fibroblast Marker: FSP1,” *The Journal of Cell Biology,* vol. 130, no. 2, pp. 393-405, 1995.

[94] F Fei et al, “Role of metastasis-induced protein S100A4 in human non-tumor pathophysiologies,” *Cell and Bioscience ,* vol. 7, no. 64, 2017.

[95] JT O'Connell et al, “VEGF-A and Tenascin-C produced by S100A4+ stromal cells are important for metastatic colonization,” *The Proceedings of the National Academy of Sciences (PNAS),,* vol. 108, no. 38, p. 16002–16007, 2011.

[96] RJ Wenstrup et al, “Regulation of Collagen Fibril Nucleation and Initial Fibril Assembly Involves Coordinate Interactions with Collagens V and XI in Developing Tendon,” *Journal of Biological Chemistry ,* vol. 286 , no. 23, p. 20455–20465, 2011.

[97] D Jia et al, “A COL11A1-correlated pan-cancer gene signature of activated fibroblasts for the prioritization of therapeutic targets,” *Cancer Letters ,* vol. 382, no. 2, pp. 203-214, 2016.

[98] OMT Perace at al, “Deconstruction of a metastatic tumor microenvironment reveals a common matrix response in human cancers,” *Cancer Discovery,* vol. 8, no. 3, pp. 304-319, 2018.

[99] D. H. a. R. Weinberg, “Hallmarks of Cancer: The Next Generation,” *Cell ,* vol. 144, no. 5, pp. 646-674, 2011.

[100] C. Roma-Rodrigues, “Targeting Tumor Microenvironment for Cancer Therapy,” *International Journal of Molecular Sciences ,* vol. 20, no. 4, p. 840, 2019.

[101] RA Glabman et al, “Cancer-Associated Fibroblasts: Tumorigenicity and Targeting for Cancer Therapy,” *Cancers (Basel),* vol. 14, no. 16, p. 3906, 2022.

[102] RD Hofheinz et al, “Stromal antigen targeting by a humanised monoclonal antibody: an early phase II trial of sibrotuzumab in patients with metastatic colorectal cancer,” *Onkologie,* vol. 26, pp. 44-48, 2003.

[103] AM LeBeau et al, “Targeting the cancer stroma with a fibroblast activation protein-activated promelittin protoxin,” *Molecular Cancer Therapy,* vol. 8, no. 5, pp. 1378-1386, 2009.

[104] FL Tansi et al, “Activatable bispecific liposomes bearing fibroblast activation protein directed single chain fragment/Trastuzumab deliver encapsulated cargo into the nuclei of tumor cells and the tumor microenvironment simultaneously,” *Acta Biomaterialia,* vol. 54, pp. 281-293, 2017.

[105] J Lee et al, “Tumor immunotherapy targeting fibroblast activation protein, a product expressed in tumor-associated fibroblasts,” *Cancer Research ,* vol. 65, no. 23, pp. 11156-11163, 2005.

[106] A Costa et al, “Fibroblast Heterogeneity and Immunosuppressive Environment in Human Breast Cancer,” *Cancer Cell,* vol. 33, no. 3, pp. 463-479, 2018.

[107] A Orimo et al, “Stromal fibroblasts present in invasive human breast carcinomas promote tumor growth and angiogenesis through elevated SDF-1/CXCL12 secretion,” *Cell,* vol. 121, no. 3, pp. 335-348, 2005.

[108] IX Chen et al, “Blocking CXCR4 alleviates desmoplasia, increases T-lymphocyte infiltration, and improves immunotherapy in metastatic breast cancer,” *Proceedings of*

[109] FA Venning et al, “Targeting ECM Disrupts Cancer Progression,” *Frontiers in Oncology,* vol. 5, p. 224, 2015.

[110] M Silacci et al, “Human monoclonal antibodies to domain C of tenascin-C selectively target solid tumors in vivo,” *Protein Engineering, Design and Selection: PEDS,* vol. 19, no. 10, pp. 471-478, 2006.

[111] DA Reardon et al, “A pilot study: 131I-antitenascin monoclonal antibody 81c6 to deliver a 44-Gy resection cavity boost,” *neuro-Oncology,* vol. 10, no. 2, pp. 182-190, 2008.

[112] DA Reardon et al, “Phase II trial of murine (131)I-labeled antitenascin monoclonal antibody 81C6 administered into surgically created resection cavities of patients with newly diagnosed malignant gliomas,” *Journal of Clinical Oncology,* vol. 20, no. 5, pp. 1389-1397, 2002.

[113] MY Kim et al, “Selection and characterization of tenascin C targeting peptide,” *Molecules and Cells,* vol. 33, no. 1, pp. 71-77, 2012.

[114] S Xu et al, “The role of collagen in cancer: from bench to bedside,” *Journal of Translational Medicine ,* vol. 17, p. 309, 2019.

[115] DM Gikes et al, “Collagen prolyl hydroxylases are essential for breast cancer metastasis,” *Cancer Research ,* vol. 73, no. 11, pp. 3285-3296, 2013.

[116] G Xiong et al, “Prolyl-4-hydroxylase α subunit 2 promotes breast cancer progression and metastasis by regulating collagen deposition,” *BMC Cancer,* vol. 14, p. 1, 2014.

[117] W Feng et al, “Exosomes promote pre-metastatic niche formation in ovarian cancer,” *Molecular Cancer ,* vol. 18, p. 124, 2019.

[118] YL Huang et al, “Collagen-rich omentum is a premetastatic niche for integrin α2-mediated peritoneal metastasis,” *eLife,* vol. 9, p. e59442, 2020.

[119] X. Ma, “The omentum, a niche for premetastatic ovarian cancer,” *Journal of Experimental Medicine ,* vol. 217, no. 4, p. e20192312, 2020.

[120] L Dai et al, “Adipocytes: active facilitators in epithelial ovarian cancer progression?,” *Journal of Ovarian Research ,* vol. 13, p. 115, 2020.

[121] S Meza-Perez et al, “Immunological Functions of the Omentum,” *Trends in Immunology ,* vol. 38, no. 7, pp. 526-536, 2017.

[122] KM Nieman et al, “Adipocytes promote ovarian cancer metastasis and provide energy for rapid tumor growth,” *Nature Medicine ,* vol. 17, pp. 1498-1503, 2011.

[123] A Mukherjee et al, “The adipocyte microenvironment and cancer,” *Cancer and Metastasis Reviews,* vol. 41, pp. 575-587, 2022.

[124] BA Dirat et al, “Unraveling the obesity and breast cancer links: a role for cancer-associated adipocytes?,” *Endocrine Development ,* vol. 19, pp. 45-52, 2010.

[125] HC Gusky et al, “Omentum and bone marrow: how adipocyte-rich organs create tumour microenvironments conducive for metastatic progression,” *Obesity Reviews,* vol. 17, no. 11, pp. 1015-1029, 2016.

[126] DH Suh et al, “Metabolic orchestration between cancer cells and tumor microenvironment as a co-evolutionary source of chemoresistance in ovarian cancer: a therapeutic implication,” *Biochemical Pharmacology ,* vol. 92, no. 1, pp. 43-54, 2014.

[127] H Chehade et al, “Regulatory Role of the Adipose Microenvironment on Ovarian Cancer Progression,” *Cancers,* vol. 14, no. 9, p. 2267, 2022.

[128] S Dogra et al, “Adipokine Apelin/APJ Pathway Promotes Peritoneal Dissemination of Ovarian Cancer Cells by Regulating Lipid Metabolism,” *Molecular Cancer Research ,* vol. 19, no. 9, pp. 1534-1545, 2021.

[129] F Miranda et al, “Salt-Inducible Kinase 2 Couples Ovarian Cancer Cell Metabolism with Survival at the Adipocyte-Rich Metastatic Niche,” *Cancer Cell,* vol. 30, no. 2, pp. 273-289, 2016.

[130] J Liu et al, “Milky spots: omental functional units and hotbeds for peritoneal cancer metastasis,” *Tumour Biology,* vol. 37, no. 5, pp. 5715-5726, 2016.

[131] A Bella et al, “Chapter Six - Omentum: Friend or foe in ovarian cancer immunotherapy?,” *International Review of Cell and Molecular Biology,* vol. 371, pp. 117-131, 2022.

[132] V Krishnan et al, “In Vivo and Ex Vivo Approaches to Study Ovarian Cancer Metastatic Colonization of Milky Spot Structures in Peritoneal Adipose,” *Journal of Visualized Experiments ,* vol. 105, p. e52721, 2015.

[133] J Fucikova et al, “Immunological configuration of ovarian carcinoma: features and impact on disease outcome,” *Journal for ImmunoTherapy of Cancer ,* vol. 9, p. e002873, 2021.

[134] J Zhou et al, “Exosomes Released from Tumor-Associated Macrophages Transfer miRNAs That Induce a Treg/Th17 Cell Imbalance in Epithelial Ovarian Cancer,” *Cancer Immunology Research,* vol. 6, no. 12, pp. 1578-1592, 2018.

[135] V Krishnan et al, “Omental macrophages secrete chemokine ligands that promote ovarian cancer colonization of the omentum via CCR1,” *Communications Biology,* vol. 3, p. 524, 2020.

[136] X Li et al, “Role of exosomes in the immune microenvironment of ovarian cancer,” *Oncology Letters ,* vol. 21, no. 5, p. 337, 2021.

[137] S Lieber et al, “Prognosis of ovarian cancer is associated with effector memory CD8+ T cell accumulation in ascites, CXCL9 levels and activation-triggered signal transduction in T cells,” *Oncoimmunology,* vol. 7, no. 5, p. e1424672, 2018.

[138] MP Pinto et al, “Patient inflammatory status and CD4+/CD8+ intraepithelial tumor lymphocyte infiltration are predictors of outcomes in high-grade serous ovarian cancer,” *Gynecologic Oncology,* vol. 151, no. 1, pp. 10-17, 2018.

[139] Y Shen et al, “The impact of neoadjuvant chemotherapy on the tumor microenvironment in advanced high-grade serous carcinoma,” *Oncogenesis ,* vol. 11, no. 1, p. 43, 2022.

[140] A Monfort et al, “A strong B-cell response is part of the immune landscape in human high-grade serous ovarian metastases.,” *Clinical Cancer Research,* vol. 23, pp. 250-262, 2017.

[141] JS Nielsen et al, “ CD20+ tumor-infiltrating lymphocytes have an atypical CD27- memory phenotype and together with CD8+ T cells promote favorable prognosis in ovarian cancer,” *Clinical Cancer Research ,* vol. 18, pp. 3289-3292, 2012.

[142] S. Labidi-Galy, “Quantitative and functional alterations of plasmacytoid dendritic cells contribute to immune tolerance in ovarian cancer,” *Cancer Research ,* vol. 71, no. 16, pp. 5423-5434, 2011.

[143] ML Drakes & PJ Stiff, “Regulation of Ovarian Cancer Prognosis by Immune Cells in the Tumor Microenvironment,” *Cancers,* vol. 10, no. 9, p. 302, 2018.

[144] Y Sun et al, “Natural killer cells inhibit metastasis of ovarian carcinoma cells and show therapeutic effects in a murine model of ovarian cancer,” *Experimental and Therapeutic Medicine ,* vol. 16, no. 2, pp. 1071-1078, 2018.

[145] Y Zhang et al, “Human omental adipose-derived mesenchymal stem cell-conditioned medium alters the proteomic profile of epithelial ovarian cancer cell lines in vitro,” *OncoTargets and Therapy,* vol. 10, pp. 1655-1663, 2017.

[146] M Castells et al, “Microenvironment mesenchymal cells protect ovarian cancer cell lines from apoptosis by inhibiting XIAP inactivation,” *Cell Death and Disease ,* vol. 4, p. e887, 2013.

[147] S Raghavan et al, “Carcinoma-Associated Mesenchymal Stem Cells Promote Chemoresistance in Ovarian Cancer Stem Cells via PDGF Signaling,” *Cancers,* vol. 12, no. 8, p. 2063, 2020.

[148] DC Ding et al, “Interleukin-6 from Ovarian Mesenchymal Stem Cells Promotes Proliferation, Sphere and Colony Formation and Tumorigenesis of an Ovarian Cancer Cell Line SKOV3,” *Journal of Cancer,* vol. 7, no. 13, pp. 1815-1823, 2016.

[149] JA Cho et al, “Exosomes from ovarian cancer cells induce adipose tissue-derived mesenchymal stem cells to acquire the physical and functional characteristics of tumor-supporting myofibroblasts,” *Gynecologic Oncology,* vol. 123, no. 2, pp. 379-386, 2011.

[150] J Cai et al, “Fibroblasts in omentum activated by tumor cells promote ovarian cancer growth, adhesion and invasiveness,” *Carcinogenesis ,* vol. 33, no. 1, pp. 20-29, 2012.

[151] Y Yang et al, “Tumor Microenvironment in Ovarian Cancer: Function and Therapeutic Strategy,” *Frontiers in Cell and Developmental Biology,* vol. 8, p. 758, 2020.

[152] S Mukherjee et al, “Homo and Heterotypic Cellular Cross-Talk in Epithelial Ovarian Cancer Impart Pro-Tumorigenic Properties through Differential Activation of the Notch3 Pathway,” *Cancers,* vol. 14, no. 14, p. 3365, 2022.

[153] A Etzerodt et al, “Tissue-resident macrophages in omentum promote metastatic spread of ovarian cancer,” *Joural of Experimental Medicine ,* vol. 217, no. 4, p. e20191869, 2020.

[154] N Di Caprio et al, “Collagen Stiffness and Architecture Regulate Fibrotic Gene Expression in Engineered Adipose Tissue,” *Advanced Biosystems ,* vol. 4, no. 6, p. 1900286 , 2020.

[155] P. Lyengar, “Adipocyte-derived collagen VI affects early mammary tumor progression in vivo, demonstrating a critical interaction in the tumor/stroma microenvironment,” *Journal of Clinical Investigation,* vol. 115, no. 5, pp. 1163-1176, 2005.

[156] Y Kubo et al, “Organization of extracellular matrix components during differentiation of adipocytes in long-term culture,” *In Vitro Cellular and Developmental Biology - Animal ,* vol. 36, no. 1, pp. 38-44, 2000.

[157] HM Micek et al, “Engineering the Extracellular Matrix to Model the Evolving Tumor Microenvironment,” *iScience ,* vol. 23, no. 11, p. 101742, 2022.

[158] VS LeBleu & R Kalluri, “A peek into cancer-associated fibroblasts: origins, functions and translational impact,” *Diease Models and Mechanisms ,* vol. 11, no. 4, p. dmm029447, 2018.

[159] RM Delaine-Smith et al, “Modelling TGFβR and Hh pathway regulation of prognostic matrisome molecules in ovarian cancer,” *iScience,* vol. 24, no. 6, p. 102674, 2021.

[160] W Sun & S Fu, “Role of cancer-associated fibroblasts in tumor structure, composition and the microenvironment in ovarian cancer,” *Oncology Letters ,* vol. 18, no. 3, pp. 2173-2178, 2019.

[161] NE James et al, “The Perfect Combination: Enhancing Patient Response to PD-1-Based Therapies in Epithelial Ovarian Cancer,” *Cancers (Basel),* vol. 12, no. 8, p. 2150, 2020.

[162] M Curtis et al, “Fibroblasts mobilize tumor cell glycogen to promote proliferation and metastasis,” *Cell Metabolism,* vol. 29, no. 1, pp. 141-155, 2019.

[163] S Dasari et al, “Cancer Associated Fibroblasts: Naughty Neighbors That Drive Ovarian Cancer Progression,” *Cancers,* vol. 10, no. 11, p. 406, 2018.

[164] MA Eckert et al, “Proteomics reveals NNMT as a master metabolic regulator of cancer-associated fibroblasts,” *Nature ,* vol. 569, pp. 723-738, 2019.

[165] A Naba et al, “The matrisome: in silico definition and in vivo characterisation by proteomics of normal and tumor extracellular matrices,” *Molecular and Cellular Proteomics ,* vol. 11, no. 4, p. M111.014647, 2012.

[166] R Iozzo, “Matrix proteoglycans: from molecular design to cellular function,” *Annual Review of Biochemistry,* vol. 67, pp. 609-652, 1998.

[167] RO Hynes et al, “Overview of the Matrisome—An Inventory of Extracellular Matrix Constituents and Functions,” *Cold Spring Harbour Perspectives in Biology ,* vol. 4, no. 1, p. a004903, 2011.

[168] MK Jansen et al, “Intracellular localization of the extracellular matrix enzyme lysyl oxidase in polarized epithelial cells,” *Matrix Biology,* vol. 26, no. 2, pp. 136-139, 2006.

[169] Y Itoh et al, “Matrix metalloproteinases in cancer,” *Essays in Biochemistry ,* vol. 38, pp. 21-36, 2002.

[170] JK Mouw et al, “Extracellular matrix assembly: a multiscale deconstruction,” *Nature Reviews Molecular and Cell Biology,* vol. 15, pp. 771-785, 2014.

[171] C Frantz et al, “The extracellular matrix at a glance,” *Journal of Cell Science ,* vol. 123, no. 24, pp. 4195-4200, 2010.

[172] J Taipale et al, “Growth factors in the extracellular matrix,” *The FASEB Journal,* vol. 11, no. 1, pp. 51-59, 1997.

[173] DE Discher et al, “Tissue cells feel and respond to the stiffness of their substrate,” *Science,* pp. 1139-1143, 2005.

[174] YL Wang et al, “Cell locomotion and focal adhesions are regulated by substrate flexibility,” *Proceedings of the national academy of sciences of the United States of America ,* vol. 94, pp. 11661-11665, 1997.

[175] M Morgan et al, “Synergistic control of cell adhesion by integrins and syndecans,” *Nature Reviews Molecular and Cell Biology ,* vol. 8, no. 12, pp. 957-969, 2007.

[176] R Sekiguchi & K Yamada, “Basement membranes in development and disease,” *Current Topics in Developmental Biology,* vol. 130, pp. 143-191, 2018.

[177] J Winkler et al, “Concepts of extracellular matrix remodelling in tumour progression and metastasis,” *Nature Communications,* vol. 11, p. 5120, 2020.

[178] LD Muiznieks et al, “Molecular assembly and mechanical properties of the extracellular matrix: A fibrous protein perspective,” *Biochimica et Biophysica Acta - Molecular Basis of Disease ,* vol. 1832, no. 7, pp. 866-875, 2013.

[179] R Kalluri et al, “Basement membranes: structure, assembly and role in tumour angiogenesis,” *Nature Reviews Cancer ,* vol. 3, pp. 422-433, 2003.

[180] P Yurchenco, “Basement Membranes: Cell Scaffoldings and Signaling Platforms,” *Cold Spring Harbour Perspectives in Biology,* vol. 3, no. 2, p. a004911, 2011.

[181] A Naba et al, “Characterization of the Extracellular Matrix of Normal and Diseased Tissues Using Proteomics,” *Journal of Proteomics Research ,* vol. 16, no. 8, pp. 3083-3091, 2017.

[182] DJ Cheon et al, “A collagen-remodeling gene signature regulated by TGF-β signaling is associated with metastasis and poor survival in serous ovarian cancer,” *Clinical Cancer Research ,* vol. 20, no. 3, pp. 711-723, 2014.

[183] S Ricard-Blum, “The Collagen Family,” *Cold Spring Harbour Perspectives in Biology,* vol. 3, no. 1, p. a004978, 2011.

[184] C Onursal et al, “Collagen Biosynthesis, Processing, and Maturation in Lung Ageing,” *Frontiers in Medicine ,* vol. 8, p. 593874, 2021.

[185] A Bonnomet et al, “Chapter thirteen - Analysis of Cell Dispersion and Migration by Video-Microscopy,” *Methods in Enzymology,* vol. 505, pp. 233-254, 2012.

[186] Y Ishikawa et al, “A molecular ensemble in the rER for procollagen maturation,” *Biochemica et Biophysica Acta - Molecular Cell Research,* vol. 1833, no. 11, pp. 2479-2491, 2013.

[187] Y Chen et al, “Oncogenic collagen I homotrimers from cancer cells bind to a3b1 integrin and impact tumor microbiome and immunity to promote pancreatic cancer,” *Cancer Cell,* vol. 40, p. 818–834, 2022.

[188] S. Pinnell, “Regulation of collagen biosynthesis by ascorbic acid: a review.,” *Yale Journal of Biology and Medicine ,* vol. 58, no. 6, p. 553–559, 1985.

[189] J Mandl et al, “Vitamin C: update on physiology and pharmacology,” *British Journal of Pharmacology,* vol. 157, no. 7, p. 2009, 2009.

[190] K Saito et al, “TANGO1 facilitates cargo loading at endoplasmic reticulum exit sites,” *Cell,* vol. 136, no. 5, pp. 891-902, 2009.

[191] L Bonfanti et al, “Procollagen Traverses the Golgi Stack without Leaving the Lumen of Cisternae,” *Cell,* vol. 95, no. 7, pp. 993-1003, 1998.

[192] J. McCaughey, “ER-to-Golgi trafficking of procollagen in the absence of large carriers,” *Journal of Cell Biology,* vol. 218, no. 3, pp. 929-948, 2019.

[193] J Hellicar et al, “Supply chain logistics – the role of the Golgi complex in extracellular matrix production and maintenance,” *Journal of Cell Science ,* vol. 135, no. 1, p. jcs258879, 2022.

[194] EG Canty et al, “Coalignment of plasma membrane channels and protrusions (fibripositors) specifies the parallelism of tendon,” *Journal of Cell Biology ,* vol. 165, no. 4, pp. 553-563, 2004.

[195] X Guo et al, “Morphological Characterization of Organized Extracellular Matrix Deposition by Ascorbic Acid-Stimulated Human Corneal Fibroblasts,” *Investigative Ophthalmology & Visual Science,* vol. 48, no. 9, pp. 4050-4060, 2007.

[196] D Greenspan, “Biosynthetic Processing of Collagen Molecules,” *Collagen ,* vol. 247, pp. 149-183, 2005.

[197] EG Canty et al, “Procollagen trafficking, processing and fibrillogenesis,” *Journal of Cell Science ,* vol. 118, no. 7, pp. 1341-1353, 2005.

[198] DE Birk et al, “Extracellular compartments in tendon morphogenesis: collagen fibril, bundle, and macroaggregate formation,” *Journal of Cell Biology,* vol. 103, no. 1, pp. 1-40, 1986.

[199] CC Banos et al, “Collagen fibrillogenesis in tendon development: Current models and regulation of fibril assembly,” *Birth Defects Research Part C: Embryo Today: Reviews,* vol. 84, no. 3, pp. 228-244, 2008.

[200] K. Kadler, “Collagen fibril formation in vitro and in vivo,” *International Journal of Experimental Pathology,* vol. 98, no. 1, pp. 4-16, 2017.

[201] T Velling et al, “Polymerization of type I and III collagens is dependent on fibronectin and enhanced by integrins alpha 11beta 1 and alpha 2beta 1,” *Journal of Biological Chemistry,* vol. 277, no. 40, pp. 37377-37381, 2002.

[202] M Musiime et al, “Collagen Assembly at the Cell Surface: Dogmas Revisited,” *Cells ,* vol. 10, no. 3, p. 662, 2021.

[203] JZ Kechagia et al, “Integrins as biomechanical sensors of the microenvironment,” *Nature Reviews Molecular Biology ,* vol. 20, pp. 457-473, 2019.

[204] DE Birk & P Brückner, “Collagens, Suprastructures, and Collagen Fibril Assembly,” *The Extracellular Matrix: An overview ,* pp. 77-115, 2010.

[205] RJ Wenstrup et al, “Type V Collagen Controls the Initiation of Collagen Fibril Assembly,” *Journal of Biological Chemistry,* vol. 279, no. 51, pp. 53331-53337, 2004.

[206] R Seegmiller et al, “A new chondrodystrophic mutant in mice. Electron microscopy of normal and abnormal chondrogenesis,” *Journal of Cell Biology ,* Vols. 580-593, no. 48, p. 3, 1971.

[207] Y Li et al, “A fibrillar collagen gene, Col11a1, is essential for skeletal morphogenesis,” *Cell ,* vol. 80, no. 3, pp. 423-430, 1995.

[208] RJ Wenstrup et al, “Reduced type I collagen utilization: A pathogenic mechanism in COL5A1 haplo-insufficient Ehlers–Danlos syndrome,” *Journal of Cellular Biochemistry ,* vol. 92, no. 1, pp. 113-124, 2004.

[209] M Sun et al, “Collagen XI regulates the acquisition of collagen fibril structure, organization and functional properties in tendon,” *Matrix Biology,* vol. 94, pp. 77-94, 2020.

[210] KM Meek & C Knupp, “Corneal structure and transparency,” *Progress in Retinal and Eye Research ,* vol. 49, pp. 1-16, 2015.

[211] H Bachman et al, “Utilizing Fibronectin Integrin-Binding Specificity to Control Cellular Responses,” *Advances in Wound Care ,* vol. 4, no. 8, pp. 501-511, 2015.

[212] TG Kapp et al, “A Comprehensive Evaluation of the Activity and Selectivity Profile of Ligands for RGD-binding Integrins,” *Scientific Reports,* vol. 7, p. 39805, 2017.

[213] SE D'Souza et al, “Arginyl-glycyl-aspartic acid (RGD): a cell adhesion motif,” *Trends in Biochemical Sciences,* vol. 16, no. 7, pp. 246-250, 1991.

[214] BS Ludwig et al, “RGD-Binding Integrins Revisited: How Recently Discovered Functions and Novel Synthetic Ligands (Re-)Shape an Ever-Evolving Field,” *Cancers,* vol. 13, no. 7, p. 1711, 2021.

[215] S Spada et al, “Fibronectin as a multiregulatory molecule crucial in tumor matrisome: from structural and functional features to clinical practice in oncology,” *Journal of Experimental and Clinical Cancer Research ,* vol. 40, p. 102, 2021.

[216] J Sottile et al, “Fibronectin Polymerization Regulates the Composition and Stability of Extracellular Matrix Fibrils and Cell-Matrix Adhesions,” *Molecular Biology of the Cell ,* vol. 13, no. 10, pp. 3546-3559, 2002.

[217] GA Hoffmann et al, “New Insights into Collagen and Fibronectin Reciprocity during Extracellular Matrix Formation,” *Chem,* vol. 5, no. 8, pp. 1930-1932, 2019.

[218] C Zhong et al, “Rho-mediated Contractility Exposes a Cryptic Site in Fibronectin and Induces Fibronectin Matrix Assembly,” *Journal of Cell Biology,* vol. 141, no. 2, pp. 539-551, 1998.

[219] P Singh et al, “Assembly of Fibronectin Extracellular Matrix,” *The Annual Review of Cell and Developmental Biology,* vol. 26, pp. 397-419, 2010.

[220] J McDonald, “Extracellular matrix assembly.,” *Annual Review of Cell Biology ,* vol. 4, p. 183–207, 1988.

[221] SL Dallas et al, “Fibronectin regulates latent transforming growth factor-β (TGFβ) by controlling matrix assembly of latent TGFβ-binding protein-1,” *Journal of Biological Chemistry ,* vol. 280, pp. 18871-18880, 2005.

[222] JA McDonald et al, “Role of fibronectin in collagen deposition: Fab' to the gelatin-binding domain of fibronectin inhibits both fibronectin and collagen organization in fibroblast extracellular matrix,” *Journal of Cell Biology,* vol. 92, no. 2, pp. 485-492, 1982.

[223] KE Kubow et al, “Mechanical forces regulate the interactions of fibronectin and collagen I in extracellular matrix,” *nature Communications ,* vol. 6, p. 8015, 2015.

[224] J Graham et al, ““Fibrillar fibronectin plays a key role as nucleator of collagen I polymerization during macromolecular crowding-enhanced matrix assembly,” *Biomaterials Science,* vol. 7, pp. 4519-4535, 2019.

[225] J Dzamba et al, “Fibronectin binding site in type I collagen regulates fibronectin fibril formation.,” *Journal of Cell Biology,* vol. 121, no. 5, pp. 1165-1172, 1993.

[226] KE Kadler et al, “Collagen fibrillogenesis: fibronectin, integrins, and minor collagens as organizers and nucleators,” *Current Opinion in Cell Biology ,* vol. 20, no. 5-24, pp. 495-501, 2008.

[227] M Colombi et al, “Matrix assembly induction and cell migration and invasion inhibition by a 13-amino acid fibronectin peptide,” *Journal of Biological Chemistry ,* vol. 278, no. 16, pp. 14346-14355, 2003.

[228] YJ WU et al, “The interaction of versican with its binding partners,” *Cell Research ,* vol. 15, pp. 483-494, 2005.

[229] SL Dallas et al, “Dynamics of Assembly and Reorganization of Extracellular Matrix Proteins,” *Current Topics in Developmental Biology,* vol. 75, pp. 1-24, 2006.

[230] G Efthymiou et al, “Shaping Up the Tumor Microenvironment With Cellular Fibronectin,” *Frontiers in Oncology ,* vol. 10, p. 641, 2020.

[231] SR Elkin et al, “Endocytic Pathways and Endosomal Trafficking: A Primer,” *Wiener Medizinische Wochenschrift,* vol. 166, no. 7-8, pp. 196-204, 2016.

[232] S Bandres-Ciga et al, “The endocytic membrane trafficking pathway plays a major role in the risk of Parkinson disease,” *Movement Disorders ,* vol. 34, no. 4, pp. 460-468, 2019.

[233] GJ Doherty & H McMahon, “Mechanisms of Endocytosis,” *Annual Review of Biochemistry ,* vol. 78, pp. 857-902, 2009.

[234] S Royle, “The cellular functions of clathrin,” *Cellular and Molecular Life Sciences,* vol. 63, no. 16, pp. 1823-1832, 2006.

[235] M Kaksonen & A Roux, “Mechanisms of clathrin-mediated endocytosis,” *Nature Reviews Molecular Cell Biology ,* vol. 19, pp. 313-326, 2018.

[236] MJ Taylor et al, “ high precision survey of the molecular dynamics of mammalian clathrin-mediated endocytosis,” *PLoS Biology,* vol. 9, p. e1000604, 2011.

[237] Y. Sun et al, “Endocytic internalization in budding yeast requires coordinated actin nucleation and myosin motor activity,” *Developmental Cell ,* vol. 11, p. 33–46, 2006.

[238] BL Goode et al, “Actin and endocytosis in budding yeast.,” *Genetics ,* vol. 199, p. 315–358, 2015.

[239] M Meinecke et al, “Cooperative recruitment of dynamin and BIN/amphiphysin/Rvs (BAR) domain-containing proteins leads to GTP-dependent membrane scission.,” *Journal of Biological Chemistry ,* vol. 288, pp. 6651-6661, 2013.

[240] S Neumann & S Schmid, “Dual role of BAR domain-containing proteins in regulating vesicle release catalyzed by the GTPase, dynamin-2.,” *Journal of Biological Chemistry ,* vol. 288, no. 288, pp. 25119-25128, 2013.

[241] C Matthaeus & JW Taraska, “Energy and Dynamics of Caveolae Trafficking,” *Frontiers in Cell and Developmental Biology ,* vol. 8, p. 614472, 2021.

[242] AL Kiss & E Botos, “Endocytosis via caveolae: alternative pathway with distinct cellular compartments to avoid lysosomal degradation?,” *Journal of Cellular and Molecular Medicine ,* vol. 13, no. 7, pp. 1228-1237, 2009.

[243] RG Parton et al, “Caveolae: Formation, dynamics, and function,” *Current Opinion in Cell Biology ,* vol. 65, pp. 8-16, 2020.

[244] P Oh et al, “Endothelin induces rapid, dynamin-mediated budding of endothelial caveolae rich in ET-B,” *Journal of Biological Chemistry ,* vol. 287, no. 21, pp. 17353-17362, 2012.

[245] DN Predescu et al, “Impaired caveolae function and upregulation of alternative endocytic pathways induced by experimental modulation of intersectin-1s expression in mouse lung endothelium,” *Biochemistry Research International ,* vol. 2012, p. 672705, 2012.

[246] M Sathe et al, “Small GTPases and BAR domain proteins regulate branched actin polymerisation for clathrin and dynamin-independent endocytosis,” *Nature Communications,* vol. 9, pp. 1-16, 2018.

[247] C Gundu et al, “Dynamin-Independent Mechanisms of Endocytosis and Receptor Trafficking,” *Cells,* vol. 11, p. 2557, 2022.

[248] M Kirkham et al, “Ultrastructural identification of uncoated caveolin-independent early endocytic vehicles,” *Journal of Cell Biology ,* vol. 168, no. 3, pp. 465-476, 2005.

[249] M Shafaq-Zadah et al, “Clathrin-independent endocytosis, retrograde trafficking, and cell polarity,” *Current Opinion in Cell Biology ,* vol. 65, pp. 112-121, 2020.

[250] M Sathe et al, “Small GTPases and BAR domain proteins regulate branched actin polymerisation for clathrin and dynamin-independent endocytosis,” *Nature Communications ,* vol. 9, p. 1835, 2018.

[251] XP Lin et al, “Macropinocytosis in Different Cell Types: Similarities and Differences,” *Membranes (Basel),* vol. 10, no. 8, p. 177, 2020.

[252] CM Buckley & JS King, “Drinking problems: mechanisms of macropinosome formation and maturation,” *The FEBS Journal,* vol. 282, no. 11, pp. 3778-3790, 2017.

[253] V Merchati et al, “Selective membrane exclusion in phagocytic and macropinocytic cups,” *Journal of Cell Science ,* vol. 119, no. 19, p. 4079–4087, 2006.

[254] Sudha Kumari et al, “Endocytosis unplugged: multiple ways to enter the cell,” *Cell Research ,* vol. 20, pp. 256-275, 2010.

[255] N Naslavsky & S Caplan, “The enigmatic endosome – sorting the ins and outs of endocytic trafficking,” *Journal of Cell Science,* vol. 131, no. 13, p. 216499, 2018.

[256] C MacDonald et al, “Cargo ubiquitination is essential for multivesicular body intralumenal vesicle formation,” *EMBO Reports ,* vol. 13, no. 4, pp. 331-338, 2012.

[257] JP Luzio et al, “Lysosomes: fusion and function,” *Nature Reviews Molecular Cell Biology,* vol. 8, pp. 622-632, 2007.

[258] RC Piper & DJ Katzmann, “Biogenesis and Function of Multivesicular Bodies,” *Annual Review of Cell and Developmental Biology ,* vol. 23, pp. 519-547, 2007.

[259] M Mathieu et al, “Specificities of secretion and uptake of exosomes and other extracellular vesicles for cell-to-cell communication,” *Nature Cell Biology,* vol. 21, pp. 9-17, 2019.

[260] PJ Cullen & F Steinberg, “To degrade or not to degrade: mechanisms and significance of endocytic recycling,” *Nature Reviews Molecular Cell Biology,* vol. 19, pp. 679-696, 2018.

[261] JRT van Weering & PJ Cullen, “Membrane-associated cargo recycling by tubule-based endosomal sorting,” *Seminars in Cell and Developmental Biology,* vol. 31, pp. 40-47, 2014.

[262] E Helfer et al, “Endosomal recruitment of the WASH complex: active sequences and mutations impairing interaction with the retromer,” *Biology of the Cell,* vol. 105, no. 5, pp. 191-207, 2013.

[263] JRT Weering et al, “SNX-BAR-mediated endosome tubulation is co-ordinated with endosome maturation,” *Traffic ,* vol. 13, no. 1, pp. 94-107, 2012.

[264] M Seaman, “The retromer complex – endosomal protein recycling and beyond,” *Journal of Cell Science ,* vol. 125, no. 20, p. 4693–4702, 2012.

[265] KE Mcnally et al, “Retriever is a multiprotein complex for retromer-independent endosomal cargo recycling,” *Nature Cell Biology,* vol. 19, no. 10, pp. 1214-1225, 2017.

[266] BD Grant & JG Donaldson, “Pathways and Mechanisms of Endocytic Recycling,” *Nature Reviews Molecular Cell Biology,* vol. 10, pp. 597-608, 2009.

[267] S Xie et al, “The endocytic recycling compartment maintains cargo segregation acquired upon exit from the sorting endosome,” *Molecular Biology of the Cell ,* vol. 27, no. 1, pp. 108-126, 2016.

[268] R Sakai et al, “The integral function of the endocytic recycling compartment is regulated by RFFL-mediated ubiquitylation of Rab11 effectors,” *Journal of Cell Science ,* vol. 132, no. 3, p. 228007, 2019.

[269] K Wennerberg et al, “The Ras superfamily at a glance,” *Journal of Cell Science ,* vol. 118, no. 5, pp. 843-846, 2005.

[270] I Kjos et al, “Rab and Arf proteins at the crossroad between membrane transport and cytoskeleton dynamics,” *Biochemica et Biophysica Acta, ,* vol. 1865, no. 10, pp. 1397-1409, 2018.

[271] C Casalou, “The Role of ARF Family Proteins and Their Regulators and Effectors in Cancer Progression: A Therapeutic Perspective,” *Frontiers in Cell and Developmental Biology,* vol. 8, p. 217, 2020.

[272] S Song et al, “Small GTPases: Structure, biological function and its interaction with nanoparticles,” *Asian Journal of Pharmaceutical Sciences ,* vol. 14, no. 1, pp. 30-39, 2019.

[273] JL Bos et al, “GEFs and GAPs: Critical Elements in the Control of Small G Proteins,” *Cell,* vol. 129, no. 5, pp. 865-877, 2007.

[274] J Cherfils & M Zeghouf, “Regulation of Small GTPases by GEFs, GAPs, and GDIs,” *Physiological Reviews,* vol. 93, no. 1, pp. 269-309, 2013.

[275] O Pylypenko et al, “Rab GTPases and their interacting protein partners: Structural insights into Rab functional diversity,” *Small GTPases,* vol. 9, no. 1-2, pp. 22-48, 2018.

[276] E Sztul et al, “ARF GTPases and their GEFs and GAPs: concepts and challenges,” *Molecular Biology of the Cell ,* vol. 30, no. 11, pp. 1245-1351, 2019.

[277] PV Sluijs, “The small GTP-binding protein rab4 controls an early sorting event on the endocytic pathway,” *Cell,* vol. 70, no. 5, pp. 729-740, 1992.

[278] EJ Hartman et al, “The Rab11-family interacting proteins reveal selective interaction of mammalian recycling endosomes with the Toxoplasma parasitophorous vacuole in a Rab11- and Arf6-dependent manner,” *Molecular Biology of the Cell,* vol. 33, no. 5, p. ar34, 2022.

[279] J Gemperle et al, “On demand expression control of endogenous genes with DExCon, DExogron and LUXon reveals differential dynamics of Rab11 family members,” *eLife,* vol. 11, p. e76651, 2022.

[280] PT Caswell et al, “Rab25 Associates with a5b1 Integrin to Promote Invasive Migration in 3D Microenvironments,” *Developmental Cell,* vol. 13, pp. 496-510, 2007.

[281] PV Sluijs, “The small GTP-binding protein rab4 controls an early sorting event on the endocytic pathway,” *Cell,* vol. 70, no. 5, pp. 729-740, 1992.

[282] K Klinkert & A Echard, “Rab35 GTPase: A Central Regulator of Phosphoinositides and F-actin in Endocytic Recycling and Beyond,” *Traffic,* vol. 17, no. 10, pp. 1063-1077, 2016.

[283] DR Sheff et al, “The receptor recycling pathway contains two distinct populations of early endosomes with different sorting functions,” *Journal of Cell Biology,* vol. 145, no. 1, pp. 123-139, 1999.

[284] K Hattula et al, “Characterization of the Rab8-specific membrane traffic route linked to protrusion formation,” *Journal of Cell Science ,* vol. 119, no. 23, pp. 4866-4877, 2006.

[285] A Knodler et al, “Coordination of Rab8 and Rab11 in primary ciliogenesis,” *The Proceedings of the National Academy of Sciences (PNAS),* vol. 107, no. 14, pp. 6346-6351, 2010.

[286] H Li at al, “Rab4 and Rab11 coordinately regulate the recycling of angiotensin II type I receptor as demonstrated by fluorescence resonance energy transfer microscopy,” *Journal of Biomedical Optics,* vol. 13, no. 3, p. 031206, 2013.

[287] W Chen et al, “Rab11 Is Required for Trans-Golgi Network–to–Plasma Membrane Transport and a Preferential Target for GDP Dissociation Inhibitor,” *Molecular Biology of the Cell,* vol. 9, no. 11, p. 3241–3257, 1998.

[288] CC Campa and E Hirsch, “Rab11 and phosphoinositides: A synergy of signal transducers in the control of vesicular trafficking,” *Advances in Biological Regulation,* vol. 63, pp. 132-139, 2017.

[289] BL Grosshans et al, “Rabs and their effectors: achieving specificity in membrane traffic,” *Proceedings of the National Academy of Sciences of the United States of America ,* vol. 103, no. 32, pp. 11821-11827, 2006.

[290] S Christoforidis & M Zerial, “Purification and identification of novel Rab effectors using affinity chromatography,” *Methods ,* vol. 20, no. 4, pp. 403-10, 2000.

[291] B Wilson et al, “Proximity labelling identifies pro-migratory endocytic recycling cargo and machinery of the Rab4 and Rab11 families,” *bioRxiv ,* p. 10.1101/2022.05.12.491689, 2022.

[292] A Rai et al, “Multivalency in Rab effector interactions,” *Small GTPases ,* vol. 10, no. 1, pp. 40-46, 2019.

[293] R Sinka et al, “Golgi coiled-coil proteins contain multiple binding sites for Rab family G-proteins,” *Journal of Cell Biology,* vol. 183, no. 4, pp. 607-615, 2008.

[294] L Perrin et al, “Rab4b controls an early endosome sorting event by interacting with the γ-subunit of the clathrin adaptor complex 1,” *Journal of Cell Science ,* vol. 126, no. 21, pp. 4950-4962, 2013.

[295] D Aivazian et al, “TIP47 is a key effector for Rab9 localization,” *Journal of Cell Biology ,* vol. 173, no. 6, pp. 917-926, 2006.

[296] H Stenmark, “Rab GTPases as coordinators of vesicle traffic,” *Nature Reviews Molecular Cell Biology ,* vol. 10, pp. 513-525, 2009.

[297] CP Horgan & MW McCaffrey, “Rab GTPases and microtubule motors,” *Biochemical Society Transactions,* vol. 39, no. 5, pp. 1202-1206, 2011

[298] E Schonteich et al, “The Rip11/Rab11-FIP5 and kinesin II complex regulates endocytic protein recycling,” *Journal of Cell Science ,* vol. 121, no. 22, pp. 3824-3833, 2008.

[299] V Marchesin et al, “ARF6–JIP3/4 regulate endosomal tubules for MT1-MMP exocytosis in cancer invasion,” *Journal of Cell Biology,* vol. 211, no. 2, pp. 339-358, 2015.

[300] PZC Chia & PA Gleeson, “Membrane tethering,” *F1000 Prime Reports ,* vol. 6, p. 74, 2014.

[301] SM Ahmed et al, “Exocyst dynamics during vesicle tethering and fusion,” *Nature Communications ,* vol. 9, p. 5140, 2018.

[302] N Polgar & B Fogelgren, “Regulation of Cell Polarity by Exocyst-Mediated Trafficking,” *Cold Spring Harbours Perspectives in Biology ,* vol. 10, p. a031401, 2018.

[303] M Prigent et al, “ARF6 controls post-endocytic recycling through its downstream exocyst complex effector,” *Journal of Cell Biology ,* vol. 163, pp. 1111-1121, 2003.

[304] JA Solinger et al, “FERARI is required for Rab11-dependent endocytic recycling,” *Nature Cell Biology ,* vol. 22, no. 2, pp. 213-224, 2020.

[305] JVD Beek et al, “CORVET, CHEVI and HOPS - multisubunit tethers of the endo-lysosomal system in health and disease,” *Journal of Cell Science ,* vol. 132, no. 10, p. jcs189134, 2019.

[306] S Ueda et al, “Membrane Tethering Potency of Rab-Family Small GTPases Is Defined by the C-Terminal Hypervariable Regions,” *Frontiers in Cell and Developmental Biology ,* vol. 8, p. 577342, 2020.

[307] M Inoshita & J Mima, “Human Rab small GTPase- and class V myosin-mediated membrane tethering in a chemically defined reconstitution system,” *The Journal of Biological Chemistry ,* vol. 292, no. 45, pp. 18500-18517, 2017.

[308] HH Ji et al, “Regulation of Myosin-5b by Rab11a and the Rab11 family interacting protein 2,” *Bioscience Reports,* vol. 39, no. 1, p. BSR20181252, 2019.

[309] J Han et al, “The Multifaceted Role of SNARE Proteins in Membrane Fusion,” *Frontiers in Physiology ,* vol. 8, p. 5, 2017.

[310] A Margiotta, “Membrane Fusion and SNAREs: Interaction with Ras Proteins,” *International Journal of Molecular Sciences ,* vol. 23, p. 8067, 2022.

[311] R Hynes, “The extracellular matrix: not just pretty fibrils,” *Science,* vol. 326, no. 5957, pp. 1216-1219, 2009.

[312] JD Humphries et al, “Emerging properties of adhesion complexes: what are they and what do they do?,” *Trends in Cell Biology ,* vol. 25, no. 7, pp. 388-397, 2015.

[313] JG Donaldson et al, “Rab and Arf G proteins in endosomal trafficking and cell surface homeostasis,” *Small GTPases,* vol. 7, no. 4, pp. 247-251, 2016.

[314] PD Allaire et al, “Interplay between Rab35 and Arf6 controls cargo recycling to coordinate cell adhesion and migration,” *Journal of Cell Science ,* vol. 126, no. 3, pp. 722-731, 2013.

[315] CCH Chen et al, “RAB-10 is required for endocytic recycling in the Caenorhabditis elegans intestine,” *Molecular Biology of the Cell,* vol. 17, no. 3, pp. 1286-1297, 2006.

[316] CM Babbey et al, “Rab10 regulates membrane transport through early endosomes of polarized Madin-Darby canine kidney cells,” *Molecular Biology of the Cell ,* vol. 17, no. 7, pp. 3156-3175, 2006.

[317] CEL CHua & BL Tang, “Rab 10-a traffic controller in multiple cellular pathways and locations,” *Journal of Cellular Physiology ,* vol. 233, no. 9, pp. 6483-6494, 2018.

[318] AJ Isabella & S Horne-Badovinac, “Rab10-Mediated Secretion Synergizes with Tissue Movement to Build a Polarized Basement Membrane Architecture for Organ Morphogenesis,” *Developmental Cell,* vol. 38, no. 1, pp. 47-60, 2016.

[319] DW Lerner et al, “A Rab10-dependent mechanism for polarized basement membrane secretion during organ morphogenesis,” *Developmental Cell ,* vol. 24, no. 2, pp. 159-168, 2013.

[320] MC Jones et al, “VEGFR1 (Flt1) regulates Rab4 recycling to control fibronectin polymerization and endothelial vessel branching,” *Traffic,* vol. 10, no. 6, pp. 754-766, 2009.

[321] G Mana et al, “PPFIA1 drives active α5β1 integrin recycling and controls fibronectin fibrillogenesis and vascular morphogenesis,” *Nature Communications,* vol. 7, p. 13546, 2016.

[322] V Glifford & Y Itoh, “MT1-MMP-dependent cell migration: proteolytic and non-proteolytic mechanisms,” *Biochemical Scoiety Transactions ,* vol. 47, no. 3, pp. 811-826, 2019.

[323] S linder and G Scita, “RABGTPases in MT1-MMP trafficking and cell invasion: Physiology versus pathology,” *Small GTPases,* vol. 6, no. 3, pp. 145-152, 2015.

[324] SH Taylor et al, “Matrix metalloproteinase 14 is required for fibrous tissue expansion,” *eLife,* vol. 4, p. e09345, 2015.

[325] J Chang et al, “The endosome is a master regulator of plasma membrane collagen fibril assembly,” *bioRxiv,* p. 10.1101/2021.03.25.436925, 2021.

[326] M Wang et al, “Cancer-Associated Fibroblasts in a Human HEp-2 Established Laryngeal Xenografted Tumor Are Not Derived from Cancer Cells through Epithelial-Mesenchymal Transition, Phenotypically Activated but Karyotypically Normal,” *PLOS ONE,* vol. 10, no. 5, p. e0128057, 2015.

[327] C Steger, “An Unbiased Detector of Curvilinear Structures,” *IEEE Transactions on Pattern Analysis and Machine Intelligence,* vol. 20, no. 2, pp. 113 - 125, 1998.

[328] NE Sanjana et al, “Improved vectors and genome-wide libraries for CRISPR screening,” *Nature Methods ,* vol. 11, no. 8, pp. 783-784, 2014.

[329] R Mhaidly & F Mechta-Grigoriou, “Fibroblast heterogeneity in tumor micro-environment: Role in immunosuppression and new therapies,” *Seminars in Immunology ,* vol. 48, p. 101417, 2020.

[330] T Liu et al, “Cancer-Associated Fibroblasts Build and Secure the Tumor Microenvironment,” *Frontiers in Cell and Developmental Biology ,* vol. 7, no. 60, 2019.

[331] M Zhang et al, “The Role of Cancer-Associated Fibroblasts in Ovarian Cancer,” *Cancers (Basel),* vol. 14, no. 11, p. 2637, 2022.

[332] PH Chang et al, “Activation of Robo1 Signaling of Breast Cancer Cells by Slit2 from Stromal Fibroblast Restrains Tumorigenesis via Blocking PI3K/Akt/β-Catenin Pathway,” *Cancer Research ,* vol. 72, no. 18, pp. 4652-4661 , 2012.

[333] A Hussain et al, “Distinct cancer-associated fibroblast states drive clinical outcomes in high- grade serous ovarian cancer and are regulated by TCF21,” *Bioarchive preprint,* p. doi: https://doi.org/10.1101/519728, 2019.

[334] JR de los Toyos Gonzalez et al, “COL11A1/(pro)collagen 11A1 expression is a remarkable biomarker of human invasive carcinoma-associated stromal cells and carcinoma progression,” *. Tumour biology : the journal of the International Society for Oncodevelopmental Biology and Medicine,* vol. 36, pp. 2213-2222, 2015.

[335] P Farmer et al, “A stroma-related gene signature predicts resistance to neoadjuvant chemotherapy in breast cancer.,” *Nature medicine ,* vol. 15, no. 1, pp. 68-74, 2009.

[336] AV Shinde et al, “The role of α-smooth muscle actin in fibroblast-mediated matrix contraction and remodeling,” *Biochemica et Biophysica Acta - Molecular Basis of Disease ,* vol. 1863, no. 1, pp. 298-309, 2016.

[337] B Hinz et al, “Smooth Muscle Actin Is Crucial for Focal Adhesion Maturation in Myofibroblasts,” *Molecular Biology of the Cell ,* vol. 14, pp. 2508-2519, 2003.

[338] R Yamin & KG Morgan, “Deciphering actin cytoskeletal function in the contractile vascular smooth muscle cell,” *The Journal of Physiology ,* vol. 590, no. 17, pp. 4145-4154, 2012.

[339] Shen Y et al, “Fibrillar type I collagen matrices enhance metastasis/invasion of ovarian epithelial cancer via β1 integrin and PTEN signals,” *The International Journal of Gynecological Cancer,* vol. 22, no. 8, pp. 1316-1324, 2012.

[340] Xu S et al, “The role of collagen in cancer: from bench to bedside,” *Journal of Translatoinal Medicine ,* vol. 17, no. 309, 2019.

[341] Y Inai et al, “The whole structure of the human nonfunctional L-gulono-gamma-lactone oxidase gene--the gene responsible for scurvy--and the evolution of repetitive sequences thereon,” *Journal of Nutritional Science and Vitaminology ,* vol. 49, no. 5, pp. 315-319, 2003.

[342] F Grinnell et al, “Collagen processing, crosslinking, and fibril bundle assembly in matrix produced by fibroblasts in long-term cultures supplemented with ascorbic acid,” *Experimental Cell Research ,* vol. 181, no. 2, pp. 483-491, 1989 .

[343] SR Pinnell et al, “Induction of Collagen Synthesis by Ascorbic Acid A Possible Mechanism,” *Archives of Dermatological Research,* vol. 123, no. 12, pp. 1684-1686, 1987.

[344] YH Wu & CY Chou, “Collagen XI Alpha 1 Chain, a Novel Therapeutic Target for Cancer Treatment,” *Frontiers in Oncology ,* vol. 12, p. 925165, 2022.

[345] YJ Wu et al, “The interaction of versican with its binding partners,” *Cell Research,* vol. 15, pp. 483-494, 2005.

[346] DJ Cheon et al, “A collagen-remodeling gene signature regulated by TGF-beta signaling is associated with metastasis and poor survival in serous ovarian cancer,” *Clinical cancer research ,* vol. 20, no. 3, pp. 711-723, 2014.

[347] TL Yeung et al, “TGF-β modulates ovarian cancer invasion by upregulating CAF-derived versican in the tumor microenvironment,” *Cancer Research ,* vol. 73, no. 16, pp. 5016-5028, 2013.

[348] T Wight, “Provisional Matrix: A Role for Versican and Hyaluronan,” *Matrix Biology ,* Vols. 60-61, pp. 38-56, 2017.

[349] J Winkler et al, “Concepts of extracellular matrix remodelling in tumour progression and metastasis,” *nature Communications,* vol. 11, p. 5120, 2020.

[350] F Calvo et al, “Mechanotransduction and YAP-dependent matrix remodelling is required for the generation and maintenance of cancer-associated fibroblasts,” *Nature Cell Biology ,* vol. 15, pp. 637-646, 2013.

[351] V Sanz-Moreno et al, “ROCK and JAK1 Signaling Cooperate to Control Actomyosin Contractility in Tumor Cells and Stroma,” *Cancer Cell ,* vol. 20, no. 2, pp. 229-245, 2011.

[352] PP Provenzano et al, “Matrix density-induced mechanoregulation of breast cell phenotype, signaling and gene expression through a FAK-ERK linkage,” *Oncogene,* vol. 28, no. 49, pp. 4326-4343, 2009.

[353] F Spill et al, “Impact of the physical microenvironment on tumor progression and metastasis,” *Current Opinions in Biotechnology,* vol. 40, pp. 41-48, 2016.

[354] PJ Asif et al, “The Role of Cancer-Associated Fibroblasts in Cancer Invasion and Metastasis,” *Cancers (Basel),* vol. 13, no. 18, p. 4720, 2021.

[355] R Kalluri, “The biology and function of fibroblasts in cancer,” *Nature Reviews Cancer,* vol. 16, no. 9, pp. 582-598, 2016.

[356] C Gaggioli et al, “Fibroblast-led collective invasion of carcinoma cells with differing roles for RhoGTPases in leading and following cells,” vol. 9, no. 12, pp. 1392-1400, 2007.

[357] E Sahai et al, “A framework for advancing our understanding of cancer-associated fibroblasts,” *Nature Reviews Cancer,* Vols. 174-186, no. 20, 2020.

[358] H Kasashima et al, “Lysyl oxidase-like 2 (LOXL2) from stromal fibroblasts stimulates the progression of gastric cancer,” *Cancer Letters ,* vol. 354, no. 2, pp. 438-446, 2014.

[359] B Erdogan et al, “Cancer-associated fibroblasts promote directional cancer cell migration by aligning fibronectin,” *Journal of Cell Biology,* vol. 216, no. 11, pp. 3799-3816, 2017.

[360] C Goertzen et al, “Three-Dimensional Quantification of Spheroid Degradation-Dependent Invasion and Invadopodia Formation,” *Biological Procedures Online ,* vol. 20, p. 20, 2018.

[361] H Liu et al, “A microcarrier-based spheroid 3D invasion assay to monitor dynamic cell movement in extracellular matrix,” *Biological Procedures Online ,* vol. 22, p. 3, 2020.

[362] M Vinci et al, “Three-Dimensional (3D) Tumor Spheroid Invasion Assay,” *Journal of Visualized Experiments ,* vol. 99, p. 52686, 2015.

[363] R Kanzaki et al, “Heterogeneity of cancer-associated fibroblasts: Opportunities for precision medicine,” *Cancer Science ,* vol. 111, no. 8, pp. 2708-2717, 2020.

[364] PY Chen et al, “Cancer-Associated Fibroblast Heterogeneity: A Factor That Cannot Be Ignored in Immune Microenvironment Remodeling,” *Frontiers in Immunology ,* vol. 12, p. 671595, 2021.

[365] JA Galvan et al, “Validation of COL11A1/procollagen 11A1 expression in TGF-β1-activated immortalised human mesenchymal cells and in stromal cells of human colon adenocarcinoma,” *BMC Cancer ,* vol. 14, p. 867, 2014.

[366] HN Chia et al, “Effect of substrate stiffness on pulmonary fibroblast activation by TGF-β,” *Acta Biomaterialia ,* vol. 8, no. 7, pp. 2602-2611, 2012.

[367] WD Joo et al, “Microscopic Omental Metastasis in Clinical Stage I Endometrial Cancer: A Meta-analysis,” *Annals of Surgical Oncology ,* vol. 22, no. 11, pp. 3695-3700, 2015.

[368] A Sykaras, “Exosomes on Endometrial Cancer: A Biomarkers Treasure Trove?,” *Cancers (Basel),* vol. 14, no. 7, p. 1733, 2022.

[369] T Simon & B Salhia, “Cancer-Associated Fibroblast Subpopulations With Diverse and Dynamic Roles in the Tumor Microenvironment,” *Molecular Cancer Research ,* vol. 20, no. 2, pp. 183-192, 2022.

[370] X Chen et al, “Exosome-mediated transfer of miR-93-5p from cancer-associated fibroblasts confer radioresistance in colorectal cancer cells by downregulating FOXA1 and upregulating TGFB3,” *Journal of Experimental and Clinical Cancer Research ,* vol. 39, p. 65, 2020.

[371] Wang Y et al, “Cancer-associated fibroblast-derived SDF-1 induces epithelial-mesenchymal transition of lung adenocarcinoma via CXCR4/β-catenin/PPARδ signalling,” *Nature,* vol. 12, no. 214, 2021.

[372] SML Anderson et al, “The effects of ascorbic acid on collagen synthesis by cultured human skin fibroblasts,” *Biochemical Soceity Transactions ,* vol. 19, no. 1, p. 48S, 1991.

[373] M Miron-Mendoza et al, “Coupling of Fibrin Reorganization and Fibronectin Patterning by Corneal Fibroblasts in Response to PDGF BB and TGFβ1,” *Bioengineering ,* vol. 7, no. 3, p. 89, 2020.

[374] E Lenselink, “Role of fibronectin in normal wound healing,” *International Wound Journal ,* vol. 12, no. 3, pp. 313-316, 2015.

[375] Y Sagae et al, “Versican provides the provisional matrix for uterine spiral artery dilation and fetal growth,” *Matrix Biology,* vol. 115, pp. 16-31, 2023.

[376] S Islam & H Watanabe, “Versican: A Dynamic Regulator of the Extracellular Matrix,” *Journal of Histochemistry & Cytochemistry,* vol. 68, no. 11, pp. 763-775, 2020.

[377] C Jensen & Yong T, “Is It Time to Start Transitioning From 2D to 3D Cell Culture?,” *Frontiers in Molecular Biosciences,* vol. 7, p. 33, 2013.

[378] KE Sung et al, “Understanding the Impact of 2D and 3D Fibroblast Cultures on In Vitro Breast Cancer Models,” *PLoS One,* vol. 8, no. 10, p. e76373, 2013.

[379] OD Wever et al, “Tenascin-C and SF/HGF produced by myofibroblasts in vitro provide convergent pro-invasive signals to human colon cancer cells through RhoA and Rac,” *FASEB Journal ,* vol. 18, no. 9, pp. 1016-1018, 2004.

[380] OD Wever et al, “Stromal myofibroblasts are drivers of invasive cancer growth,” *International of Cancer ,* vol. 123, no. 10, pp. 2229-2238, 2008.

[381] Y Sun et al, “Cancer-associated fibroblasts secrete FGF-1 to promote ovarian proliferation, migration, and invasion through the activation of FGF-1/FGFR4 signaling,” *Tumor Biology,* vol. 39, no. 7, 2017.

[382] R Zaidel-Bar et al, “A paxillin tyrosine phosphorylation switch regulates the assembly and form of cell-matrix adhesions,” *Journal of Cell Science ,* vol. 120, no. 1, pp. 137-148, 2007.

[383] Y Attieh et al, “Cancer-associated fibroblasts lead tumor invasion through integrin-β3–dependent fibronectin assembly,” *Journal of Cell Biology ,* vol. 216, no. 11, p. 3509–3520, 2017.

[384] R Kalluri &. M Zeisberg, “Fibroblasts in cancer,” *Nature Reviews Cancer,* vol. 6, no. 5, pp. 392-401, 2006.

[385] J Winkler et al, “Concepts of extracellular matrix remodelling in tumour progression and metastasis,” *Nature Communications,* vol. 11, p. 5120, 2020.

[386] Y Itoh & H Nagase, “Matrix metalloproteinases in cancer,” *Essays in Biochemistry ,* vol. 38, no. 21, p. 36, 2002.

[387] TH Klopper et al, “Untangling the evolution of Rab G proteins: implications of a comprehensive genomic analysis,” *BMC Biology,* vol. 10, p. 71, 2012.

[388] NA Guadagno & C Progida, “Rab GTPases: Switching to Human Diseases,” *Cells ,* vol. 8, no. 8, p. 909, 2019.

[389] RL Nokes et al, “Rab13 regulates membrane trafficking between TGN and recycling endosomes in polarized epithelial cells,” *Journal of Cell Biology ,* vol. 182, no. 5, pp. 845-853, 2008.

[390] Y Pei et al, “RAB21 controls autophagy and cellular energy homeostasis by regulating retromer-mediated recycling of SLC2A1/GLUT1,” *Autophagy,* pp. 1-17, 2022.

[391] E Frittoli et al, “A RAB5/RAB4 recycling circuitry induces a proteolytic invasive program and promotes tumor dissemination,” *Journal of Cell Biology ,* vol. 206, no. 2, pp. 307-328, 2014.

[392] H Huang et al, “A dominant negative variant of RAB5B disrupts maturation of surfactant protein B and surfactant protein C,” *PNAS,* vol. 119, no. 6, p. e2105228119, 2022.

[393] A Hamm et al, “Efficient transfection method for primary cells,” *Tissue Engineering ,* vol. 8, no. 2, pp. 235-245, 2002.

[394] M Breunig et al, “Breaking up the correlation between efficacy and toxicity for nonviral gene delivery,” *PNAS,* vol. 104, no. 36, pp. 14454-14459, 2007.

[395] AMA Rømer et al, “Immune Modulatory Properties of Collagen in Cancer,” *Frontiers in Immunology ,* vol. 12, p. 791453, 2021.

[396] T Koorman et al, “Spatial collagen stiffening promotes collective breast cancer cell invasion by reinforcing extracellular matrix alignment,” *Oncogene,* vol. 41, p. 2458–2469, 2022.

[397] CR Esquibel et al, “Second Harmonic Generation Imaging of Collagen in Chronically Implantable Electrodes in Brain Tissue,” *Frontiers in Neuroscience ,* vol. 14, p. 95, 2020.

[398] S Hashimoto et al, “Requirement for Arf6 in breast cancer invasive activities,” *PNAS,* vol. 101, no. 17, pp. 6647-6652, 2004.

[399] G Efthymiou et al, “Shaping Up the Tumor Microenvironment With Cellular Fibronectin,” *Frontiers in Oncology ,* vol. 10, p. 641, 2020.

[400] DP White et al, “αvβ3 and α5β1 integrin recycling pathways dictate downstream Rho kinase signaling to regulate persistent cell migration,” *Journal of Cell Biology,* vol. 177, no. 3, pp. 515-525, 2007.

[401] MR Morgan et al, “Syndecan-4 Phosphorylation Is a Control Point for Integrin Recycling,” *Developmental Cell,* vol. 24, no. 5, pp. 472-485, 2013.

[402] O Nadiarnykh et al, “Alterations of the extracellular matrix in ovarian cancer studied by Second Harmonic Generation imaging microscopy,” *BMC Cancer ,* vol. 10, p. 94, 2010.

[403] J Chang et al, “Circadian control of the secretory pathway maintains collagen homeostasis,” *Nature Cell Biology ,* vol. 22, no. 1, pp. 74-86, 2020.

[404] WJ Lee et al, “Neutrophils facilitate ovarian cancer premetastatic niche formation in the omentum,” *The Journal of Experimental Medicine,* vol. 216, no. 1, pp. 176-194, 2019.

[405] T Serdiuk et al, “Trypsinization-dependent cell labeling with fluorescent nanoparticles,” *Nanoscale Research Letters ,* vol. 9, p. 568, 2014.

[406] P Vehviläinen et al, “Latent transforming growth factor-beta-binding protein 2 is an adhesion protein for melanoma cells,” *Journal of Biological Chemistry ,* vol. 278, no. 27, pp. 24705-24713, 2003.

[407] H Zang et al, “Roles of Fibulin-2 in Carcinogenesis,” *Medical Science Monitor ,* vol. 26, pp. e918099-1–e918099-9, 2020.

[408] A Yorozu et al, “Upregulation of adipocyte enhancer-binding protein 1 in endothelial cells promotes tumor angiogenesis in colorectal cancer,” *Cancer ,* vol. 111, no. 5, p. 1631–1644, 2020.

[409] F Prica et al, “The life and works of S100P - from conception to cancer,” *American Journal of Cancer Research ,* vol. 6, no. 2, pp. 562-576, 2016.

[410] T Mirzapoiazova et al, “HABP2 is a Novel Regulator of Hyaluronan-Mediated Human Lung Cancer Progression,” *Frontiers in Oncology ,* vol. 5, p. 164, 2015.

[411] A Bera et al, “Functional role of vitronectin in breast cancer,” *PLoS One ,* vol. 15, no. 11, p. e0242141., 2020.

[412] S Royle, “The cellular functions of clathrin,” *cellular and Molecular Life Sciences,* vol. 63, no. 16, pp. 1823-1832, 2006.

[413] Z Zhang et al, “Size and Dynamics of Caveolae Studied Using Nanoparticles in Living Endothelial Cells,” *ACS Nano ,* vol. 3, no. 12, pp. 4110-4116, 2009.

[414] O Olivares et al, “Collagen-derived proline promotes pancreatic ductal adenocarcinoma cell survival under nutrient limited conditions,” *Nature Communications,* vol. 8, p. 16031, 2017.

[415] Y Bi et al, “Endocytosis of collagen by hepatic stellate cells regulates extracellular matrix dynamics,” *The American Journal of Physiology-Cell Physiology,* vol. 307, no. 7, pp. C622-C633, 2014.

[416] Z Gu et al, “Integrins traffic rapidly via circular dorsal ruffles and macropinocytosis during stimulated cell migration,” *Journal of Cell biology ,* vol. 193, no. 1, pp. 61-70, 2011.

[417] T Hongu et al, “Arf6 regulates tumour angiogenesis and growth through HGF-induced endothelial β1 integrin recycling,” *Nature Communications,* vol. 6, p. 7925, 2015.

[418] AM Powelka et al, “Stimulation-dependent recycling of integrin beta1 regulated by ARF6 and Rab11,” *Traffic,* vol. 5, no. 1, pp. 20-36, 2004.

[419] C Zeltz & D Gullberg, “The integrin–collagen connection – a glue for tissue repair?,” *Journal of Cell Science ,* vol. 129, no. 4, pp. 653-664, 2016.

[420] JG Donaldson, “Macropinosome formation, maturation and membrane recycling: lessons from clathrin-independent endosomal membrane systems,” *Philosophical Transactions of The Royal Society B ,* vol. 374, p. 20180148, 2019.

[421] CD Williamson & JG Donaldson, “Arf6, JIP3, and dynein shape and mediate macropinocytosis,” *Molecular Biology of the Cell ,* vol. 30, no. 12, pp. 1477-1489, 2019.

[422] RM Sears et al, “BioID as a Tool for Protein-Proximity Labeling in Living Cells,” *Methods in Molecular Biology ,* vol. 2012, pp. 299-313, 2019.

[423] AF Majdalawieh et al, “AEBP1 is a Novel Oncogene: Mechanisms of Action and Signaling Pathways,” *Journal of Oncology ,* vol. 2020, p. 8097872, 2020.

[424] L Cheng et al, “Adipocyte enhancer binding protein 1 (AEBP1) knockdown suppresses human glioma cell proliferation, invasion and induces early apoptosis,” *Pathology - Research and Practice ,* vol. 216, no. 2, p. 152790, 2020.

[425] PR Blackburn et al, “Bi-allelic Alterations in AEBP1 Lead to Defective Collagen Assembly and Connective Tissue Structure Resulting in a Variant of Ehlers-Danlos Syndrome,” *The American Jounral of Human Genetics ,* vol. 102, no. 4, p. 696–705., 2018.

[426] Gonda A et al, “Extracellular Vesicle Molecular Signatures Characterize Metastatic Dynamicity in Ovarian Cancer,” *Frontiers in Oncology,* vol. 11, p. 718408, 2021.

[427] M Jager et al, “Aortic carboxypeptidase-like protein enhances adipose tissue stromal progenitor differentiation into myofibroblasts and is upregulated in fibrotic white adipose tissue,” *PLoS ONE,* vol. 13, no. 5, p. e0197777, 2018.

[428] D Li et al, “AEBP1 Is One of the Epithelial-Mesenchymal Transition Regulatory Genes in Colon Adenocarcinoma,” *BioMed Research International ,* vol. 2021, p. 3108933, 2021.

[429] JM Gebauer et al, “COMP and TSP-4 interact specifically with the novel GXKGHR motif only found in fibrillar collagens,” *Scientific Reports ,* vol. 8, p. 17187, 2018.

[430] NES Sibinga et al, “Collagen VIII Is Expressed by Vascular Smooth Muscle Cells in Response to Vascular Injury,” *Circulation Research ,* vol. 80 , no. 4, pp. 532-541, 1997.

[431] NUB Hansen et al, “Type VIII collagen is elevated in diseases associated with angiogenesis and vascular remodeling,” *Clinical Biochemistry,* vol. 49, no. 12, pp. 903-908, 2016.

[432] W Wang et al, “Type VIII collagen is elevated in diseases associated with angiogenesis and vascular remodeling,” *The FEBS Journal ,* vol. 280, no. 5, p. Type VIII collagen is elevated in diseases associated with angiogenesis and vascular remodeling, 2013.

[433] H Li et al, “PRELP (proline/arginine-rich end leucine-rich repeat protein) promotes osteoblastic differentiation of preosteoblastic MC3T3-E1 cells by regulating the β-catenin pathway,” *Biochemical and Biophysical Research Communications ,* vol. 470, no. 3, pp. 558-562, 2016.

[434] R Hong et al, “PRELP has prognostic value and regulates cell proliferation and migration in hepatocellular carcinoma,” *Journal of Cancer,* vol. 11, no. 21, pp. 6376-6389, 2020.

[435] H Kosuge et al, “Proteomic identification and validation of novel interactions of the putative tumor suppressor PRELP with membrane proteins including IGFI-R and p75NTR,” *Journal of Biological Chemistry ,* vol. 296, p. 100278, 2021.

[436] B Chiavarina et al, “Tumor-Antagonizing Fibroblasts Secrete Prolargin as Tumor Suppressor in Hepatocellular Carcinoma,” *Oncogene,* vol. 41, no. 10, pp. 1410-1420, 2022.

[437] E Bengtsson et al, “The leucine-rich repeat protein PRELP binds fibroblast cell-surface proteoglycans and enhances focal adhesion formation,” *Biochemical Journal ,* vol. 473, no. 9, pp. 1153-1164, 2016.

[438] S Chakraborty et al, “Agrin Mediates Angiogenesis in the Tumor Microenvironment,” *Trends in Cancer ,* vol. 6, no. 2, pp. 81-85, 2020.

[439] ZQ Wang et al, “Agrin promotes the proliferation, invasion and migration of rectal cancer cells via the WNT signaling pathway to contribute to rectal cancer progression,” *Journal of Receptors and Signal Transduction,* vol. 41, no. 4, pp. 363-370, 2020.

[440] X Lv et al, “Agrin para-secreted by PDGF-activated human hepatic stellate cells promotes hepatocarcinogenesis in vitro and in vivo,” *Oncotarget,* vol. 8, no. 62, pp. 105340-105355, 2017.

[441] DI Leavesley et al, “Vitronectin—Master controller or micromanager?,” *IUBMB Life,* vol. 65, no. 10, pp. 807-818, 2013.

[442] R Burgos-Panadero et al, “Vitronectin as a molecular player of the tumor microenvironment in neuroblastoma,” *BMC Cancer,* vol. 19, p. 479, 2019.

[443] Y Fukushima et al, “Induction of glioma cell migration by vitronectin in human serum and cerebrospinal fluid,” *Journal of Neurosurgery ,* vol. 107, no. 3, p. 578–585, 2007.

[444] L Heyman et al, “Mesothelial vitronectin stimulates migration of ovarian cancer cells,” *Cell Biology International,* vol. 34, no. 5, pp. 493-502, 2013.

[445] HA Kenny et al, “The initial steps of ovarian cancer cell metastasis are mediated by MMP-2 cleavage of vitronectin and fibronectin,” *The Journal of Clinical Investigation,* vol. 118, no. 4, p. 1367–1379., 2008.

[446] C Chen et al, “Formation of pre-metastatic bone niche in prostate cancer and regulation of traditional chinese medicine,” *Frontiers in Pharmacology,* vol. 13, p. 897942, 2022.

[447] Y Maru, “The lung metastatic niche,” *Journal of Molecular Medicine,* vol. 93, no. 11, pp. 1185-1192, 2015.

[448] H Peinado et al, “Pre-metastatic niches: organ-specific homes for metastases,” *Nature Reviews Cancer ,* vol. 17, p. 302–317, 2017.

[449] M Paolillo & S Schinelli, “Extracellular Matrix Alterations in Metastatic Processes,” *International Journal of Molecular Sciences ,* vol. 20, no. 19, p. 4947, 2019.

[450] Z Yu et al, “Pancreatic cancer-derived exosomes promote tumor metastasis and liver pre-metastatic niche formation.,” *Oncotarget,* vol. 8, pp. 63461-63483, 2017.

[451] R Baghban et al, “Tumor microenvironment complexity and therapeutic implications at a glance,” *Cell Communication and Signalling ,* vol. 18, p. 59, 2020.

[452] G Biffi & D Tuveson, “Diversity and Biology of Cancer-Associated Fibroblasts,” *Physiological Reviews ,* vol. 101, no. 1, pp. 147-176, 2021.

[453] ME Fiori et al, “Cancer-associated fibroblasts as abettors of tumor progression at the crossroads of EMT and therapy resistance,” *Molecular Cancer ,* vol. 18, no. 1, p. 70, 2019.

[454] G Gunaydin, “CAFs Interacting With TAMs in Tumor Microenvironment to Enhance Tumorigenesis and Immune Evasion,” *Frontiers in Oncology ,* vol. 11, p. 668349., 2021.

[455] X Li et al, “Single-cell RNA sequencing reveals a pro-invasive cancer-associated fibroblast subgroup associated with poor clinical outcomes in patients with gastric cancer,” *Theranostics,* vol. 12, no. 2, pp. 620-638, 2022.

[456] M Hong et al, “RNA sequencing: new technologies and applications in cancer research,” *Journal of Hematology & Oncology ,* vol. 13, p. 166, 2020.

[457] D Lavie et al, “Cancer-associated fibroblasts in the single-cell era,” *Nature Cancer ,* vol. 3, pp. 793-807, 2022.

[458] CX Dominguez et al, “Single-Cell RNA Sequencing Reveals Stromal Evolution into LRRC15+ Myofibroblasts as a Determinant of Patient Response to Cancer Immunotherapy,” *Cancer Discovery ,* vol. 10, no. 2, pp. 232-253, 2020.

[459] A Sebastian et al, “Single-Cell Transcriptomic Analysis of Tumor-Derived Fibroblasts and Normal Tissue-Resident Fibroblasts Reveals Fibroblast Heterogeneity in Breast Cancer,” *Cancers (Basel) ,* vol. 12, no. 5, p. 1307, 2020.

[460] S Olalekan et al, “Characterizing the tumor microenvironment of metastatic ovarian cancer by single-cell transcriptomics,” *Cell Reports ,* vol. 35, p. 109165, 2021.

[461] A Bauernfeind, “The predictive nature of transcript expression levels on protein expression in adult human brain,” *BMC Genomics,* vol. 18, p. 322, 2017.

[462] E D'Arcangelo et al, “The life cycle of cancer-associated fibroblasts within the tumour stroma and its importance in disease outcome,” *British Journal of Cancer ,* vol. 122, pp. 931-942, 2020.

[463] M Clague, “Molecular aspects of the endocytic pathway.,” *Biochemical Journal ,* vol. 336, no. 2, pp. 271-282, 1998.

[464] KJ Roux et al, “BioID: A Screen for Protein-Protein Interactions,” *Current Protocols in Protein Science ,* vol. 91, pp. 19.23.1-19.23.15, 2019.

[465] SP Rebelo et al, “3D-3-culture: A tool to unveil macrophage plasticity in the tumour microenvironment,” *Biomaterials,* vol. 163, pp. 185-197, 2018.

[466] T Qin et al, “Harnessing preclinical models for the interrogation of ovarian cancer,” *Journal of Experimental and Clinical Cancer Research ,* vol. 41, p. 277, 2022.

[467] J Kwon et al, “USP13 promotes development and metastasis of high-grade serous ovarian carcinoma in a novel mouse model,” *Oncogene,* vol. 41, no. 13, pp. 1974-1985, 2022.

[468] E Maniati et al, “Mouse Ovarian Cancer Models Recapitulate the Human Tumor Microenvironment and Patient Response to Treatment,” *Cell Reports,* vol. 30, p. 525–540, 2020.

[469] Y Mo et al, “Tumor-secreted exosomal miR-141 activates tumor-stroma interactions and controls premetastatic niche formation in ovarian cancer metastasis,” *Molecular Cancer ,* vol. 22, p. 4, 2023.

[470] JH Yoo et al, “ARF6 Is an Actionable Node that Orchestrates Oncogenic GNAQ Signaling in Uveal Melanoma,” *Cancer cell,* vol. 29, no. 6, pp. 889-904, 2016.

[471] E Fiola-Masson et al, “Activation of the GTPase ARF6 regulates invasion of human vascular smooth muscle cells by stimulating MMP14 activity,” *Science Reports,* vol. 12, no. 1, p. 9532, 2022.

[472] S Hashimoto et al, “Requirement for Arf6 in breast cancer invasive activities,” *PNAS,* vol. 101, no. 17, pp. 6647-6652, 2004.

[473] R Li et al, “Roles of Arf6 in cancer cell invasion, metastasis and proliferation,” *Life Sciences,* vol. 182, pp. 80-84, 2017.

[474] JK Schweitzer et al, “ARF6-mediated endocytic recycling impacts cell movement, cell division and lipid homeostasis,” *Seminars in Cell and Developmental Biology,* vol. 22, no. 1, pp. 39-47, 2011.